UNIVERSITY OF SALERNO

UNIVERSITÀ DEGLI STUDI DI SALERNO

DEPARTMENT OF CIVIL ENGINEERING

DIPARTIMENTO DI INGEGNERIA CIVILE

PHD COURSE IN RISK AND SUSTAINABILITY IN CIVIL, ARCHITECTURE AND ENVIRONMENTAL ENGINEERING SYSTEMS

DOTTORATO DI RICERCA IN RISCHIO E SOSTENIBILITA' NEI SISTEMI DELL'INGEGNERIA CIVILE, EDILE E AMBIENTALE

TOPIC

INTEGRATED STRUCTURAL AND THERMAL UPGRADING OF EXISTING MASONRY WALLS USING TEXTILE-STRENGTHENED MORTARS WITH JUTE FIBERS: A CROSS-SCALE EXPERIMENTAL STUDY

XXXV Cycle/ Ciclo: (2020-2022)

Ph.D. Student
Arnas Majumder

Supervisor/Il Tutor
Prof. Enzo Martinelli

Co-Supervisors
Prof. Fernando Fraternali
Prof. Flavio Stochino (Unica)

The coordinator/
Il Coordinatore
Prof. Fernando Fraternali

Some of the sections of this Thesis are part of the following articles:

Majumder, A., Stochino, F., Frattolillo, A., Valdes, M., Mancusi, G. and Martinelli, E., 2023. Jute fiber strengthened mortars: Mechanical response and thermal performance. *Journal of Building Engineering*, p.105888.

Majumder, A., Stochino, F., Farina, I., Valdes, M., Fraternali, F. and Martinelli, E., 2022. Physical and mechanical characteristics of raw jute fibers, threads and diatons. *Construction and Building Materials*, *326*, p.126903.

Majumder, A., Farina, I., Stochino, F., Fraternali, F. and Martinelli, E., 2022. Natural Fibers Strengthened Mortars: Composition and Mechanical Properties. In *Key Engineering Materials* (Vol. 913, pp. 149-153). Trans Tech Publications Ltd.

Majumder, A., Stochino, F., Frattolillo, A., Valdes, M., Fraternali, F. and Martinelli, E., 2022. Sustainable Building Material: Recycled Jute Fiber Composite Mortar for Thermal and Structural Retrofitting. In *International Conference on Computational Science and Its Applications* (pp. 657-669). Springer, Cham.

Majumder, A., Stochino, F., Fernando, F. and Enzo, M., 2021. Seismic and Thermal Retrofitting of Masonry Buildings with Fiber Strengthened Composite Systems: A State of the Art Review.

Majumder, A., Stochino, F., Frattolillo, A., Valdes, M., Fraternali, F. and Martinelli, E., 2022. Jute fiber mortar composites for integrated retrofitting Proc. of the 14th fib International PhD Symposium in Civil Engineering, Sep. 5 to 7, 2022, Rome, Italy (Yet to be publish officially).

Acknowledgments

At the beginning I would like to express my sincere gratitude to my supervisor and respected Prof. Enzo Martinelli, for extending his support and guidance throughout three years of my PhD course. Also, I would like to thank him for providing me, with a friendly environment and pleasant workplace, during my staying at the University of Salerno. He is very kind, gentle and always helped me like a friend, and advised, encouraged and guided me like a true mentor and supervisor, and of course he is a wonderful person. Without his assistance and guidance, it won't be possible to complete the PhD research activities and this Thesis.

Thank you, Prof.

I would like to thank and express my sincere gratitude to my co-supervisor, PhD coordinator and respected Prof. Fernando Fraternali for his kind advice, support and guidance during my research activities. Also, he was kind to help me to solve many problems during these last three years as a co-supervisor and PhD coordinator.

I would like to thank and express my sincere gratitude to my external co-supervisor and respected Prof. Flavio Stochino of the University of Cagliari, being a wonderful mentor and guide during my staying for my research activities, at the University of Cagliari, Italy. I heartly acknowledge his useful advice, support, guidance and fund, which he has provided for my research work and experimental activities. Without his guidance and support it would be impossible to conduct so many and long experimental campaign.

Also, I would like to thank and express my sincere gratitude and respected Prof. Andrea Frattolillo for his support, guidance and allowing to use the engineering thermodynamics laboratory and the Climate Chamber of the University of Cagliari, Italy, for my research activities.

Further I would convey my sincere gratitude to respected Prof. Gianvittorio Rizzano the Head of the department (DICIV, UNISA), respected Prof. Luciano Feo, the head of the Strength Laboratory of the University of Salerno and respected Prof. Mauro Sassu the Head of the department (Civil engineering and architecture, UNICA) for allowing me to use the laboratories for conducting various tests.

I am expressing my gratitude to the research fellow engineer Monica Valdes and technician Mr. Roberto Lai from the University of Cagliari, Italy, and the research fellows Engineer Francesco Perri and Engineer Ciro Esposito of the

University of Salerno, Italy, for extending their help whenever I needed during my experimental and research activities.

I would like to thank and express my sincere gratitude to Dr. Giuseppe Ferrara for his valuable suggestions and advice on conducting tests and writing this thesis.

Similarly, I would like to thank and express my sincere gratitude Prof. Satyajit Pattanayak of the Madanapalle Institute of Technology & Science, AP, India for hosting me and guiding my research activities during my visit in India.

Moreover, I would like to thank Mr. Uttam Patra, the General Manager of the Ganges jute Pvt. Ltd., Bansberia, Hooghly, India for is kindness, hospitality and also for providing valuable information and data on jute thread(s) production process.

I cordially thank and convey my gratitude to Prof. Giacomo Viccione, Prof. Salvatore Barba, Prof. Ada Amandola and Dr. Marco Pepe for helping me whenever I needed it the most.

I have to thank jute plant cultivators from village of Chakdaha and Bilpar for their kind hospitality during my visit for the on-field survey and also for answering my questions.

I would like to thank Mr. Pier Luigi Damiani owner of the Brebey S.c.a.r.l., for providing the woolen insulation panel samples, which has been used as heat guards, during the composite sample's thermal conductivity tests.

Also, I would like to convey my gratitude to Prof. Mariano Modano, Prof. Ilenia Farina, Prof. Gianluca Gatto, Prof. Roberto Innamorati, Prof. Roberto Ricciu, Prof. Roberto Baccoli, Prof. Amit Kumar, Prof. Costantino Carlo Mastino and Prof. Giovanna Concu.

I would like to specially thank Dr. Sara Antinozzi for her help and kindness, during my staying at the university campus.

Last but not least, I would like to thank my family and friends: my father, mother and Tiash & Samir, Elisabetta Piras and family, Antonio Fadda and family, Antonio Pinese and family, Rento Tetti, Simone Vacca, Biplab Mistry, Nagendra Baku, Narindar Singh, Francesco Nigro, Sumit Saha, Aviru Sarkar and all my PhD colleagues.

Index

1. Introduction

1.1 Motivation

The present PhD Thesis has been developed considering the existing housing problem, which our society is facing today, in both villages and cities. Based on the aforesaid problem, this PhD research work focuses mainly two areas:

1) The rural (Villages) and urban (Slums) poor housing conditions (Fig. 1-1);
2) Need for urgent thermo-structural retrofitting or upgrading mainly for the urban existing old and historical buildings.

As data provided by World Bank (2021), approximately 39.44% of the total world population still live in rural villages. While in 63 (out of 196) countries this number is much higher, as it ranges between 50% to 86.65 %.

The rural houses are mostly constructed with poor building materials, such as plastic, paddy straw, grass, thatch, bamboo, mud, wood, stones, asbestosis, GI metal sheet etc. Mostly these types of living places and conditions are unhealthy, and also lack basic amenities like potable water, electricity etc.

While as reported by the United Nations Development Program (UNDP), 17 out of 100 people do not have access to proper shelter, whereas 33 people out of every 100 people do not have access to electricity (UNDP 2022).

Notably, a major part of the buildings in urban city center are made of masonry (many of these are old and historical buildings) and these were built to withstand the gravitational loads. Therefore, during a strong earthquake event these buildings sometime are uncapable to stand to the horizontal loads (Ferrara et al. 2021).

(a): Mud and metal house.

(b): Jute steak, plastic cover and metal

(c): Metal (Tin).

(d): Bamboo.

(e): Wooden

Fig. 1-1. Some traditional houses can be found in India.

Considering the aforesaid problems, newer composite construction materials could be right choice, with good structural behavior and thermal insulating property.

The individual and integrated (structural and/or thermal) properties could be achieved by using conventional or recycled (end life) construction products enhanced with natural materials, like locally available and cheap natural fibers.

The use of fibers is getting more and more common in construction sector. While both man-made and natural fibers are widely used for various purposes as highlighted below.

More commonly Fiber Strengthened Polymers (FRP) configurations are used for structural retrofitting or upgrading due to its higher strength and durability (Alecci et al. 2019). Mostly the man-made carbon (as stated in Alecci et. al. 2019, Rahman et al. 2016, Can 2018), glass (as highlighted in Kalali et al. (2012), Gattesco et al. (2015), Stratford et al. (2004) and basalt (as mentioned in Padalu 2019, Punurai 2018, Zhou et al. 2013) fibers are used for this purpose.

As highlighted by Ferrara et al. (2021), there are some known drawbacks and compatibility problems, of the use of FRPs in masonry reinforcement, such as the non-permeable nature of the polymeric resins used in the process and the strength of FRP found to be much higher than that of retrofitted masonry.

At the same time, FRP are non-ductile in nature and to deterioration of mechanical properties with elevated temperature Bisby et al. (2002).

Some installation-related problems are also observed as the process of thermosetting adhesive is affected by moisture and temperature conditions and the resin may have toxic effects, which requires specialized workers.

Therefore, to overcome the aforesaid issues and to have similar type of strength as of FRP, the inorganic matrix composite systems have been developed for masonry retrofitting or upgrading, where a fiber matrix is generally embedded in cement or lime-based mortar (Ferrara et al. 2021). In this case to the carbon, glass and basalt (Koutas et al. 2020, De Santis et al. 2019) and as well as steel (De Santis

et al. 2019, Dalalbashi et al. 2018, Ascione et al. 2020) fibers are used in Textile Strengthened Mortar (TRM).

In order to improve sustainability, recyclability and to reduce the carbon footprint and production cost of the construction and building materials, scientists and researchers are working on developing newer and smarter natural fiber-composite building materials and their mechanical properties are being studied (Elanchezhian et al. 2018, Francesconi et al. 2016, Pani et al. 2020, Sassu et al. 2016, Martínez-Barrera et a. 2020). Works on the natural fiber based FRP (or NFRP) can be found in Jirawattanasomkul et al (2019). There are some promising studies on the use of natural fiber TRM, particularly for structural upgrading can be found in Menna et al. (2015) on hemp fiber and Ferrara et al. (2021) on flex fiber.

While highlighting the studies conducted on the thermal property of the composite building materials, it is important to highlight that the natural fibers are mainly used in raw form or mixed with other nature materials like lime putty (Elanchezhian et al. 2018), clay (Majumder et al. 2021, El Azhary et al. 2017), opus signinum (Majumder et al. 2021), potato starch and starch (Ferrandez-García et al. 2020) etc., whereas in other cases the fibers are mainly fused with polyester or bicomponent to fabricate thermal insulating materials.

According to de Beus et al.(2019) natural fibers (like flax, hemp, jute or kenaf) have 78%-79.4% lower carbon footprint, when compared with glass or mineral fibers. Few notable studies conducted on the thermo-mechanical performance of the composite mortar systems fabricated with natural fibers (like date palm, hemp, sheep wool and oil palm fibers) can be found in (Benmansour et al.2014, Elfordy et al. 2008, Valenza et al. 2015, Raut et al.2016). In this contest, a promising new idea is the development of hybrid fibers composite in which both natural and man-made fibers are applied together by Hari et al.(2019).

It is worth highlighting that no studies have been yet conducted on the application of jute fiber net & jute fiber diatons together for structural masonry retrofitting and

the combination of jute composite mortar, jute fiber net & jute fiber diatons together for thermo-structural masonry retrofitting or upgrading.

Interestingly jute fiber accounts for nearabout 7% of the total natural fiber production (Townsend 2019).

Notably, every part of the jute plant can be used as food and herbal medicine (leaves), industrial and household materials (fibers) and for paper production, as fuel mainly used for cooking in villages and building materials (stalks/sticks) (Islam et al. 2012).

Fig. 1-2 presents different derivatives which come from the jute fiber plants, and also it represents various uses and products (Islam et al. 2012, Codispoti et al.2015, Mohanty et al. 1995, Majumder et al. 2021, Ferrandez-García et al. 2020).

The jute fiber production and its products require lower-energy during their production process and these are less hazards during manufacturing (Bambach 2020), when compared with man-made and mineral fibers. The jute fiber is known to be cheap, recyclable, whereas its strength and insulating capacity (Islam et al. 2012) make it attractive and competitive as construction material. Same as other natural fibers, jute fiber too inherits some disadvantages, when the fiber come in contact with water the strength of the fiber decrease and increase the moisture absorbability (Chand et al.2020).

At the same time, there are many positive sides of the jute plant cultivation like it improves the fertility of the soil, purify the air by absorbing CO_2 and emitting O_2 (Islam et al. 2012). The jute fiber and it derived products are quickly gaining importance in the Construction and Building (C&B) sector.

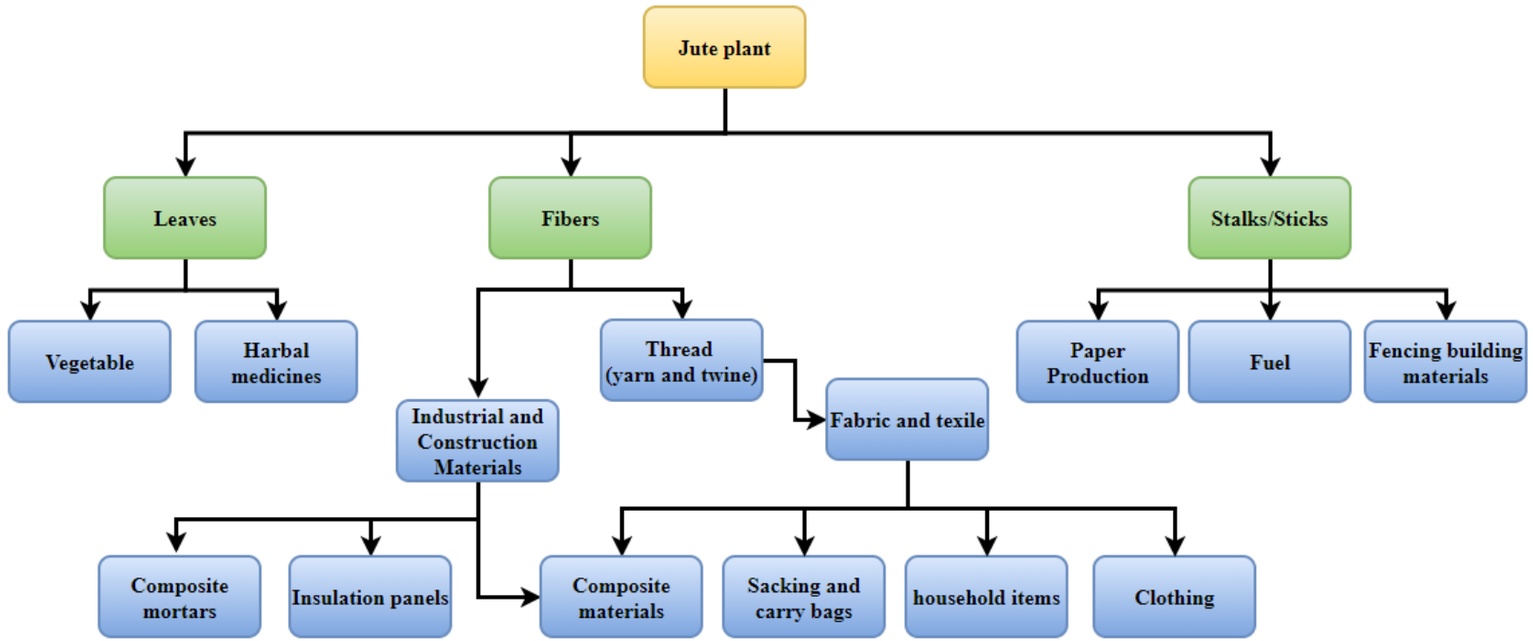

Fig. 1-2. Jute plant uses.

Some interesting research works conducted on the use jute fiber in the C&B field could be underlined as: concrete retrofitting or upgrading (Zakaria et al. 2017, Islam et al 2018, Razmi et al. 2017), Jute-FRP (Ascione et al. 2020), jute TRM (Codispoti et al. 2015), recycled jute fiber (collected from packaging bag) insulating materials (Majumder et al. 2021, Ferrandez-García et al. 2020), jute composite mortar (Formisano et al. 2020 a&b), jute epoxy composites (Ferreira et al. 2016), jute fiber crude earth bricks (Saleem et al. 2016), jute fiber burnt bricks (Rashi et al. 2019) etc.

For jute fiber, as well as for other types of natural fibers. very few studies have been conducted on the thermo-mechanical properties of the jute fiber composite mortar and thermo-structural behavior masonry retrofitting or upgrading (with jute fiber products like nets, diatons etc.).

Therefore, being felt the need to fulfil the existing gap the present study proposes:

1) A detailed analysis of the physical and mechanical properties of the jute fiber and it biproducts (threads and diatons);
2) The assessment of the thermo-mechanical properties of the jute fiber composite mortars prepared with various combinations of fiber lengths and fiber percentages (with respect to the dry mortar mass);
3) An experimental study on various combination of composite masonry wall systems, upgraded with jute fiber composite mortar, diatons (made of jute fiber) and jute TRM system.

Later Structural behavior and thermal insulation property of the upgraded masonry walls have been evaluated. Therefore, the Dual Upgrading Strategy (DUP) to optimize the masonry upgrading with respect to the anti-seismic and energetic standards has been evaluated.

While, the final objectives and contribution of this research work would be to promote the use of jute fiber and its products (diatons, net and jute fiber composite

mortars): (1) to construct new sustainable, Affordable and Healthy houses in rural areas (like in Indian villages, where the jute fiber is abundantly available) to contribute to create smarter villages and (2) to use these green and eco-friendly building materials for upgrading the existing buildings in urban areas (like historical cities), therefore contributing towards creating smart cities.

1.2 Vision of the project and the project development

The vision of the present project is to develop smart and green building matreials for thermo-structural retroftting purposes. To fullfill the project vision, the research work had gone through and accomplish two objectives or missions, which are:

1) To develop and study the thermo-mechanical behavior of the new jute-fiber composite mortars;
2) To study thermo-structural behavior of the composite masonry wall systems retrofitted with jute-fiber products.

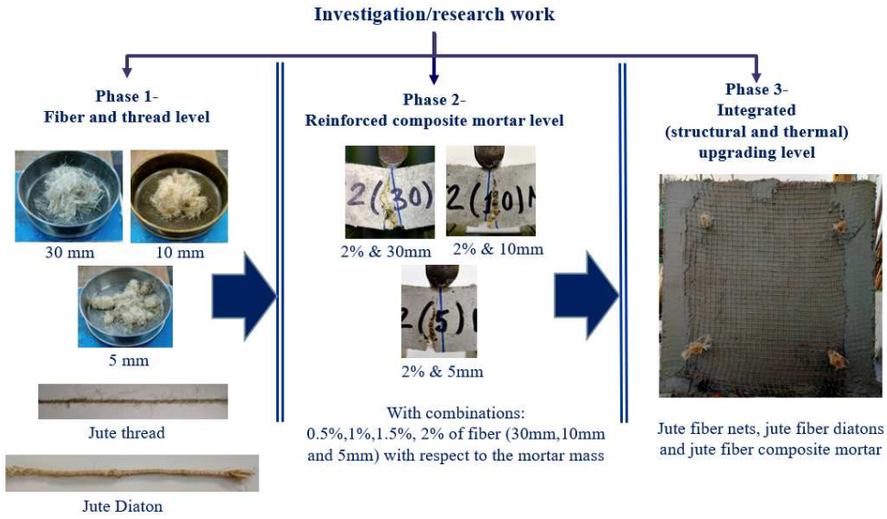

Fig. 1-3. The main three phases of the PhD research activities/works.

Fig. 1-3 presents the three main phases of this PhD research work. While these phases too have some other sub phases:

1) First phase: Fiber and thread level, in which the physical characteristics and mechanical behaviors of the raw jute fibers and its derivatives (threads and diatons) were studied.
2) Second phase: Strengthened composite mortars level. In this phase jute fiber composite mortars were prepared. Two types of mortars, and jute fibers with three different lengths (30 mm, 10 mm and 5 mm) and four different fiber percentages (0.5%, 1%, 1.5% and 2%) with respect to the mortar masses have been used to prepare the composite mortars. In this phase a total to 24 combinations of composite mortar sample have been prepared and tests were conducted to study the mechanical behaviors and thermal performances of these samples.

   Further developments: three different typed of composite mortars have been carried out in following sub-phases.

   Case 1 – Composite mortars prepared with Same Average Water (SAW) and with Recycled Aggregates (RA)

   Case 2 – Thermal composite mortars prepared with 1 % fiber (with respect to the dry mortar mass) and without Recycled Aggregates (nRA)

   Case 3: Thermal mortar without Recycled Aggregates (nRA) and Same water (SW).
3) Third phase: Integrated (Thermo-Structural) upgrading level. In this phase different combinations of the integrated masonry upgrading were done by using the knowledge gained and results obtained during the Phase 1 and phase 2 for this research work.

   Further developments: In this case or sub-phase: the recycled jute net fiber composite mortar was prepared by using jute fiber scraps collected during

the jute net fabrication. Recycled fibers were applied in the place of pre-fabricated insulation materials (i.e., RA) present in the original mortar.

It is worth to highlight that integrated (Structural and Thermal) retrofitting or upgrading with TRM system is a subject of current relevance. The recent research activities in this field are repported in the Chapter 2; Section 2.3.

The novelties of this PhD reserch work could be highlighted are:

1) a natural fiber has been used for dual purpose (structural and thermal) or integrated upgarating of a masonry wall/structure with a Natural Fiber (NF) TRM system.
2) jute fiber products like nets, diatons and chipped raw fibers (for composite mortar) have been used for NFTRM upgrading.
3) a *TRM system package* composded of jute fiber nets, jute fiber diatons and jute fiber composite mortar, has been created with the aim not only to improve the stuctural behavior but also to enhance the thermal performance of the upgraded masonry wall/structure. (it has been nominated as *TRM system package* due the fact that it is a complete TRM-system which has the capability to improve both structural and thermal properties. Notably in most of the previous cases, researchers have integrated the insulation material mainly the Expanded Polystyrene (EPS) inside the TRM-system, while in our case a composite mortar has been prepared to be one of the components of the TRM system)
4) the thermal properties have been evaluated expermentally in a dedicated climate chamber with pre-set desired enviromental (i.e., room/internal and ambient/external) conditions.

1.3 Contents and Structure of the Thesis

The present Thesis presents analytical results of the experimental campaigns conducted at each phase, during the period of three years of the PhD course. All the experiments were performed in the Material Testing Laboratory of the University of Cagliari, Italy and the Strength Laboratory of the University of Salerno, Italy.

In this ambitious research and development project, the various properties (physical, thermal and mechanical) and the applicability (structural upgrading) of jute fiber and it derived products in the C&B sector have been evaluated.

The experimental observations, results and critical analysis of each phase (as highlighted in section 1.2) are reported in detail in progressive chapters as below:

Chapter 1 proposes a general background and motivation for this PhD research and development project.

Chapter 2 highlights the state of the art literature review reinforcement and /or retrofitting and upgrading strategies.

Chapter3 underlines the in brief the existing regulations, guidelines and recommendations, particularly provided by the Government of Italy, for the Textile Strengthened Mortar (TRM) and for the thermal transmittance or heat transfer coefficient (U) calculations.

Chapter 4 provides in detail the information about the materials used during this research work. The Physical and mechanical behaviors of three jute products (i) raw fibers, (ii) threads and (iii) diatons, have been studied in detail during this phase. The Physical characteristics and mechanical properties all the jute fiber products were determined through water absorption and tensile strength tests, respectively.

Chapter 5 deals with jute fiber composite mortar preparation, using various combinations of fiber (30mm, 10mm and 5mm) lengths and fiber percentages (0.5%, 1.0%, 2.0% and 2.0%) with respect to the mortar mass. Later

mechanical behavior and insulation property of composite mortars have been evaluated, through flexural, compression and thermal conductivity tests.

Chapter 6 highlights further developments of the composite mortar preparation, based on the observations and results obtained in the previous chapter. Only 0.5% and 1.0% of fiber with respect to the mortar mass have been used for the preparing the composite mortar and particular attention was made on the amount of water used for the mortar mix. Here too the mechanical behavior and insulation property of composite mortars have been evaluated, through flexural, compression and thermal conductivity tests.

Chapter 7 explains the procedure of the jute net/textile fabrication, using the class 1mm jute threads. Further it highlights the criteria, characteristics and procedure followed for the hollow brick wall masonry upgrading using the jute fiber products: (i) jute diatons, (ii) jute net/textile and (ii) jute fiber composite mortar. Later the structural behavior and insulation capacity of the retrofitted masonry composite wall systems with various configurations were studied.

Chapter 8 shows the use scrap jute net fiber for the preparation of recycled jute net fiber composite mortar. The mechanical behavior and insulation property of this recycled composite mortars have been evaluated, through flexural, compression and thermal conductivity tests.

Chapter 9 reports the results of Digital Image Correlation (DIC) procedures intended at analyzing the crack/opening in the prismatic samples and masonry wall specimens after failure.

Chapter 10 presents the carbon-footprint analysis of the masonry wall upgrading with jute fiber products.

Chapter 11 points out the main conclusions of the present research and subsequently figures out some possible future developments.

2. State of Art Review

This chapter presents a State-of-the-Art review of all known techniques, for retrofitting and upgrading of masonry structures. There are many techniques which are in use for the retrofitting and upgrading purpose (structural and/or thermal) of the entire building and/or individual element(s), based on various standards adopted in various countries.

The majority of the buildings around the world have been constructed without following any anti-seismic standard, and/or these buildings too are not always energy efficient. While the natural disasters, notably, the earthquake is responsible for causing major damages, to the masonry structures and buildings (Chuang et al. 2005).

In Italy, there are about 7 million masonry buildings (Pittau et al. 2017) and according to the Italian Institute of Statistics, around 57% of the total residential buildings are masonry buildings (Formisano et al.2019) out of which almost 90 % of these are constructed before nineties (Mistretta et al. 2019).

As highlighted in Ferrara et al. (2020), the improvement in seismic capacity of a building can be achieved through the reduction of the ultimate effect of the earthquake force, and with the upgrading against the earthquake load.

The optimization of buildings earthquake force resistance can be achieved by installing of base isolation and/or damper devices. Thus, these mechanisms can optimize the structural dynamic behavior. while the earthquake loads on masonry walls could be countered with upgrading of the individual elements, like (a) Confinement techniques (with new strengthened concrete column) and (b) Jacketing techniques (like FRP, steel rings, strengthened concrete etc.) (Ferrara et al. 2020, Chuang et al. 2005).

The studies on the natural (plant and animal) fiber composite mortars or materials are gaining interest rapidly with the aim to be used as newer, smarter and greener building materials, most commonly the thermal and/or the mechanical behaviors of the same have been studied.

The carbon, basalt and steel fiber-based textiles are commonly used as commercial Textile Strengthened Masonry (TRM) composite for retrofitting or upgrading purpose. While the plant fiber-based textile TRM composite systems have studied by Ferrara et al. (2020) for flex fiber and by Menna et al. (2015) for hemp fiber, and in both cases promising results have been obtained. As cited by Ferrara et al. (2020), although the plant fibers have great potential, but still lack in structural applications due to the limited availability of tested and reliable data on their (for plant-based fibers) mechanical performance.

On the other hand Each and every building, in its complete life cycle, directly or indirectly consume a huge amount of energy and at the same time emit a significant amount of CO_2, therefore they are responsible for damaging the environment and eco-system, and also somehow harm the human health. Table 2-1 represents total energy consumption and CO_2 emission by the building sector.

Table 2-1. Out of total energy consumption and CO_2 emission.

	Energy consumption	CO_2 emission
Global (Benzar et al. 2020)	36%	39%
European Union (EC. 2019)	40% (Out of which 50% used for heating and cooling (Pohoryles et al. 2020)	36%

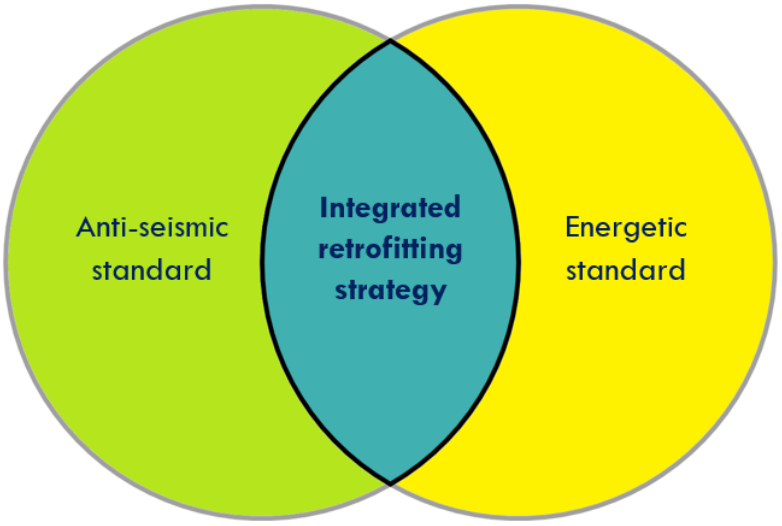

Fig. 2-1. Integrated retrofitting or upgradtion scheme (Self)

Notably the European Union (EU) aims to (i) reduce the greenhouse gas emissions of 40% (from 1990 levels), (ii) have the renewable energy production share of 32%, and (iii) improve the efficient use of energy of 32.5% by 2030 as stated in the Paris agreement (UNFCCC V. 2015, EC 2030 C&E framework).

To accomplish these goals, integrated retrofitting or upgrading techniques and strategies (as represented Fig. 2-1), and the use of fibers and its products, composite material(s) for thermo-structural retrofitting or upgrading could be game changers, considering cost effectiveness and sustainability.

During this PhD research work, priority has been given to the jute fiber due to its low cost and high abundancy, as well as for its competitive strength and thermal conductivity (i.e., insulation property).

The mechanical behaviors and thermal priority of the jute fiber composite mortar rarely have been studied deeply and simultaneously. Similarly, very few information is available in the literature on jute fiber textile TRM composite systems application.

Moreover, this is absolutely the first research work, in which the hollow brick masonry walls have been strengthened with jute textile (TRM composite) & jute fiber diatons (made of jute fibers) and jute fiber composite mortars for integrated (i.e., structural and thermal) masonry wall upgrading.

This chapter presents a state of art review of the literatures particularly deal with the classification of various masonry retrofitting and upgrading techniques.

2.1 Fiber classifications and use of fiber-strengthened composites for masonry retrofitting or upgrading

Composite systems are mainly composed of two main components: fibers and mortar. The fibers are mainly categorized into natural and man-made fibers. Fig. 2-2 elaborated based on Amaral et al. 2018, Deopura and Padaki 2015, Barbosa et al. 2004, Saba et al. 2014, Saleem et al. 2020 and Ferrara et al. 2020, and presents a comprehensive idea of the natural and man-made fibers and their sub-categories.

Fibers in the construction in building application are known to used either in raw or fabrics forms. In the fiber composite production process, the raw fibers are generally chopped into desired sizes. Application of fibers in textile forms with various patterns of mesh configurations are also in use. Whereas, hybrid fabrics are prepared, by using one or more kinds of fiber.

The man-made organic and mineral fibers are fabricated using metals, carbon, glass and basalt etc. and due to their known good structural performances, they are prioritized for retrofitting or upgrading purpose. The man-made fibers very often found to be applied in various forms in composite systems, such as Fiber-Strengthened Polymer (FRP) and Textile Strengthened Mortar (TRM).

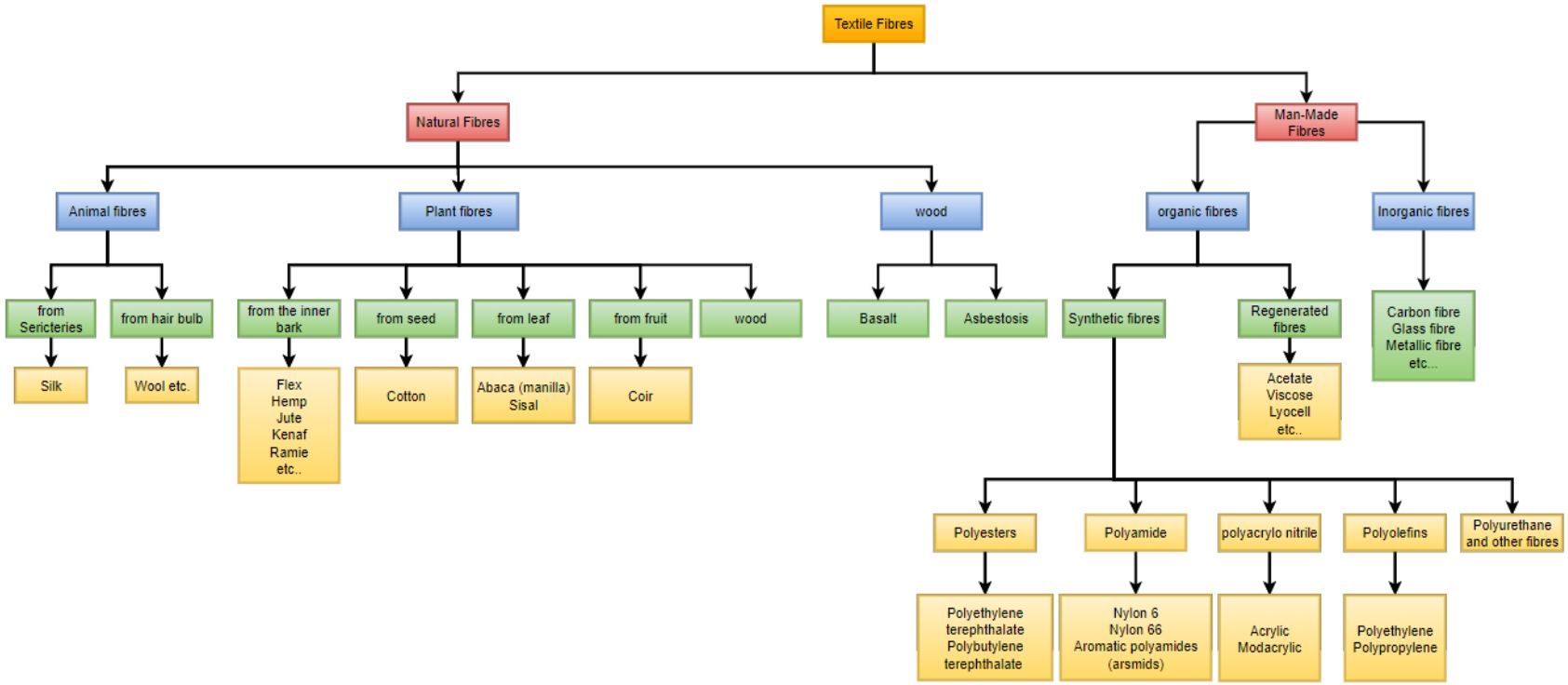

Fig. 2-2. Classification of fibers

As highlighted by Kim et al. (2020) Natural Fiber Composites (NFCs) are composite materials composed of reinforcing fibers, which come from renewable and CO2 neutral resources.

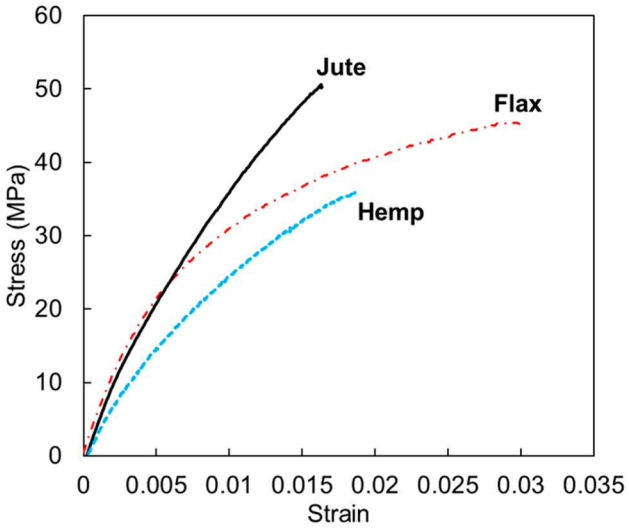

(a): Nature fibers.

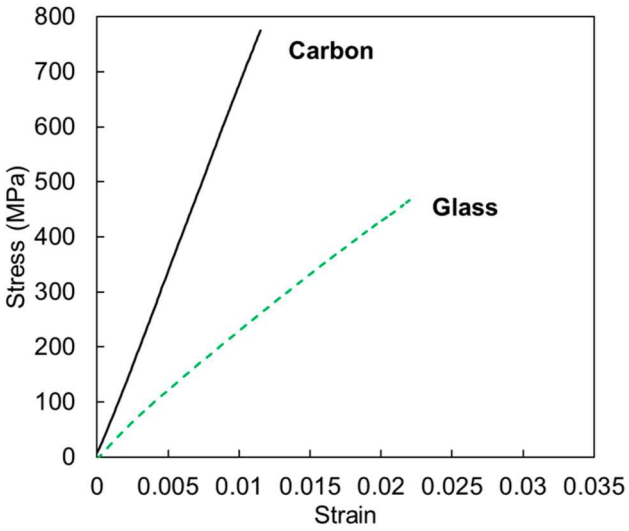

(b): Man-made fibers.

Fig. 2-3. Fibers composite laminate (Bambach 2020).

The use of plants and animal fibers are becoming more and more acceptable for the sustainable retrofitting or upgrading purposes of the buildings. Due to their competitive thermo-mechanical behavior, cheap availability, biodegradability and recyclability, these fibers and the composites made of them are becoming a focal point of the sustainable building material research and development.

Bambach (2020) compared the natural and man-made fibers in terms of stress-strain relation. It is clearly noticeable that the plant fibers (jute, hemp and flax) have nonlinear behavior (Fig. 2-3.a), whereas man-made fibers (carbon and glass) tend to have linear behavior (Fig. 2-3.b).

2.1.1 Plant fibers

The plant fibers can be sub-divided into five categories based on their origin. Mainly the plant fibers come from the inner bark, from seed, from leaf, from fruit and their wood/stick/stalks, which can be seen in the Fig. 2-2.

Table 2-2. World production of vegetable (Plant) origin fibers (2018) (Townsend 2020)

Plant/vegetable origin	Production estimated (Metric ton)
Abaca	83000
Bast fibers, other	190000
Coir	970000
Cotton lint	26120000
Fiber crops not specified elsewhere	280000
Flex fiber and tow, ex scutching mill	310000
Hemp fiber and tow	70000
Jute, kenaf and allied fibers	2500000
Kapok fiber	96000
Ramie	100000
Sisal, henequen and similar hard fiber	210000
Total	30929000

As stated by Ferrara (2020), the plants fibers can be classified under wood and non-wood fibers. As reported in the Table 2-2, according to Townsend 2020

total vegetable (Plant) fiber produced globally in the year 2018 was around 30 (+) million tons.

2.1.1.1 Jute fiber

India, Bangladesh and China are the main jute producing countries (Arunavathi et al. 2016). Jute fiber commonly known as *pat* in local Bengali language, mainly concentrated around the Gangetic delta of India (West Bengal) and Bangladesh. Due to its yellowish color, popularly also it is known as golden fiber.

In last 57 years jute fiber production increased by 1 million tons. Notably around 6 million households engage with jute fiber production and the value of the jute fiber production is around 1.2 billion dollar (Townsend 2020).

The jute plant cultivation needs warm and humid climate conditions as highlighted in the Table 2-3.

Table 2-3. Ideal condition for jute cultivation. (Townsend 2020).

Rainfall (weekly) [mm]	Humidity [%]	Temperature [°C]
150-200	70	25-30

Table 2-4 Chemical compositions of jute fiber (Yan et al. 2016)

Cellulosic fiber	Cellulose [%]	Hemi-cellulose [%]	Lignin [%]	Pectin [%]	Wax [%]
Jute	67.0	16.0	9.0	0.2	0.5

Jute come under *corchorus* species and belongs to *malvaceae* family (Islam et al. 2017). Although there are 100 plus corchorus species only two *corchorus olitorius* (also known as *tossa*) and *corchorus capsularis* (also known as *white jute*) are cultivated for commercial purposes (Islam et al. 2017, Mohanty et al 1995).

Jute fiber derives from the middle of the bark and stick (Mohanty et al 1995). Notably it holds nearabout 80% of the total global bast fiber production

(Islam et al. 2017). Due to partial presence of textile fiber and wood fiber, jute fiber is also stated as lignocellulosic fiber (Chand et al. 2020).

The chemical composition of the jute fiber can be found in the Table 2-4. Fig. 2-4. presents the different constitutive elements of the jute fiber, notably three prime constituents are cellulose, hemicellulose and lignin (Shahriar et al. 2018, Yan et al. 2016), whereas other elements also like waxes, pectin, protein, nitrogenous compounds (Ashraf et al. 2019).

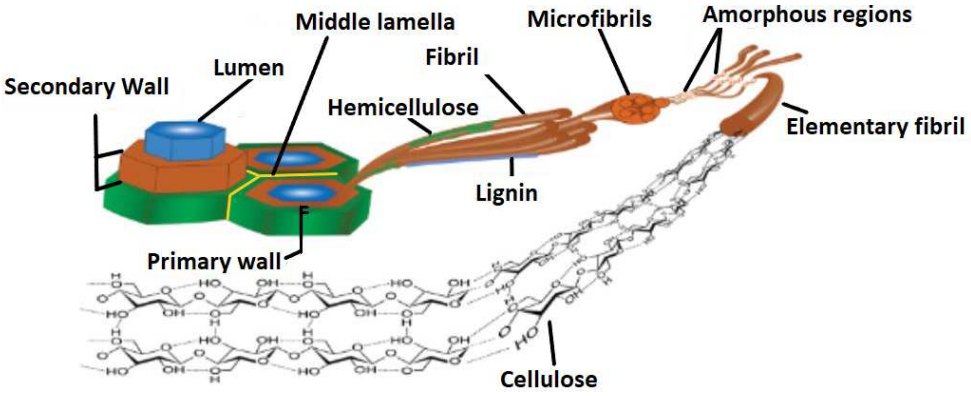

Fig. 2-4. Cross section of the jute filament and microstructure (Shahriar et al. 2018)

It is evident that the cellulose occupies and constitute more than fifty percent of the total jute fiber structural components (Yan et al. 2016) and the amount of cellulose determine the strength, stiffness and stability (Ferrara et al. 2021).

Notably due to the presence of lower percentage of wax in jute fiber structure, it considered to be a harsh and rough fiber (Yan et al.2016).

Normally very fine micro-fibrils combine to form the jute fiber cell and it is composed of thin primary and thick secondary wall (Gopinath et al. 2014).

Jute fiber can absorb water due to the presence of lumen (Ferrara et al. 2020), the physical properties of the jute fiber are presented in the Table 2-5, which includes the moisture up-taking amount.

Table 2-5. Physical properties of jute fiber (Yan et al. 2016)

Cellulosic fiber	Diameter [μm]	Length [mm]	Density [kg/m^3]	Moisture gain [%]	Micro-fibril angle [degree]
Jute	20.0-200.0	2.6	1400.0	17.0	8.1

Like all natural fibers, jute fibers too inherents some advantages as well as some disadvantages as underlined by Shahriar et al. (2018) and Antov et al. (2017), and highlighted in the Table 2-6.

Table 2-6. Jute fiber usable and negative properties.

Pros	Cons
High tensile strength	Hydrophobic
High tensile modulus	brittleness
Low elongation break	Poor drapability
Biodegradability	Subjected to microbe attack at humid-condition
Recyclability	
Lower density	
Lower risk to human and nature	

2.2 Classification retrofitting or upgrading techniques for masonry buildings

Structural retrofitting or upgrading mainly aim to protect masonry structures and buildings from external loads, considering their vulnerability to the seismic actions.

As highlighted in Ferretti (2019), the buildings or the structures' characteristics and location of the same, influence in choosing the correct strengthening method and right strategies to improving ductility or strength (or a balance approach), and also this selection is based on the on the available budget for this purpose (Fig. 2-5).

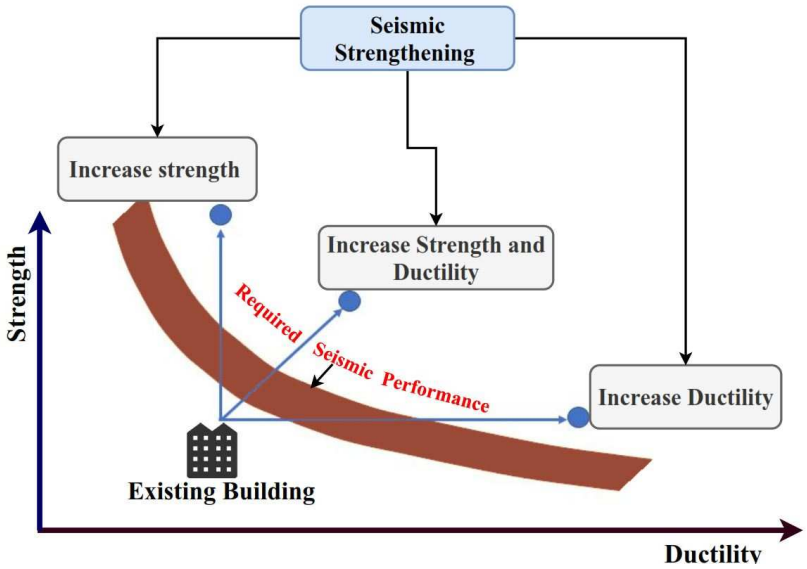

Fig. 2-5. Strategies for seismic retrofitting and upgrading (Ferretti 2019).

Masonry retrofitting or upgrading can be classified according to different reinforcement scheme and can be categorized based on the following criteria:

1) Different retrofitting or upgrading techniques.
2) Type of fibers used.
3) Purpose of the retrofitting or upgrading, enhancing structural or thermal performance.

2.2.1 Retrofitting or upgrading Techniques

2.2.1.1 Strengthened Mortar (with natural and man-made fibers)

Mortar is a mixture of a binder (either cement- or lime-based), fine aggregates and water, mainly used to bond masonry or other structural units. While in case of strengthened mortars, some reinforcing agent like fibers are also added in the mixture, with the aim to enhance the thermos-structural properties of the material. Different types of natural fibers derive from the plant and animal sources which have been used for retrofitting purposes can found literature.

Fig. 2-6 presents oil palm waste from a mill in Malaysia, and these wastes known for creating huge environmental problem. Therefore, to mitigate this problem (Raut et al. 2016) considered the possibility to re-use the industrial residuals like oil palm and fly ash as a binder along with cement. While the oil palm fiber has been used as strengthening material.

Fig. 2-6. Oil palm waste at Kian Hoe Plantation Mill, Malaysia (Raut et al. 2016).

Benmansour et al (2014) have mixed palm fibers (two different sizes as in Fig. 2-7) with cement and sand, of various proportions, with the aim to formulate a new building insulating material. The thermo-mechanical behaviors of these samples have been assessed by the authors.

(a): 6mm (b): 3mm

Fig. 2-7. Date palm wood fiber of two different sizes (Benmansour et al 2014).

Fig. 2-8 represents hemp fibers and hemp shives, these hemp plant products have been used by Formisano et al. (2017) to prepared mortars and bricks, respectively.

(a): Fiber (b): Shives

Fig. 2-8. Hemp products (Formisano et al. 2017).

Later, in another study, Formisano et al. (2019) have studied the usability of jute fibers along with lime mortar.

Recently Ferrandez-García et al. (2020) have fabricated cement based panels by using recycle jute fibers from jute bags, potato starch and Portland cement.

Valenza et al. (2015) fabricated cement matrix using the scrap sheep wool (from Sicily) at various percentages, and the thermal insulation and the mechanical properties the samples were studied. For these composite mixtures authors have used three different sizes of washed and un-washed sheep wool, as in Fig. 2-9.

(a): 20mm (b): 6mm (c): 1mm

Fig. 2-9. Sheep wool three different fiber lengths (Valenza et al. 2015).

Fig. 2-10. Carbon fiber-mortar mix (Babaeidarabad et al 2014).

Babaeidarabad et al (2014) have formulated carbon-mortar cementitious element to retrofit six un-strengthened masonry clay brick walls, using TRM technique (Fig. 2-10).

The mortars also can be applied as a plaster layer. While the plaster is a composite material in which commonly clay, cement, lime, gypsum etc. are mixed with water and in addition sand or other reinforcing materials (like fibers).

In the literature the use of plaster can be found both as structural and thermal retrofitting agent, for masonry retrofitting or upgrading.

While Aizi et al. (2020) also have developed a composite plaster reinforcement material using gypsum and natural fiber retama monosperm (Fig. 2-11).

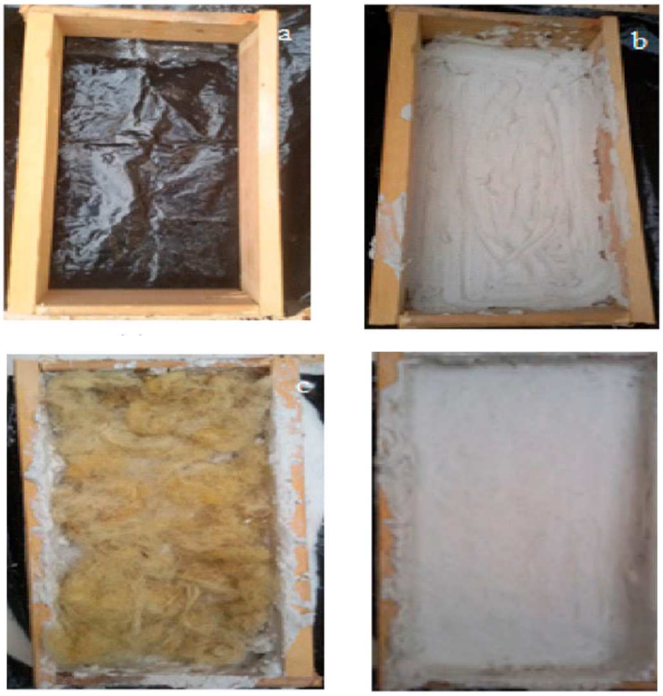

Fig. 2-11. preparation of composite plaster-fiber (Aizi et al 2020).

Liuzzi et al. (2017) prepared a bio-based plaster with clay, sand and olive pruning waste fibers (leaves and branches), and the product has proven to enhance the insulation capability.

Basaran et al. (2013) have prepared two types of strengthened plasters by using sand, Portland cement and fibers, whereas the authors have used the polypropylene and the steel fibers as additives for masonry structural reinforcement.

Furthermore, Mustafaraj et al. (2020) also have used polypropylene fiber, as in

Fig. 2-12 for the purpose of masonry reinforcement. It has to be noticed that the characteristics of materials strengthened with natural fibers directly depend on the size of the fiber as well as on the percentage/amount of the fiber used in the mixture.

Fig. 2-12. Polypropylene fiber (Mustafaraj ed at. 2020).

2.2.1.2 Ferrocement

Ferrocement is a mixture of cement mortar and reinforcement elements, without any coarse aggregate Sakthivel and Jagannathan (2011).

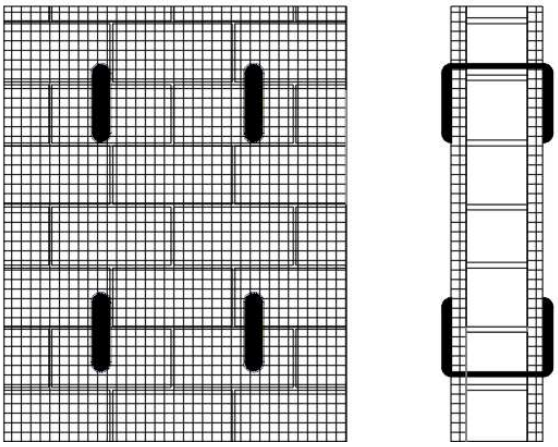

Fig. 2-13. Ferrocement retrofitting scheme (Wang et al 2018).

Fig. 2-13 presents a typical ferrocement retrofitting scheme in Wang et al (2018). The use of ferrocement found to be very common in the construction and building sector (Nedwell and Swamy 1994). When it is put on the structure surfaces for reinforcement or retrofitting purposes, it can significantly enhance both the in-plane and out-of-plane capacity (Lizundia et al. 1997), as well as lateral load capacity (Ashraf et al. 2012, Ali Shah et al. 2017).

2.2.1.3 Shotcrete Sprayed

Shotcrete is a technique in which concrete or mortar is directly sprayed on the structure (Warnar 1996) and for shotcrete reinforcements usually mesh and bars are used (Shabdin et al. 2018). Some advantages of this process, as mentioned by Warnar (1996) can be highlighted as it enhances the structures strength capacity and in addition it helps in dissipating the seismic energy (Shabdin et al. 2018). In some cases, the filler or binding materials like hemp fibers (Yun et al. 2019) and Silica-Fume (US Army 1993) can be used in the shotcrete spraying mixture.

Fig. 2-14. Shotcrete spraying process (Wang et al 2018).

While Banthin (2019) also has reported that there are mainly two processes for the shotcrete reinforcement, (i) the wet-process and the (ii) the dry-process. In the former case, shotcrete is ready to use as a concrete mixture, while in the latter case the water is added separately along with the bone-dry cementitious mixture.

Elgawady et al. (2006) have retrofitted both sides of a masonry wall using shotcrete process, in Fig. 2-14 presents the process.

2.2.1.4 Application of fiber net

A quite common approach can be found for masonry retrofitting is the application of a reinforcing net on the external wall surfaces. This net could be the open fabrics made of various kinds of fiber roving, as mentioned in Oskouei (2018).

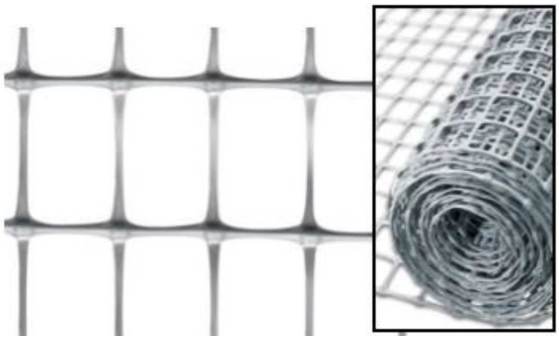

Fig. 2-15. Polypropylene net (Mustafaraj ed at. 2020).

Mustafaraj ed at. (2020) mentioned to have used the polypropylene net (as in Fig. 2-15) for masonry panels reinforcement.

Papanicolaou et al. (2011) have used bitumen-coated polyester fiber net (Fig. 2-16.a) and Polypropylene net (Fig. 2-16.b) for masonry retrofitting.

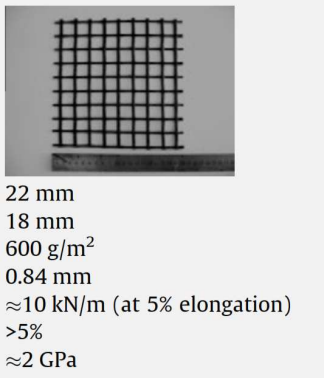

(a): Bitumen-coated polyester fiber net *(b): Polypropylene net*

Fig. 2-16. Fiber nets (Papanicolaou et al. 2011).

2.2.1.5 Grout and epoxy injection

Grouting is a process where any filler materials is injected into the structural element that need to be retrofitted or upgraded. The injecting materials mainly used are cement (Vintzileou and Tassios 1995) and lime-based mortar (Almeida et al. 2012).

As stated by (Isfeld et al. 2016), through this process the masonry walls can be retrofitted and restored, keeping originality of the wall and improving the structural performance.

Vintzileou et al (2015) have used the grouting process for retrofitting a masonry building with natural hydraulic lime-based grout.

Fig. 2-17 shows the installation of the grout through rubber tubes in the wall (Christou and Elliotis 2016).

Fig. 2-17. Grouting (Christou and Elliotis 2016).

2.2.1.6 The insertion of a Reinforced Concrete (RC)

As reported in Mistretta et al. (2019), the improvement in seismic energy dissipation capacity and ductility of the structure can be also achieved through Strengthened Concrete (RC) frames insertion.

2.2.1.7 Horizontal connectors (Diatons)

Horizontal-connectors, sometimes nominated as transversal connectors or diatons and these are the structural elements inserted orthogonally into the masonry wall to connect its two external surfaces and this is done to strongly

improve the shear resistance. Traditionally, various types of horizontal connectors made of timber, bamboo, reed and stones, which have been used all around the world as highlighted by Ortega et al. (2017).

Fig. 2-18 presents different kinds of transversal connectors have been used to improve the strength of the Multi-Leaf Masonry (MLM) specimens Cascardi et al. (2020).

For modern masonry buildings, more advanced transversal reinforcement elements or diatons are also used (Mistretta et al. 2019). They are made of two plastic anchoring parts that hold a fiber mesh or a combination of stainless-steel micro cords and plastic mesh, as can be seen in Fig. 2-19. In addition, a specific liquid mortar has been injected inside the mesh in order to create a real strengthened mortar transversal beam (Fig. 2-20).

(a): Stone transversal

(b): Glass L-shape

(c):Glass rope connector

(d): Steel rope

(e): Steel helical bar.

Fig. 2-18. Various types of transversal connectors (Cascardi et al. 2020).

Fig. 2-19. Transversal diaton.

Fig. 2-20. Mortar injection in the diatons cavity.

Mustafaraj et al. (2020) have created the transversal connectors by wrapping the fiberglass around the GFRP bar, as in Fig. 2-21.

Fig. 2-21. GFRP bar and fiberglass sheet wrapped to use as horizontal connector (Mustafaraj et al. 2020).

As stated by Siddiqui et al. 1996, these horizontal connectors improve the out-of-plane bending and in-plane shear resistance. In case of the application of a fiber net reinforcement (for example FRP, TRM), this type of connector as in is very important because it influence the stability of the wall and helps to grip the fiber mesh on the two external sides.

2.2.1.8 Strengthened Mortar (RM) with Metallic Cross Strips

Dong et al. (2019) have retrofitted Un-Strengthened Masonry (URM) walls with mortar and cross steel bars that are placed diagonally (Fig. 2-22).

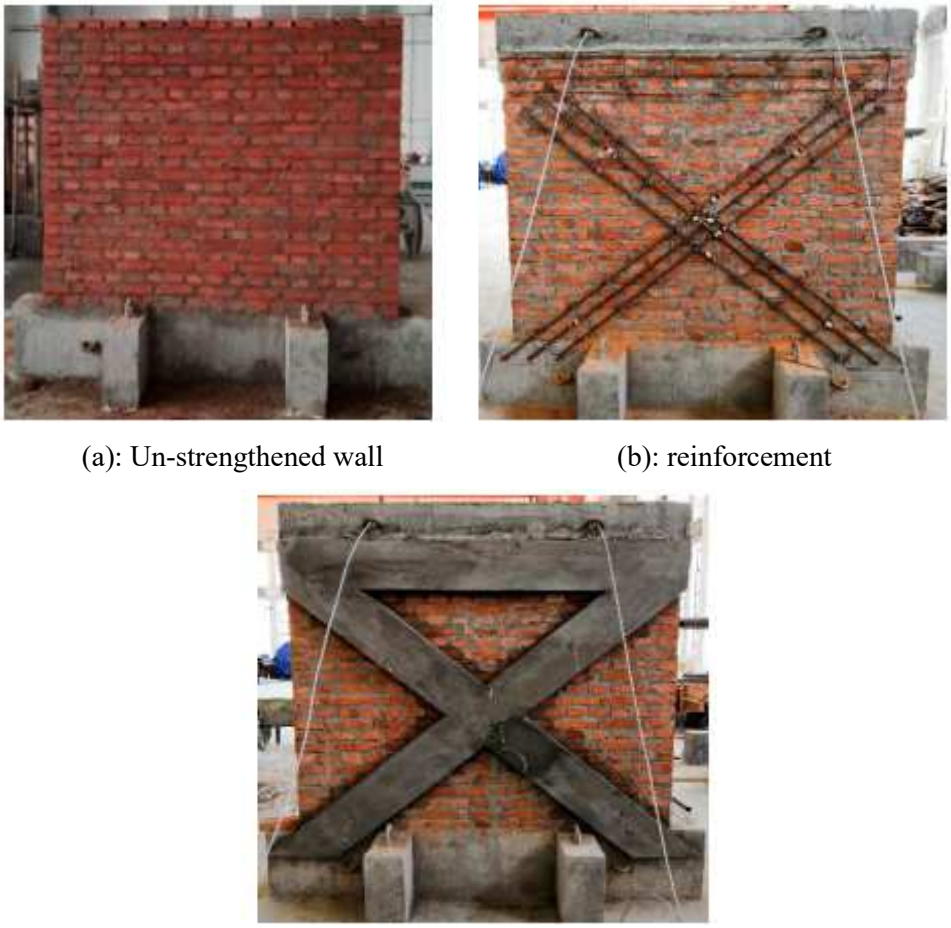

(a): Un-strengthened wall (b): reinforcement

(c): strengthened wall

Fig. 2-22. Reinforcement construction process (Dong et al. 2019).

Single and double-faced URM walls were strengthened and tested applying low-cyclic load keeping the vertical load constant. An increase of around 38.2% was observed in terms of shear capacity.

2.2.1.9 Textile strengthened mortar (TRM) composite systems

The textile strengthened mortar (TRM) is obtained by embedding fiber textile (Fig 2-23) inside an inorganic matrix.

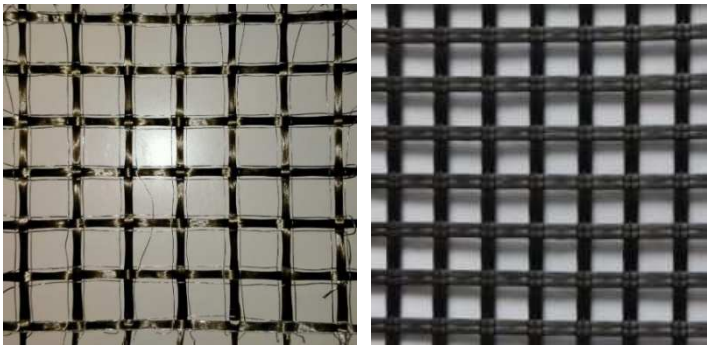

(a): Basalt fabric (b): Carbon fabric

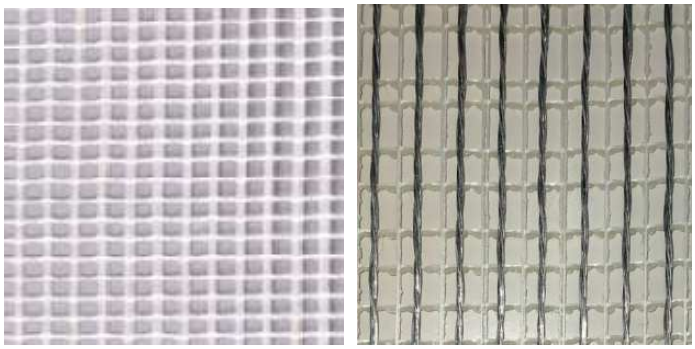

(c): Glass fabric (d): Metal (steel) fabric

Fig. 2-23. Fibers in textile form.

TRM is sometimes referred also as Fabric-Strengthened Cementitious Matrix (FRCM) or Textile-Strengthened Concrete (TRC) as stated by Kouris and Triantafillou (2018). It is usually applied on existing masonry structures to improve

their mechanical characteristics. Notably many examples of this technique can be found in the literature.

Basalt fibric TRM

Fig. 2-24 presents a typical use of Basalt fiber mesh, for masonry wall retrofitting. This picture has been taken during masonry wall retrofitting process at the University of Cagliari, Italy.

Fig. 2-24. TRM retrofitting.

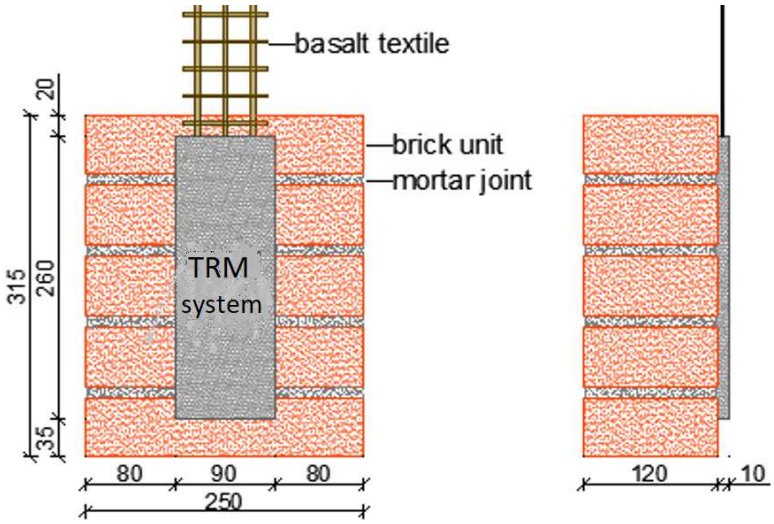

Fig. 2-25. Specimens' geometry (measures in mm) (Ferrara et. Al. 2019).

Ferrara et. Al. (2019) have conducted shear-bond tests (Fig. 2-25) to analyze the adhesion between BTRM and brick masonry. For retrofitting purpose, three types of basalt textile of different patters (Fig 2.26) were chosen for retrofitting purpose.

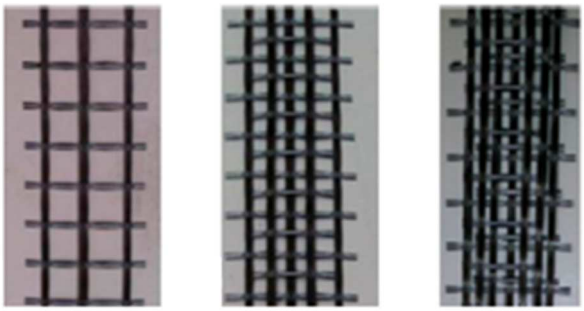

Fig. 2-26. Basalt textile configuration arrangements (Ferrara et. Al. 2019).

In Barducci et al (2019), Fiber-Reinforcement Cementitious Matrix (FRCM) is applied on a brick substrate. The composites were prepared using basalt textile fiber coupled with four different mortar matrices.

Fig. 2-27. BFRCM reinforcement (Fossetti and Minafò 2016).

Fossetti and Minafò (2016) have strengthened brick masonry column with Basalt Fiber–Strengthened Cementitious Matrix (BFRCM). During this process steel wire collaring with two different types of mortar have been used. One of the mortars

was prepared with hydraulic lime and sand, while other with Portland cement, hydraulic lime and sand (Fig. 2-27).

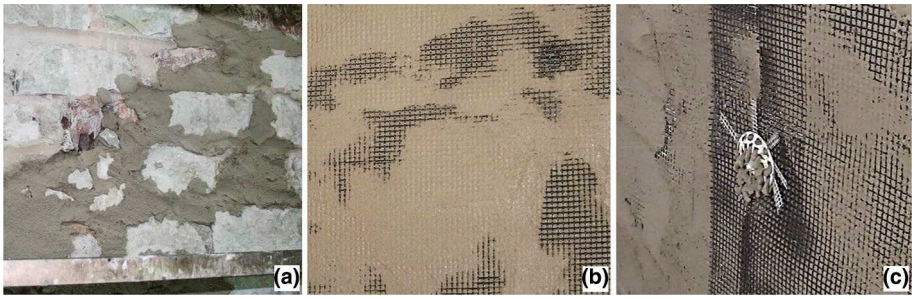

(a): repointing of the crushed joints *(b): Installation of the basalt mesh* *(c): Steel connector and grout injection*

Fig. 2-28. Retrofitting of the stone wall with BTRM (De Santis et al 2019).

De Santis et al (2019) repaired an un-strengthened stone wall after the out-of-plane test. Specifically, the damaged wall was retrofitted on both sides the bidirectional basalt mesh, transversal connectors and lime-based mortar (Fig. 2-28), thereafter these walls were tested again.

Steel fibric TRM

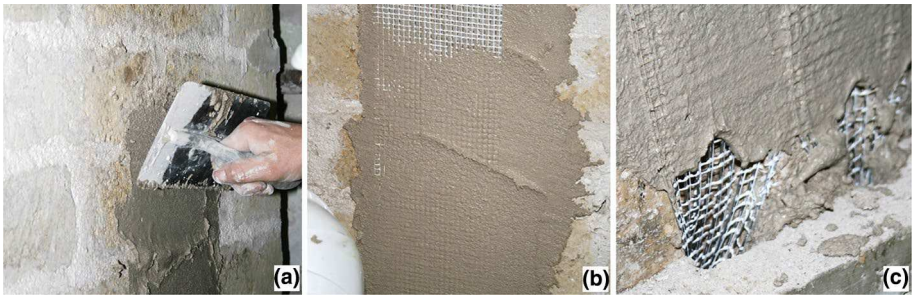

(a): laying of the first mortar layer *(b): Installation of the steel textile* *(c): Steel connector and grout injection*

Fig. 2-29. Retrofitting of the tuff wall with SRG De Santis et al (2019).

Same as above, in De Santis et al (2019) have tested the un-strengthened tuff wall, the damaged wall then repaired and retrofitted on both sides with Steel

Strengthened Grout (SRG). Therefore, a unidirectional Ultra High Tensile Strength Steel (UHTSS) textile, steel connectors and lime-based mortar have been used for the purpose, (Fig. 2-29). After reinforcement the wall was subject to out-of-plane test.

Carbon fabric TRM

Faella et al (2010) utilized the fiber-strengthened cement mortar technique to retrofitted tuff brick walls with carbon fiber mesh. The carbon fiber mesh placed within two layers of mortar, as in Fig. 2-30.

(a): Un-strengthened wall *(b): Strengthened wall*

Fig. 2-30. Tuff brick wall (Faella et al 2010).

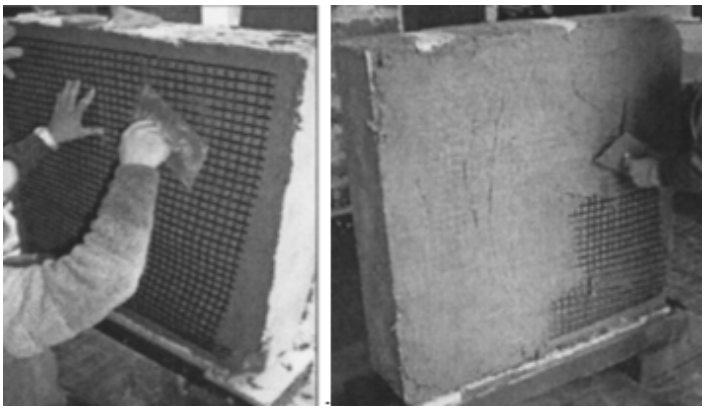

(a): grid installation *(b): troweling of final mortar layer*

Fig. 2-31. Tuff masonry walls were retrofitted (Prota et al 2006).

Fig. 2-31 presents tuff masonry walls retrofitted with a Cement-based Matrix-coated alkali resistant Glass grid system (CMG + TMR) as reported by Prota et al (2006). During the experiment different combination of innovative Cementitious Matrix–Grid CMG are created and applied on one or both sides of the tuff masonry wall.

(a): first layer of mortar *(b): precut carbon fabric* *(c): second layer of mortar*

Fig. 2-32. FRCM installation (Babaeidarabad et al 2014).

(a) Application of a layer of spray mortar *(b) Embedding the carbon mesh* *(c) Application of another layer of spray mortar.*

Fig. 2-33 carbon mesh and spring mortar (Bischof and Suter 2014)

Babaeidarabad et al (2014) have used layers of Fiber-Strengthened Cementitious Matrix FRCM with carbon-mortar cementitious mortar as in Fig. 2-32, to retrofit six un-strengthened masonry clay brick walls.

To achieve the static and seismic retrofitting of masonry wall, as can be seen in Fig. 2-33 Bischof and Suter (2014) have sprayed a mortar mixture on single and applied bidirectional coated carbon mesh strips. They have used four different types of retrofitting strategies as in Fig. 2-34.

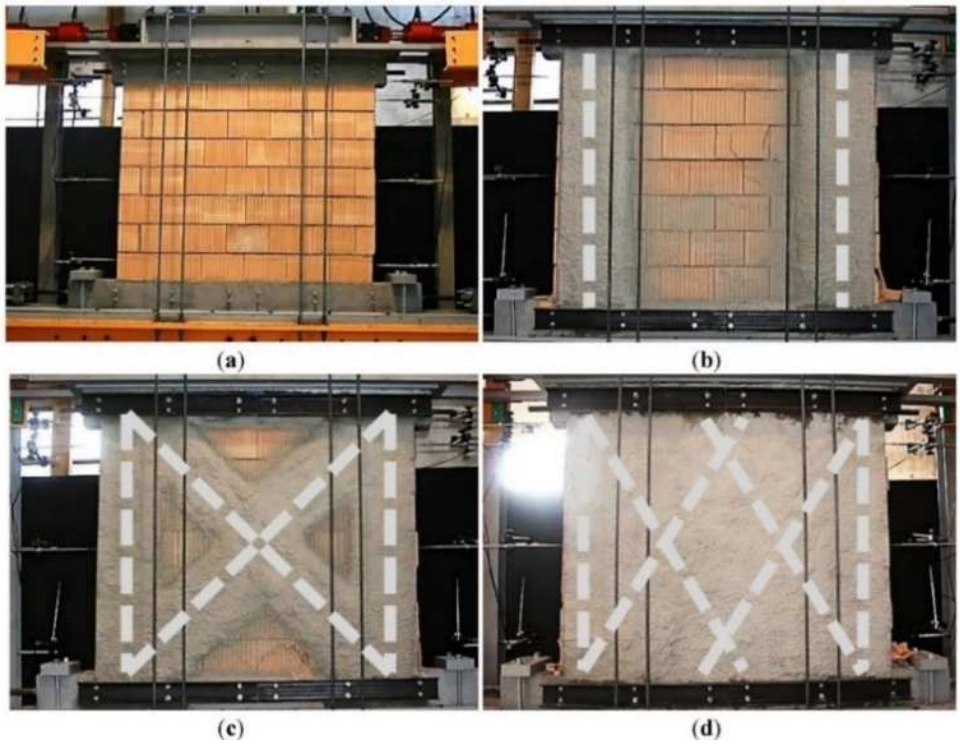

Fig. 2-34. Different pattern of application of carbon mesh for retrofitting masonry walls (Bischof and Suter 2014).

Glass fabric TRM

Akhoundi et al (2018a) and Akhoundi et al (2018b) have used textile glass fiber meshes embedded in mortar to retrofit the brick masonry infilled frames.

Bernat et al. (2013) have used Glass TRM and carbon TRM to strengthen, a total of five and three brick walls, respectively.

(a): Masonry wall with connectors *(b): TRM and connectors retrofitted wall*

Fig. 2-35. Masonry retrofitting (Bernat et al. 2013).

They have used two types of fiber grides with various combinations of single layer of glass fiber grid and Portland-based mortar, glass fiber grid and lime-based mortar and carbon fiber grid and pozzolan-based mortar, and they also have tested two wall samples, with double layered fiber grids embedded into lime-based and Portland-based mortars.

Other two sample walls are additionally retrofitted with six and nine fiber grid connectors. Also, connectors (rectangular shape) of same glass and carbon fiber specifications have been used enhance bonding between the TRM and masonry (Fig. 2-35).

Righetti et al. (2016) have used GFRP grids with two different dimensions along with lime based or cement based mortar, to reinforce the historically old masonry (Fig. 2-36). .

(a): 66x66 mm² *(b): 33x33 mm²*

Fig. 2-36. Two types of GFRP grids, (Righetti et al. 2016).

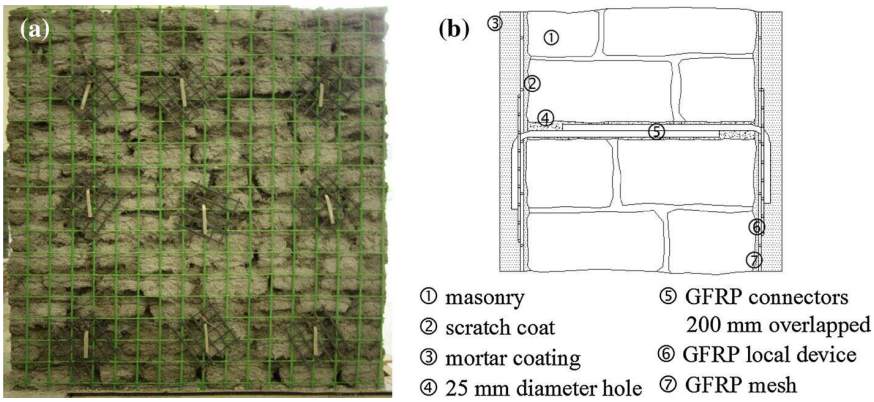

(a): GFRP mesh application *(b): Connectors application*

Fig. 2-37. Masonry wall retrofitted with hydraulic lime mortar (Gattesco et al. 2015).

Gattesco et al. (2015) used five types of GFRP mesh along with three different types of mortars (hydraulic lime) in various combinations, to retrofit four different types of masonry walls. The transversal and longitudinal fibers impregnated in resin have been crisscrossed to form the GFRP mesh. Fig. 2-37 presents the GFRP application on masonry wall.

Furtado et al. (2020) have retrofitted masonry walls made of hollow clay horizontal bricks, using polypropylene mesh and strong glass fiber mesh (GFRP) along with M5 class mortar for plastering, and also they have used steel connectors to anchor the textile mesh, as in Fig. 2-38 (c).

(a): Glass fiber *(b): Glass fiber application*

(c): Steel connectors

Fig. 2-38. GFRP retrofitting (Furtado et al. 2020).

Moreover, Papanicolaou et al. (2011) have retrofitted various masonry wall configurations (brick shear walls, beam-column type walls and beam type walls) using five different types of textiles (Carbon, Basalt, E-glass, Polyester fiber and Polypropylene net).

Natural (Plant based) fiber TRM

Recently use of Natural (mainly plant origin) fiber TRM (NTRM), particularly for masonry retrofitting is gaining momentum. Very rear but some interesting NTRM retrofitting examples can be found in literature.

Codispoti et al. (2015) have studied the mechanical performance of the natural fiber strengthened cementitious matrices (NFRCM). The authors have used jute Fig. 2-39.(a), Sisal Fig. 2-39.(b), hemp Fig. 2-39.(c) and flex Fig.

2-39.(d) fabric and inorganic nature mortar (prepared with pozzolana lime and natural siliceous with max. diameter of 2 mm). Fig. 2-39.(e) represents one of the NFRCM sample after tensile failure.

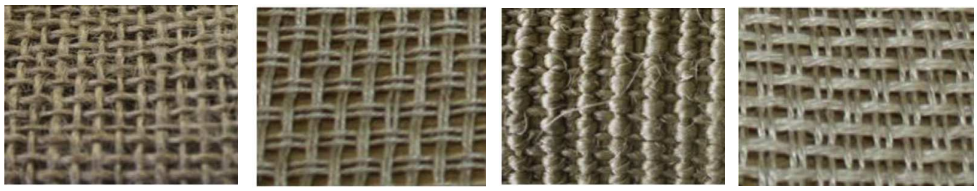

(a): Jute *(b): Sisal* *(c): Hemp* *(d): Flex*

(e): Tensile failure

Fig. 2-39. Some of the nature fiber fabric used and NFRCM sample (Codispoti et al. 2015).

As in Fig. 2-40., Meena et al. (2015) have used different combinations of Hemp Fiber Composite (HFC) and two different binding materials for retrofitting purposes, as tabled in Table 2-7. They also have used HFC ties/connectors. Later diagonal compression tests have been carried out.

Table 2-7. Hemp Fiber Composite (HFC) retrofitting scheme

	Natural hydraulic lime	Pozzolanic mortar
Yellow tuff brick	HFC	HFC
Solid clay brick	HFC	HFC

(a): Placement of one ply of HFC grid on each side of the panel

(b): Installation of the anchor system on each panel side.

Fig. 2-40. Hemp fiber TRM retrofitting (Meena et al. 2015).

Ferrara et al. (2020) have utilized flex textile for two combinations of Flex-TRM retrofitting. One of the masonry walls has been retrofitted with single textile layer (Fig. 2-41. b), while another wall was retrofitted with two textile layers (Fig. 2-41. c). Textile and mortar have been applied on both faces of the masonry walls. Structural behaviors were determined through the diagonal compression test.

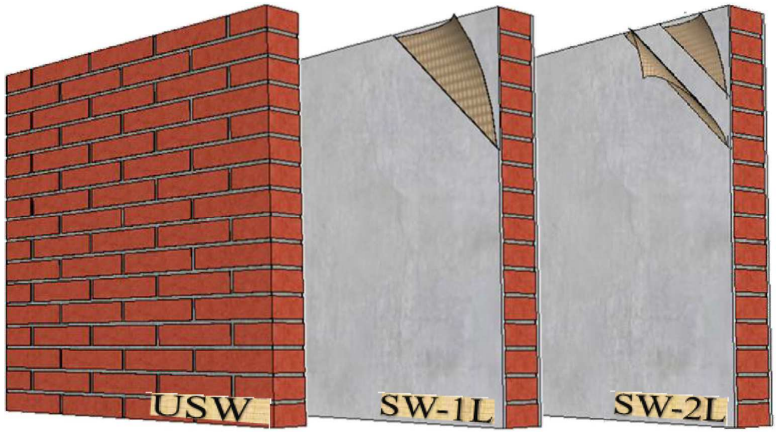

(a): Un-strengthened

(b): Strengthened with one textile panel

(c): Strengthened with two textile panels

Fig. 2-41. Flex fibric retrofitted masonry walls (Ferrara et al. 2020).

2.2.2 Fibers used for Masonry Retrofitting or upgrading: Fiber strengthened polymer (FRP)

Fiber-Strengthened Polymer (FRP), also sometimes represented as Fiber-Strengthened Plastics, is a composite system made of a polymer matrix strengthened with fibers, and notably they are rust proof and have high strength-to-weight and stiffness-to-weight ratios (Masuelli 2013).

All man-made or natural fiber strengthened with plastic or polymer matrix material can be defined as FRP, this is the nomenclature commonly known among the professionals.

Most commonly glass, carbon, or aramid are used, while other fibers like paper, wood and asbestos, also found to be used for this purpose. While the polymer used usually are epoxy, vinylester or polyester thermosetting plastic, and also phenol formaldehyde resins (Masuelli 2013).

The Glass Fiber Strengthened Polymer (GFRP), Basalt Fiber Strengthened Polymer (BFRP) and Carbon Fiber Strengthened Polymer (CFRP), represent the main FRP groups (see Fig. 2-42) and most commonly used for masonry retrofitting or upgrading.

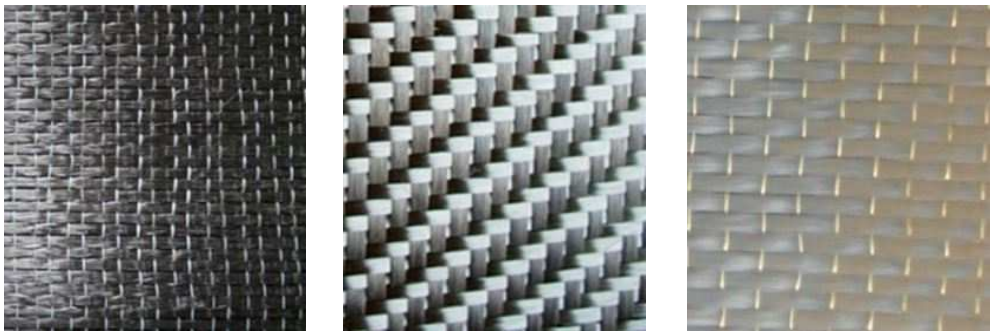

(a): Basalt Fiber sheet *(b): Carbon Fiber sheet* *(c): Glass Fiber sheet*

Fig. 2-42. Fiber Sheets (Zhao et al. 2017).

Considering its lightweight and strength, the FRP composites are widely used in civil engineering applications, both for newer constructions or for

retrofitting or upgrading the existing structures and buildings. Some interesting use of FRPs can be found in the literature, some notable applications are in bridges (Smits 2016), for underwater steel pipeline (Shamsuddoha ed al. 2013) and also for concrete and masonry structures (Buchan and Chen 2007).

The Fig. 2-43 presents the constitutive laws of different fibers (used in FRP form) in comparison with common steel used for rebars.

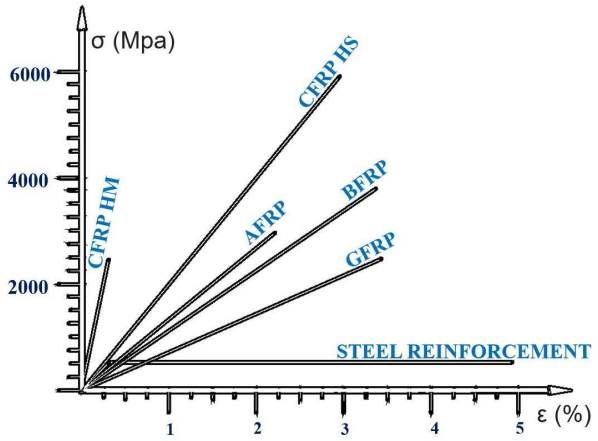

Fig. 2-43. Constitutive laws for different fibers (Sonnenschein et al. 2016).

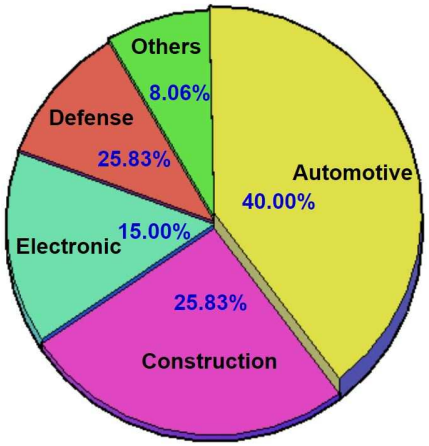

Fig. 2-44. Fiber Strengthened Polymer (FRP) composites global market, elaborated from (GVR 2017).

Industries which commonly use FRPs are the aerospace, automotive, marine, and construction industries (Masuelli 2013).

According to GVR (2017) the automotive industry is still the prime user of FRP. At the same time the application of FRPs in the construction sector also has gained quite a momentum, as can be seen in Fig. 2-44. Here to be noted that the values used in the chart are approximated.

2.2.2.1 Glass fiber strengthened polymer (GFRP) masonry retrofitting or retrofitting

Glass fiber, also known as fiberglass, is made of micro-fibers of glass combined with a plastic matrix (Masuelli 2013). The glass fibers can be categorized into short fiber particles, yarns and textiles.

As stated in Bakis et al. (2002) the glass fibers are predominantly used to prepare the early FRP's and the application of GFRP to masonry retrofitting is becoming quite common. The GFRP application requires first the surfaces smoothing, then the application of a primer epoxy coat. After this it is possible to apply the epoxy-saturated glass fabric. Then the glass fiber anchors are placed inside the predrilled holes in order to apply others Glass fabric layer.

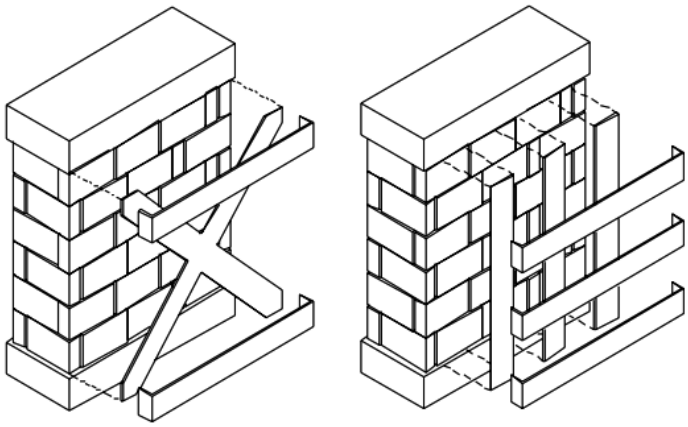

Fig. 2-45. U-wrap system for cross layout (left) and grid layout (right) (Marcari et al. 2007).

In Marcari et al. (2007), tuff masonry walls were prepared with historical mortar and retrofitted with GFRP by fixing on the walls with epoxy glue, following wet lay-up systems. Two types of FRP layout were used for retrofitting, as shown below in Fig. 2-45. The shear strength of the retrofitted masonry walls improved significantly. Tensile failure of GFPR strips was observed.

Sivaraja et al. (2013) have strengthened burnt clay brick masonry walls with GFRP externally, glued with epoxy resin (Fig. 2-46). The mechanical tensile and shear bond behavior of GFRP retrofitted walls have been studied and improvement have been observed.

Fig. 2-46. GFPR wrapped wall (Sivaraja et al. 2013)

Mahmood and Ingham (2011) have studied the solid clay brick masonry sample walls were retrofitted with externally bonded uniaxial and biaxial GFRP fabrics.

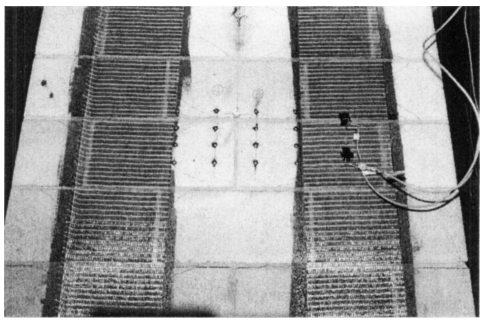

Fig. 2-47. Typical diagonal crack pattern in masonry (Kuzik et al. 2003).

Kuzik et al. (2003) have retrofitted eight concrete brick samples with different dimensions but of same type and characteristics of GFPR sheet, one example is presented in Fig. 2-47.

Silva et al. (2008) reported to have used polyurea and GFRP to retrofit the masonry walls (prepared with Portland cement-sand mortar.). Different GFRP grid strengthened polyurea layouts, in either vertical or horizontal direction and single- and double-sided layouts were used.

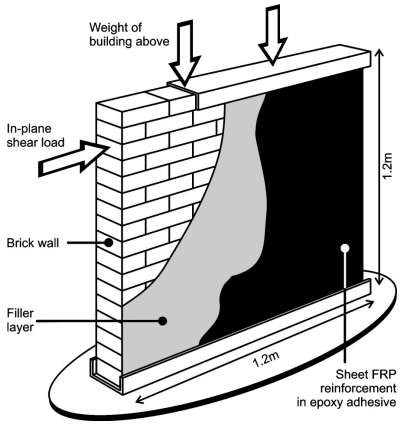

Fig. 2-48. In-plane shear strengthening (Stratford et al. 2004).

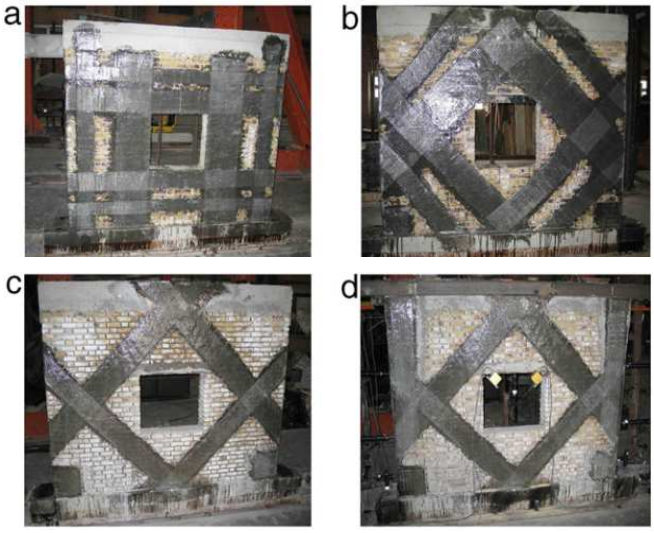

Fig. 2-49. Various schemes of the GFRP strengthened test specimens (Kalali and Kabir 2012).

Stratford et al. (2004) used the GFRP sheets to retrofit two different type of masonry walls, made of clay and concrete bricks. GFRP sheets are fixed on the surfaces with epoxy adhesive. Fig. 2-48 presents the schematic arrangement of glass-fiber strengthened polymer.

Kalali and Kabir (2012) have used GFRP and epoxy to retrofit a simulated Iranian style traditional wall constructed with solid clay bricks and cement mortar and both sides have been strengthened, as in Fig. 2-49.

2.2.2.2 Basalt fiber strengthened polymer (BFRP) masonry retrofitting or upgrading

Basalt fibers are produced out of a volcanic stone (Mahltig 2018). The physical performance and mechanical behavior of the basalt fiber are superior to that of glass fiber (Rajak et al 2019).

Zhou et al (2013) have tested eight (1) un-retrofitted solid clay bricks walls and (2) the failed masonry walls retrofitted walls with Basalt Fiber Strengthened Polymer (BFRP) to analyzing the mechanical performances pre and post the damage tests. The application BFRP have shown in increasing the ultimate shear strength and drift at the range of 44–61%, 203–265%, respectively. Fig. 2-50 represents a specimen with mixed strengthening configuration.

Fig. 2-50. BFRP retrofitting (Zhou et al 2013).

In Lei et al. (2014), BFRP was used to retrofit the RC-brick wall specimen (Fig. 2-51) with opening, and the in-plane mechanical behavior has been investigated. The BFRP was attached to the wall using TGJ FRP-special adhesive. As stated by the authors The use of BFRP composite materials can efficiently improve the energy dissipation capacity and bearing stability and postpones the rate of stiffness degradation, and also demonstrated higher maximum lateral strength and ultimate drift.

Fig. 2-51. BFRP-strengthened wall (Lei et al. 2014).

(a): Application of first layer of epoxy *(b): Placement of BFRP strip* *(c): Application second layer of epoxy*

Fig. 2-52. Finished specimen after application of to achieve full saturation of fibers (Padalu et al. 2019).

Padalu et al. (2019) have applied BFRP composite applied in various configurations (a total of eight) along with epoxy to retrofit un-strengthened masonry. A Bi-directional basalt fabric has been used for this purpose. They have used epoxy resin to fix the BFRP to reinforce masonry wall. In this case also, the authors have used bi-directional weaved fiber. Fig. 2-52 presents one of the masonry walls retrofitting process: the application of epoxy and placement of BFRP.

Tempesta (2018) conducted some on-site tests on wall samples inside a historical masonry building and based on these suggested to retrofit the building using BFRP and transversal element system, that provides grip to the basalt fiber strip and stability to the structure.

2.2.2.3 Carbon Fiber Strengthened Polymer (CFRP) masonry retrofitting or upgrading

Carbon fiber is an organic fiber with a 5-10 micrometers diameter. It is also known as graphite fiber when there is more than 99% of carbon (Masuelli 2013). It is a long chain of molecules tie together by carbon atoms (Bhatt and Goe 2017) and according to (Wu et al 2020) it can be fabricated by fibrillation of acrylic resin.

CFRP is light and strong (Masuelli 2013) and due its advantageous mechanical properties like high strength, excellent creep level, resistance to chemical effects, low conductivity, low density and high elastic modulus, it is suitable for reinforcement and retrofitting new as well as historical masonry buildings (Günaslan et al. 2014).

Carbon fiber was commercialized in 70's and due to higher cost, the CFRP was mainly used in the aviation industry until 1980, but currently given its comparative lower cost and its excellent mechanical performance, it is widely used also in the building construction sector (Mouritz 2012). In many civil-structural applications the use of CFPR, can be found in the literature.

Rahman and Ueda (2016) have used unidirectional CFRP fibers to retrofit masonry.

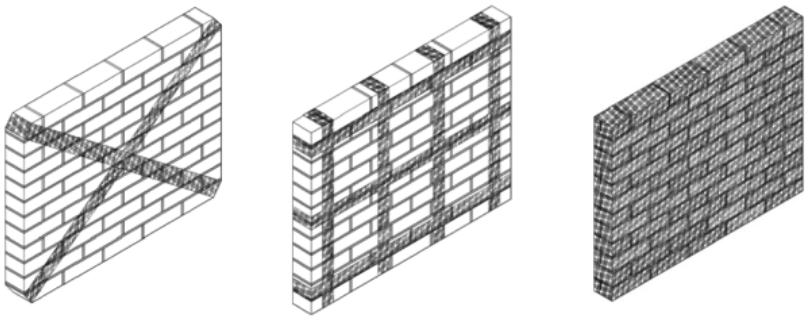

(a): cross-diagonal *(b): grid system* *(c): fully wrapped*

Fig. 2-53. CFRP and PET-FRP retrofitting configurations (Rahman and Ueda 2016).

They adopted a wet layup procedure where two-component epoxy resin is mixed, and a primer layer is first applied where the composite is to be bonded. Epoxy putty (filler) have been used to fill the cavities on the wall to have smoother surface for fiber application. Fiber strip was fully saturated using resin and thereafter applied on the wall. In-plane shear performance of a total of three retrofitted wall configurations (Fig. 2-53) have been tested. CFRPs increases the shear capacity but reduces ductility of the wall system.

Fig. 2-54. The masonry wall retrofitted on one side (Arifuzzaman and Saatcioglu 2012).

Arifuzzaman and Saatcioglu (2012) have conducted experiments on a masonry wall retrofitted with double layered epoxy bonded CFRP sheets (Fig. 2-54). The sheets were placed parallel and perpendicular to the bed joint and CFPR was placed on the masonry wall using the wet layup procedure. As highlighted by the authors under simulated seismic loading the overall wall behavior has improved, with improved shear capacity.

Fig. 2-55. The eight stone columns after installation of the CFRP wrapping through the columns (Hemeda 2018).

Fig. 2-56. Debonding of CFRP plate (Mahmood and Ingham 2011).

In Marcari et al. (2007), tuff masonry walls were prepared with historical mortar and retrofitted with GFRP by fixing on the walls with epoxy glue, following wet lay-up systems. Two types of FRP layout were used for retrofitting.

As mentioned by Hemeda (2018), the circular masonry stone columns (Fig. 2-55) can be structurally retrofitted against the seismic load using the CRPF laminates. The author reports on the cases of a historical church and other monuments strengthened in this way.

Mahmood and Ingham (2011) have used pultruded CFRP plates (Fig. 2-56) and near-surface mounted rectangular bars to retrofit solid clay brick masonry walls.

2.2.2.4 Polyethylene terephthalate fiber strengthened polymer (PET-FRP)

Rahman and Ueda (2016) have used unidirectional PET-FRP fibers to retrofit masonry. They adopted a wet layup procedure where two-component epoxy resin is mixed, and a primer layer is first applied where the composite is to be bonded. Epoxy putty (filler) have been used to fill the cavities on the wall to have smoother surface for fiber application. Fiber strip was fully saturated using resin and thereafter applied on the wall. In-plane shear performance of a total of three retrofitted wall configurations, exactly similar as Fig. 2-53 have been tested. As stated by (Rahman and Ueda 2016) PET-FRP has a better seismic performance than CFRP, as it shows a better ductile behavior than CFRP,

2.2.2.5 Natural fiber strengthened polymer (NFRP)

The natural fibers are extracted from both plants and animal sources. In the literature it is possible to find several applications of natural fibers retrofitting or upgrading that improve the structural and thermal insulation performance of masonry staructure. In recent years some studies have been done on the Natural FRPs (NFRP).

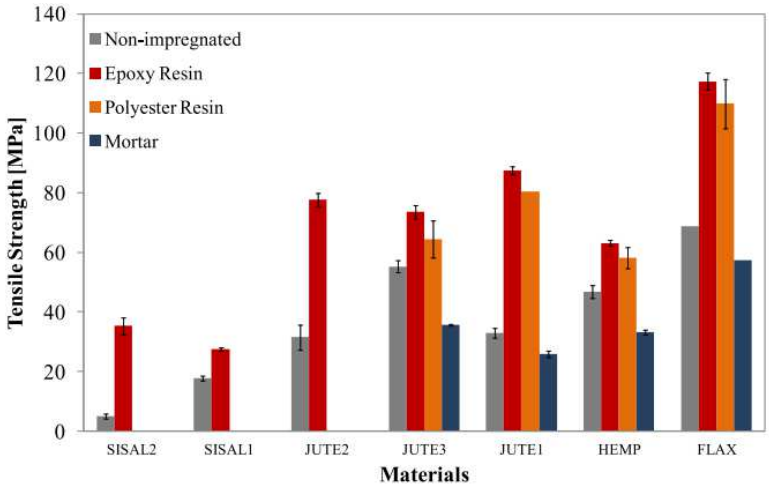

Fig. 2-57. Tensile strength of the fibers tested as a function of the matrix used (Codispoti 2015)

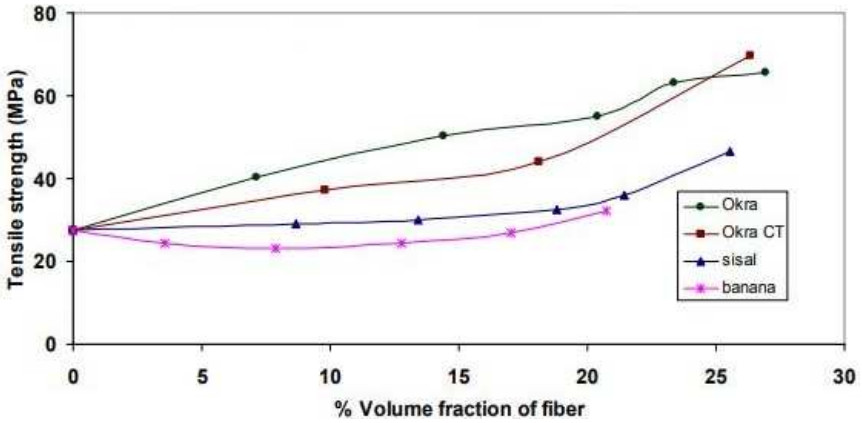

Fig. 2-58. Effect of % volume fraction of fiber with tensile strength (Srinivasababu et al. 2009).

Codispoti (2015) have developed a very extensive study to understand the mechanical performances of Natural Fiber Strengthened Polymers (NFRP), with the aim to strengthen masonry. The authors have chosen natural fibers like Jute, Sisal, Hemp and Flax. While, Epoxy resin, polyester resin (organic nature), cement-free mortar made with pozzolana lime and natural siliceous aggregate (inorganic nature) that are typically used for the matrix composites. The NFRP-epoxy and NFRP-polyester were manufactured for mechanical tests. The tensile

strengths of the tested fibers are reported in Fig. 2-57. Codispoti (2015) also have stated that Flax fiber is the most suitable for manufacturing (composite martials) and useful for structural strengthening (in terms of strength and stiffness). Fig. 2-57 Presents the obtained tensile for each non-impregnated and NFRP matrix.

Whereas, Srinivasababu et al. (2009) have studied the okra, sisal and banana fiber strengthened polyester composites. As stated by the authors, the chemically treated (CT) okra fiber strengthened composites have demonstrated better choice performance than those of other composites studied, because it has shown highest tensile strength and tensile modulus.

2.2.2.6 Various Fiber mesh layouts

In order to complete the fiber retrofitting or upgrading description, it is important to present a synthetic review of the possible fiber mesh layouts, based on and mainly found in the literatures.

Fig. 2-59 presents a synthetic review of the possible configurations. The application of the fiber mesh or net and its size, usable numbers and the layout combinations for masonry retrofitting or upgrading can vary, depending on the desirable mechanical performance that to be achieved from the reinforcement.

The presence of empty spaces (like window, doors etc.) in the masonry walls makes the structure vulnerable towards the seismic events, and the damage due to these activities could be minimized by retrofitting or upgrading the walls with FRPs, different configurations have been shown in Fig. 2-60.

Notably, the horizontal connectors are used in both for FRP and TRM retrofitting or upgrading purposes, some schemes are shown in Fig. 2-61.

The number of horizontal connectors (diatons) may vary depending on the type and size of the used fiber mesh, and also on the personal choice and as studied and tested in Giresini et al. (2020) to ensure an optimum grip of the composite to the masonry.

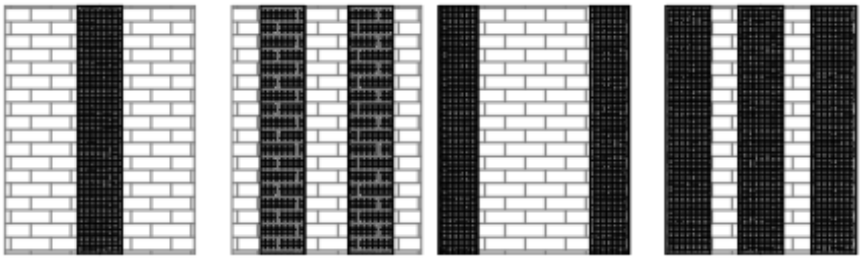

(a): Vertical bending configuration.

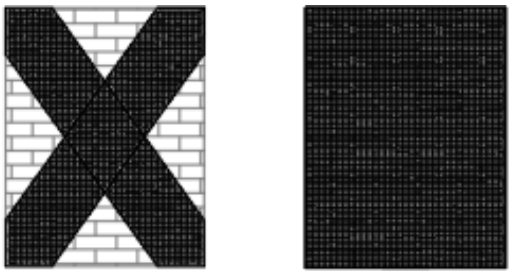

(b): Shear configuration (c): Complete configuration

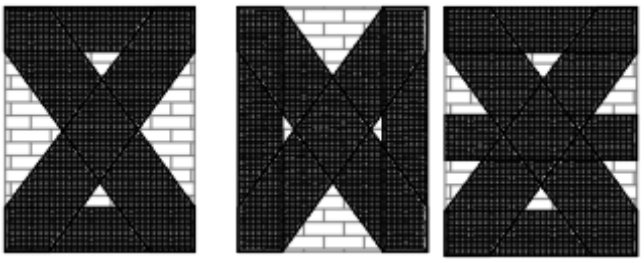

(d): Simple hybrid configurations

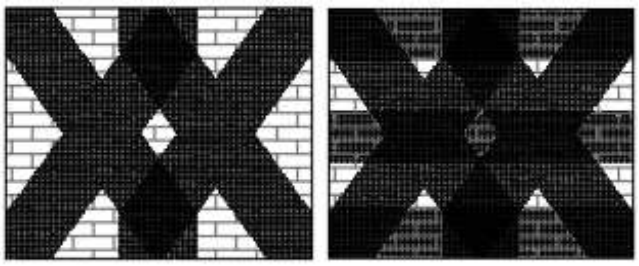

(e): Complex hybrid configurations

Fig. 2-59. Different FRP layouts.

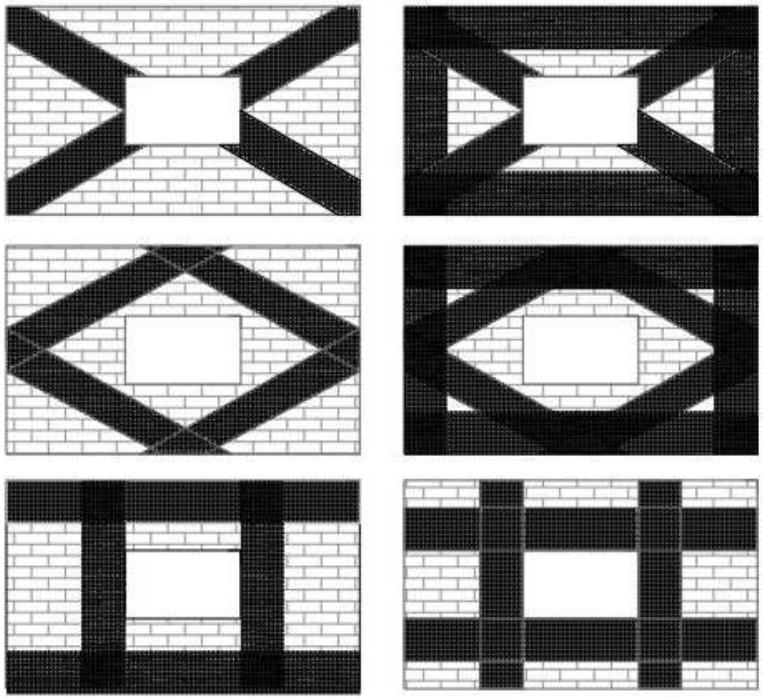

Fig. 2-60. Masonry wall structure with hollow space in the middle and FRP retrofitting or upgrading schemes.

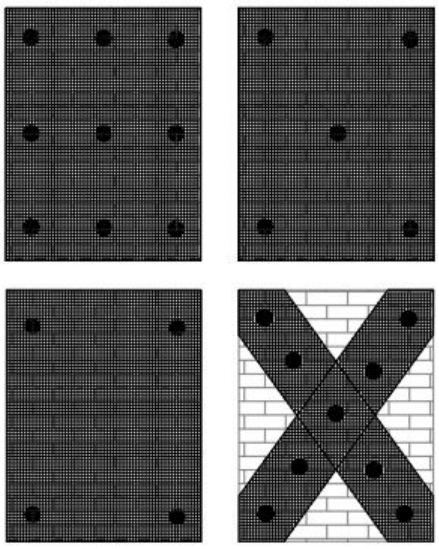

Fig. 2-61. TRM & FRP with horizontal connectors.

2.2.3 Masonry upgrading of structural and thermal performance

Another way to describe the various applications of masonry retrofitting or upgrading with fiber-strengthened composite systems is to distinguish the purpose of the retrofitting and upgrading and mainly these can be categorized under: (a) structural retrofitting or upgrading and (b) thermal retrofitting or upgrading, whereas third category could be placed under (c) integrated retrofitting or upgrading which are the cases where both structural and thermal performances of the wall are enhanced by the fibers.

Indeed, the various fibers have been tested and used for structural and/or thermal retrofitting or upgrading, but very rarely found to be used for the integrated retrofitting or upgrading.

FRP retrofitting or upgrading predominantly has been used as (a) external and (b) internal reinforcement (Zaman et al. 2013), due to the composite materials ability to minimize or solve the problem of over-loading and demonstrate to be better performer in compared to other retrofitting materials (Ferrara et al. 2020).

The advantages of FRP, as highlighted by Zaman et al. (2013), high ratio of strength to density, it can be fit according to certain mechanical characteristics, also known to have excellent corrosion behavior, and convenient electrical, magnetic and thermal properties.

While according to Zaman et al. (2013), FRPs show brittle and anisotropic behavior, of course rate of loading, environmental condition and temperature affect the mechanical properties.

As mentioned by Ferrara et al. (2020), TRM technique is specifically suitable for masonry elements reinforcement or retrofitting purposes.

When natural fibers are used to improve the mortar performances, notably the fiber size and mixing percentage significantly influence the final results. In particular both structural and thermal performances results are inversely proportional to each other, and this phenomenon has been observed in Raut et al

(2016) for palm oil fiber, in Benmansour et al. (2014) for date palm fiber and in Valenza et al. (2015) for sheep wool fiber.

Notably, the thermal insulation improvement due to the retrofitting or upgrading yields to the reduction of energy consumptions used for the building climate control. Therefore, the correct use of fiber in masonry retrofitting or upgrading not only can improve the structural performance of the masonry structures but also it can improve its thermal insulation, and further boost the thermal performance of the building as whole.

The plant and animal based natural fiber's ability to work as insulating materials depend on the capability to trap the air in the fiber cavity, inside it or in the fiber's matrix, notably can be observed in the case of fiber insulation panels, for example the sheep wool fiber insulation panel (Ahmed et al 2019) and formation of compact/composite insulating layers in cases where fibers are mixed with binders (Valenza et al. 2015).

When natural mineral fiber like basalt or man-made inorganic fibers like glass and carbon are used as FRP or in textile form (as TRM), these fibers can also influence the overall heat transfer due to their presence in the structure. Whereas to have a dedicated improvement in the thermal performance, these fibers must be used along with other heat insulating materials to achieve the thermal retrofitting (Borri et al. 2016).

A synthetic scheme of the possible masonry retrofitting or upgrading with fibers is presented in Fig. 2-62. Importantly, to achieve thermal insulation or integrated retrofitting or upgrading, the textile fabrics must be paired with fiber (mainly plant or animal) composite mortar(s).

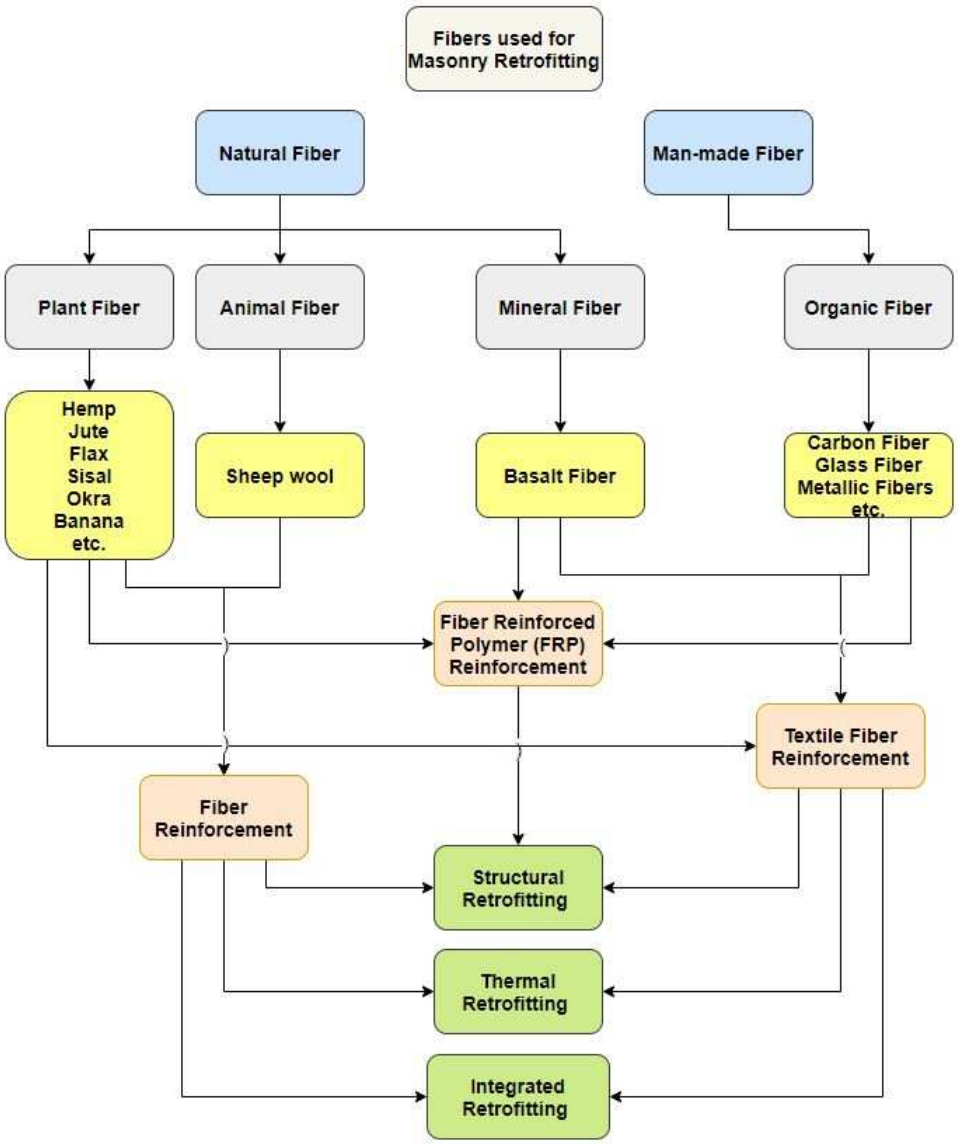

Fig. 2-62. The use of fibers for strengthening of masonry.

The use of natural fibers for different retrofitting or upgrading use, has been reported in Table .2.8.

Table 2-8 – Fiber use in Masonry retrofitting or upgrading .

Type of Fiber Used	Thermal retrofitting or upgrading	Structural retrofitting or upgrading		Possible Integrated Retrofitting
	Thermal conductivity tests	Mechanical tests	Structural tests	
Jute 1. Ferrandez-García et al. (2020) 2. Formisano et al. (2019)	1.Recycled Jute Fiber (waste jute bags) + Portland cement + Potato Starch	1. Recycled Jute Fiber (waste jute bags) + Portland cement + Potato Starch 2. Plaster block made of Fiber (of various sizes) + lime binder	X	1. Right choice of fiber size & percentage and fabric/net, might satisfy both thermal and structural retrofitting
Flex Ferrara et al. (2020)	X	Flex fiber + mortar	Flex fiber fabric + mortar	1. Right choice of fiber size & percentage and fabric/net, might satisfy both thermal and structural retrofitting
Hemp 1. Formisano et al. (2017) 2. Menna et al. (2015) 3. Sassu et al. (2016)	1. Hemp shives + Hydrated lime + with and without cement 2. Concrete blocks made of hemp shives (lower %) + hydrate lime +	1. Mortar – made of Fiber + Hydrated lime 2. Brick- made of, Shives + Hydrated lime + silica sand + volcanic sand	1. Neapolitan yellow tuff & solid clay bricks both sides strengthened with hemp fiber composite	1. Concrete blocks made of hemp shives (optimum size and %) + hydrate lime + pozzolanic material + hydraulic binder

	pozzolanic material + hydraulic binder	3. Concrete blocks made of hemp shives (higher %) + hydrate lime + pozzolanic material + hydraulic binder	(HFC) and using both pozzolanic and lime-based mortar	
Oil Palm Raut et al (2016)	Fiber + Palm Oil Fly Ash + cement + Sand	Palm Oil Fly Ash + cement + Sand	X	Right choice of fiber size & percentage and fabric/net, might satisfy both thermal and structural retrofitting or upgrading
Date Palm Benmansour et al (2014)	Fiber* + cement + sand	Fiber# + cement + sand	X	Right choice of fiber size & percentage and fabric/net, might satisfy both thermal and structural retrofitting or upgrading
Sheep Wool Valenza et al (2015)	Fiber* + Portland cement	Fiber# + Portland cement	X	Right choice of fiber size & percentage and fabric/net, might satisfy both thermal and

				structural retrofitting or upgrading
Banana, Reed, Palm and Coconut Zubaidi, A.B. (2018)	Fibers* + Portland cement + Sand	Fibers# + Portland cement + Sand	X	Right choice of fiber size & percentage and fabric/net, might satisfy both thermal and structural retrofitting or upgrading
Use of Carbon, Glass, Basalt and Metal (Steel) as 1. TRM or 2. FRP	X	X	1. Textile Fabric + Mortar 2. FRP mesh + Epoxy (adhesive, putty)	Right choice of fiber size & percentage and fabric/net, might satisfy both thermal and structural retrofitting or upgrading
* better with higher fiber % & # better with lower fiber %				

2.2.4 Structural upgrading

Man-made fibers (like, glass, basalt, steel, carbon etc.) have been predominantly used for many years for structural strengthening interventions, intended at either retrofitting or upgrading the existing buildings. The use and some examples of these fibers are highlighted below:

As reported in Sivaraja et al. (2013), GFRP retrofitted masonry walls were subjected to shock table tests, exposed to a simulated earthquake event. It has been observed that the total seismic energy withstanding capacity of the GFRP retrofitted sample is almost 20 times greater than the one of similar non-retrofitted sample.

Stratford et al. (2004) tested all the masonry walls subjected to a combination of vertical and in-plane shear load. The performance improvements are patent also in this case: 65% increase in load-capacity for the GFRP strengthened clay walls, 38% and 63% for the concrete walls (lower value due to faulty production process). As reported by the authors, no change in the stiffness and deformation-capacity of the specimens have been observed.

Silva et al. (2008) have studied the in-plane share capacity of the GFRP retrofitted masonry and concrete walls. Improvements in shear capacity of the strengthened walls were significant and horizonal strips have demonstrated more effectiveness over vertical strips and at the same time when GFRPs are put on both wall sides their efficacy increased twice.

In Kuzik et al. (2003) cyclic loading was applied to study the out-of-plane flexural behavior of the GFRP retrofitted masonry walls. They have reported excellent overall flexural performance and highlight that the linear response of the bending moment versus centerline deflection hysteresis and the variation in the wall stiffness and the ultimate strength depend on amount of bonded GFRP sheet reinforcement.

Kalali and Kabir (2012) have tested GFRP-strengthened masonry walls subjected to constant gravity load and under increasing in-plane loading cycle,

obtaining improvement are the strength, deformation capacity, and energy absorption.

Mahmood and Ingham (2011) have developed diagonal compression tests and report to achieve improvement in shear strength (up to 325%), in ductility and toughness of the pultruded CFRP and GFPR retrofitted masonry.

Also, Marcari et al (2007) have used CFRP and GFRP strips applied on the walls using epoxy, for strengthening tuff masonry walls and have studied the in-plane shear performance when these were subjected to monotonic shear-compression loading in a quasi-static test. Improvements in shear strength, lateral strength and non-significant variation of elastic stiffness have been reported.

Zhou et al (2013) have studied the in-plane behavior of unstraightened and strengthened with BFRP masonry subjected to static cyclic loading. Enhancement in shear capacity (44-61%), whereas no difference from the initial stiffness was observed.

Lei et al. (2014) have studied BFRP strengthened and the un-strengthened RC-brick masonry walls were tested to investigate in-plane behavior. All the samples were subjected to low frequency cyclic loading. The application of BFPR enhances the lateral strength (16%) both also the ultimate drift, the energy dissipation capacity and the bearing stability.

Padalu et al. (2019) have tested the wall samples (including BFRP retrofitted ones) in one-way bending condition under two point out-of-plane loading by putting wallettes horizontally. Comparing BFRP retrofitted samples with unstrengthened masonry samples it is possible to assess improvement of flexural strength (up to 6.4 times), the maximum midspan displacement (up to 30 times), effective stiffness (up to 5.3 times).

Padalu et al. (2020) have studied the out-of-plane behavior of the strengthened masonry walls. The unstrengthened masonry walls were structurally retrofitted with BFRP + Epoxy resin, basalt fiber mesh (BFM) + 1:4 cement-sand mortar and welded wire mesh + 1:3 cement-sand mortar. A notable improvement approx. 73% in

flexural capacity, 482% in stiffness and 72% in the energy absorbing have been observed.

Tempesta (2018) has stated that a structure retrofitted using BFRP with transversal element system presents an excellent resistance to shear as well as to the combined compressive and bending actions.

Rahman and Ueda (2016) have reported on the use of CFPR to reinforce the masonry walls and found an improvement of in-plane shear strength but a reduction in the ductility. Also, CFRP application can modify the elastic stiffness.

Arifuzzaman and Saatcioglu (2012) have demonstrated that with CFRP a masonry wall can withstand to an improvement of 150% in the applied lateral force. Also, the wall shear capacity, the flexural capacity, and the overall behavior under applied seismic loading are enhanced.

Righetti et al. (2016) have conducted the on-site shear compression, as shown in Fig. 2-63(a) and diagonal compression tests, as in Fig. 2-63(b) on the masonry walls retrofitted with GFRP and inorganic mortar, and as stated enhancement of the mechanical behavior was achieved.

(a) Shear compression test (b) Diagonal compression test

Fig. 2-63. On-site tests (Righetti et al. 2016).

Alecci et. al (2020) have carried out diagonal compression tests on masonry walls before damaging these walls and after repairing using CFRP strips placed at various patterns and the shear strength found to be similar for damaged and undamaged walls.

Furtado et al. (2020) have studied the out-of-plane behavior of the masonry infill walls, strengthened with Glass fiber textile and mortar. The GFRP-TRM increase the flexural strength and deformation capacity by 54% and 4.18 times respectively. Also, the plaster enhances the approx.57 % the flexural capacity.

Papanicolaou et al. (2011) have tested both CFRP and TRM retrofitting by applying out-of-plane or in-plane loading on masonry walls. TRM produce better performances in terms of maximum load and displacements at failure in the case of out-of-plane loading but for in-plane loading the effectiveness of TRM is lower than the one of FRP. It has been observed that the TRM retrofitted samples present a higher deformation capacity (15-30% more). The authors have concluded that TRM retrofitting is more promising for out-of-plane than in-plane seismic loading.

Prota et al (2006) have experimented the in-plane behavior of the TRM+CMG retrofitted tuff masonry walls. With the CMG grid application, it has been found that the average shear strength increases by factor equal to 2.

Fossetti and Minafò (2016) have developed uniaxial compressive tests until failure, on the BFRCM and steel retrofitted masonry columns. Strength improvement has been observed for the column with BFRCM jacketing while an increase in ultimate strain and energy absorption when reinforcing steel wires has been observed.

Barducci et al (2019) have compared the bond behavior of the FRCM systems, composed of basalt fiber and four different types of mortar matrices.

2.2.4.1 Innovative natural fiber building materials studied for structural applications

Actually, when compared to natural fibers and Natural FRPs, the man-made fibers and their FRPs are less sustainable due to the constraints associated with

their production processes like fossil fuel depletion, air pollution, smog, and acidification as mentioned in Masuelli (2013) and Osugi et al (2009). Therefore, to contribute to the global sustainability and reduction in CO_2 production, it is important to look for natural materials for retrofitting existing buildings or for the construction of new ones.

Sassu et al. (2016) have develop two types of sustainable building materials as reported in Fig. 2-64. In this case, new kinds of blocks are fabricated by mixing hemp shives and cork granules with natural hydraulic lime. They achieved mixed results in terms of mechanical performances with the hemp and cork samples. The hemp samples have low mechanical performances but might be effective as insulating panels, basement layers or separating walls. The cork samples have demonstrated optimum structural properties achieving quite high maximum stain, compressive strength and tensile strength.

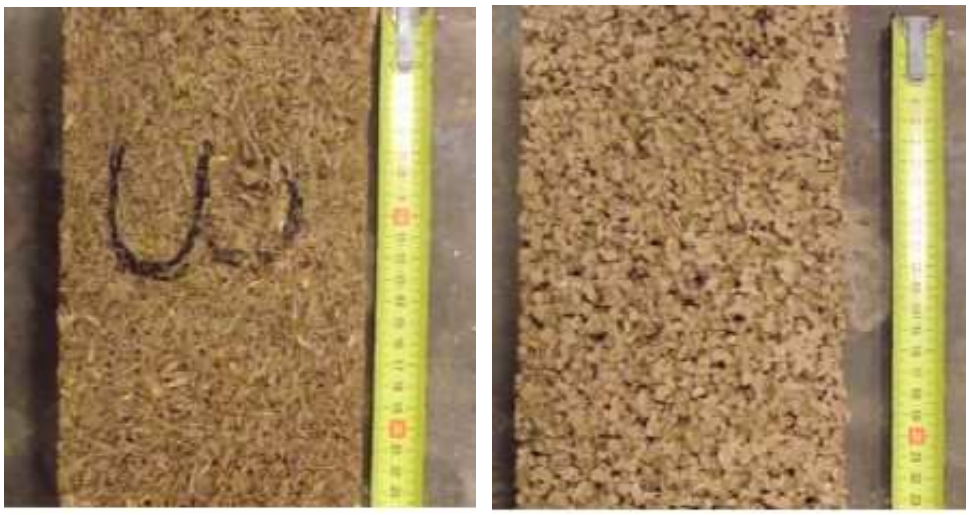

(a): hemp (b): cork

Fig. 2-64. Blocks of granules (Sassu et al. 2016).

Formisano et al. (2020) have used jute fiber and lime of M15 class (NTC 18 standard) to prepared fiber strengthened mortar. The value of the average failure compression stress has remained above the class M10-NTC 18 standard

for almost all fiber-strengthened mortars, as in Fig. 2-65. Therefore, these products can be used as building product, also in seismic zones.

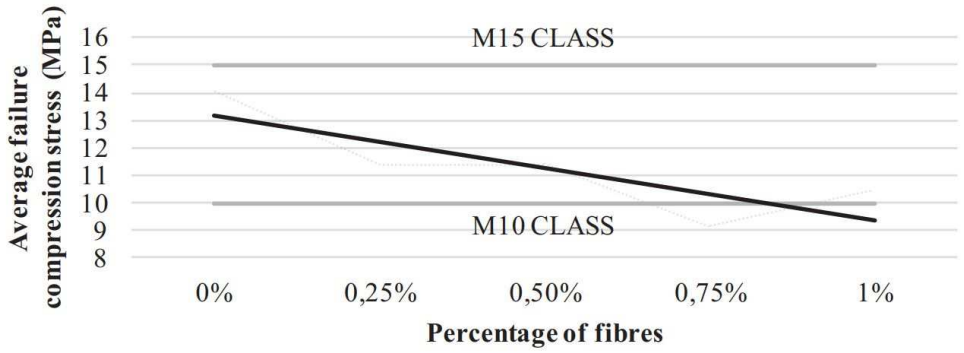

Fig. 2-65. Influence of the fiber percentage in Average failure compression stress (Formisano 2020).

Formisano et al. (2017) have used hemp fibers and shives to prepare mortar and bricks, in order to evaluate their mechanical behaviors. It has been found that the performance increment was of about 29% in strengthened mortar specimens under bending tests. The ultimate displacement of strengthened specimen is 0.63 mm, whereas for the un-strengthened specimen is about 0.49 mm.

Menna et al. (2015) have studied the diagonal compression tests on retrofitted tuff and clay masonry wall panels with hemp fiber mesh, pozzolanic and lime-based mortar. The authors have studied the in-plane behaviors strengthened Neapolitan yellow tuff (NYT) and clay masonry panels. The tests have proved capable to enhance the mechanical properties for the strengthened members. Maximum shear strength increased by a factor about 2–3 and 5 in the case of NYT panels and clay panels respectively.

Elfordy et al (2008) have prepared the hempcrete (hemp shives + lime based binder) blocks with various densities. According to authors hempcrete blocks need to be denser and stronger for structural use purposes.

Table 2-9 presents some of the advantages and disadvantages of the natural and men made fibers.

Table 2-9. Comparison of advantages and disadvantages of man-made and natural fiber for masonry retrofitting or upgrading.

Man-made FRP		Natural Fiber Retrofitting or upgrading / Natural FRP	
Advantages	Disadvantages	Advantages	Disadvantages
Higher mechanical performance	High production cost	Low production cost	Lower mechanical performance
Well known characterization data	Less-sustainable – more energy consumption	Lower environmental Impact	Sustainable but new to the users
Majorly used for structural retrofitting	Limitation to recyclability	Mostly recyclable when used with other natural/biomaterials	Perfect candidates for Integrated retrofitting
Durability	Glass fiber is Hazardous	Non-Hazardous	Degradable, sometime need treatment

2.2.5 Thermal- retrofitting building materials

Notably for thermal-retrofitting purposes, the mineral wool and plastics are widely used in C&B sector, and these insulating materials (including it derived products) occupy approx. 52% and 41% of the market shares, respectively (as stated by Asdrubali et al. 2015). These insulation materials also known to have detrimental effect towards the environment, considering that these materials are generally produced by using non-renewable and non-organic materials. Also, these materials are quite difficult to be recycled or re-used, and are known to be hazardous towards human health, as expressed in De Vuyst et al (1995).

Valenza et al. (2015) have used washed and unwashed Sicilian sheep wool at various proportion along with cement to prepare the composite samples. They have

studied the thermo-mechanical properties of these samples. As stated by the author, specimen with fiber size and proportion respectively equal to 1 (mm) and 46% has the best and lowest thermal conductivity value equal to 0.096 (W/mK).

While Elfordy et al (2008) have reported that the hempcrete block with lower density 417 (kg/m^3) has better thermal conductivity 0.179 (W/mK) in comparison to 0.485 (W/mK) when density is 551 (kg/m^3). Therefore, the blocks with lower conductivity value can be used as thermal insulating material.

As stated by Sassu et al. (2016), the hemp shives might be used to create insulating panels. While both Raut et al (2016) and Benmansour et al. (2014) have demonstrated that higher fiber percent in the composite mixture directly influence the thermal conductivity, i.e., lower thermal conductivity value demonstrated ton have better insulation capacity. Therefore, the authors have stated that the products created by them might be used as thermal insulation materials in buildings.

2.2.6 Integrated retrofitting or upgrading building materials

When the retrofitting or upgrading strategy is aimed to enhance both structural and thermal properties, the integrated retrofitting or upgrading might be an approach. While it is quite difficult to achieve the ultimate improvement of both these properties simultaneously using the same materials. Indeed, structural strength and thermal resistance, found to have opposite trend.

Extensive research work/activities need to be carried out, to optimize both structural and thermal insulation properties simultaneously and it might not always cost effective. Conversely, Giresini et al. (2020) have conducted an analytical study, to evaluate the cost-effectiveness of the integrated approaches for the masonry building façades.

Notably, Raut et al (2016) have prepared mortars using oil-palm fibers, available as waste product to attain certain thermo-structural characteristics and to have a sustainable building material. The optimized values are obtained when fiber addition is equal to 1,5% of the weight of the binder and the compressive

strength is compliant with ASTM C270, therefore a balance between the thermal performance and in the flexural strength have been detected. This composite product might be used as integrated building material.

Benmansour et al. (2014) have reported on the thermal and mechanical properties of mortar strengthened with date palm fibers. Although the goal was to develop an insulating building material. Authors have claimed that these innovative mortars are suitable for thermo-structural or integrated retrofitting use when fiber concentration is low, and the optimum ratio is found to be 5-15%.

Valenza et al. (2015) have fabricated environmentally friendly mortar and plaster with good thermal performance by mixing sheep wool with cement. The optimum thermo-structural value found to be with when the fibers length is equal to 6 mm and weight content to 13%.

Al-Zubaidi (2018) have prepared cement composite strengthened with natural fibers like banana, reed, palm and coconut. According to the author the size, morphology and fiber contents mainly affect the reinforcement performance. Therefore, right combination should be chosen to enhance integrated retrofitting.

Ferrandez-García et al. (2020) have studied the thermo-mechanical properties of the cement panels retrofitted with recycled jute fiber (collected from jute bags) and potato starch plasticizer. As claimed by the authors, the thermal and mechanical properties are in line with European building standards.

Borri et al. (2016) have inserted GFRP grids into thermo-insulating mortars by and reported to have achieved low value for conductivity 0.106 (W/mK) for the sample fabricated using plaster board and mortar with clay, cork and natural lime with glass fiber strengthened grid (GFRP grid). This technique also improves the lateral load capacity.

2.3 Integrated retrofitting or upgrading with TRM system

In last few years, scientist and researchers are working to find the best solution for integrated retrofitting techniques (Fig. 2-66) for structural and thermal upgrading or retrofitting of masonry walls using TRM-system. Most of the studies are stated to have integrated the insulation materials in the TRM system. As reported in majority of these studies, only experimental results based on structural tests have been provided, whereas no experimental data on improvement in thermal property are reported. While only exception Facconi et al. (2021) where the calculated values for both Structural and thermal behaviors are stated. Notably, Longo et al.(2021) is the first to provide experimental data for both structural and thermal parameters.

Structural and thermal retrofitting of masonry structure with TRM system

	Fabric	Mortar	Insulation material	Structural test	Thermal test
First research **Triantafillou et al. (2017)**	Commercially available (Not specific)	Cement-based	Expanded polystyrene (EPS)	Out-of-plane	No information available (Only fire test results are reported)
Triantafillou et al. (2018)	Glass	General-purpose cement mortar	Expanded polystyrene	In-plane	No information available
Gkournelos et al. (2020)	Glass	General-purpose masonry mortar	Polystyrene	In-plane and out-of -pane	No information available
Karlos et al. (2020)	Glass	Cementitious mortar	EPS plate	Out-of-plane test, analytical and numerical model	No information available
Facconi et al. (2021)	Steel	Aerogel, light and heavy wood fiber.	Cement	Numerical model	Computed using COMSOL software
First research to provide experimental data for both parameters **Longo et al. (2021)**	Glass and steel	Hydraulic lime and GeoPolymer lime	Hydraulic lime and GeoPolymer lime	In-plane	Wall surface (one side) heated with 4 halogen lights, temp. of surfaces measured, ambient temp. measured and other parameters are assumed to calculate thermal transmittance value

Fig. 2-66. Notable works on integrated retrofitting or upgrading with TRM-system.

Triantafillou et al. (2017) claimed to be the first to coin the idea of structural and energy retrofitting (Fig. 2-67). Actually, they investigated the possible retrofitting of masonry wall by using TRM system of various configurations, which

consisted of a cement-based mortar internally reinforced with a commercially available fabric, whereas Expanded Polystyrene (EPS) and foamed cement were used as insulation materials. Improvement in structural parameters has been evaluated through out of plane tests. Some samples were subjected to fire tests.

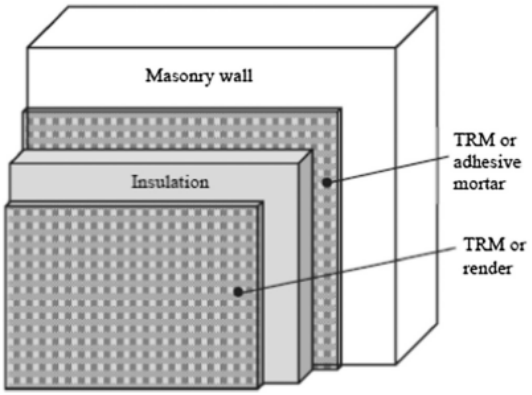

Fig. 2-67. Integrated retrofitting scheme Triantafillou et al. (2017).

Again Triantafillou et al. (2018) have reinforced (with the aim structural and energy retrofitting) masonry wallets (Fig. 2-68) with Glass-TRM system, in this case authors have used a general-purpose cement mortar and integrated EPS in the TRM system. Although authors highlight in-plane test results, no experiment related to thermal properties are reported. For aforesaid cases, it could be guessed that due to presence of insulation material in the TRM system, the thermal performance would improve.

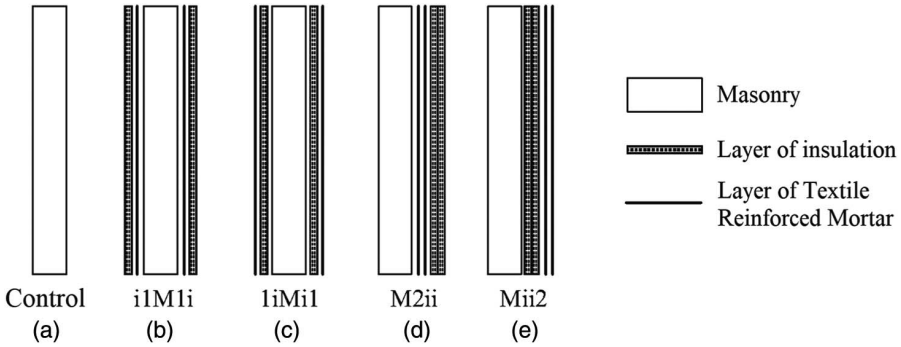

Fig. 2-68. Various integrated retrofitting schemes Triantafillou et al. (2018).

Structural performances of integrated retrofitted wallets (Fig. 2-69) are evaluated by Gkournelos et al. (2020) through in-plane and out-of-plane tests, and improvements are reported. Notably these wallets were retrofitted with a Glass-TRM system, which includes the insulation material (polystyrene) and general-purpose masonry mortar. Authors do not provide any information regarding the thermal performance.

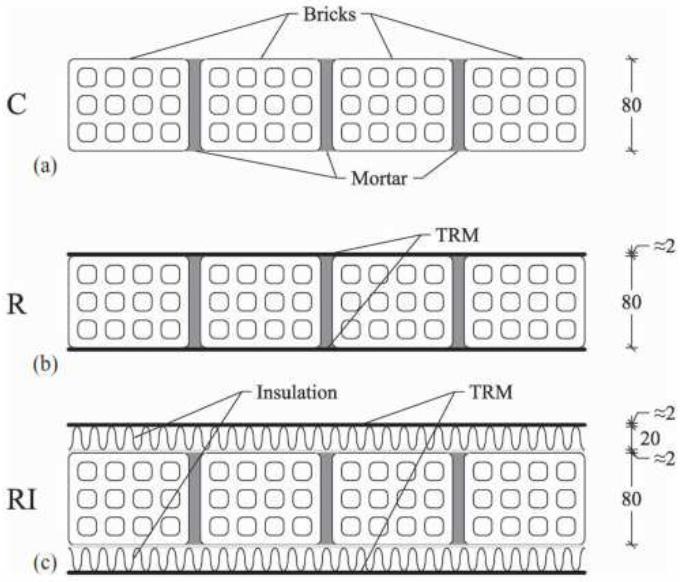

Fig. 2-69. Retrofitting configurations: (a) control; (b) TRM only; (c) TRM combined with insulation, all dimensions are in mm Gkournelos et al. (2020).

Similarly, Karlos et al. (2020) also have retrofitted masonry walls with TRM system consist of glass fibric, cementitious mortar and an EPS plate integrated as protective insulating layer. No experimental results have been provided on thermal performance of the masonry wall, which was supposed to be improved due to the presence of EPS. While detailed experimental (out-of-plane test), analytical and numerical model results justifying the improvement in strength and deformation capacity of the retrofitted walls have been presented.

While Facconi et al. (2021) have reported to have evaluated structural and thermal performance of the integrated retrofitted masonry (Fig. 2-70) structure using numerical model and COMSOL software, respectively. In this case the masonry

walls simulated to be retrofitted with Steel-TRM made with cement and insulation materials like aerogel, light and heavy wood fiber.

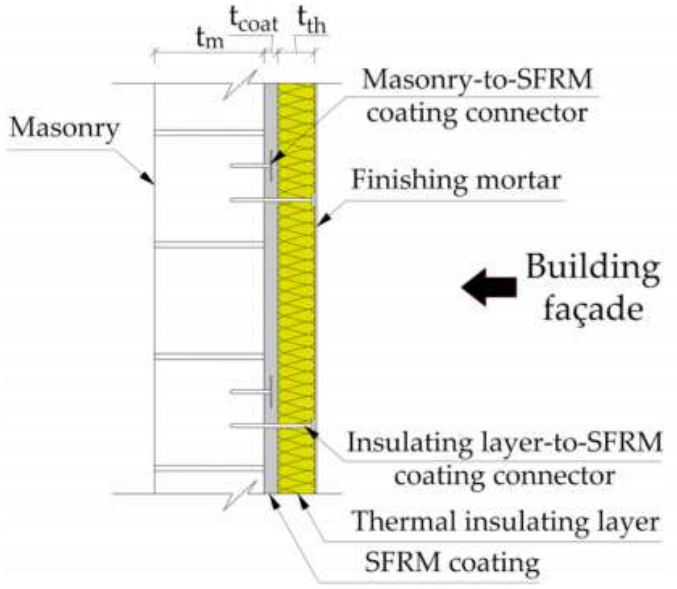

Fig. 2-70. Proposed retrofitting scheme Facconi et al. (2021).

Longo et al.(2021) supposed to be the first to provide in detail the experimental results on integrated property i.e., both structural and thermal behaviors of the masonry walls retrofitted with various configurations of TRM systems (consist of glass and steel fabric used with natural hydraulic lime and GeoPolymer lime) (Fig. 2-71). Interestingly, authors have used four halogen lamps to heat one side of the wall specimen, and the surface temperatures of both surfaces were measured. Thereafter, calculated the thermal transmittance value of each wall. Geopolymer based system found to have higher ductility and improved thermal insulation capacity.

(a) Glass fabric

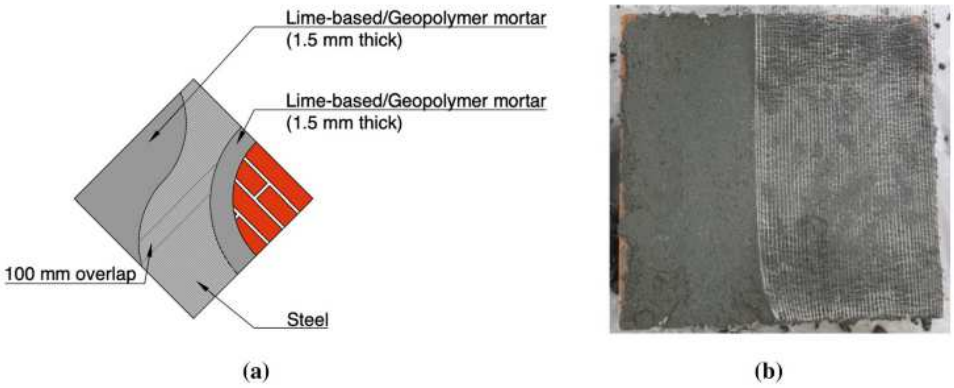

(b) Steel fabric

Fig. 2-71. Two different retrofitting schemes Longo et al.(2021).

2.4 Conclusions

This chapter has presented a review on the current state of knowledge of both structural and thermal masonry retrofitting or upgrading with a particular attention to the use of fiber-strengthened composed systems. This topic is quite relevant considering that the largest part of the European traditional buildings is composed of masonry buildings and most of these did not follow the anti-seismic and thermal standards. Thus, the needs of the structural and thermal retrofitting

or upgrading is quite clear. On the other hand, the buildings impact on the environment represents one of the most important challenges for mankind.
Therefore, it is necessary to reduce the environmental impact of construction materials and find new and more sustainable solutions. Natural fibers represent a promising approach to this target. Therefore jute, hemp, oil palm, flax, but also sheep wool are sustainable materials that can play a key role for building retrofitting or upgrading.

An integrated approach aimed at improving both thermal and structural performances would be a right approach for future developments.

3. Some general aspects on strengthening masonry walls with TRM systems and the basics of thermal conductance calculations.

The ultimate objective of this thesis is to use the jute fiber composite mortar and jute net or Textile Reinforcement Mortar (TRM), to obtain thermo-structural upgrading of masonry walls.

This chapter is subdivided into two parts and it briefly highlights the aspects, regulations & guidelines and formulae which would be necessary to design, strengthen and test the masonry walls.

Further the importance of the TRM retrofitting or upgrading of masonry systems is discussed.

Particular attention has been made to discuss, only the arguments (on the TRM masonry retrofitting or upgrading) which are provided in the guidelines and recommendation prepared by the national research council of Italy and recognized by the Italian government.

While in the second part of this chapter, it has been discussed the concept of the heat flow through masonry walls, and the formulae necessary to calculate the thermal transmittance/ heat transfer coefficient (U).

Also, it highlights the regulations and the limitations of the thermal transmittance/ heat transfer coefficient (U) as provided by the Italian Ministry of Economic Development.

3.1 TRM strengthening/reinforcement

The use of Textile Strengthened Mortar or Textile Reinforced Mortar (TRM) composites is becoming very common in Construction & Building (C&B) sector for structural retrofitting or upgrading purposes. Here in Italy, these inorganic matrix composites are nominated in Italian ministerial documents as Fiber-Reinforcement Cementitious Matrix/Mortar (FRCM). While among scientist, professionals and research communities these composites are also called as Textile Strengthened Concrete (TRC), Fabric Strengthened Mortar (FRM) and sometimes also called as Inorganic Matrix-Grid (IMG) Composites. For simplicity, hereafter the acronym TRM has been used in all following chapters.

These inorganic matrix composites are created by coupling nets/fabrics (man-made or natural fibers) and with an inorganic matrix mortar (lime based or cement based). Commercially the man-made nets/fabrics fabricated with carbon, glass, aramid, steel fibers and PBO (Polyparaphenylene benzobisoxazole) are used for the structural rehabilitation interventions. While most recently, the use of natural fiber made nets/fabrics (hemp by Menna et al. 2015 and flex by Ferrara et al. 2020) for TRM retrofitting can found in the literature.

As stated by De Santis et al. (2017) and confirmed in Ferrara et al. (2020), no dedicated standards to design, test and/or qualify the TRM systems are available around the world, other than the standard and guidelines developed by United States (US) like RILEM TC 250-CSM and ACI 549, and the guidelines and recommendation prepared by CNR DT 215 (2018) and recognized by the Italian government.

Also, it is worth highlighting that there are no guidelines and/or standard exist on or specifying the Natural Fiber Textile Strengthened Mortar (NFTRM) systems. Recently TRM retrofitting or upgrading became a widely recognized masonry retrofitting or upgrading techniques, and strongly competing with the FRP retrofitting or upgrading techniques due to various known advantages of the TRM over FRP system (Table 3-1).

Table 3-1. Some advantages of TRM over FRP system.

TRM	FRP
Inorganic matrix CNR DT 215 (2018).	Organic matrix CNR DT 200 (2004).
High strength to weight ratio enhancing the mechanical performance CNR DT 215 (2018).	Higher strength
Easily applicable and installed Ferrara et al. (2020).	Need special attention during application Einde et al. (2003).
No organic additives needed (if used, CNR DT 215 (2018) recommends it should not exceed 10% weight of the inorganic binder).	organic additives needed for its application CNR DT 200 (2004).
Ideal for countering limited deformations in masonry, CNR DT 215 (2018). Applied mostly all over the retrofitting or upgrading element(s) or structure.	High specific strength, therefore applied in form of strip laminates Ferrara et al. (2020).
Stress is less concentrated due to more homogeneous application of TRM fabric over the masonry.	Concentration of stress and low adhesion capacity Ferrara et al. (2020).
Don't have this problem. Good chemical-physical compatibility between composite and masonry substrates Ferrara et al. (2020).	Polymeric resins generally in use are non-permeable and can leads to compatibility problem between composite and masonry Ferrara et al. (2020).
Can retain its performance even at high temperature Raoof et al. (2017).	Totally lost its effectiveness at high temperature Raoof et al. (2017).
Improve ductility.	Lack ductility and susceptibility to fire Ferrara et al. (2020).

Papanicolaou et al. (2008) have strengthening un-strengthened masonry buildings (URMs) using both FRP and TRM techniques. The authors have reported that under out-of-plane cyclic loading, the TRM systems have shown better results and improved effectiveness in terms of strength and deformability.

As recommended by CNR DT 215 (2018), the TRM could be applied for various masonry retrofitting or upgrading applications, for example strengthening:

1) Panels or whole wall surface: to enhance the shear and combined axial and bending moment capacity.
2) Vaults and arches: to improve the tensile capacity of the structure.
3) Floor and roof ring beams: to increase the collapse multiplies.
4) Columns: with the aim to increase ductility.

This research has been developed with the aim to strengthen (in-plane strengthening) of masonry wall through retrofitting or upgrading with Jute Fiber Textile Strengthened Mortar (JFTRM), mainly to improve the shear capacity of the composite wall structures, which were later subjected to in-plane cyclic loads.

Therefore, in this chapter it would focus only on the arguments linked to the masonry retrofitting or upgrading.

Some recommendations, as stated in CNR DT 215 (2018), to improve the in-plane shear capacity are provided below,

1) Both sides symmetrical masonry wall TRM reinforcement.
2) Application TRM preferably should be on the entire wall surfaces (or specific case could be applied in strips).
3) Fibric should have vertical and horizontal grid orientation.
4) For crack intervention, fabric should be applied in orthogonal direction.
5) Also, it to be noted that the area of the fibers arranged parallel to the shear force only should be considered for the design of shear strengthening.
6) If one side strengthened, then connectors should be used (as minimum 30% reduction in strength could be observed).

According to the CNR DT 215 (2018) guideline, the strength of a TRM retrofitted/strengthened masonry wall or the shear capacity of the strengthened wall ($V_{t,R}$) could be determined by calculating the minimum shear capacity of the un-strengthened masonry wall (*Vt*) and the contribution of the TRM ($V_{t,f}$) and summing these two values:

$$V_{t,R} = V_t + V_{t,f} \text{ [kN]} \tag{3.1}$$

The shear capacity of un-strengthened brick masonry (V_t) could be evaluated following the Italian Building Code (NTC- Circolare n.7 del 21 gennaio 2019 – 8.7.1.16) as,

$$V_t = H.t.\frac{1.5\,\tau_{0d}}{p}\sqrt{(1+\frac{\sigma_0}{1.5\,\tau_{0d}})} \text{ [kN]} \tag{3.2}$$

where:

H, l and *t* are the length, height and thickness, respectively of the solid clay brick masonry wall (m).

P is the corrective coefficient of the stresses in the cross section.

τ_{0d} is the shear stress capacity due to gravity load (MPa).

σ_0 is the stress due to gravity load (MPa).

Conversely, the contribution of the FRCM system could be calculated as,

$$V_{t,f} = \frac{1}{\gamma_{Rd}}.n_f.t_{vf}.l_f.\alpha_t.\varepsilon_{fd}.E_f \text{ [kN]} \tag{3.3}$$

where,

γ_{Rd} is a partial safety factor equal to 2, according to current knowledge.

n_f is the total number of the strengthened layers arranged at the sides of the wall (numbers on each side).

t_{vf} is the equivalent thickness of a single layer of the TRM system

l_f is the design dimension of the reinforcement measured orthogonally to the shear force, it can't be longer than length of the masonry wall. Therefore $l_f \leq H$.

α_t is the coefficient to account for reduced tensile strength of fibers when stressed in shear. When experimental values not available, can be assumed as 0.80.

E_f is the Young's/elastic modulus of elasticity of dry fabric/textile.

ε_{fd} is the design strain of TRM. This value can be derived from $\varepsilon_{lim,conv}^{(\alpha)}$.

The design strain of the TRM system could be calculated using the below mentioned formula:

$$\varepsilon_{fd} = \eta \frac{\varepsilon_{lim,conv}^{(\alpha)}}{\gamma_m} = \eta \frac{\boldsymbol{\alpha}.\, \varepsilon_{lim,conv}}{\gamma_m} = \eta \frac{\boldsymbol{\alpha}.\, (\sigma_{lim,conv}/E_f)}{\gamma_m} \tag{3.4}$$

where,

$\varepsilon_{lim,conv}^{(\alpha)}$ is the conventional stain limit (intermediate condition).

γ_m is the partial factor for materials and products. Is equal to 1.5 for Ultimate Limit State (ULS) and to 1.0 for Serviceability Limit States (SLS).

η is the conversion factor (accounting for special design problems), should be only used the values (i.e., $\eta = \eta_a$) from the Table 3-2, when no specific value available.

Table 3-2. Environmental conversion factors (η_a)

Internal	0.90
External	0.80
Aggressive environment	0.70

Moreover,

$$\varepsilon_{lim,conv} = \sigma_{lim,conv}/E_f \tag{3.5}$$

$$\Rightarrow \sigma_{lim,conv} = \varepsilon_{lim,conv}/E_f \tag{3.6}$$

where,

$\varepsilon_{lim,conv}$ is the conventional stain limit.

$\sigma_{lim,conv}$ is the conventional stress limit.

$$\varepsilon_{lim,conv}^{(\alpha)} = \boldsymbol{\alpha}.\, \varepsilon_{lim,conv} \tag{3.7}$$

$$\sigma_{lim,conv}^{(\alpha)} = E_f . \varepsilon_{lim,conv}^{(\alpha)} \tag{3.8}$$

where,

α is the amplification coefficient, for all TRM strengthening system can be taken equal to 1.5.

$\sigma_{lim,conv}^{(\alpha)}$ is the conventional stress limit (intermediate condition).

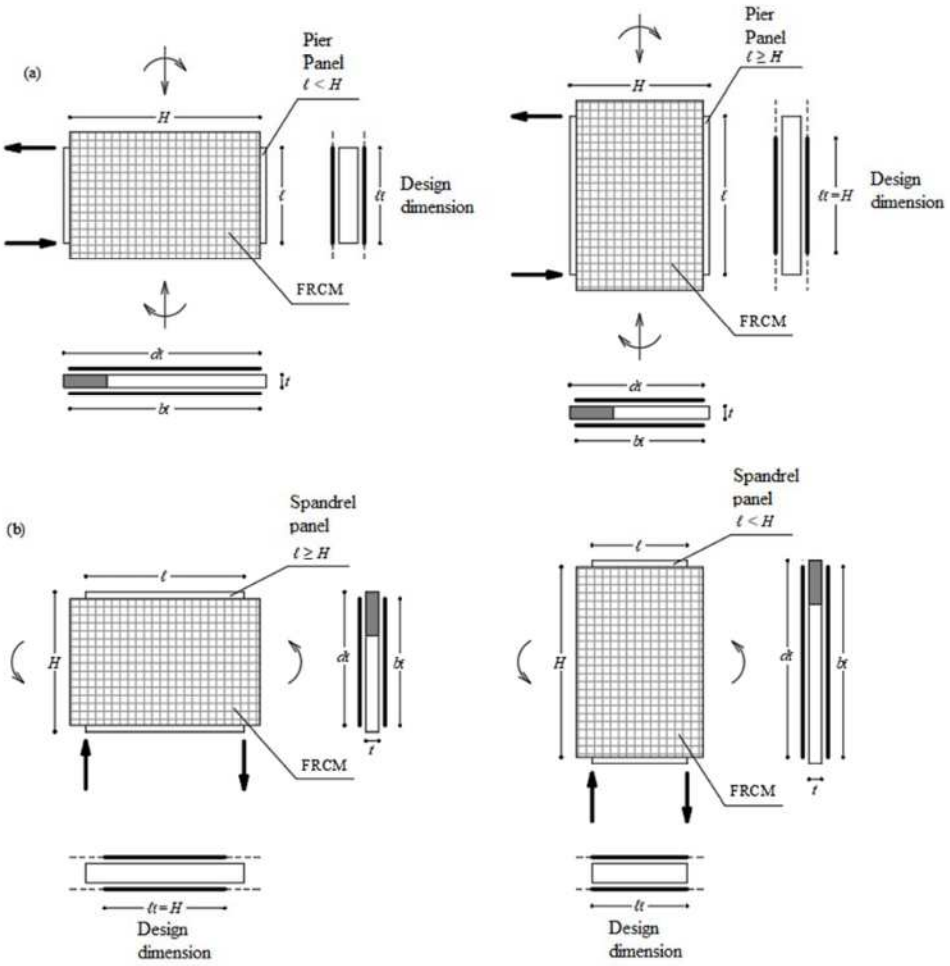

Fig. 3-1. FRCM in-plane strengthening of panels: (a) strengthening of pier panel; (b) strengthening of spandrel panel (CNR DT 2018).

3.1.1 Various types of shear-bond failure could be obtained for TRM strengthening.

As highlighted and mentioned in CNR DT 215 (2018) and Ferrara et al. (2020) there are mainly three (debonding, slippage and textile failure) types of failures could be observed in TRM strengthened element. The below mentioned failures (CNR DT 215 2018 and Ferrara et al. 2020) occur due to the substrate-strengthening matrix interaction, when external load is applied.

Case 1 - Loss of cohesion and debonding occur due to shear failure and the substrate collapse into two, while one of the pieces remained attached to TRM matrix (Fig. 3-2).

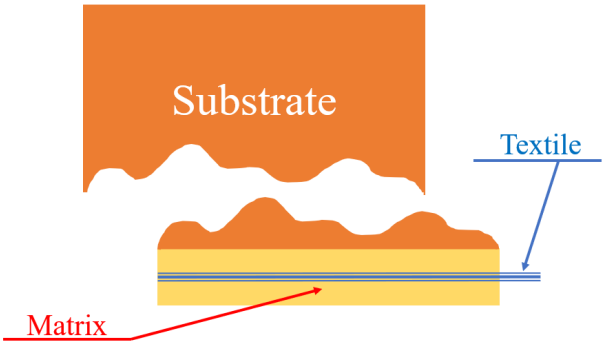

Fig. 3-2. Debonding with cohesive failure within the support.

Case 2 – In this case the TRM matrix (textile and mortar) get separated/detached from the substate as in Fig. 3-3.

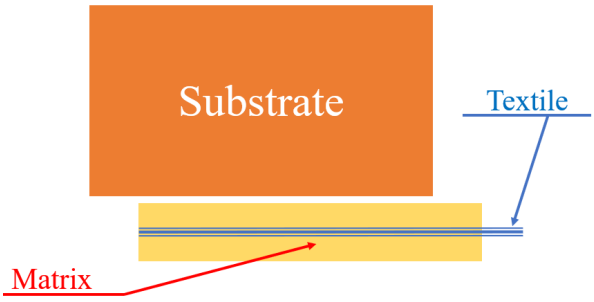

Fig. 3-3. Debonding at matrix-to-substrate interface.

Case 3 – Fig. 3-4 represents the disintegration of the TRM matrix, i.e., the detachment of the textile along with the outer layer of the mortar, while another portion of the mortar from the matrix remained attached to the substrate.

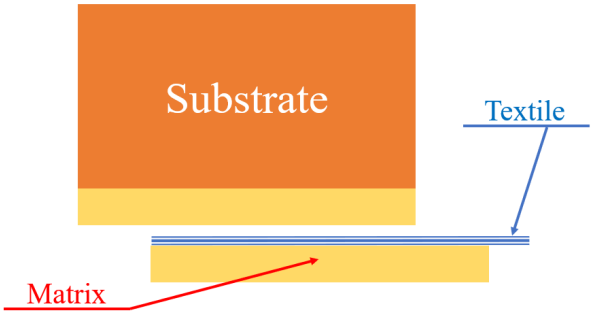

Fig. 3-4. Debonding at the matrix-to-textile interface.

Case 4 – In this case the imbodied textile used in the TRM matrix, slides in between the inner and outer mortar layer, as in the Fig. 3-5.

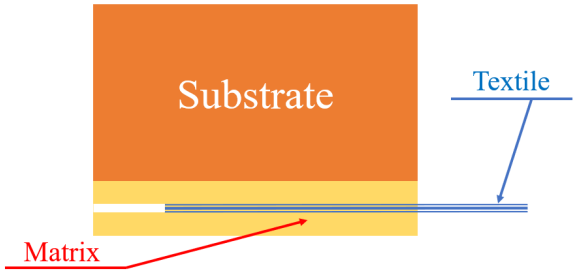

Fig. 3-5. Slippage of textile within the matrix.

Case 5 – This is an interesting case (Fig. 3-6), where both slipping of textile as well as disintegration of mortar matrix outer layer could be observed.

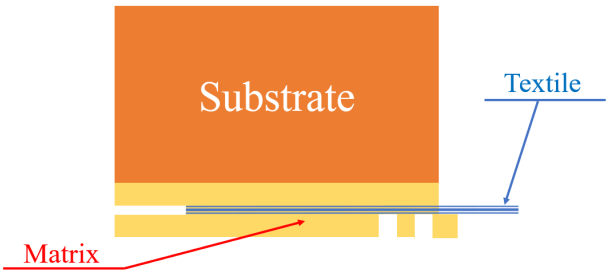

Fig. 3-6. Slippage of the textile and cracking in matrix.

Case 6 – This is a case in which the tensile failure of the textile observed out of the matrix, as can be seen in Fig. 3-7.

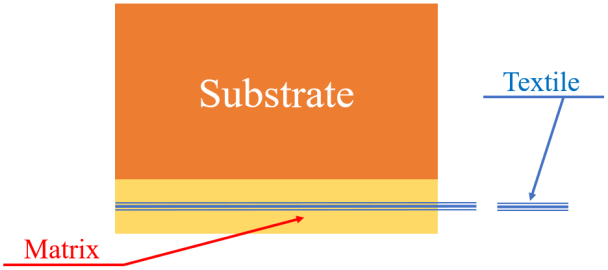

Fig. 3-7. Tensile failure of the textile.

Case 7 – Same as above but in the case the tensile failure, as in Fig. 3-8 the textile observed with in the matrix

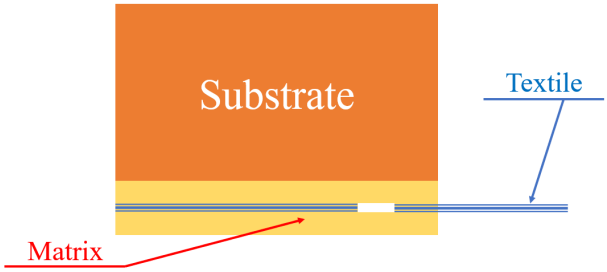

Fig. 3-8. Tensile failure of the textile within the matrix.

3.2 Thermal transmittance of a masonry wall

Pohoryles et al. (2020) highlighted that a building as an individual unit, consumes near about half of its total energy demand for heating and cooling operations. Therefore, loss of these energy through undesired heat transfer not only responsible to provide discomfort to its occupants, but also leads to huge economical loss.

The heat loss from a building envelope mainly happens due transmission and/or infiltration (Vosper et al. 1988), while as stated by Wallin (2014) ventilation is one of the main sources and account about 50% of total heat loss from a building, particularly in cold climate.

The transmission and heat losses are influenced due to physical parameters (including thermal conductivity), air and vapor permeabilities of the materials used, further these losses occur and depend on the building's construction quality and thermal bridge effects (Echarri et al. 2017).

Therefore, the use of suitable building materials with better insulation capacity could minimize the effect of the heat loss.

As it has been already mentioned, our research mainly focuses on masonry wall upgrading with JFTRM and jute fiber composite, therefore the thermal transmission capacity of the composite wall system has been studied.

The rate of heat flow through a material with flat surfaces can be determined using the Fourier's law:

$$q = -\lambda \Delta T \tag{3.9}$$

where, q = Local heat flux density (W/m2)

λ = Thermal conductivity of the material (W/mK)

ΔT =Temperature gradient (°C)

As stated by Kutz, M. (2006), the heat loss ($\dot{Q}$) or heat transfer/flow due to convection through a wall (build with homogeneous material) from indoor room condition (with temperature ($T_{in.}$)) to outdoor ambient condition (with temperature ($T_{Amb.}$)) can be calculated as follows:

$$\dot{Q} = U.A.\Delta T \tag{3.10}$$

where, U is the thermal transmittance/ heat transfer coefficient (W/m^{2}K); A is the surface area (m^2); ΔT= ($T_{Amb.}$- $T_{in.}$) is the temperature difference (K).

For a multi-layer or composite materials (Fig. 3-9) in series, the total thermal transmittance or heat transfer coefficient (U) due to mutual conduction and convection heat transfer, can be written as follows:

$$\frac{1}{U} = \frac{1}{h_{in}} + \mathbf{\Sigma}\frac{x}{\lambda} + \frac{1}{h_{Amb}} \tag{3.11}$$

where, h_{in} is the heat transfer coefficient of the internal surface [W/m^{2}K], h_{Amb} is the heat transfer coefficient of the outer surface [W/m^{2}K], λ is the thermal conductivity of materials [W/mK] and x is the wall layer thickness [m].

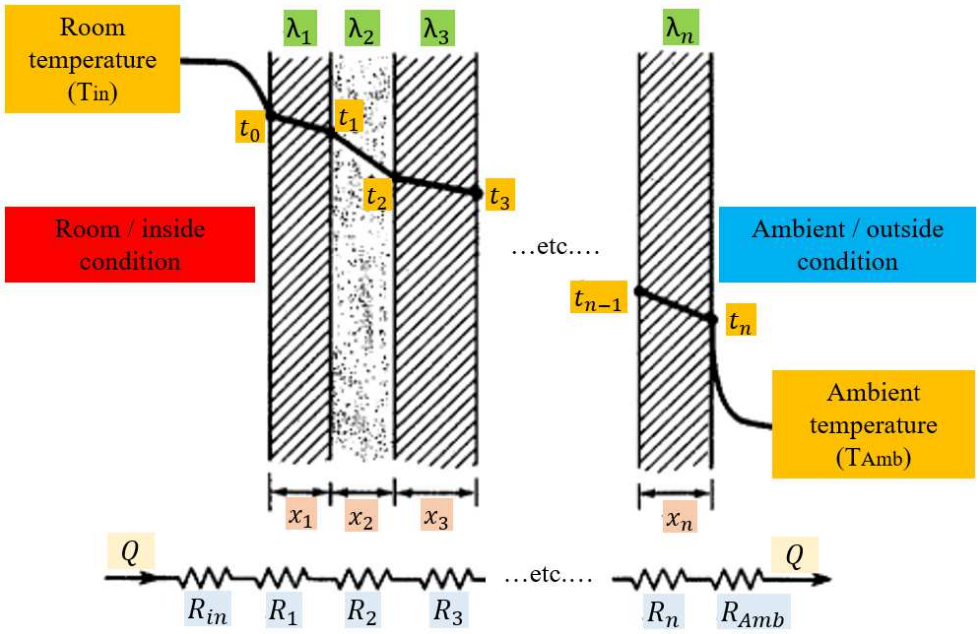

Fig. 3-9. Thermal resistance and heat flow through the masonry wall layers (Kutz, M. 2006).

In principle, thermal resistance (R) is the reciprocal of the total thermal transmittance or heat transfer coefficient (U) for unit area, therefore

$$U = \frac{1}{R_{total}} = \frac{1}{R_{in} + \mathbf{\Sigma}\frac{x}{\lambda} + R_{Amb}} \tag{3.12}$$

where R_{Total} is total thermal resistance [m^{2}K/W], R_{in} is the resistance of the internal surface [W/m^{2}K], R_{Amb} is the heat transfer coefficient of the outer surface [W/m^{2}K].

Regulation which are in use, for the calculation of total thermal transmittance or heat transfer coefficient (U) are highlighted below:

- The ISO 10077-1:2018 - (Thermal performance of windows, doors and shutters — Calculation of thermal transmittance — Part 1: General), specifies methods for the calculation of the thermal transmittance of

windows and pedestrian doors consisting of glazed and/or opaque panels fitted in a frame, with and without shutters.

- UNI EN ISO 6946:2018 - (Building components and building elements - Thermal resistance and thermal transmittance - Calculation methods).
- UNI/TR 11552:2014 - The technical report provides the main thermophysical parameters (thermal transmittance, air thermal capacity and periodic thermal transmittance) of the opaque components of the envelope most used in existing buildings. These parameters can be used for energy assessments of existing buildings in the absence of more detailed information on the materials that make up the structure.

While the reference of thermal conductivity (λ) values of the of homogeneous materials can be found in the UNI 10351: 1994 and UNI EN ISO 10456: 2008 standards.

Italian Ministry of Economic Development (IMED 2015) provides the regulation for the application of the methodologies for calculating energy performance and defining the prescriptions and minimum requirements for buildings.

Which also includes the minimum requirements values of the thermal transmittance/heat transfer coefficient (W/m^2K), particularly designated for each climate zones (Table 3-3 and Table 3-4) and the details could be found in Inter-Ministerial Decree 26 June 2015.

As obliged by the decree, Table 3-3 represents the required thermal transmittance/ heat transfer coefficient (W/m^2K) requalification values for the existing buildings. The values highlighted in the Tables are updated and are in use from 01/07/2021.

Table 3-3. According to IMED 2015 the thermal transmittance/heat transfer coefficient (W/m²K) reference value for requalification (existing buildings).

Climate zones	Opaque vertical structures	Opaque horizontal structures/Roof	floors	doors and windows
A	0.40	0.32	0.42	3.00
B	0.40	0.32	0.42	3.00
C	0.36	0.32	0.38	2.00
D	0.32	0.26	0.32	1.80
E	0.28	0.24	0.29	1.40
F	0.26	0.22	0.28	1.00

Similarly, Table 3-4 represents the required thermal transmittance/ heat transfer coefficient (W/m²K) requalification values for the newer constructions. According to the decree these values are to be followed from 1 January 2019 by all public buildings and from 1 January 2021 by all other buildings.

Table 3-4. According to IMED 2015 the thermal transmittance/ heat transfer coefficient (W/m²K) reference value for new constructions.

Climate zones	Opaque vertical structures	Opaque horizontal structures/Roof	floors	doors and windows
A	0.43	0.35	0.44	3.00
B	0.43	0.35	0.44	3.00
C	0.34	0.33	0.38	2.20
D	0.29	0.26	0.29	1.80
E	0.26	0.22	0.26	1.40
F	0.24	0.20	0.24	1.10

4. Physical and mechanical characterization of raw jute fibers, jute fiber threads and jute diatons

The main objective of this research work is to formulate a technical solution for thermo-structural retrofitting or upgrading of existing/new masonry by using the jute fiber composite mortar and jute net i.e., Natural Fiber Textile Reinforcement Mortar (NFTRM).

Before accomplishing the aforementioned objective, in Phase I the research and analysis was conducted at the material level. The physical and mechanical behaviors of three jute products: (i) raw fibers, (ii) threads and (iii) diatons (Fig.4-2) were studied in detail.

This chapter reports on the geometric properties of the aforesaid jute fiber products (raw fibers, threads and diatons) in terms of length, size, cross-section, density etc., as well as the physical property of the same products (raw fibers, threads and diatons) was determined in terms water absorption capacity.

Further, the durability of the jute threads was evaluated under three environmental conditions, represented with respective aging protocol. This was done to imitate the threads exposure to different natural conditions. Later, their mechanical properties were evaluated through tensile tests, and these values were compared with the tensile test values obtained for the untread threads.

Thereafter, the mechanical property of the jute diatons was evaluated through tensile tests. Later these jute diatons to be used for the structural upgrading.

All the tests were conducted in the Material Testing Laboratory of the University of Cagliari, Italy and the Strength Laboratory of the University of Salerno, Italy. While the information gained in the Phase I have been used in the subsequent phases.

4.1 Materials

The raw jute fibers (Fig. 4-1) and threads (Fig. 4-6) are directly collected from the farmers of the West Bengal, India. These materials are handcrafted products and are not subjected to any pre-treatment.

4.1.1 Raw jute fibers

The raw jute fiber type considered in this study is generally referred to as Bangla Tosha - *Corchorus olitorius* (golden shine), with original lengths found to be between 3 and 4 meters (Fig. 4-1). while the diameter measured randomly found to be 0.08 mm on average.

Fig. 4-1. A bunch of Jute fibers.

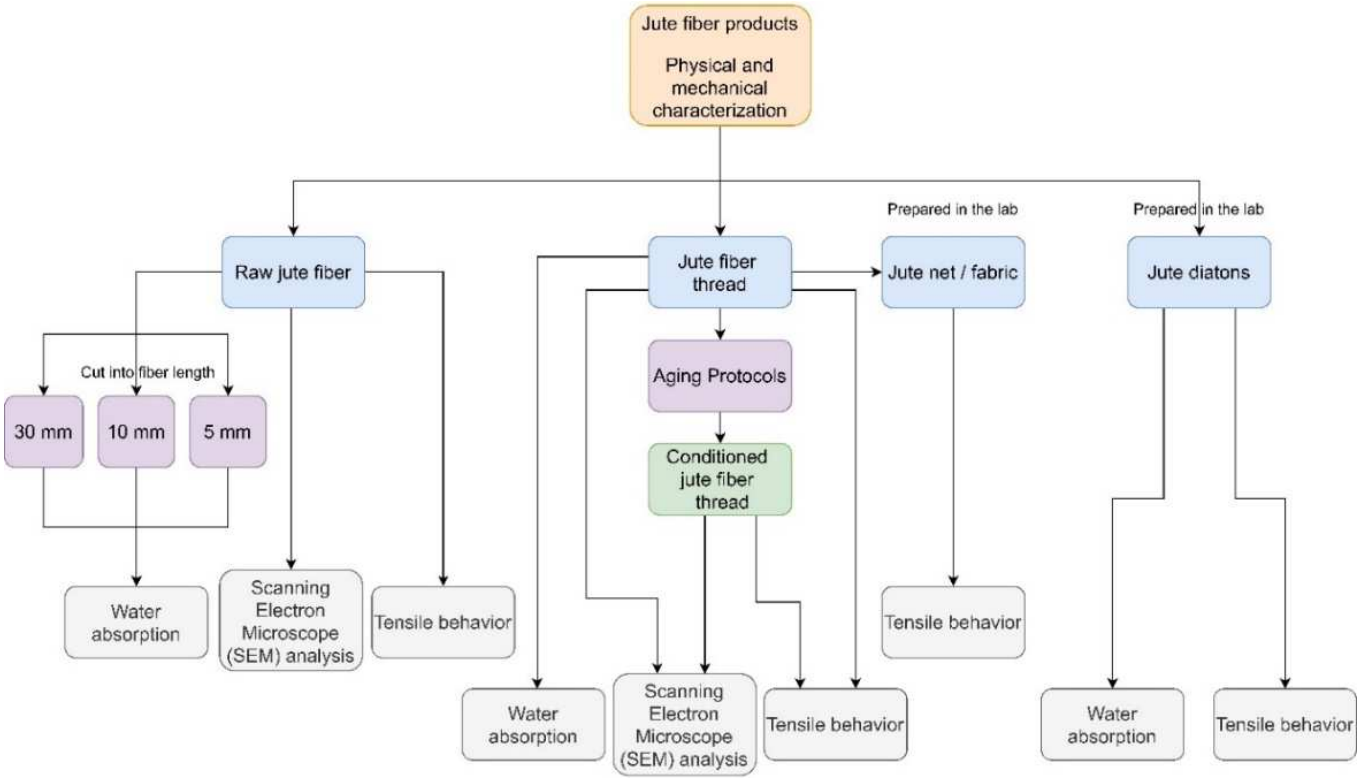

Fig.4-2. Jute fiber products tests scheme.

The present work considers mainly three jute products: raw fibers, threads and diatons (Fig. 4-2). The jute diatons and jute net-fabrics were prepared using the raw jute fibers and jute fiber threads respectively. The physical characteristics and mechanical behavior of the raw jute fibers, threads and diatons were determined by water absorption tests and tensile strength tests respectively (Fig. 4-2).

Three type jute fiber lengths of 30 mm, 10 mm and 5 mm were manually cut from the original long fibers. Fig.4-3 and Fig. 4-4 present the 30 mm fiber cutting process.

(a): Fiber cutting process 30 mm

(b):30 mm chopped fiber

Fig.4-3. Manual cutting process for jute fibers.

These fiber samples were later soaked in water to measure their water absorption capacity. This was done to determine the amount of water would be necessary in the second phase to prepare the mortar matrices of the jute-fiber-strengthened composite systems.

(a): 30 mm

(b): 10 mm

(c): 5 mm

Fig.4-4. 10 grams of chopped jute fibers.

Fig.4-5 presents the SEM pictures of the jute fibers captured at 500X and 1500X magnification, highlights the irregular pattern of natural jute fibers.

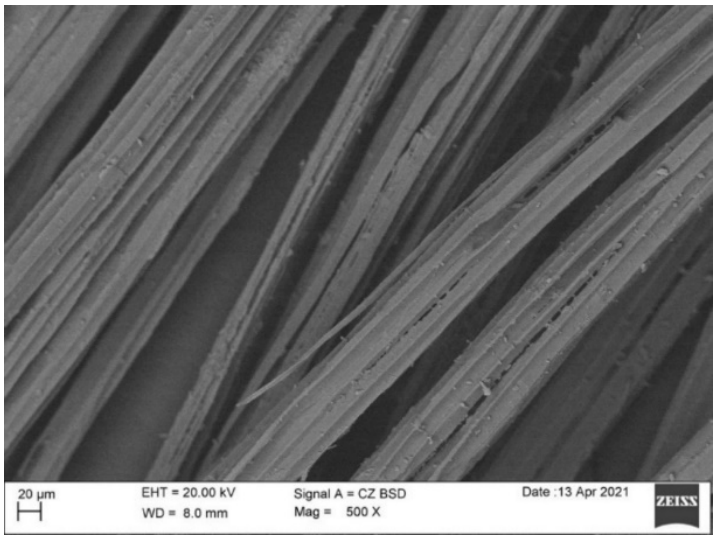

(a): 500X magnification

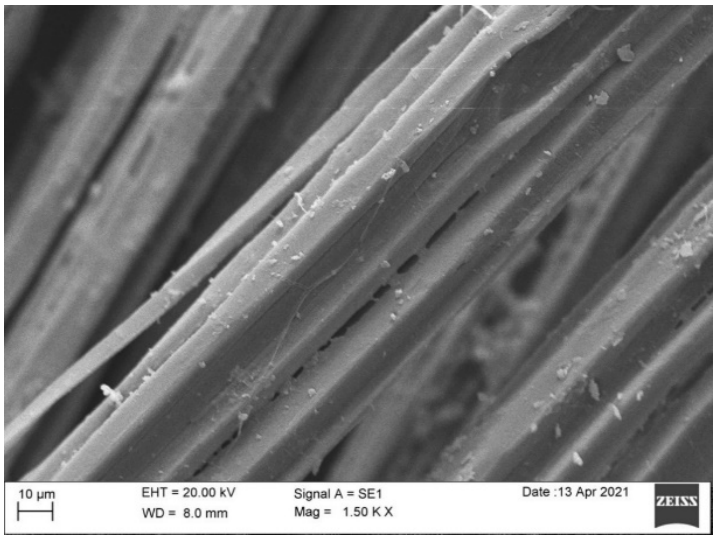

(b): 500X magnification

Fig.4-5. SEM images of jute fibers.

4.1.2 Jute fiber threads

The 3 yarns jute threads fabricated with the same Bangla Tosha jute fiber, as described above were imported from India. Two classes of threads with different diameters (Fig. 4-7) were used for tensile tests; the thinner thread type has been

denoted as 1mm class while the thicker thread has been labeled as 2 mm class. While Fig. 4-6 presents class 1mm jute thread lot.

Fig. 4-6. Jute threads

These threads were nominated as the Class 1 mm in Fig.4-7 (a) and Class 2 mm in Fig.4-7 (b), based on the measured diameters.

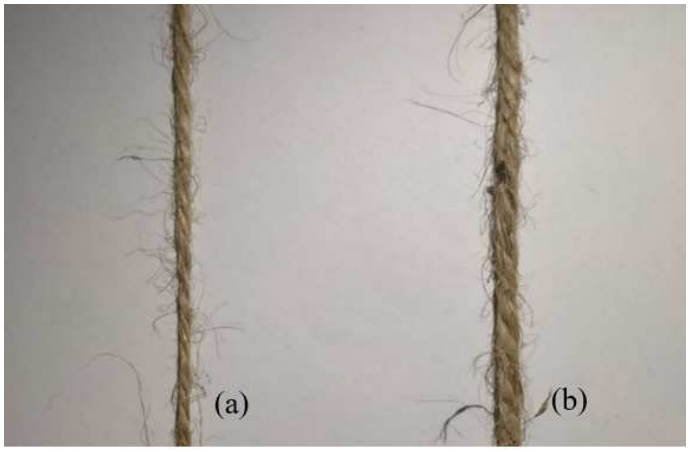

(a): class 1 mm *(b): class 2 mm.*

Fig.4-7. Two classes of jute threads.

Fig. 4-8 presents the 3 yarns jute threads sample of the Class 1 mm.

Fig.4-8. 3 yarns jute threads sample.

The geometric properties these two types of threads (Class 1 mm and Class 2 mm) were determined in terms of the yarn diameter and the TEX (reported in Table 4-1) by using a total of 20 samples of 35cm length (in average). These samples were cut randomly from both types of thread lots.

Table 4-1. Jute thread geometric properties

	average yarn diameter		yarn weight	
	mm	Co.V	tex	Co.V
Class 1 mm	1.17	6.39%	1118.74	12.04%
Class 2 mm	2.15	5.59%	2140.41	12.91%

A total of 5 thread samples from each lot (1mm class and 2mm class) were used for water absorption tests (Fig.4-19). While 15 thread samples of 1mm class and 2 mm class, respectively were used for the aging treatment and subsequently subjected to tensile tests. Moreover, another 5 untreated thread samples from both classes were used as reference and they were subjected to tensile tests only.

4.1.3 Jute diaton(s) fabrication

Jute diatons (Fig.4-9) are intended as connectors aimed to improve the mechanical performance of masonry walls. Whereas the mechanical performance of these diatons were also determined by tensile test.

Approximately 25 grams of raw jute fiber have been used to fabricate a single diaton sample. The diatons are made of the same raw jute variety as described in the Section 2.1.1.

Fig.4-9. Jute diaton

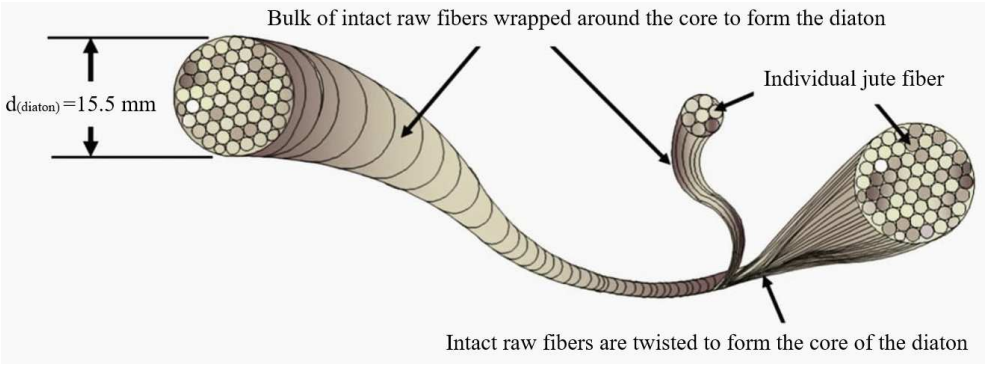

Fig. 4-10. Diaton fabrication scheme

The diatons were fabricated by wrapping long raw fibers around the core fibers. While the core of a diaton was made of 65cm long twisted raw fibers as in the Fig. 4-10. The diaton diameter was found to be 15.5 mm (9.68% Co.V.). Therefore, these diatons were nominated under class 15 mm category.

4.2 Methods

The durability of the jute threads i.e., the effect of different aging conditions (Table 4-2) on the strength of these threads were determined by treating and exposing them to different aging conditions (Table 4-2.) and followed by determining their tensile strength.

Table 4-2. presents the characteristics of these aging protocols. Three different solutions were prepared:

- solution 1 (deionized water) was obtained with 2 liters of pure deionized water (Fig.4-12a);
- solution 2 (salty solution) was prepared by mixing 35g/l of salt with 2 liters of deionized water (Fig.4-12b)
- solution 3 (alkaline solution) was prepared by mixing 1.05 (g/l) of $NaHCO_3$, 9.724 (g/l) of Na_2CO_3 and 6 drops of NaOH in 0.1 normal solution respectively with 2 liters of deionized water, to achieve 9.5 pH level (Fig.4-11 and Fig.4-12c).

Threads were cut randomly from the lot, and all samples measured to be approximately 35 cm (with Co.V. of 5.95%) long.

Five thread samples, each from class 1 mm and class 2 mm, were soaked inside three different solutions i.e., deionized water, salty solution and alkaline solution, respectively. All these thread samples were left inside the solutions (Fig.4-12) for a total period of 42 days, i.e., approximately for 1000 hours (Fig. 4-13).

Threads placed in the deionized water were labeled as D1 and D2 for the class1 mm and the class 2 mm threads, respectively. While for those threads were placed in the salty solution were labeled as DS1 and DS2 for the class1 mm and the class 2 mm threads, respectively. Similarly, samples places in the alkaline solution were labeled as DA1 and DA2 for the class1 mm and the class 2 mm threads, respectively.

Table 4-2 Aging protocol solutions

	Solution 1 Deionized water (DW)	Solution 2 Salty solution (DS)	Solution 3 Alkaline solution (DA)
Deionized water	2 liters	2 liters	2 liters
NaCl	x	70 g	x
$NaHCO_3$	x	x	2.10 g
Na_2CO_3	x	x	19.45 g
NaOH	x	x	6 drops in 0.1 N solution

Fig.4-11. Case 3 - Preparation of alkaline solution with 9.5 pH

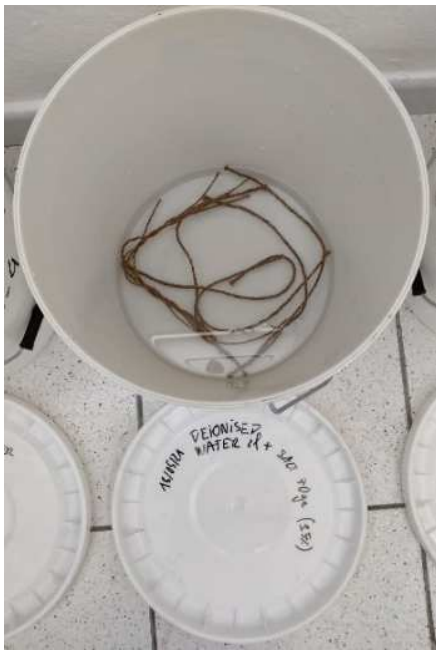

(a): Deionized water

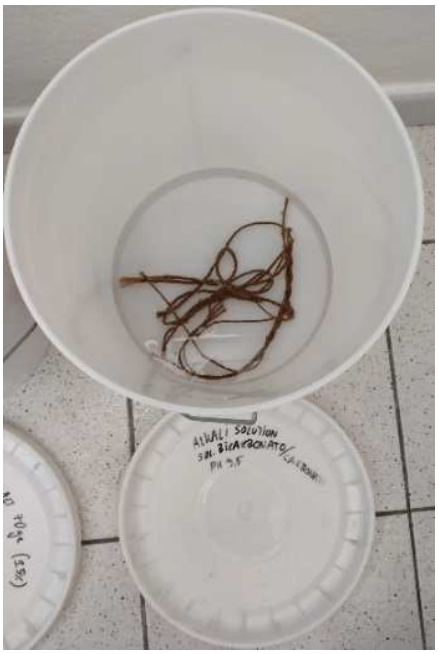

(b): Salty solution

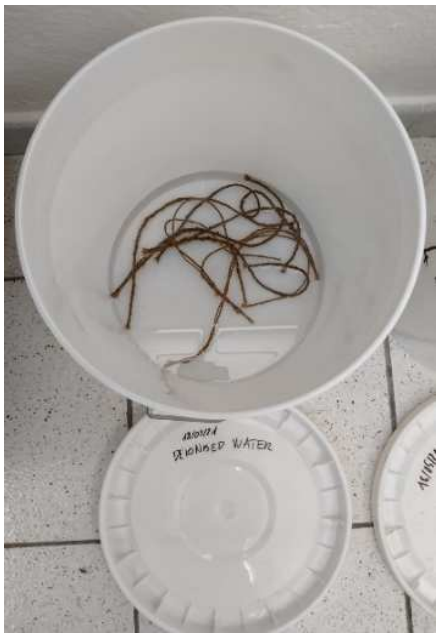

(c): Alkaline solution

Fig.4-12. Jute treads placed (1st day)

(a): Treated in deionized water

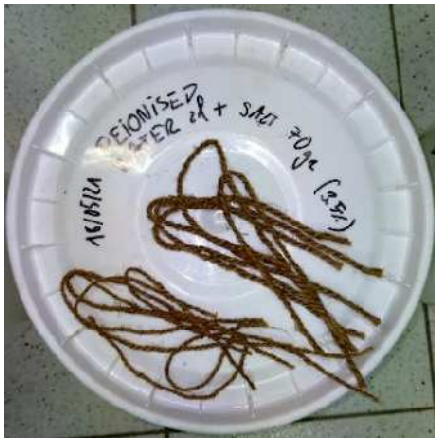

(b): Treated in salty solution

(c): Treated in alkaline solution

Fig.4-13. Jute treads after 1000 hours treatment and drying

Table 4-3 presents the geometric properties of the 20 jute fiber thread samples (un-treated and treated) from both the classes (class 1 mm and class 2 mm) which have been used for the tensile strength tests. These measurements have been done before placing the samples in the ageing solution, for all those 15 samples of each class for the ageing treatment.

Table 4-3 Raw jute threads and treated Jute threads diameters and densities

Nomenclatures	Thread diameter	Thread density	Nomenclatures	Thread diameter	Thread density
Class 1 mm threads	mm	g/cm^3	Class 2 mm threads	mm	g/cm^3
Raw jute fiber thread, without any treatment					
N1.1	1.33	0.87	N2.1	2.01	0.94
N1.2	1.14	1.25	N2.2	2.00	0.73
N1.3	1.22	0.96	N2.3	1.86	0.81
N1.4	1.07	1.05	N2.4	1.91	0.77
N1.5	1.18	1.01	N2.5	1.85	0.82
Jute fiber threads immersed in deionized water for 1000 hours					
D1.1	1.28	0.76	D2.1	1.72	0.76
D1.2	1.21	0.79	D2.2	2.08	0.55
D1.3	1.21	0.94	D2.3	2.30	0.48
D1.4	1.08	1.08	D2.4	1.99	0.56
D1.5	1.21	1.12	D2.5	2.32	0.56
Jute fiber threads immersed in Salty solution for 1000 hours					
DS1.1	1.28	0.70	DS2.1	1.82	0.83
DS1.2	1.21	1.08	DS2.2	1.94	0.71
DS1.3	1.21	1.11	DS2.3	2.10	0.62
DS1.4	1.08	1.24	DS2.4	2.10	0.56
DS1.5	1.21	0.87	DS2.5	2.13	0.70
Jute fiber threads immersed in alkaline solution for 1000 hours					
DA1.1	1.39	0.90	DA2.1	1.87	0.77
DA1.2	1.21	1.06	DA2.2	2.20	0.58
DA1.3	1.18	0.97	DA2.3	2.05	0.64
DA1.4	1.16	1.21	DA2.4	1.94	0.74
DA1.5	1.10	1.16	DA2.5	2.01	0.59

The Fig.4-14 (a) and (b) show the SEM micrographs of the examined class 1mm fiber at 500x and 1000X magnification, respectively.

(a):

(b):

Fig.4-14. SEM images of untreated class 1 mm threads (N1)

Similarly, Fig.4-15 (a) and (b) show the SEM micrographs of the examined class 2mm fiber at 500x and 1000X magnification, respectively.

(a):

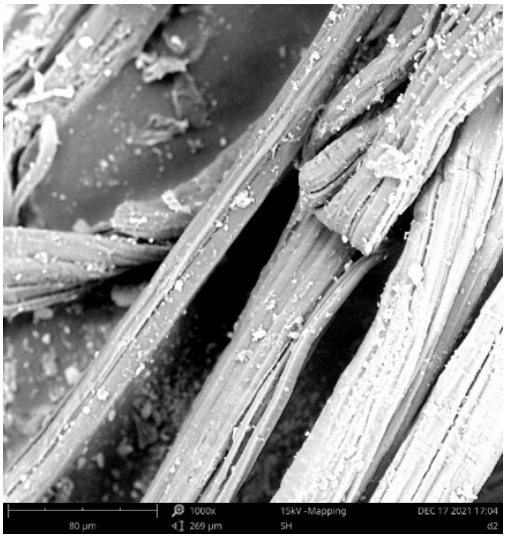

(b):

Fig.4-15. SEM images of untreated class 1 mm threads (N2)

4.3 Experimental results: physical properties

4.3.1 Jute fibers

Raw jute fibers of three different lengths 30 mm (Fig. 4-16), 10 mm and 5 mm (Fig. 4-4), respectively, were used for the water absorption tests. In order to have real worksite/onsite conditions test data, the tests were conducted under normal environmental temperature and humidity, and no modifications in the physical state of the fibers have been made. Therefore, the fibers were not subjected to pre-drying or any pre-treatment. This was done to determine the quantity/amount of water that would be necessary (for different percentages and sizes of jute fiber) while preparing the composite mixtures in the second phase of the project.

A total of 5 tests were performed on 10 g of each type of fiber lengths (30 mm, 10 mm and 5 mm) and the test results are presented in the following Section.

The chopped fibers (30 mm, 10 mm and 5 mm) were immersed in water for a total period of 3 hours.

Dry fiber masses (W_{dry}) of the 30 mm (Fig. 4-16.a), 10 mm and 5 mm fibers were measured before putting the fibers inside the water. At an interval of every 30 mins, the wet mass (W_{wet}) (as in (Fig. 4-16.c) of each fiber type were measured. Before every W_{wet} measurement, extra water was drained by keeping the fibers in fine mesh strainers for about 2 mins. All fiber type (30 mm, 10 mm and 5 mm) reached its saturation point nearabout 2 hours after the first immersion and notably after this point, fibers unable to absorb or trap any more water.

The jute fibers water absorption WA is defined by equation (1) as in Momoh et al. (2017):

$$WA = \frac{W_{wet} - W_{dry}}{W_{dry}} \times 100\ (\%) \tag{4.1}$$

where W_{dry} is the fiber weight before immersion while W_{wet} fiber weight after immersion.

(a): Dry jute fibers

(b): Jute fibers socked in water

(c): wet jute fibers

Fig.4-16. Water absorption test.

Interestingly, the water absorption rate (which also includes the extra trapped water) increased rapidly until 2 hours (the point corresponding from W_{dry} to 120 mins

in the Fig.4-17). Moreover, the water imbibition remained quasi constant from 120 mins to 180 mins, averaging in the range from 58.87 g to 58.89 g for 30 mm, from 81.38 g to 81.38g for 10 mm and from 91.78 g to 91.84 g for 5 mm, respectively. Therefore, it can be said that the fibers reach the saturation point and these results are comparable to those obtained by Formisano et al. (2020).

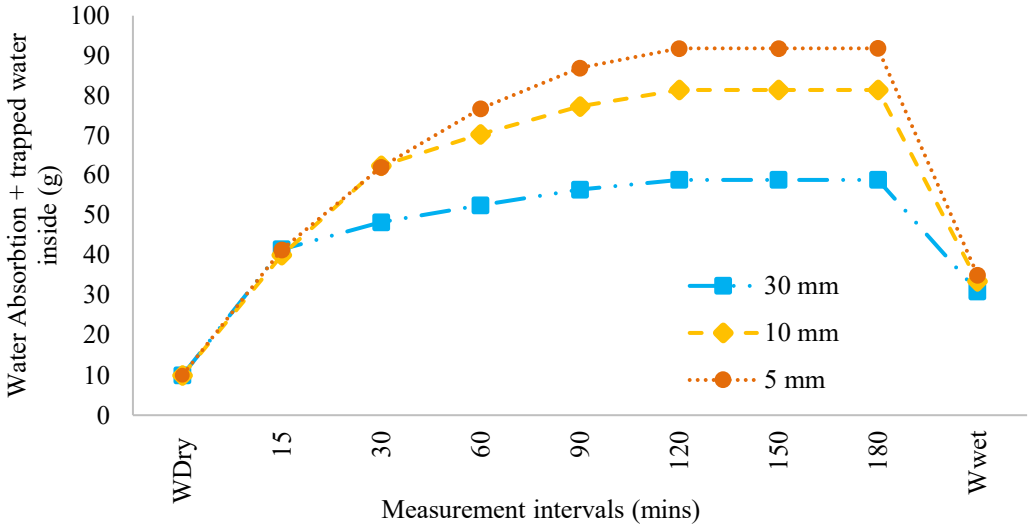

Fig.4-17. Jute fibers water absorption

Based on these observations, it is worth highlight that the fibers not only absorb water singularly by itself, but they have the tendency to stick to each other due to electrostatic force also in wet state, similar alike happen in dry state.

It has been noticed that whenever fibers come in contact with water, the fibers have the tendency to stick together to form fiber-balls (Fig.4-18). These fiber bundles as a whole behave exactly like a sponge and they too soak and trap extra additional water inside its cavity. With the increase in fiber amount, the tendency to trap water trap water also increase. It has been observed that 10 grams of jute fiber with 5 mm length can trap 10 g more water when compared to 10 mm fibers, and 33 g when compared to 30 mm fibers (Fig.4-17).

Fig.4-18. Fiber-balls formed as fibers come in contact with water.

After the fibers were taken out from water after 3 hours from the time of immersion (the point corresponding to 180 min in the (Fig.4-17), the additional trapped water was squeezed out (the point corresponding to W_{wet} in the Fig.4-17).

The W_{wet} (g) masses were measured and it has been found that the 30 mm, 10 mm and 5 mm jute fibers can absorb on average 210% (average); 235% (average) and 250% in weight, respectively, when the values were compared with respect to its dry mass (W_{dry}).

Therefore, these observations would be used in the next phase and these obtained values would be applied during the jute fiber composite preparation.

4.3.2 Jute fiber threads

Five samples of class 1 mm and class 2 mm of approximately 7 cm long (Fig.4-19) were cut randomly from each thread class lot. Notably both types of jute threads have shown a similar absorption trend. In this case, the water absorption saturation point reached after 150 mins from the time of immersion.

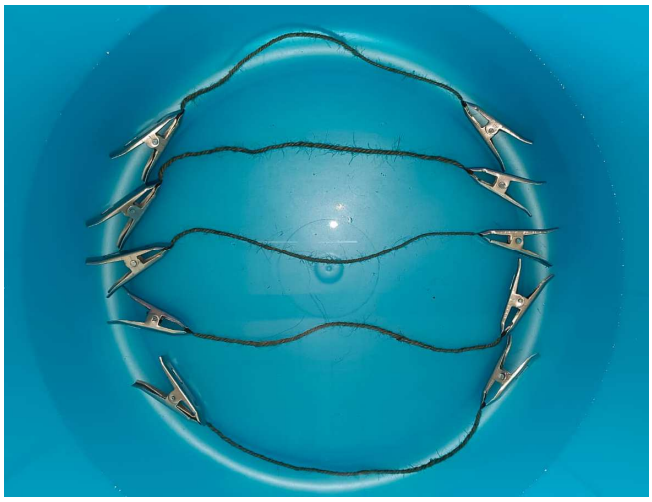

(a): Class 1 mm fibers immersed in water.

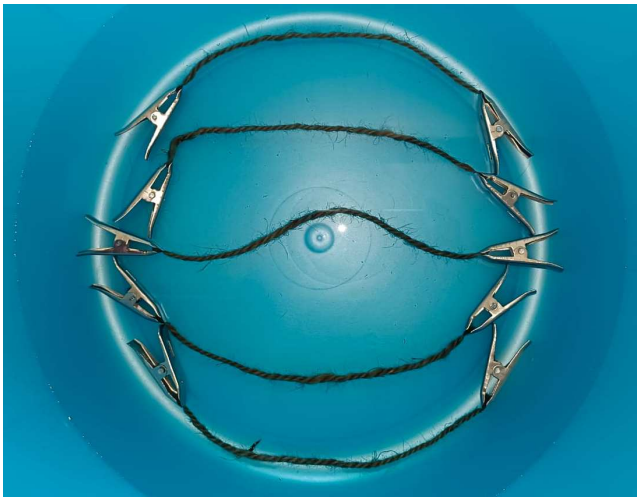

(b): Class 2 mm fibers immersed in water.

Fig.4-19. Threads water absorption tests

Finally, after 3 hours, both type of threads was taken out from the water (the point corresponding to 180 min, in the Fig.4-20. Before measuring W_{wet} (g) masses the additional trapped water was squeezed out (the point corresponding to W_{wet}, in Fig.4-20 from each sample.

The water absorption percentage obtained using Equation 4.1, for the class 1mm thread group equal to 197.89% in average and for class 2 mm thread group is equal to 209.59% in average.

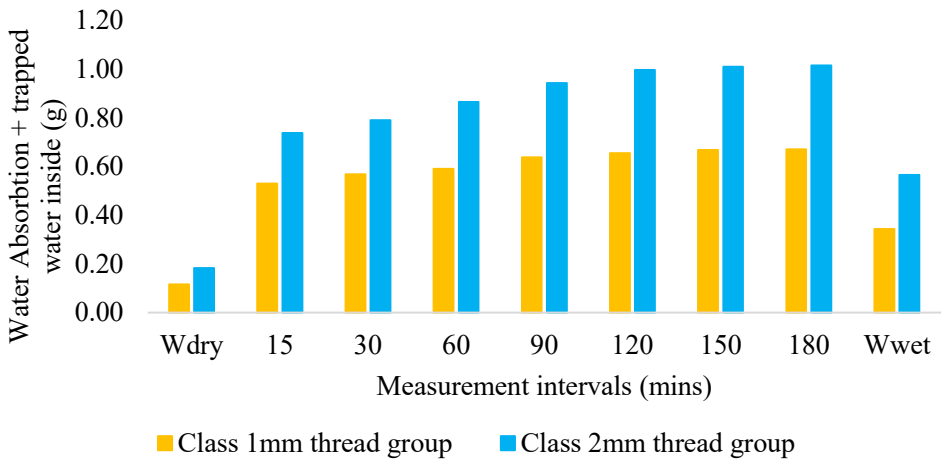

Fig.4-20. Jute threads water absorption.

4.3.3 Jute fiber diatons

The water absorption tests were conducted on five diatons samples of approximately 17 cm long. These samples were cut randomly form five original diatons.

In this case too, the water absorption saturation period was observed almost after 150 mins from the time of immersion (Fig.4-21).

Before W_{wet} (g) mass was measured, the additional trapped water was squeezed out (the point corresponding to W_{wet}, in the Fig.4-21.

The calculation done according to Equation 4.1 and it has demonstrated that diatons can absorb on average 183.46% of water with respect to its dry mass (W_{dry}).

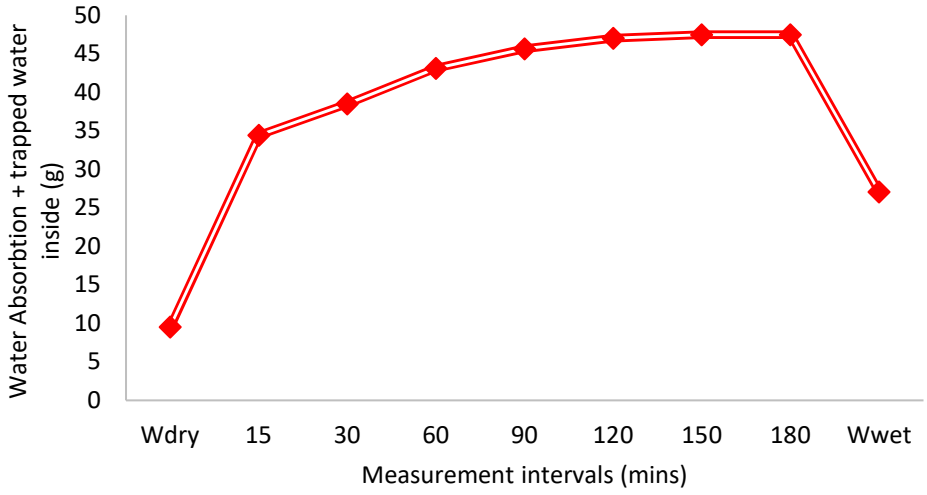

Fig.4-21. Jute diatons average water absorption.

4.4 Experimental results: mechanical characteristics of the jute products

4.4.1 Fibers

A total of 12 individual jute (Fig.4-22) fibers were collected randomly from the raw and intact jute stock. The tested jute samples measured to be 10 cm long (with Co.V of 2.64%) and have 81.08 μm (with Co.V. of 20.94%) of diameter (Fig.4-23.a).

Tensile strength tests were conducted to determine the strain energy (U), tensile strength (ft) and axial strain/deformation ratio (ε) of the jute fiber.

A digital force gauge (Fig.4-23.b) was used for the tensile tests, and it has maximum capacity of 50 N and displacement rate of 0.5 mm/min. The fibers used for these tests are raw and no pre-test treatments were done.

Fig.4-22. A total of 20 jute fibers used for tensile strength tests.

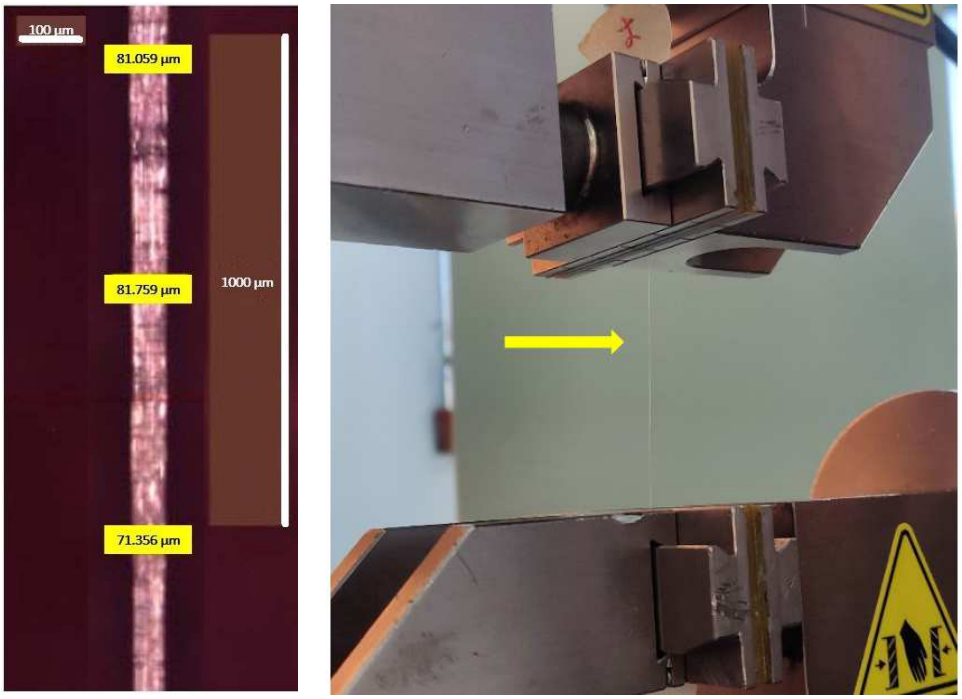

(a): Fiber diameter *(b): Sample JF7*

Fig.4-23. (a) Scanning electron microscopy (SEM) analysis and Tensile strength test.

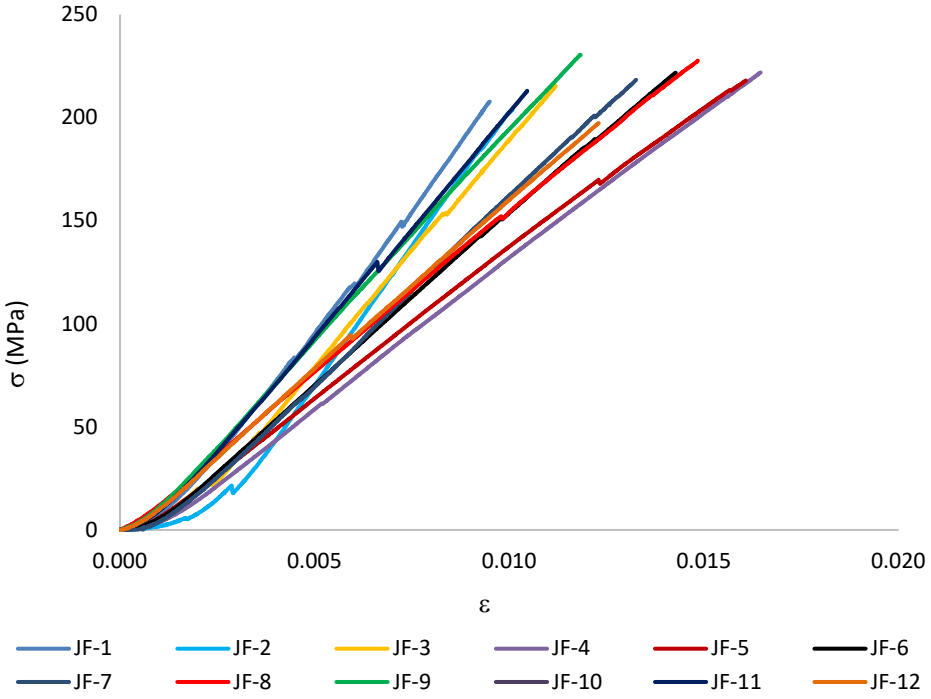

Fig.4-24. Tensile stress-strain diagrams of the jute fiber

Fig.4-24 shows an initially narrower branch of the stress-strain curve due to the fact that the fibers were tested in an initially slack configuration.

The minimum and minimum tensile loads were obtained, 0.59 N (sample JF-1) and 1.96 N (sample JF-4), respectively. While maximum strain energy of equal to 1.54 N.mm and the maximum axial strain of 0.017 were found for the sample JF-4.

The mechanical properties of the tested fibers are present in Table 4-, where the strain energy has been determined by calculating the area beneath the stress-strain curves presented in Fig.4-24.

The Young Modulus has been estimated by calculating the ratio between the maximum stress and the corresponding strain.

Table 4-4.Mean mechanical properties of jute fiber samples.

Strain energy (U)		Tensile strength (f_t)		Maximum Axial strain (ε)		Young's modulus (E)	
Mean Nmm	CoV %	Mean MPa	CoV %	Mean	CoV %	Mean GPa	CoV %
0.77	58.85	215.11	4.42	0.0131	19.08	16.97	17.89

4.4.2 Fiber threads

Displacement controlled tensile tests have been conducted to determine the mechanical properties of the untreated and treated jute samples and the strain energy (U), tensile strength (f_t) and axial strain/deformation ratio (ε) of these fiber samples were determined, according to the ISO 2062:2009 (Fig. 4-25 and Fig. 4-26). A total of 20 thread samples from both classes (Fig.4-7) were tested.

A total of 5 samples were not treated (raw natural state), while other 15 samples were subjected to aging protocols as described in the previous section.

For the tensile tests a *Metrocom* universal machine was used and it has maximum load capacity of 735 N, a sensitivity/scale division of 2.5 N and a load rate of 2mm/min.

Conversely, a Baoshishan ZP-200N digital force gauge was used to measure the tensile force. It has a capacity of 500 N with ± 0.2% of accuracy and featured with display (resolution of 0.1 N.

A linear variable displacement transducer (LVDT) was used to measure the fiber samples elongation. The instrument has the following characteristics: max. range of 50 mm, nominal sensitivity of 2 mV/V and linearity ±<0.10 % of span.

Also, for threads the strain energy has been evaluated by calculating the area underneath the stress-strain curves. While the ratio between the maximum stress and the corresponding strain has been considered to evaluate the Young Modulus.

Fig. 4-25: Three yarns class 1 mm thread, after complete failure

Fig. 4-26: Three yarns class 1 mm thread, after complete failure

The synthesis of the tensile test results is presented in the Table 4-5.

Interestingly, the reduction in strength and strain energy were observed when the samples from both classes (class 1 mm and class 2 mm) were treated in the salty solution for 1000 hours. These reductions found to be around 16% and 34% lower respectively for class 1mm thread samples and 20% and 26% lower, respectively, for class 2 mm thread samples, when compared with the untreated normal raw threads.

Similarly, when compared with the corresponding untreated threads the reduction in the strength and strain energy found to be 20% and 16% lower respectively for class 1mm thread and 8% and 12% lower, respectively, for class 2 mm thread, when the threads were treated in the alkaline solution for 1000 hours.

Table 4-5. Mechanical properties of jute threads samples tested in tension.

Thread type	Strain energy (U)		Tensile strength (f_t)		Maximum Axial strain (ε)	
	Mean kNmm	CoV %	Mean MPa	CoV %	Mean	CoV %
N1	1.03	34.59	112.45	26.16	0.07	11.71
D1	0.42	17.67	53.27	18.19	0.05	18.28
DS1	0.68	19.05	94.17	12.99	0.06	5.23
DA1	0.86	38.50	101.40	23.73	0.06	25.32
N2	2.05	10.86	56.95	9.73	0.12	29.78
D2	1.27	28.31	36.44	23.81	0.07	4.36
DS2	1.52	34.27	45.63	14.71	0.08	21.17
DA2	1.81	24.41	52.31	12.98	0.09	6.94

N = Normal; D = Deionized water; DS =Salty solution; DA = Deionized water and Alkaline solution

Moreover, the samples treated in the deionized water have demonstrated the worst performance when compared with the untreated samples and the reductions in the

strength and strain energy found to be significantly high being more than 50% for class 1mm thread and more than 35% for class 2 mm thread.

Interestingly the deionized water aging treatment has induced major damage to both classes of thread samples, as this damage was significantly low for both classes of thread samples treated in alkaline solution.

Although the explanation of the physic-chemical reasons which make deionized water the most harmful agent for the considered jute is complex and beyond the scope of this thesis, but it is worth highlighting that similar results have been obtained by other researchers (Zukowski et al. 2018, Ray et al. 2001, Bera et al. 2019).

Looking at the results in the Table 4-5, the scattering in values/data can be explained considering that these thread samples were handmade, therefore these samples quality is not constant.

The stress-strain diagrams for untreated and treated thread samples in three different solutions are shown, in the figures from Fig.4-27 to Fig.4-34.

In all cases the mechanical behaviors found to be almost linear elastic. While depending on the failure scenarios, it worth to mention that there could be a small ductility linked to the timing of each yarn collapse.

Three types of thread failure have been observed during the tensile tests.

1) The first mode implies the failure of all three yarns occurred together, for example in the sample N1.2 from the class 1 mm (Fig.4-27) and in the sample N2.3 from the class 2 mm (Fig.4-31).
2) The second mode consists of the failure in one of the three yarns and thereafter the failure occur in the other two or this phenomenon observed reversed; for example the sample D1.3 from the class 1 mm (Fig.4-28) and the sample D2.5 from the class 2 mm (see Fig.4-32).
3) The third mode was with failure occurring one after another at each single yarn; for example, the case of the sample DA1.3 in the class 1 mm (Fig.4-30).

Table 4-6. Threads Young's modulus

Thread type	Mean [MPa]	Co.V [%]
Class 1 mm	1454.15	20.00
Class 2 mm	531.05	10.66

Every singular thread from each class presents a quite similar elastic behavior. due to the fact that the Young's modulus of every sample from each thread class have shown quite similar to the average values of that respective class (Table 4-6).

The result of the tensile tests (Table 4-5) has demonstrated that the thinner thread samples (from the class 1mm) have shown better mechanical performance when compared with the thicker samples (from class 2 mm threads). Strain energy and maximum strain (Table 4-5) also have shown the similar trend.

Notably, untreated samples have demonstrated the optimum performance. While samples treated in deionized water are the worst performers (Table 4-7). Whereas in comparison to the standard construction materials, it should be highlighted the very high value of strain reached at collapse.

Table 4-7. Collapse loads

		Un-treated (N)	Deionized water solution (D)	Salty solution (DS)	Alkaline solution (DA)
		[N]	[N]	[N]	[N]
Class 1mm thread	Maximum	166.81	73.94	119.15	125.13
	Minimum	99.83	45.40	81.00	56.29
Class 2mm thread	Maximum	195.25	147.30	187.99	216.73
	Minimum	139.94	88.95	105.91	132.49

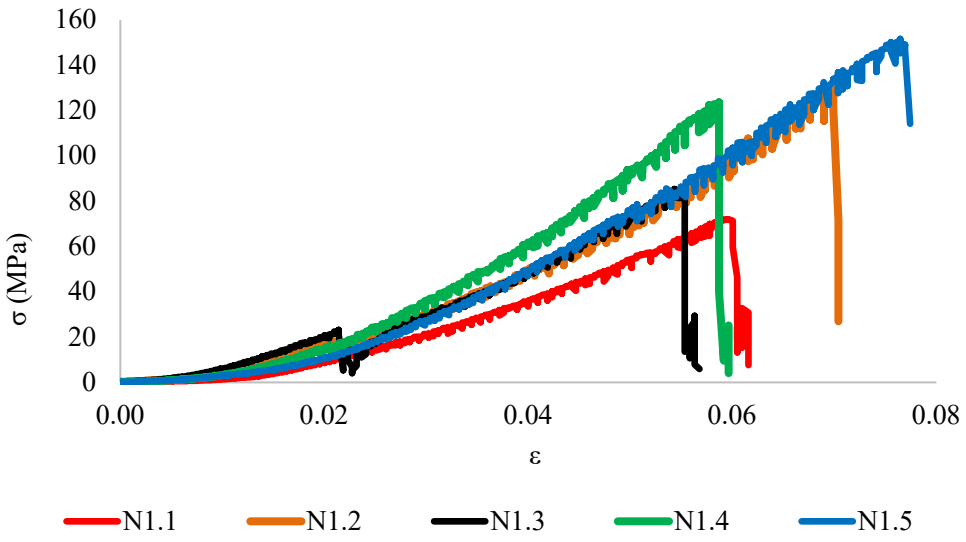

Fig.4-27. Tensile stress-strain diagrams of the jute fiber threads of N1 category with diameter class 1 mm, without any treatment.

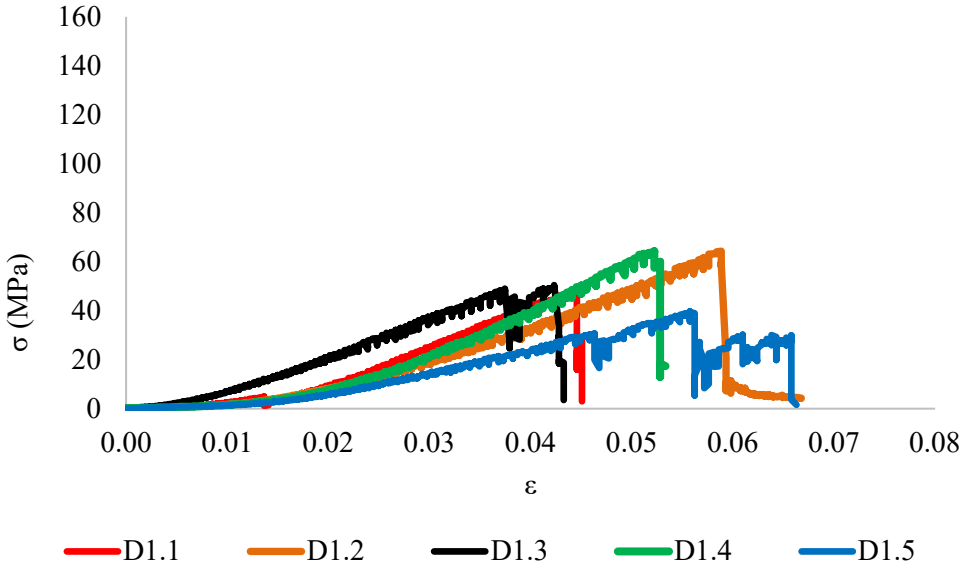

Fig.4-28. Tensile stress-strain diagrams of the jute fiber threads of D1 category with diameter class 1 mm, treated in deionized water.

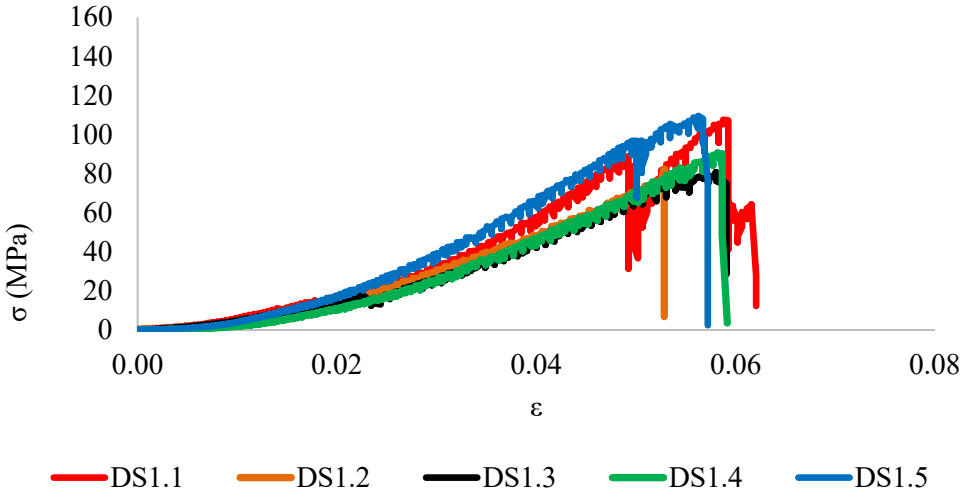

Fig. 4-29. Tensile stress-strain diagrams of the jute fiber threads of DS1 category with diameter class 1 mm, treated in salty solution.

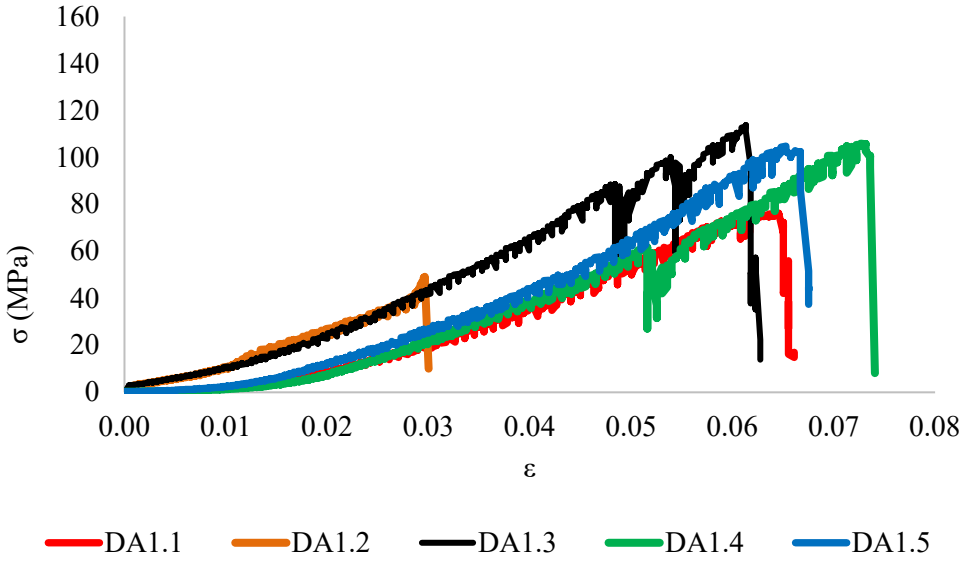

Fig.4-30. Tensile stress-strain diagrams of the jute fiber threads of DA1 category with diameter class 1 mm, treated in alkaline solution.

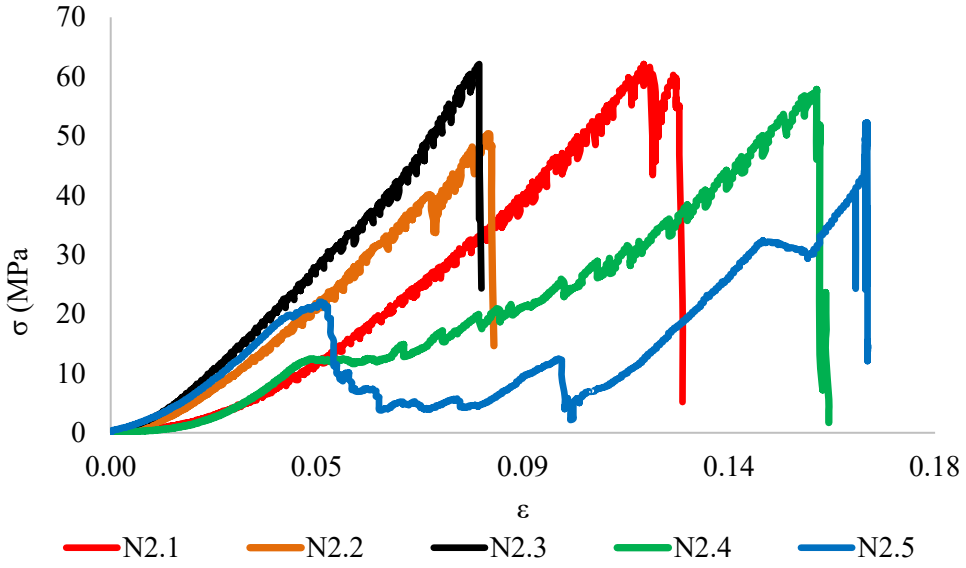

Fig.4-31. Tensile stress-strain diagrams of the jute fiber threads of N2 category with diameter class 2mm, without any treatment.

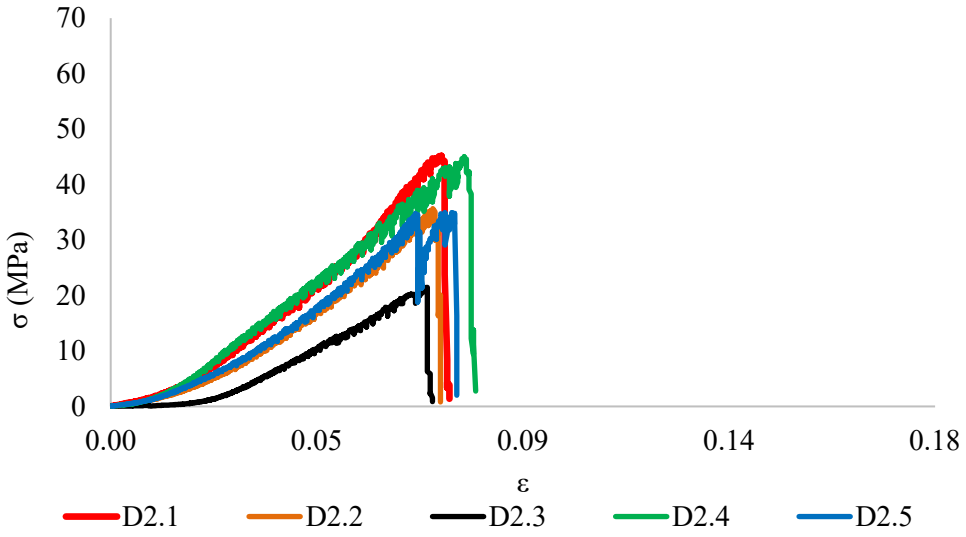

Fig.4-32. Tensile stress-strain diagrams of the jute fiber threads of D2 category with diameter class 2 mm, treated in deionized water.

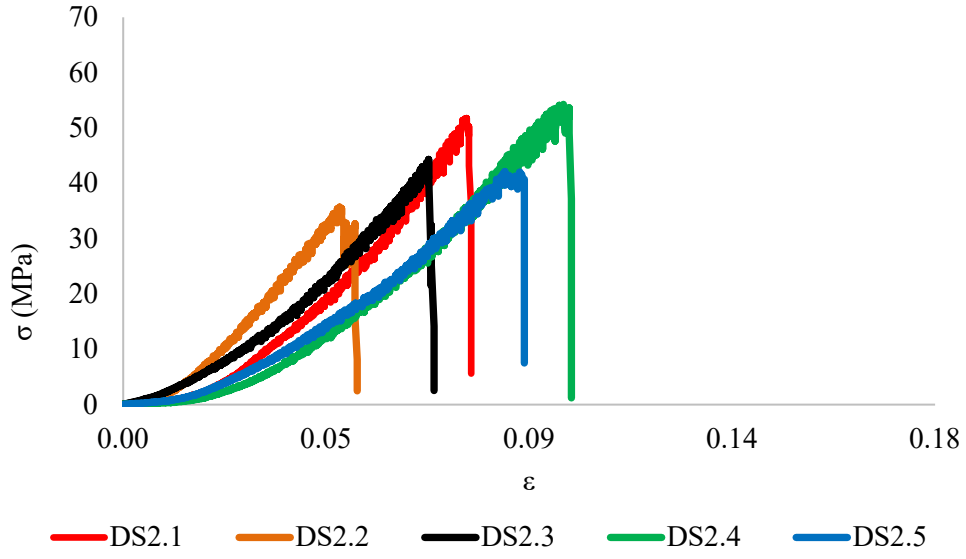

Fig.4-33. Tensile stress-strain diagrams of the jute fiber threads of DS2 category with diameter class 2 mm, treated in the salty solution.

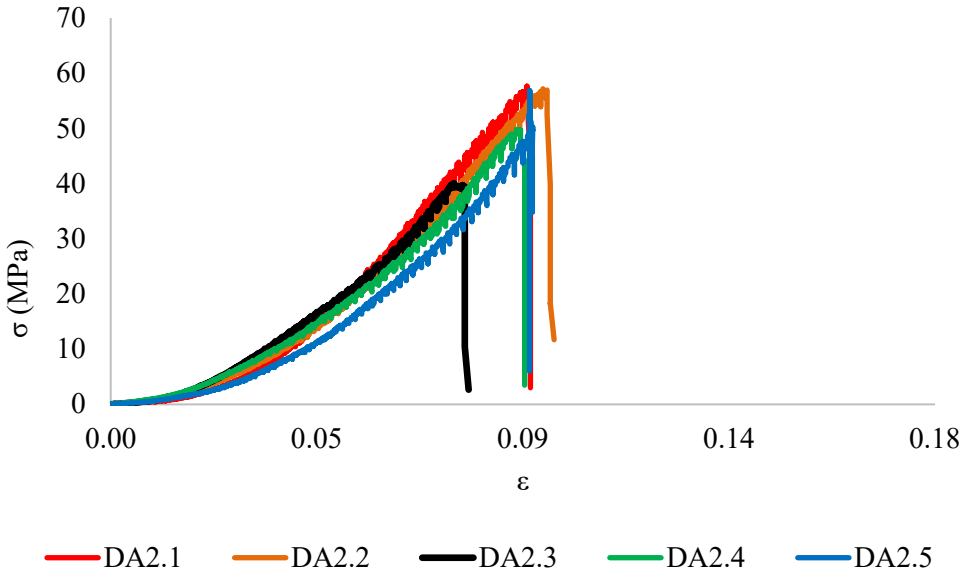

Fig.4-34. Tensile stress-strain diagrams of the jute fiber threads of DA2 category with diameter class 2 mm, treated in the alkaline solution.

4.4.3 Diatons

Jute diatons have been used for retrofitting or upgrading masonry walls in the third phase of this research work. Indeed, diatons were applied through walls to connect and grip the reinforcing nets applied on the wall external surfaces. At the same time, their application can further increase the wall shear resistance.

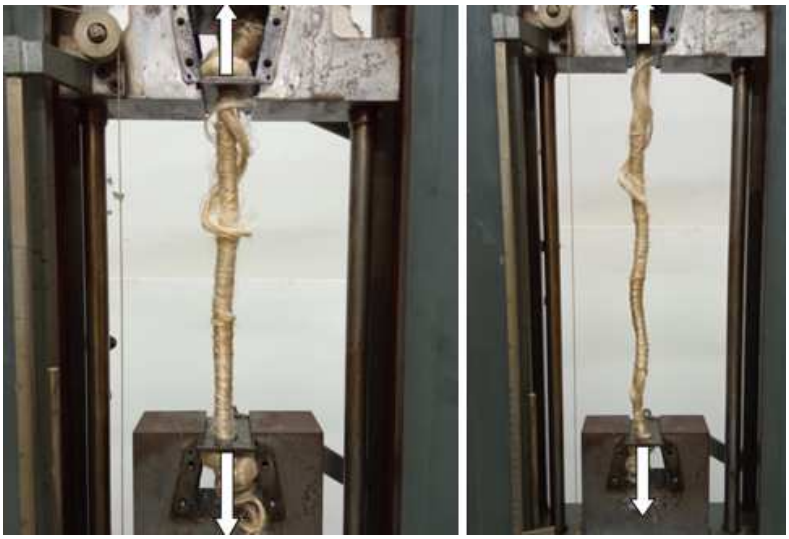

(a): before tensile test (b): after tensile test

Fig.4-35. Jute diaton (a)

A displacement-controlled tensile strength test was conducted on 5 diaton samples (specifications as described in Section 4.1.3) using Metrocom-2 universal machine (Fig.4-35). It has maximum load capacity, sensitivity/scale division and imposed displacement rate of 9.8 kN, 39 N and a of 0.5 mm/min, respectively.

The maximum tensile load was observed to be equal to 3.92 kN for Diaton-2, while the minimum of 2.09 kN for Diaton-4. The maximum strain energy found to be equal to 27.21 kNmm, for the Diaton-1. The maximum axial strain measured equal to 0.04, for the Diaton-1.

The specific mechanical properties of the diatons found to be lower, when compared with threads (Table 4-8). The strain energy has been evaluated calculating the area underneath the stress-strain curve.

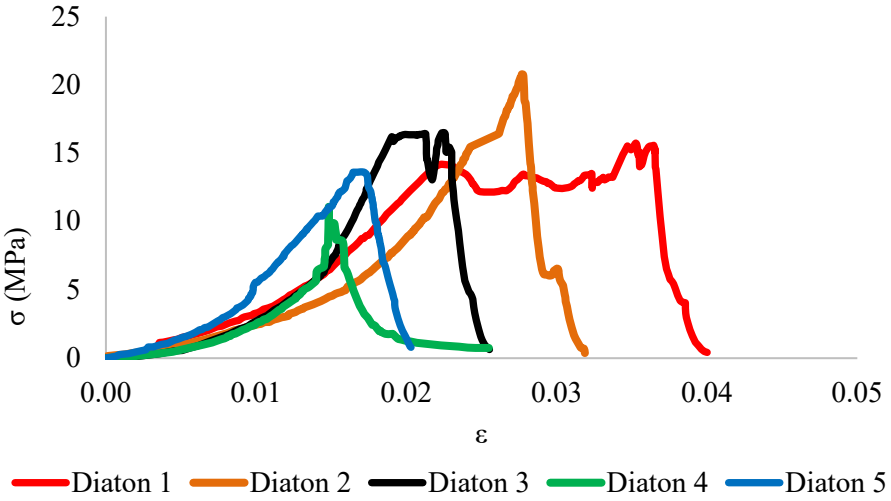

Fig.4-36. Tensile stress-strain diagrams of the jute fiber diatons.

Table 4-8 Mechanical properties of jute diaton samples tested in tension.

Strain energy (U)		Tensile strength (f_t)		Axial strain (ε)	
Mean [kNmm]	Co.V [%]	Mean [MPa]	Co.V [%]	Mean [-]	Co.V [%]
14.18	53.87	15.54	20.77	0.03	23.62

The stress-strain diagrams of 5 diatons are presented in Fig.4-36. Non-linearity in the stress-strain behaviors have been observed, with different shapes at the collapse point. The significant scatter performances have been observed as jute fibers are 3-4 meter long and their diameter vary from top to bottom, so as their mechanical properties. Diatons are manually fabricated with these fibers, therefore the wide result range observed in the above Fig.4-36.

4.5 Cross scale comparison

Although, all the jute fiber products are made from the same source material, notably every single product has different and its own physical and mechanical characteristics.

Table 4-9 Cross-scale comparison: Physical Properties

Type of jute products		Group behavior (Absorbed + trapped)		Material Behavior (Absorbed)	
		Mean [g(water)/g(fiber)]	Co.V [%]	Mean [g(water)/g(fiber)]	Co.V [%]
Jute fiber	Class 0.1mm (5mm)	8.18	6.60	2.50	5.55
Jute fiber	Class 0.1mm (10mm)	7.14	10.07	2.35	8.56
Jute fiber	Class 0.1mm (30mm)	4.89	3.30	2.10	7.67
Jute thread	Class 1mm	3.94	10.40	1.98	12.96
Jute thread	Class 2mm	4.56	4.68	2.10	8.55
Jute diaton	Class 15mm	2.97	5.52	1.83	4.67

This uniqueness can be highlighted through the physical and the mechanical cross scale comparison, represented in Table 4-9 and Table 4-10, respectively. Considering the material behavior, the water absorption of jute fibers in every product found to be almost similar, ranging in between 1.83-2.50 g(water)/g(fiber) (Table 4-9). The behavior a single fiber changes when it works together with other fibers (group behavior). Indeed, length and density of fibers significantly affect the

water trapping capacity. Similar variations can be seen in threads as considered, but in this case the group behavior is less important while diameter and density play a key role. As for the mechanical properties, Table 4-10 shows that the stiffness tends to be lower for elements of bigger equivalent size and diameter.

This can be explained by considering that bigger samples may have a higher number of imperfections that yields to high stress localization points, which can trigger collapse mechanism.

Table 4-10 Cross-scale comparison: Mechanical Properties

Type of jute products		Ultimate stress		Ultimate strain		Specific Modulus	
		Mean [MPa]	Co.V. [%]	Mean	Co.V. [%]	Mean [MPa/(kg/m^3)]	Co.V. [%]
Jute fiber	Class 0.1mm	215.11	4.42	0.013	19.08	11.32	17.89
Jute thread	Class 1mm	112.45	26.16	0.064	12.75	1.70	14.72
Jute thread	Class 2mm	56.95	9.73	0.120	29.45	0.65	33.65
Jute diaton	Class 15mm	15.54	20.77	0.024	31.68	1.99	18.32

4.6 Scanning Electron Microscopy (SEM) analysis of the threads with aging treatment

The following Fig. 4-5, Fig. 4-37, Fig. 4-38, Fig. 4-39, Fig. 4-40, Fig. 4-41 and Fig. 4-42 show two SEM micrographs for each examined fiber at 500x and 1000X magnification. Such pictures prove evidence of similar microstructures of the untreated samples (N); deionized water-treated samples (D); alkali solution-treated

samples (DA); salty solution-treated samples (DS). In particular, the presence of relevant crystalline phases on the DA1 sample (large white spots) can be highlighted.

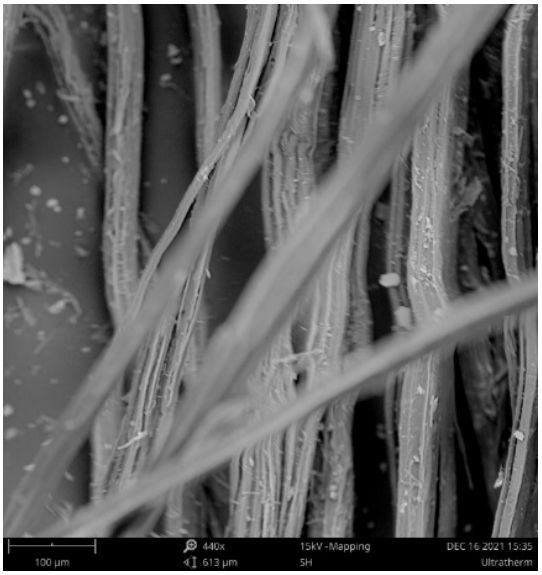

(a): 500X magnification

(b): 1500X magnification

Fig.4-37. SEM magnification: Jute fiber threads of class 1 mm (D) treated in. deionized water.

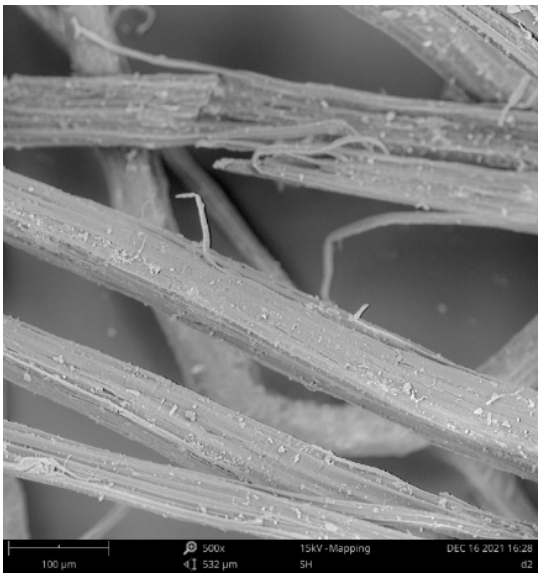

(a): 500X magnification

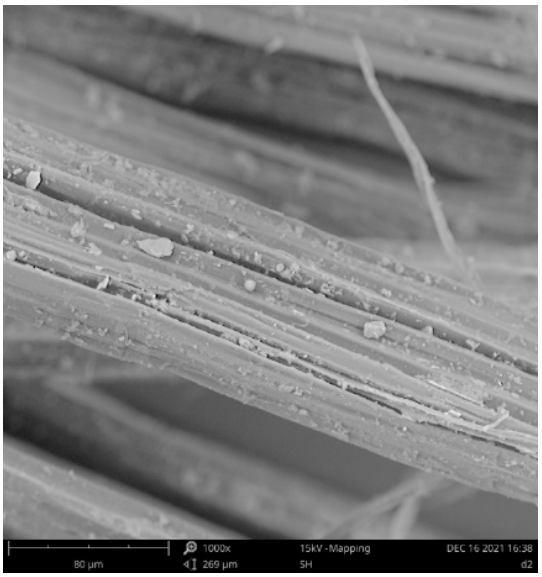

(b): 1500X magnification

Fig.4-38. SEM magnification: Jute fiber threads of class 2 mm (D) treated in. deionized water.

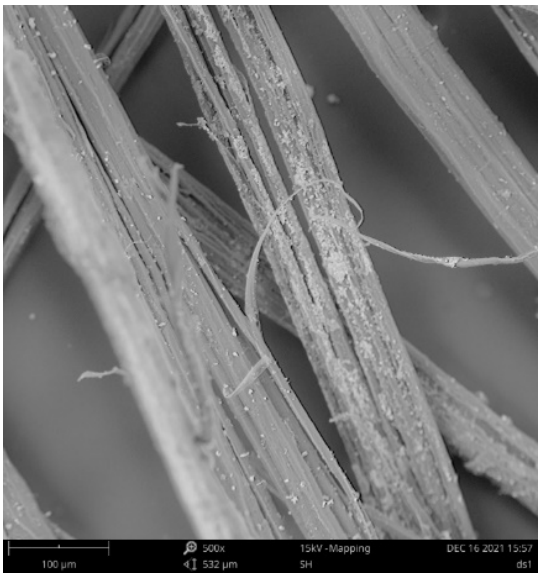

(a): 500X magnification

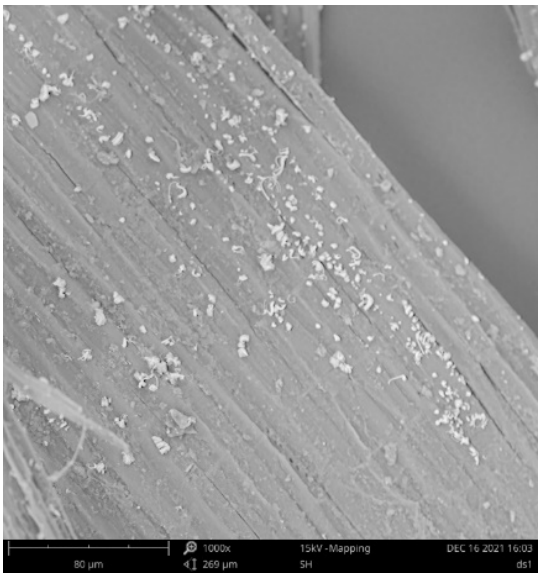

(b): 1500X magnification

Fig.4-39. SEM magnification: Jute fiber threads of class 1 mm) treated in slaty water solution (DS1).

(a): 500X magnification

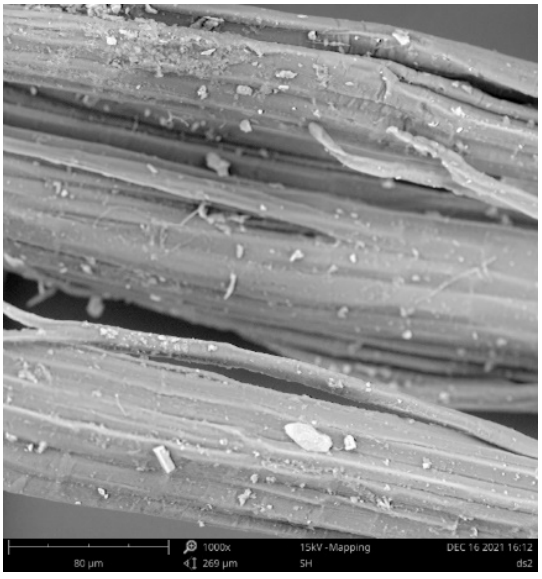

(b): 1500X magnification

Fig.4-40. SEM magnification: Jute fiber threads of class 2 mm) treated in slaty water solution (DS2).

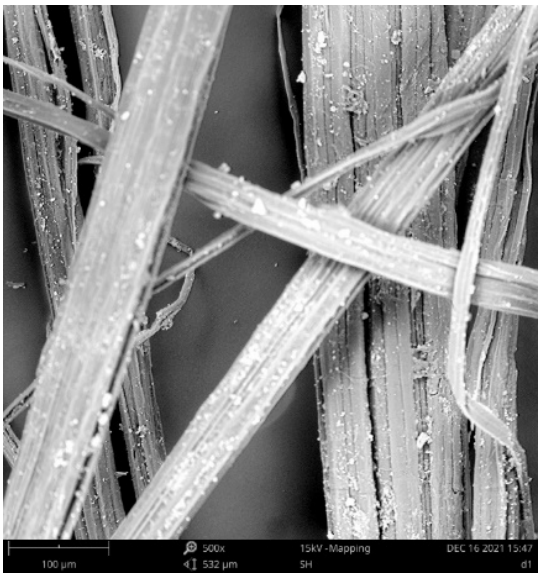

(a): 500X magnification

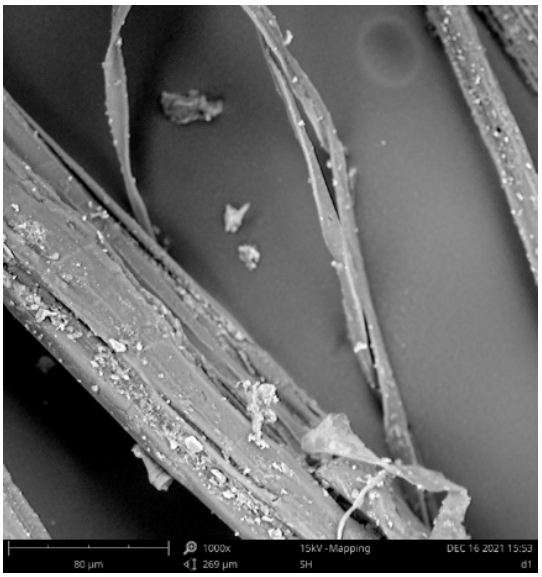

(b): 1500X magnification

Fig.4-41. SEM magnification: Jute fiber threads of class 1 mm) treated in. alkaline solution (DA1).

(a): 500X magnification

(b): 1500X magnification

Fig.4-42. SEM magnification: Jute fiber threads of class 2 mm) treated in. alkaline solution (DA2).

4.7 Conclusions

In this chapter the physical and mechanical properties of the raw jute fibers (of Bangla Tosha - Corchorus olitorius or golden shine origin), threads and diatons prepared with the same type of raw jute fibers have been evaluated, with objective to use these for thermo-structural retrofitting or upgrading of the masonry walls.

Jute fibers absorption capabilities are very important for designing the mixture composition of fiber strengthened mortars. It has been observed that different fiber lengths produced different absorption rate, in particular smaller fiber present the highest absorption values. In case of jute threads bigger diameter corresponds to highest absorption.

Every single product has different and its own physical and mechanical characteristics. While considering the material behavior, it has been found that the jute fiber can absorb near about 183% (minimum observed for diaton) to 250% (maximum obtained for 5 mm chopped fiber), notably the obtained absorption capacities are lower than the value i.e., about 300% (length between 5mm to 15mm) as reported by Formisano et al. (2020).

However, particular attention has been devoted to the durability properties of jute threads that has been subjected to different aging protocols. The same anti-aging treatment procedures have been followed, as conducted by Farrara et al. (2020) for the flex fiber threads and they have reported no significant loss of strength due to these treatments in water, salt solution and alkaline solution. While in our case the maximum deterioration has been recorded in case threads immersed in the deionized water, while salty solution and alkaline solution did not produce significant damages.

In this phase of the experimental research work, it has been demonstrated that the jute fiber and it derived products have interesting physical and mechanical properties. Jute fibers, threads and diatons present quite good tensile strength that can be useful for construction composite materials design. The tensile obtained in our case found to be about 215 MPa and this value is lower than that of reported in Gupta et al. (2015).

In our case the tensile strength of jute threads found to be about 101 MPa (for Class 1mm) to 112 MPa (for Class 2mm), whereas Nouri et al. (2015) have to achieved 104 MPa (for 2.7 mm) to 123 MPa (for 0.95 mm). To study the physical and mechanical properties of the jute fiber diaton the new concept, and all these additional information would enrich the scientific knowledge.

Results obtained in this phase are used in the subsequent phases for the composite mortar preparation, jute net preparation and masonry wall upgrading (or structural upgrading).

5. Phase II – Mechanical, thermal and integrated performance of the jute fiber strengthened mortars

This chapter deals with the behavior of the composite system is based on and following to the research activities were conducted in the phase-I of this current project. The integrated (mechanical and thermal) behavior of the various composite mortars systems was analyzed with prime focus to achieve dual positive effect with improving the thermal insulating property and as well as to achieve acceptable structural properties. In addition, other objectives are to develop newer sustainable building materials with bio-degradable and recyclable properties.

The jute fiber composite mortar systems were developed and prepared using different combinations of three different fiber lengths (30mm,10mm and 5mm) and four different fiber percentages (0.5%,1%,1.5% and 2%) with respect to the dry mortar masses. For this purpose, two types of commercially available mortars were used, one lime based and other cementitious. The workability of the various mortar – fiber mixture compositions were established through the shaking table tests. The mechanical properties of these composite systems were determined by flexural and compression tests. Where the flexural strength, compression strength and strain energy of each individual composite mortar combinations was analyzed. Thermal property of the composite systems was determined by analyzing the insulation capacity, through the thermal conductivity tests. All the aforesaid studied properties and their respective obtained values were compared with each-other (dry mortar categories) and particularly with the thermos-mechanical performance values of the normal mortar specimens. All the above-mentioned tests were conducted in the Material Testing Laboratory of the University of Cagliari, Italy and the Strength Laboratory of the University of Salerno, Italy.

5.1 Materials and methods

The present section represent the thermo-mechanical characterization of the normal Thermal Mortar (TM) without fiber, normal Structural Mortar (SM) without fiber and jute fiber composite mortars prepared using TM and SM. Fig. 5-1 describes the underlying methodologycal for the mortar and composite mortar preparation.

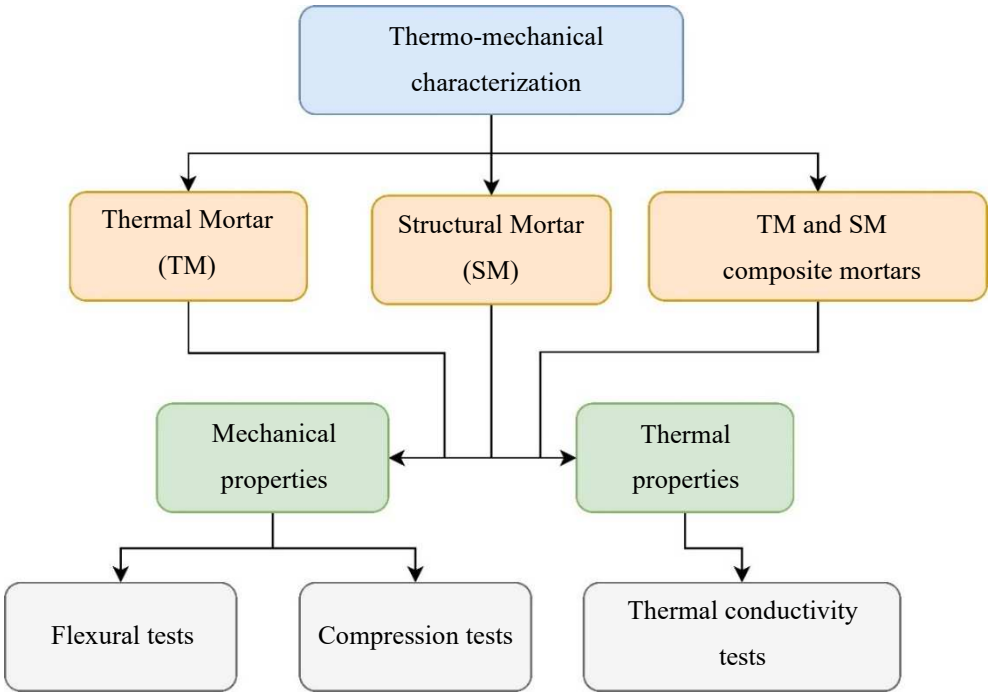

Fig. 5-1. Experimental procedures

5.1.1 Materials

5.1.1.1 Jute raw fibers

The origin of jute fibers and the physical and mechanical properties of the same, as well as their cutting process can be found in Chapter 4.

In this section, three jute fiber lengths (30 mm, 10 mm and 5 mm) (Fig. 4-4) were used for the preparation of the composite mortar samples. To prepare the

composite samples various combinations fibers lengths and percentages have been used, as you can see in the Table 5-1.

Table 5-1. Thermal Mortar (TM) and Structural Mortar (SM) preparation and Composite TM and SM preparation

		Fiber length categories			
		No fiber	30mm	10mm	5mm
Normal sample	No fiber	yes	-	-	-
Composite samples	0.5%	-	yes	yes	yes
	1.0%	-	yes	yes	yes
	1.5%	-	yes	yes	yes
	2.0%	-	yes	yes	yes

5.1.1.2 Mortars

Two types of mortars were used to prepare the jute fiber composite mortar samples Namely a lime based Thermal Mortar (TM) (Fig. 5-2a) and cement-based Structural Mortars (SM) (Fig. 5-2.b) were chosen for this purpose.

The TM is a thermo-dehumidifying plaster certified R and T/CSII (EN 998-1) that denotes a compressive strength between 1.5 and 5 MPa. Its nominal thermal conductibility is 0.14 W/m^2K, while it is characterized by a dry density of 750 kg/m^3. TM has pre-fabricated insulation materials (which are Recycled Aggregates (RA) in it (Fig. 5-3.b).

The SM is a premixed mortar for masonry with hydraulic binders and selected aggregates. Its compressive strength is 10 MPa, while its shear strength is 0.15 MPa. It is characterized by a thermal conductibility of 0.82 W/m^2K and a dry density of 1545 kg/m^3.

Fig. 5-2. Cement-based Structural mortar

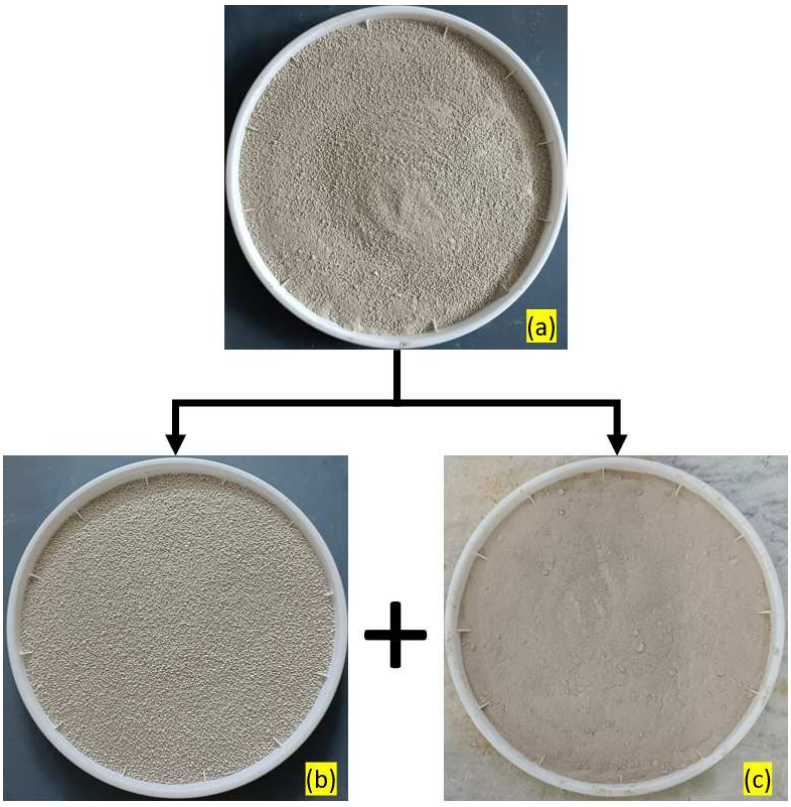

Fig. 5-3. Lime-based thermal mortar: (a) Original Thermal Mortar (TM), Separated (b) insulation materials (Recycled Aggregates (RA) and (c) separated mortar

For identification purposes, the samples are labelled as reported in Table 5-2. The labels start with M and MS, respectively representing the thermal and structural

mortars. Thereafter there is the casting number (x), the mortar sample type with fiber (F), the fiber percentage (0.5%, 1.0%, 1.5% and 2.0%), the fiber length (30 mm, 10 mm and 5 mm), the serial of the mold (M) number (y) and finally the sample (S) serial number (z). For example: MxF0.5(10) MySz denotes the sample number z, realized with thermal mortar M, using the mold x, with fiber percentage 0.5% and fiber length 10 mm.

Table 5-2. Composite mortar preparing scheme

		Fiber length		
		30 mm	10 mm	5 mm
Fiber percentage	0.5%	MxF0.5(30)MySz	MxF0.5(10)MySz	MxF0.5(5)MySz
		MSxF0.5(30)MySz	MSxF0.5(10)MySz	MSxF0.5(5)MySz
	1.0%	MxF1(30)MySz	MxF1(10)MySz	MxF1(5)MySz
		MSxF1(30)MySz	MSxF1(10)MySz	MSxF1(5)MySz
	1.5%	MxF1.5(30)MySz	MxF1.5(10)MySz	MxF1.5(5)MySz
		MSxF1.5(30)MySz	MSxF1.5(10)MySz	MSxF1.5(5)MySz
	2.0%	MxF2(30)MySz	MxF2(10)MySz	MxF2(5)MySz
		MSxF2(30)MySz	MSxF2(10)MySz	MSxF2(5)MySz

* M=Thermal mortar; MS = Structural mortar; x= Mortar casting sequence; y=number of molds; z=Sample number

5.1.2 Test procedure

5.1.2.1 Mortars and jute fiber composite mortars preparation.

Fig. 5-4 demonstrated that, first of all, the thermal and structural mortar samples grouts were prepared following EN 1015-2 and their workability were verified through shaking table tests as prescribed in EN 1015-3.

The workability tests values of the first thermal and mechanical grouts were used as a benchmark for the composite mixtures. Also, while preparing the composite-mortar samples, the EN 1015- 2 and EN 1015-3 standards have been followed.

The jute fiber composite-mortars were fabricated with three different fiber lengths 30mm, 10mm and 5mm and using four different percentages (0.5%, 1.0%, 1.5% and 2.0%) with respect to the dry mortar mass. In this phase of the experimental campaign, the amount of water was different for each mix in order to take into account the fiber absorption capabilities already studied in the previous chapter. For this reason, in Table 5-3 (for TM) and Table 5-4 (for SM) the details of the mix design have been reported.

Two molds were used to prepare 6 samples (160 mm x 40 mm × 40 mm) for the mechanical test. Moreover, another two molds were used to prepare 2 samples (160 mm × 140 mm × 40 mm) for thermal conductivity tests.

While preparing the composite samples, the fibers were initially mixed with the dry mortar for 30 seconds inside the mixture (Fig. 5-4) without any water. Thereafter, an appropriate amount of water was added (Table 5-3 for TM and Table 5-4 for SM) and mixed for 7 minutes.

The amount of water, necessary for the mixture was determined through the water absorption test (for more details see chapter 4).

After mixing, the shaking table test was performed to evaluate the mortar workability. During this process a hollow conical bronze mold was used to cast the test specimens on the shaking table (see, Fig. 5-4).

The mortar was put inside this conical mold and 15 strokes were applied to the half-filled grout, to distribute the mixture uniformly around the bottom of the mold. Thereafter, another portion of the mixture was put into completely fill the mold.

Then, 15 more strokes were applied, and then the extra materials were removed from the top. The mold was removed vertically and the table was shaken for 15 times by rotating a lever attached to the table at a frequency of 1 sec/rotation. After the first shaking table test, the orthogonal diameters of the spread normal-mortars or composite mortars were measured with a digital vernier caliper. An average +/-10% variation range between two consecutive tests assured the mixtures composition correctness.

Otherwise, the normal-mortar or composite-mortars were re-prepared and the shaking table tests were re-conducted. While preparing the samples inside the molds, 25 strokes were applied for each mechanical samples (160 mm × 40 mm × 40 mm), while 75 strokes were applied for each thermal sample (160 mm × 140 mm × 40 mm).

This was done to remove the trapped air in the samples. The EN 1015-11: 2019 standard has been followed for samples maturation.

The curing period consists of a total of 28 days from the day of casting. After casting, all the samples were kept inside airtight plastic bags and left inside molds for first two days after casting date.

On day 3, samples were taken out from the respective first plastic bag and mold and re-put inside another plastic bag for 5 days.

This controlled drying period corresponds 2nd to 8th day in Fig. 5-5 and Fig. 5-6 reporting the samples mass variation during the drying period.

On day 8 after casting, all the samples were extracted from plastic bags and placed in a room with ambient temperature 25 °C and relative humidity 65 %, until 28th day.

On day 28, rectangular prism specimens with dimensions 160mm × 40mm × 40mm were used to conduct the mechanical tests, and their flexural properties and compressive strength were evaluated.

While other rectangular prism specimens with dimensions 160 mm × 140 mm × 40 mm, on 28th day were place inside an oven for forced drying to remove the moistures form these samples, before conducting the thermal conductivity tests.

Raw fibers: 30mm, 10mm and 5mm + Fiber percentages 0.5% or 1.0% or 1.5% or 2.0% +Water amount as necessary, based on the calculation.

Jute +Mortar (Mixed for 30 secs).

Jute +Mortar +water (Mixed for 7 mins). secs)

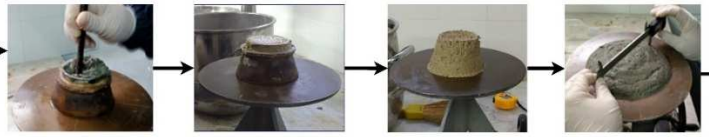

Shaking table test.

1 Sample (160 x 140 x 40 mm) for thermal conductivity test.

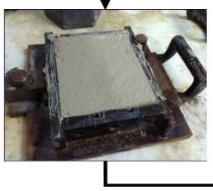

3 Samples (160 x 40 x 40 mm) for mechanical conductivity. test)

Initial drying period in molds and inside plastic bags from the casting day to 3rd day.

Intermediate drying period inside plastic bag from 3rd day to 8th day.

Final drying period from 8th day to 28th

Fig. 5-4. Jute fiber composite mortar preparation

Table 5-3. Mixture composition for the normal thermal composite mortar.

	Thermal Mortar [%]	Jute Fiber used [%]	Water used [%]
M (No fiber)	75.000	0.000	25.000
MF0.5(30)	72.134	0.362	27.503
MF0.5(10)	71.186	0.358	28.457
MF0.5(5)	70.764	0.356	28.880
MF1(30)	69.452	0.701	29.846
MF1(10)	66.825	0.702	32.473
MF1(5)	66.969	0.676	32.355
MF1.5(30)	67.251	1.027	31.723
MF1.5(10)	64.925	0.991	34.084
MF1.5(5)	63.922	0.976	35.102
MF2(30)	64.968	1.326	33.706
MF2(10)	62.088	1.267	36.645
MF2(5)	60.865	1.242	37.893

Table 5-4. Mixture composition for the normal and composite mortar.

	Structural Mortar [%]	Jute Fiber used [%]	Water used [%]
MS (No fiber)	84.753	0.000	15.247
MSF0.5(30)	82.865	0.418	16.716
MSF0.5(10)	82.295	0.415	17.290
MSF0.5(5)	82.039	0.414	17.547
MSF1(30)	81.059	0.819	18.122
MSF1(10)	79.962	0.808	19.230
MSF1(5)	79.477	0.803	19.719
MSF1.5(30)	79.497	1.211	19.293
MSF1.5(10)	78.207	1.191	20.602
MSF1.5(5)	77.340	1.178	21.482
MSF2(30)	77.635	1.584	20.781
MSF2(10)	75.652	1.544	22.804
MSF2(5)	74.784	1.526	23.689

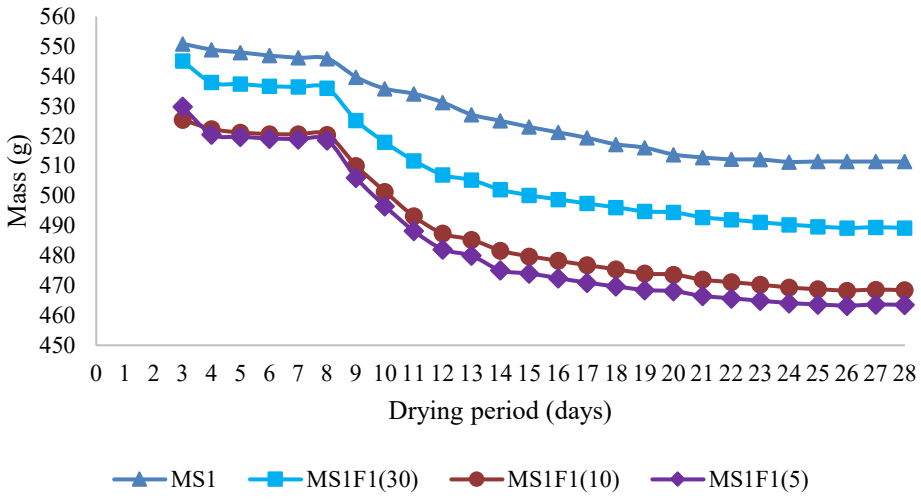

Fig. 5-5. A typical example of samples drying period of a structural mortar and composite mortars with different fiber lengths (30 mm, 10 mm and 5 mm) and 1% of jute fiber (with respect to the mortar dry mass).

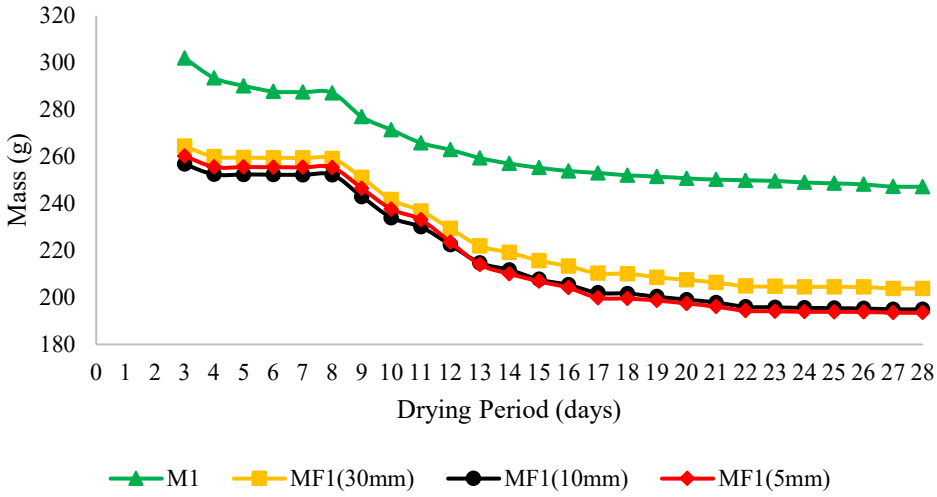

Fig. 5-6. A typical example of samples drying period of a thermal mortar and composite mortars with different fiber lengths (30 mm, 10 mm and 5 mm) and 1% of jute fiber (with respect to the mortar dry mass).

5.1.2.2 Mechanical Tests

The mechanical properties of both thermal and structural mortar samples (without fiber) and fiber-strengthened mortar samples were evaluated through flexural and compression tests, on the 28th day from the casting date.

Before conducting the tests, mass and dimensions of each sample were measured, and later these values were used while calculating flexural and compressive values.

Different mix-compositions of thermal composite mortar samples are shown in Fig. 5-7, Fig. 5-8, Fig. 5-9 and Fig. 5-10 , while the structural mortar samples are shown in Fig. 5-11, Fig. 5-12, Fig. 5-13 and Fig. 5-14.

Fig. 5-7. Thermal mortar samples prepared using 0.5% fiber (with respect to the dry mortar mass), with 30 mm, 10 mm and 5 mm fiber lengths, respectively.

Fig. 5-8. Thermal mortar samples prepared using 1% fiber (with respect to the dry mortar mass), with 30 mm, 10 mm and 5 mm fiber lengths, respectively.

Fig. 5-9. Thermal mortar samples prepared using 1.5% fiber (with respect to the dry mortar mass), with 30 mm, 10 mm and 5 mm fiber lengths, respectively.

Fig. 5-10. Thermal mortar samples prepared using 2% fiber (with respect to the dry mortar mass), with 30 mm, 10 mm and 5 mm fiber lengths, respectively.

Fig. 5-11. Structural mortar samples prepared using 0.5% fiber (with respect to the dry mortar mass), with 30 mm, 10 mm and 5 mm fiber lengths, respectively.

Fig. 5-12. Structural mortar samples prepared using 1% fiber (with respect to the dry mortar mass), with 30 mm, 10 mm and 5 mm fiber lengths, respectively.

Fig. 5-13. Structural mortar samples prepared using 1.5% fiber (with respect to the dry mortar mass), with 30 mm, 10 mm and 5 mm fiber lengths, respectively.

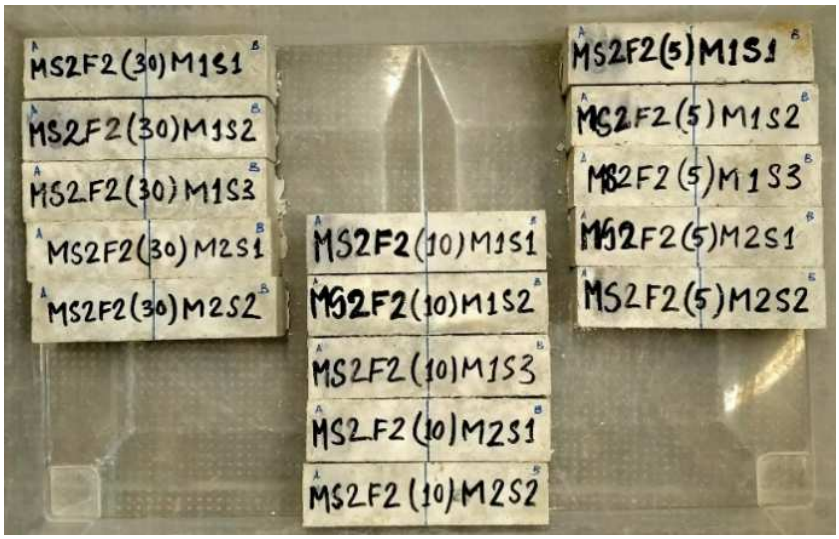

Fig. 5-14. Structural mortar samples prepared using 2% fiber (with respect to the dry mortar mass), with 30 mm, 10 mm and 5 mm fiber lengths, respectively.

Fig. 5-15. Flexural strength test (Sample MS1F1.5(30)M2S1).

The three-point bending flexural test was run according to EN 1015-11:2019, using a universal displacement-controlled machine: Metrocom-1 (Fig. 5-15) characterized by a maximum load capacity of 4.9 kN and sensibility of 0.02 kN. The tests were conducted on prismatic specimens (160 mm × 40 mm × 40 mm) with displacement rate of 1.5 mm/min.

The applied force was measured by using a load cell of class 1 (Fig. 5-15) having a maximum capacity of 5 tons and nominal sensibility of 2 mV/V. A Linear Variable Displacement Transducer (Fig. 5-15) was used to measure the displacement, its specifications are max. range 50 mm, nominal sensibility output 2mV/V and linearity -<0.10%.

(a): Thermal mortar *(b): Structural mortar*

Fig. 5-16. Composite mortars with 2% of fiber with respect to the binder weight, without fiber and with 30 mm, 10 mm and 5 mm of fiber lengths.

After the flexural strength test, the remaining two parts (Fig. 5-16) of the tested specimens have been subjected to the compression tests (Fig. 5-17). These tests were conducted using a universal load-controlled machine Metrocom-2 that has a load capacity of 100 kN.

Fig. 5-17. Compression strength test (Sample MS1F1.5(30)M2S1).

5.1.2.3 Thermal Properties Tests

A heat flow meter instrument was used to evaluate the thermal properties of the mortar (without fiber) (Fig. 5-18), the thermal composite mortar (Fig. 5-19) and structural composite mortar (Fig. 5-20) samples.

The measurements were conducted following ISO 8301 and EN 1946-3 using the heat flow meter measuring device *TAURUS TCA* 300 (Fig. 5-21) (for simplicity hereafter it will be called only *TAURUS*).

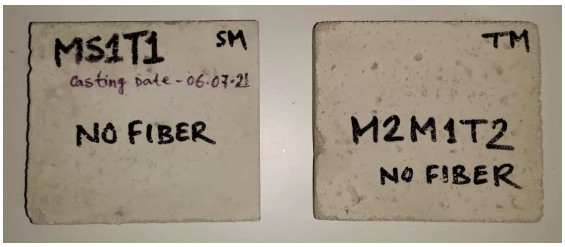

Fig. 5-18. Structural mortar sample without fiber (MS1T1) and thermal mortar sample without fiber (M2M1T2) used for thermal conductivity tests.

Fig. 5-19. Thermal composite mortar samples prepared using fiber percentages (0.5%, 1.0%, 1.5% and 2.0%) (with respect to the dry mortar mass) and fiber lengths (30 mm, 10 mm and 5 mm).

Fig. 5-20. Structural composite mortar samples prepared using fiber percentages (0.5%, 1.0%, 1.5% and 2.0%) (with respect to the dry mortar mass) and fiber lengths (30 mm, 10 mm and 5 mm).

On some selected samples from all combination categories (fiber length and fiber percentages (with respect to the fiber dry mass) as specified in the Table 5-2), a total of 5 measurements were conducted on each sample, out of which four were executed during the natural drying period, i.e., on 10^{th}, 15^{th}, 22^{nd} and 28^{th} day. This was done to study the effect of moisture on thermal conductivity. Therefore, measurements were done to register the change in the thermal conductivity with the reduction in water /humidity content, for all samples tested.

Fig. 5-21. Heat flow meter: TAURUS TCA 300

All samples were subjected to forced drying in an oven at constant temperature of 50°C, according to EN 12667. The oven drying (Fig. 5-22) was done to remove all residual moisture present inside the samples, as the presence of humidity influences the measurement and provides higher values of the Thermal Conductivity (TC). The forced oven drying time varied ranging from 5 to 14 days, depending on the moisture contain in each individual 'sample.

While drying in the oven, the mass of each sample was daily monitored, and it measurements continued until two successive measurements were almost equal (with a margin of error of +/- 0.1 g).

When constant weight for samples was achieved, the samples were wrapped and kept inside airtight plastic bags and taken out only before putting inside so-called TAURUS for measurements. Samples masses were also measured before and after

every thermal conductivity test. All sample mass measurements were carried out in the laboratory where temperature is controlled at 25±3°C and relative humidity is 60± 10%.

Fig. 5-22. Normal mortar (without fiber) and composite mortar samples are placed inside the oven for forced drying or moisture removal.

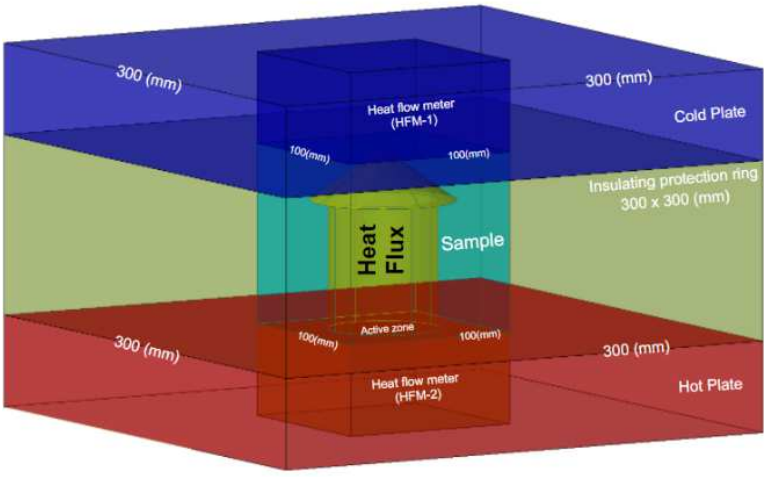

Fig. 5-23. Schematic diagram of heat flow meter (TAURUS).

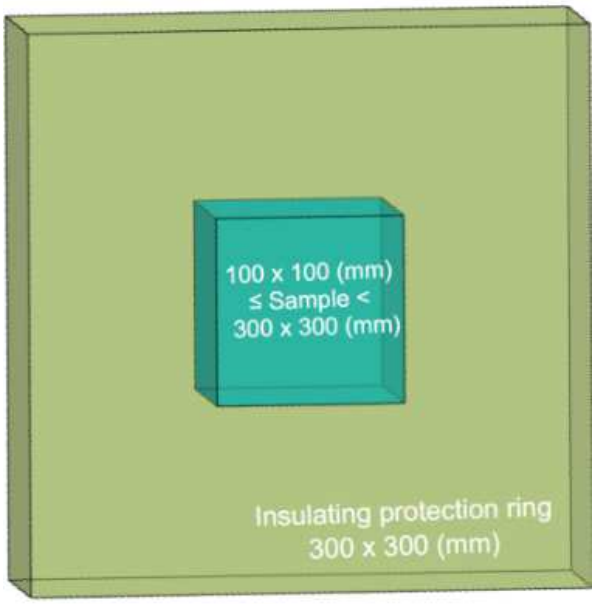

Fig. 5-24. The size of the sample 100x100 (mm^2)≤ Sample<300x300 (mm^2), in green represents the insulating protection materials like EPS or sheep wool (must be used around the samples).

TAURUS is equipped with hot and cold plates (Fig. 5-23). The instrument has a total workable surface area of 300 mm × 300 mm, whereas both plates active zone has a surface area of 100 mm × 100 mm and is situated at the center of the plates. These active measuring zones are equipped with one heat flux sensor per plate arranged symmetrically in this area. Protective zones are located outside the plates active zone.

The intermediate sampling time was set at 1 minute; therefore, the instrument provides the calculated value of thermal conductivity at an interval of each minute for 300 mins (set as total measuring time period).

A heat loss protective ring, made of insulation material (like EPS or wool) must be placed around the samples (Fig. 5-24). Samples used for the thermal conductivity test are placed exactly at the middle of the measuring plates (as in the Fig. 5-25 and Fig. 5-26), where the active zones of the plates are located. According

to EN 12939, the sample mean temperatures were chosen to be equal to 10 °C, 20 °C and 30 °C, with the plate's temperature difference selected to be 10 °C.

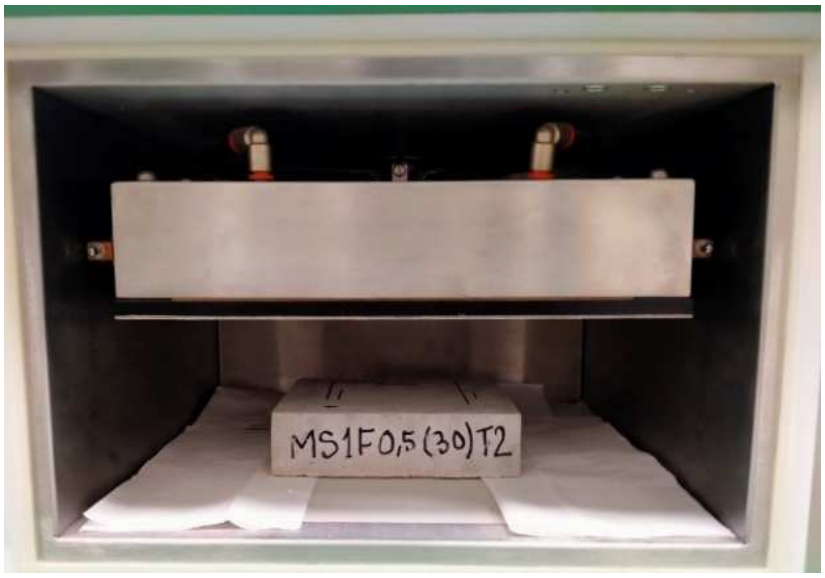

Fig. 5-25. Sample MS1F0.5(30)T2 placed exactly at the middle of the plates.

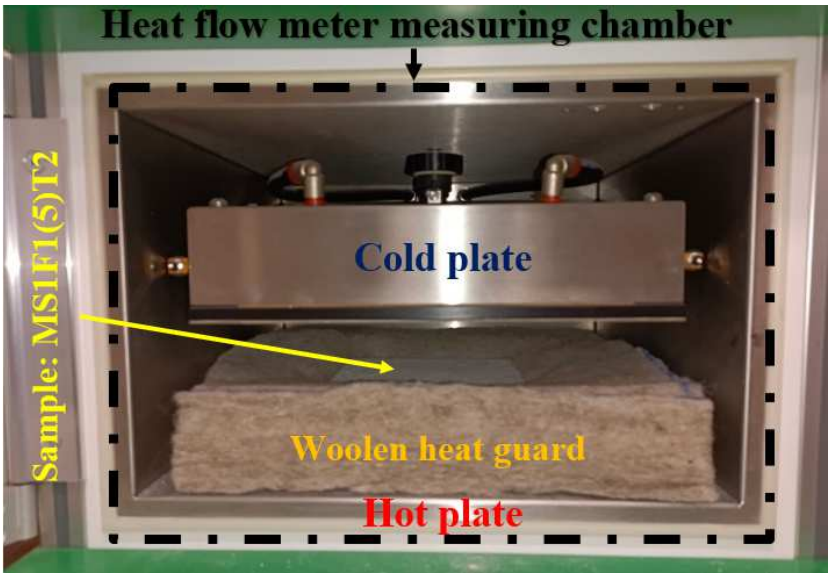

Fig. 5-26. (a) Samples used with surface areas 160 x 140 mm^2 and (b) Sample place inside the measuring chamber.

Fig. 5-27. Woolen heat guard is placed around the sample (MS1F0.5(30)T1)

All the thermal samples have the upper and lower surface areas equal to 160×140 mm^2 with thickness equal to 40 mm. Being greater than that of active zone surface areas 100×100 mm^2 but being smaller than total plate areas 300×300 mm^2, a protective woolen insulating ring was used (Fig. 5-26 and Fig. 5-27) around each sample. This was done to avoid the heat losses along around the sample's edges and also to have a uniform heat flux passing through the sample, under observation. The sheep wool was chosen as it has one of the lowest thermal conductivity values among other thermo-insulating materials, which is approximately around 0.0378 W/m^{2}K. The heat fluxes were measured and the thermal conductivity λ value was calculated by enforcing its definition as in Majumder et al. (2021):

$$\lambda = \dot{Q} \frac{S}{(t_H - t_C)} \tag{5.1}$$

where $\dot{Q}$ is the heat flux in W/m^2, s is the sample thickness in m, t_H is the hot plate temperature in °C, t_C is the cold plate temperature in °C.

5.2 Results and discussion

5.2.1 Physical and mechanical properties

The workability of the mortars was evaluated through the shaking table test. Whereas the samples mechanical performances were assessed through flexural and compression tests.

5.2.1.1 Shaking table test results

The mortars (with and without fiber-strengthened) workability threshold was judged by comparing the average spreading diameter of each mortar sample (with and without fiber-strengthened) with the average spreading diameters (used as reference value) of the normal-thermal mortar (M-without fiber) and normal structural mortars (MS- without fiber) spreading diameters, 151.65 mm and 163.64 mm, respectively.

The workability limit state is fulfilled if the percentage difference between the spreading diameters is +/- 10%. The accepted shaking table tests values are listed in the Table 5-5 (thermal mortars) and Table 5-6 (thermal mortars).

Table 5-5. Shaking table tests: Jute fiber thermal composite mortars

Values with respect to +/-10% of the thermal mortar (M)			
	[%]		[%]
MF0.5(30)	10.0	MF1(30)	3.09
MF0.5(10)	9.9	MF1(10)	4.12
MF0.5(5)	0.70	MF1(5)	8.27
MF1.5(30)	3.08	MF2(30)	6.03
MF1.5(10)	6.88	MF2(10)	1.66
MF1.5(5)	9.55	MF2(5)	9.18

Table 5-6. Shaking table tests: Jute fiber structural composite mortars

Values with respect to +/-10% of the structural mortar (MS)			
	[%]		[%]
MSF0.5(30)	2.58	MSF1(30)	5.78
MSF0.5(10)	3.17	MSF1(10)	1.17
MSF0.5(5)	0.50	MSF1(5)	3.65
MSF1.5(30)	6.30	MSF2(30)	9.90
MSF1.5(10)	5.50	MSF2(10)	9.10
MSF1.5(5)	2.33	MSF2(5)	9.85

5.2.2 Mechanical properties and observations

In total of 240 mortar samples of various combinations and mix have been used for the flexural tests. Moreover, around 480 samples have been used for the compression tests.

5.2.2.1 Flexural Test

Fig. 5-28.a represents a typical complete collapse of the structural mortar sample without fiber. In this case the samples break immediately after reaching the ultimate flexural strength. The similar collapse has been recorded for both thermal and structural mortar samples without fiber.

In the case of samples with fibers (Fig. 5-28.b, Fig. 5-28.c and Fig. 5-28.d), it has been observed that even after reaching the maximum flexural strength limit the samples keep a residual softening behavior and continue dissipating the applied load. Indeed, the presence of fibers improved the maximum deflection of the specimens, but also their strain energy capacity increased.

Fig. 5-29 and Fig. 5-30 it is quite clear that, the presence of fibers (30 mm, 10 mm and 5 mm) had help in holding broken pieces together. Further these presence of fiber in the composite mortar help in absorbing and dissipating energy of the applied load.

(a): MS1M1S2 without fiber.

(b): MS2F2(30)M1S2 with 2% fiber (with respect to mortar mass) and 30mm fiber length

(c): MS2F2(10)M1S2 with 2% (with respect to mortar mass) and 10 mm fiber length.

(d): MS2F2(5)M1S1 with 2% (with respect to mortar mass) and 5mm fiber length

Fig. 5-28. Structural composite mortar samples with fiber.

. *(a): Thermal composite mortar with 1.5% fiber (with respect to mortar mass) and 30mm fiber length*

(b): Structural composite mortar with 2% fiber (with respect to mortar mass) and 30mm fiber length

Fig. 5-29. Closed view after flexural failure and ultimate displacement.

(a): 30mm fiber length *(b): 10mm fiber length* *(c): 5mm fiber length*

Fig. 5-30. Zoomed view of samples with imbodied fiber

Table 5-7. Thermal mortar and composite mortars flexural test properties-1

	deflection max. (d)		Strain energy	
	Mean [mm]	Co.V. [%]	Mean [kN.mm]	Co.V. [%]
M (no-fiber)	0.603	9.403	0.186	29.723
MF0.5(5)	0.483	19.653	0.176	20.935
MF0.5(10)	0.840	12.135	0.200	20.434
MF0.5(30)	0.839	44.548	0.538	48.984
MF1(5)	0.137	26.334	0.020	19.551
MF1(10)	0.996	28.624	0.229	25.624
MF1(30)	0.666	40.240	0.563	42.170
MF1.5(5)	0.549	31.646	0.121	23.748
MF1.5(10)	0.611	26.956	0.272	7.662
MF1(30)	0.613	45.588	0.543	51.208
MF2(5)	0.512	28.570	0.054	38.430
MF2(10)	0.908	44.539	0.187	30.480
MF2(30)	0.604	32.781	1.095	28.192

Table 5-8. Thermal mortar and composite mortars flexural test properties-2

	Flexural stress (σ)		Flexural strain (ε)		Moment of inertia (I)	
	Mean [MPa]	Co.V [%]	Mean	Co.V [%]	Mean [mm^4]	Co.V [%]
MF0.5(30)	1.156	6.487	0.013	9.701	229219.484	1.051
MF1(5)	0.978	7.852	0.010	19.084	238651.134	3.969
MF1(10)	0.919	6.014	0.018	12.188	236889.402	2.025
MF1(30)	1.214	2.877	0.017	44.838	232294.789	2.483
MF1.5(5)	0.429	10.245	0.003	35.624	235590.026	3.523
MF1.5(10)	0.662	7.264	0.021	29.221	243081.565	2.553
MF1(30)	0.634	8.907	0.015	37.575	239004.001	0.885
MF2(5)	0.505	5.091	0.011	31.299	238988.136	1.458
MF2(10)	0.490	10.212	0.013	27.151	242856.595	2.158
MF2(30)	0.563	16.549	0.013	45.218	259554.012	2.594
MF0.5(30)	0.283	29.895	0.011	28.672	235421.779	0.714
MF1(5)	0.373	7.695	0.019	45.214	242024.499	2.395
MF1(10)	0.630	6.050	0.013	32.830	244984.576	1.874

Table 5-9. Structural mortar and composite mortars flexural test properties-1

	deflection max. (d)		Strain energy	
	Mean [mm]	Co.V [%]	Mean [kN.mm]	Co.V [%]
MS (no-fiber)	0.578	23.219	0.447	13.904
MSF0.5(5)	0.381	22.855	0.677	28.459
MSF0.5(10)	0.395	16.949	0.580	24.888
MSF0.5(30)	0.402	20.196	0.903	18.180
MSF1(5)	0.486	53.980	0.769	13.796
MSF1(10)	0.350	5.229	0.959	25.123
MSF1(30)	0.477	10.067	0.551	67.009
MSF1.5(5)	0.372	17.944	0.688	13.872
MSF1.5(10)	0.668	57.634	1.209	28.018
MSF1.5(30)	0.461	24.379	1.470	41.546
MSF2(5)	0.286	12.177	0.668	12.258
MS F2(10)	0.331	19.738	1.180	16.676
MSF2(30)	0.530	45.370	2.687	34.841

Table 5-10. Structural mortar and composite mortars flexural test properties

	Flexural stress (σ)		Flexural strain (ε)		Moment of inertia (I)	
	Mean [MPa]	Co.V [%]	Mean	Co.V [%]	Mean [mm^4]	Co.V [%]
MS (no-fiber)	7.789	8.446	0.012	23.378	218301.931	1.872
MSF0.5(5)	5.045	13.572	0.008	23.405	243885.014	2.728
MSF0.5(10)	5.825	8.929	0.008	16.951	234638.973	1.794
MSF0.5(30)	6.287	3.701	0.008	21.916	235917.934	5.057
MSF1(5)	3.914	6.393	0.010	54.246	239304.314	3.153
MSF1(10)	4.131	16.062	0.007	5.540	233765.911	1.843
MSF1(30)	5.068	7.931	0.010	10.186	238971.074	2.457
MSF1.5(5)	3.062	9.176	0.008	18.528	230956.559	2.092
MSF1.5(10)	3.733	10.518	0.014	57.603	233274.868	0.618
MSF1.5(30)	4.455	8.069	0.010	24.534	236707.824	2.199
MSF2(5)	2.389	8.438	0.006	12.917	233151.347	2.644
MS F2(10)	2.719	6.838	0.007	20.645	236396.515	3.685
MSF2(30)	3.611	10.919	0.011	46.069	230882.531	3.098

Table 5-11. Structural mortar and composite mortars flexural test properties

	Flexural stress (σ)		Flexural strain (ε)		Moment of inertia (I)	
	Mean [MPa]	Co.V [%]	Mean	Co.V [%]	Mean [mm^4]	Co.V [%]
MS (no-fiber)	7.789	8.446	0.012	23.378	218301.931	1.872
MSF0.5(5)	5.045	13.572	0.008	23.405	243885.014	2.728
MSF0.5(10)	5.825	8.929	0.008	16.951	234638.973	1.794
MSF0.5(30)	6.287	3.701	0.008	21.916	235917.934	5.057
MSF1(5)	3.914	6.393	0.010	54.246	239304.314	3.153
MSF1(10)	4.131	16.062	0.007	5.540	233765.911	1.843
MSF1(30)	5.068	7.931	0.010	10.186	238971.074	2.457
MSF1.5(5)	3.062	9.176	0.008	18.528	230956.559	2.092
MSF1.5(10)	3.733	10.518	0.014	57.603	233274.868	0.618
MSF1.5(30)	4.455	8.069	0.010	24.534	236707.824	2.199
MSF2(5)	2.389	8.438	0.006	12.917	233151.347	2.644
MS F2(10)	2.719	6.838	0.007	20.645	236396.515	3.685
MSF2(30)	3.611	10.919	0.011	46.069	230882.531	3.098

Table 5-7 and Table 5-8 present the flexural behaviors of the thermal mortar samples without fiber and thermal composite mortar samples of various combinations (see, Table 5-1) of fiber lengths and fiber percentages (with respect to the dry mortar mass).

While Table 5-9 and Table 5-10 present the flexural behaviors of the structural mortar samples without fiber and thermal composite mortar samples of various combinations (see, Table 5-1) of fiber lengths and fiber percentages (with respect to the dry mortar mass).

Notably for both cases (i.e., TM and SM), it has been found that the flexural strength and strain energy decrease, with the decrease of the fiber length. It has been observed that the longer fibers present a better mechanical performance in comparison to shorter ones. While considering in each fiber length category (30mm or 10mm or 5mm), with the increase of fiber percentage (with respect to the mortar dry mass), the stain energy found to be increased significantly in both for thermal and structural composite mortars.

Fig. 5-31, Fig. 5-32, Fig. 5-33 and Fig. 5-34 represent the experimental stress-strain curves comparison between the composite thermal mortar samples (with fibers) and the normal thermal mortar samples without fibers.

Looking at Fig. 5-31 it can be seen that samples with 0.5% fiber (with respect to the dry mortar mass) present a flexural strength reduction of 12.84% for 30 mm long fiber, 33.62% for 10mm long fiber and 37.43% for 5 mm long fiber.

Similarly, in Fig. 5-32, samples with 1% fiber (with respect to the dry mortar mass) presents a strength drop of 54.29% for 30 mm long fiber, 53.79% for 10 mm long fiber and 68.17% for 5 mm long fiber. Fig. 5-34 shows that samples with 1.5% fiber (with respect to the dry mortar mass) have a drop around 54.96% for 30 mm long fiber, 64.47% for 10 mm long fiber and 67.82% for 5 mm long fiber.

Finally, Fig. 5-34 highlights that samples with 2% fiber (with respect to the dry mortar mass) present a strength reduction of 57.49% for 30 mm long fiber, 76.29% for 10 mm long fiber and 81.44% for 5 mm long fiber.

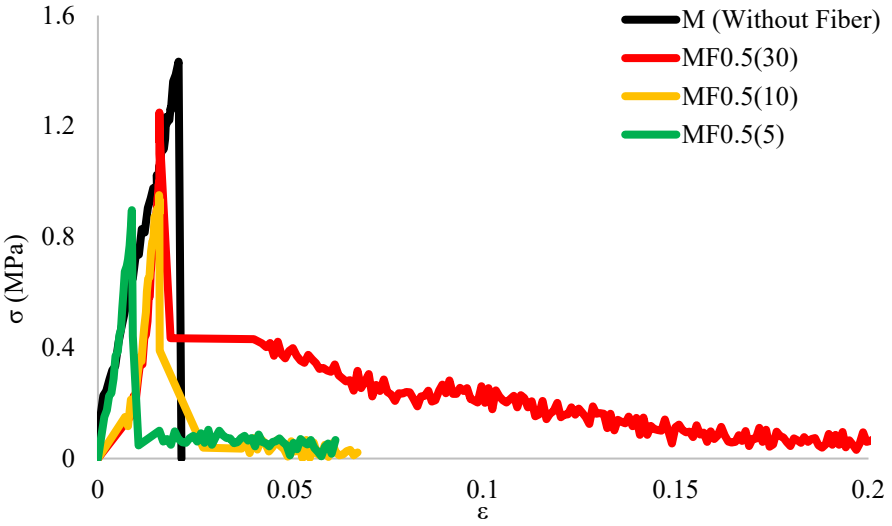

Fig. 5-31. Thermal mortar stress-strain curves: mortar sample Vs composite mortars samples with fiber lengths 30 mm, 10 mm and 5 mm with 0.5% fiber with respect to the dry mortar mass.

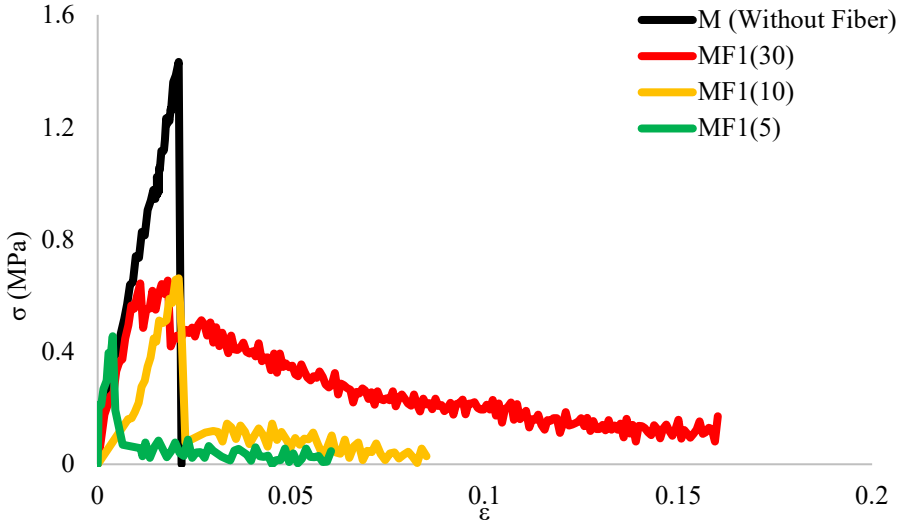

Fig. 5-32. Thermal mortar stress-strain curves: mortar sample Vs composite mortars samples with fiber lengths 30 mm, 10 mm and 5 mm with 1% fiber with respect to the dry mortar mass.

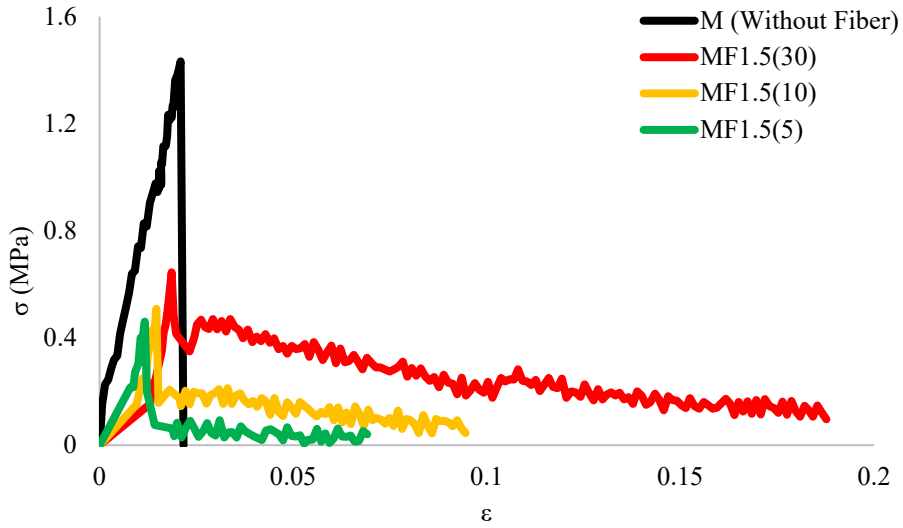

Fig. 5-33. Thermal mortar stress-strain curves: mortar sample Vs composite mortars samples with fiber lengths 30 mm, 10 mm and 5 mm with 1.5% fiber with respect to the dry mortar mass.

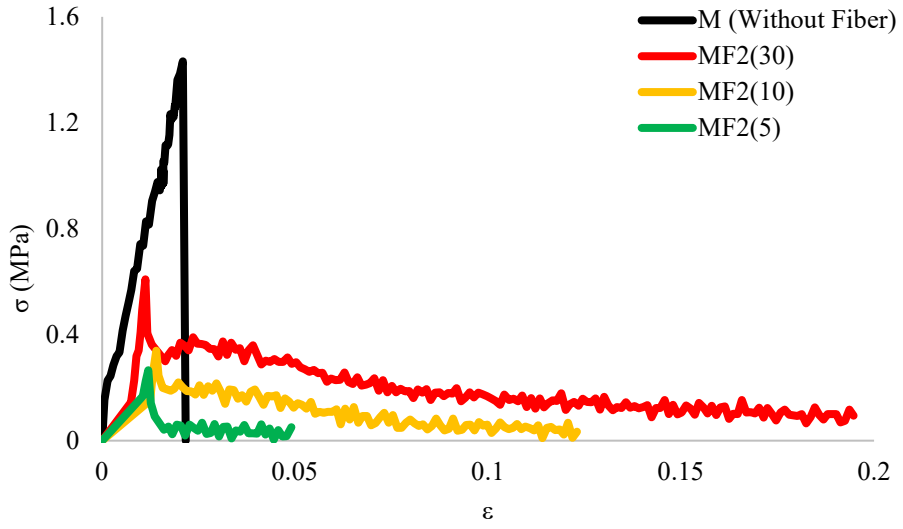

Fig. 5-34. Thermal mortar stress-strain curves: Normal mortar sample Vs composite mortars samples with fiber lengths 30 mm, 10 mm and 5 mm with 2% fiber with respect to the dry mortar mass.

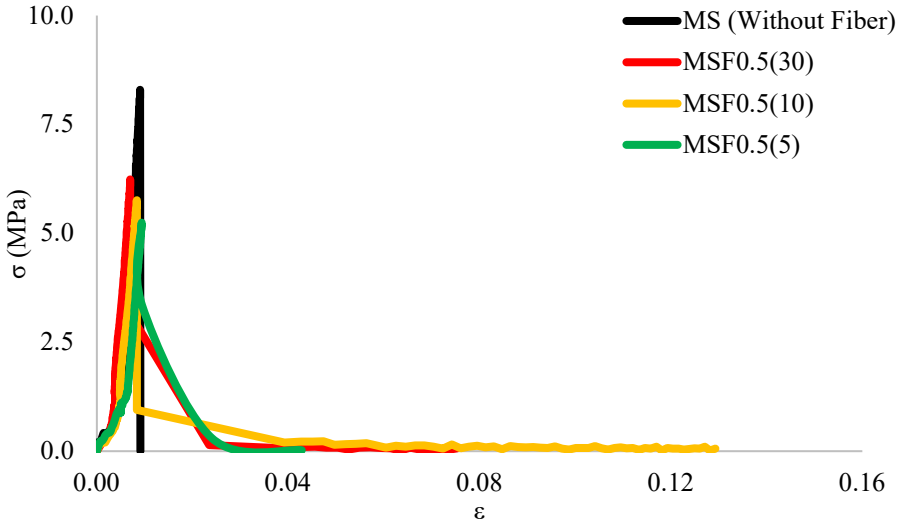

Fig. 5-35. Structural mortar stress-strain curves: mortar sample Vs composite mortars samples with fiber lengths 30 mm, 10 mm and 5 mm with 0.5% fiber with respect to the dry mortar mass.

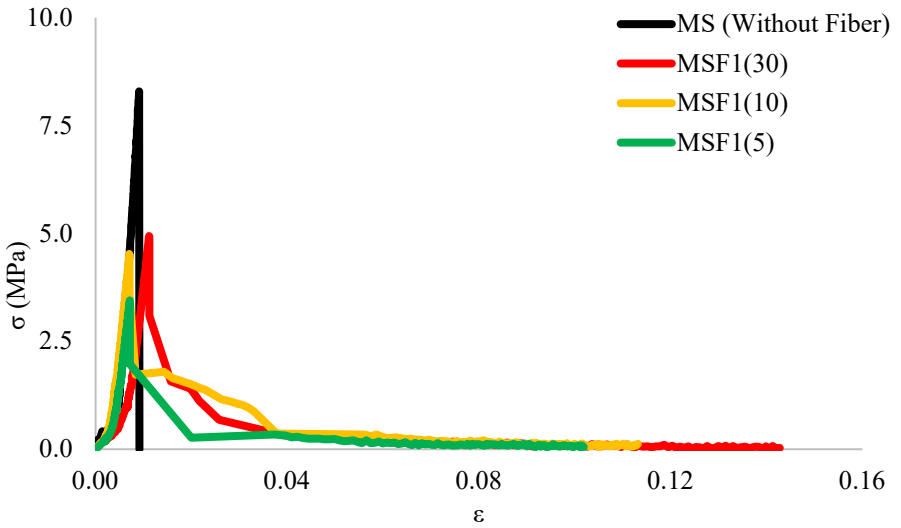

Fig. 5-36. Structural mortar stress-strain curves: mortar sample Vs composite mortars samples with fiber lengths 30 mm, 10 mm and 5 mm with 1% fiber with respect to the dry mortar mass.

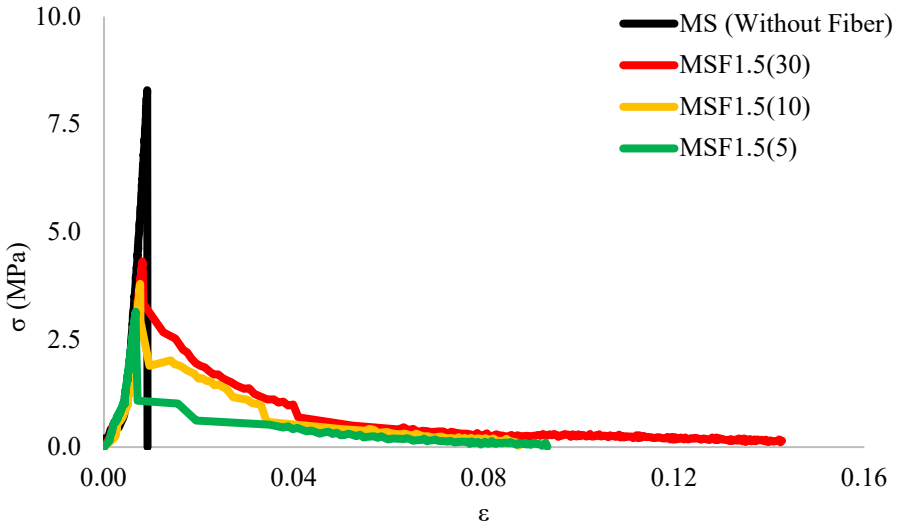

Fig. 5-37. Structural mortar stress-strain curves: mortar sample Vs composite mortars samples with fiber lengths 30 mm, 10 mm and 5 mm with 1.5% fiber with respect to the dry mortar mass.

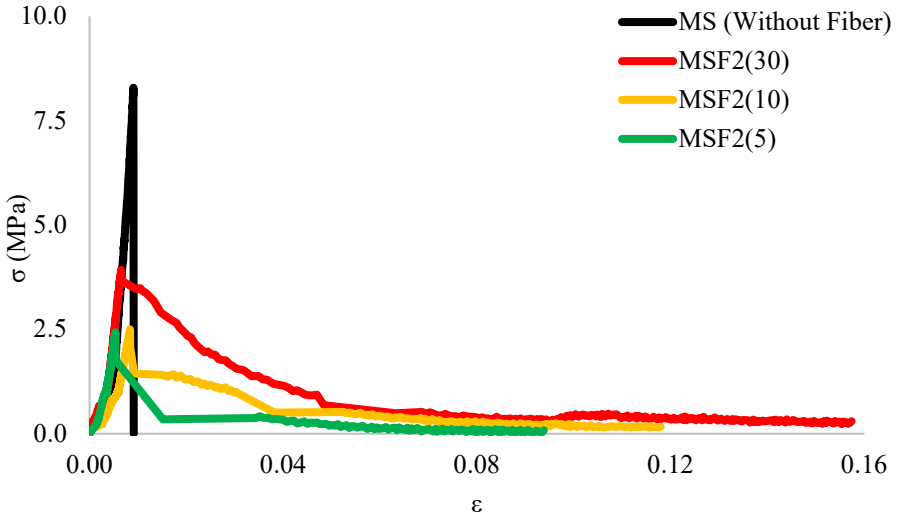

Fig. 5-38. Structural mortar stress-strain curves: mortar sample Vs composite mortars samples with fiber lengths 30 mm, 10 mm and 5 mm with 2% fiber with respect to the dry mortar mass.

Moreover, Fig. 5-35, Fig. 5-36, Fig. 5-37 and Fig. 5-38 depict the stress-strain curves comparison of composite structural mortar samples (with fibers) and normal structural mortar samples without fibers. Fig. 5-35 shows that samples with 0.5% fiber (with respect to the dry mortar mass) have a flexural strength reduction of 24.81% for 30 mm long fiber, 30.59% for 10 mm long fiber, and 36.77% for 5mm long fiber. Similarly, Fig. 5-36 presents the results of samples with 1% fiber (with respect to the dry mortar mass) the strength drops by 40.45% for 30mm long fiber, 45.49% for 10 mm long fiber, and 58.41% 5 mm long fiber. The results for specimens with 1.5% fiber (with respect to the dry mortar mass) are presented in Fig. 5-37 and the strength reductions have been recorded as of 47.99% for 30 mm long fiber, 54.30% 10mm long fiber and 62.09% for 5mm long fiber. Lastly in Fig. 5-38 it is possible to see the results for the specimens with 2% fiber (with respect to the dry mortar mass) where the strength reductions have been measured as equal to 52.67% for 30mm long fiber, 69.89% for 10mm long fiber and 70.71% for 5mm long fiber.

5.2.2.2 Compression Test

The compression tests were performed following the EN 1015-11:2019. Fig. 5-39, Fig. 5-40 and Fig.5-41 represent the collapse condition of sample without fiber, it has shown a perfect hourglass collapse at compression failure and the similar pattern has been observed for all structural and thermal mortar samples without fibers.

In the case of the composite mortar samples after reaching the ultimate compressive load, these samples do not present a physical separation between broken parts, as in Fig. 5-42 and Fig. 5-43.

In the enlarged picture (Fig.5-42.c) it is clearly visible that the embodied fibers present in the mortar sample, help to hold the broken pieces together. Therefore, in the case of composite samples (for both structural and thermal samples), in all cases like hour-glass collapse has been observed.

Fig. 5-39. Structural mortar: ultimate compression rapture for sample without fiber.

Fig. 5-40. A Structural mortar sample without fiber, after compression failure.

Fig. 5-41. A thermal mortar sample without fiber, after compression failure.

Fig. 5-42. Structural mortar: compression test failure for sample with 0.5% jute fiber (30mm) with respect to the dry mortar mass.

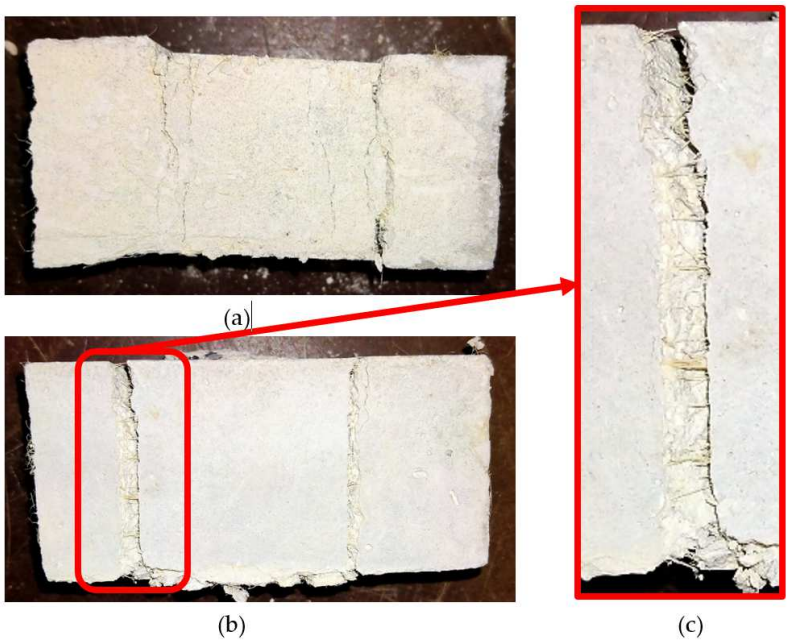

Fig. 5-43. A structural mortar sample (a) bottom view, (b) back view and (d) enlarged view, retrofitted with 0.5% jute fiber (30 mm) with respect to the dry mortar mass

Table 5-12. Compressive strength (R_c): Thermal mortar and composite mortars

	Mean [MPa]	Co.V [%]
M (No fiber)	3.50	9.69
MF0.5(5)	2.48	7.79
MF0.5(10)	2.35	6.62
MF0.5(30)	3.15	2.33
MF1(5)	1.16	12.56
MF1(10)	1.38	3.62
MF1(30)	1.59	3.49
MF1.5(5)	0.75	10.03
MF1.5(10)	0.66	16.27
MF1.5(30)	1.28	6.16
MF2(5)	0.36	34.77
MF2(10)	0.57	9.37
MF2(30)	2.05	9.19

Table 5-13. Compressive strength (R_c) Structural mortar and composite mortars

	Mean [MPa]	Co.V [%]
MS (No fiber)	32.25	5.61
MSF0.5(5)	24.24	4.84
MSF0.5(10)	26.75	2.12
MSF0.5(30)	26.16	6.89
MSF1(5)	14.68	15.82
MSF1(10)	18.03	10.41
MSF1(30)	21.83	5.79
MSF1.5(5)	10.79	4.72
MSF1.5(10)	13.97	3.02
MSF1.5(30)	17.79	3.97
MSF2(5)	6.03	7.47
MSF2(10)	8.40	12.35
MSF2(30)	10.15	7.41

Table 5-12 and Table 5-13 presents the compressive strength values of the thermal and structural mortar samples without fiber, as well as thermal and structural composite mortar samples of various combinations (as reported in Table 5-1) of fiber lengths and fiber percentages (with respect to the dry mortar mass), respectively.

The compressive strength of the composite mortars decreases with increase fiber percentages (0.5%, 1.0%, 1.5% and 2.0%) with respect to the mortar mass, or vice versa. As well, the fiber lengths also influence the compressive strength of the composite mortar samples, therefore with the decrease in fiber length (i.e., 30mm, 10mm and 5mm) the compressive strength also decrease linearly.

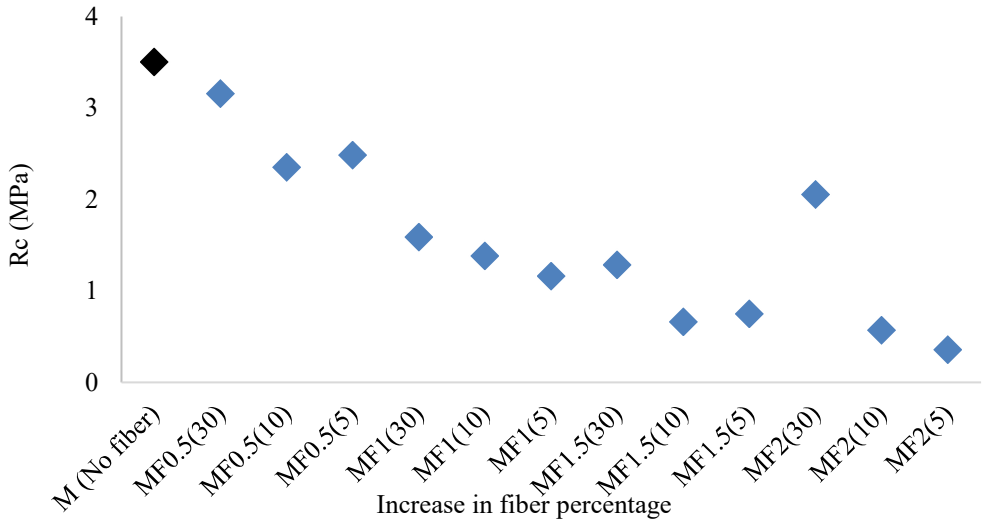

Fig. 5-44. Compression strengths of the thermal mortar and composite mortars with different fiber lengths (30 mm, 10 mm and 5 mm) and various fiber percentages (0.5%, 1%, 1.5% and 2% w.r.t mortar mass).

In the case of thermal composite-mortar samples (Fig. 5-44, when compared with the normal thermal mortar samples, the reduction in the compressive strengths for those samples prepared with 0.5 % fiber is 29.05% (5 mm fibers length), 32.85% (10 mm fibers length) and 9.81% (30 mm fibers length). For samples with 1% fiber there is a compressive strength drop of 66.77% (5 mm fibers length), 60.51% (10 mm fibers length) and 54.58% (30 mm fibers length).

Samples with 1.5% fiber present a compressive strength drop of 78.65% (5 mm fibers length), 81.11% (10 mm fibers length) and 63.34% (30 mm fibers length). Finally, samples with 2.0% fibers show a compressive strength drop of 89.85% (5 mm fibers length), 83.70% (10 mm fibers length) and 41.37% (30 mm fibers length).

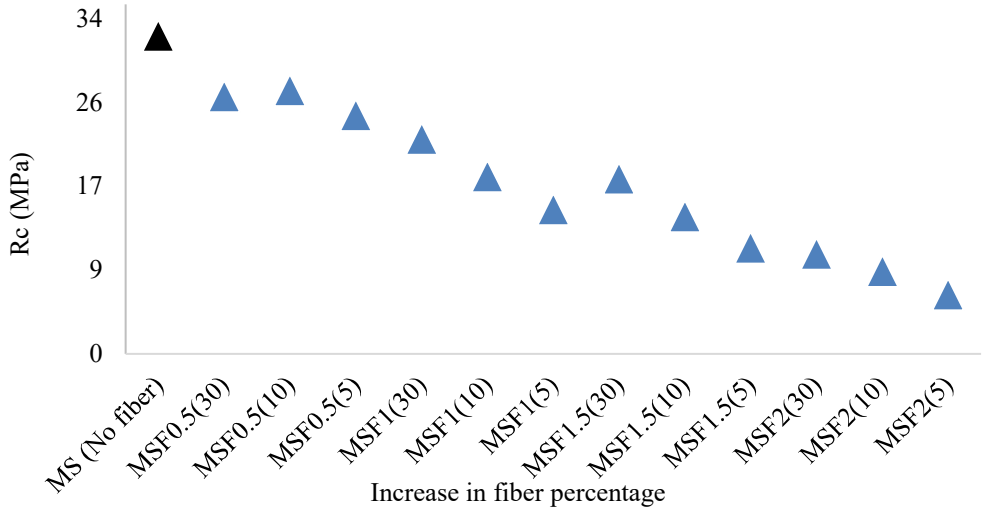

Fig. 5-45. Compression strengths of the structural mortar and composite mortars with different fiber lengths (30 mm, 10 mm and 5 mm) and various fiber percentages (0.5%, 1%, 1.5% and 2% w.r.t mortar mass).

Similarly, in the case of structural composite mortars the reduction in the compressive strengths are respectively: for 0.5% fiber 24.84% (5 mm fibers length), 17.06% (10 mm fibers length) and 18.90% (30 mm fibers length); for 1.0% fiber 54.48% (5 mm fibers length), 44.09% (10 mm fibers length) and 32.33% (30 mm fibers length); for 1.5% fiber 66.56% (5 mm fibers length), 56.69% (10 mm fibers length) and 44.84% (30 mm fibers length); for 2.0% fiber 81.30% (5 mm fibers length), 73.96% (10 mm fibers length) and 68.53% (30 mm fibers length).

Fig. 5-44 and Fig. 5-45 show the linear trends of reducing the compressive strengths with respect to the combination of increase in fiber percentages and variation in fiber lengths.

While as observed by Formisano et al. (2020) (Chapter 2, Fig. 2-65), in our case too for structural mortar the average compression stress failure (Fig. 5-58) with different fiber percentage (0.5%, 1.0% & 1.5%) with respect to the dry mass mortar and fiber length (30 mm, 10 mm and 5 mm) combinations has remained above the class M10 (NTC 18 standard). Therefore, the aforesaid combinations of composite products (Fig. 5-58) qualify to be used as building products, also in seismic zones. Moreover, the combination of fiber 2.0% (with respect to the dry mortar mass) and 30mm fiber length exactly meet this criterion (M10 Class).

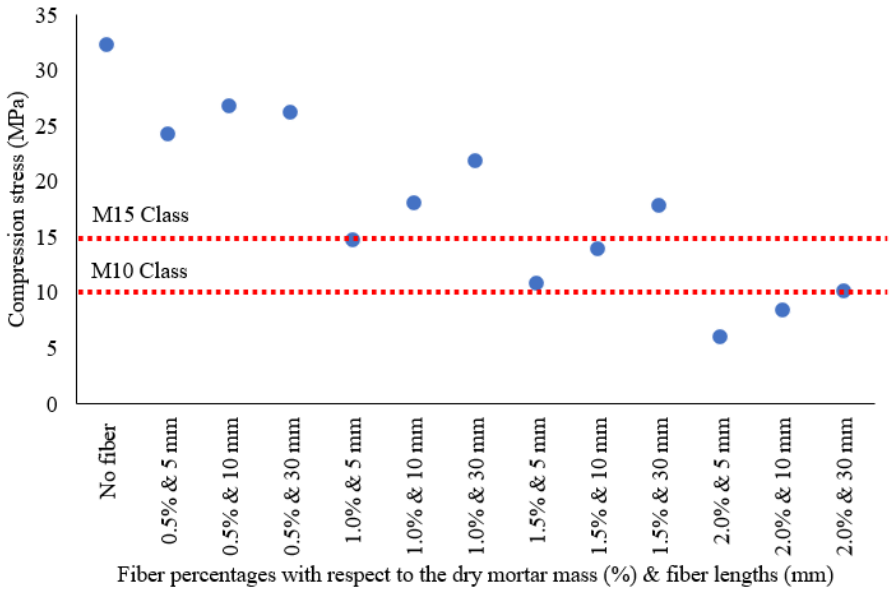

Fig. 5-46. SM and composite SM remained mostly above class M10 (NTC 18 standard).

Notably, all jute fiber percentage (with respect to the dry mass mortar) and fiber length combinations for the thermal mortars have too low compressive strength

values (Fig. 5-49), therefore these composite products prepared with thermal mortar can only be used as thermal insulating elements.

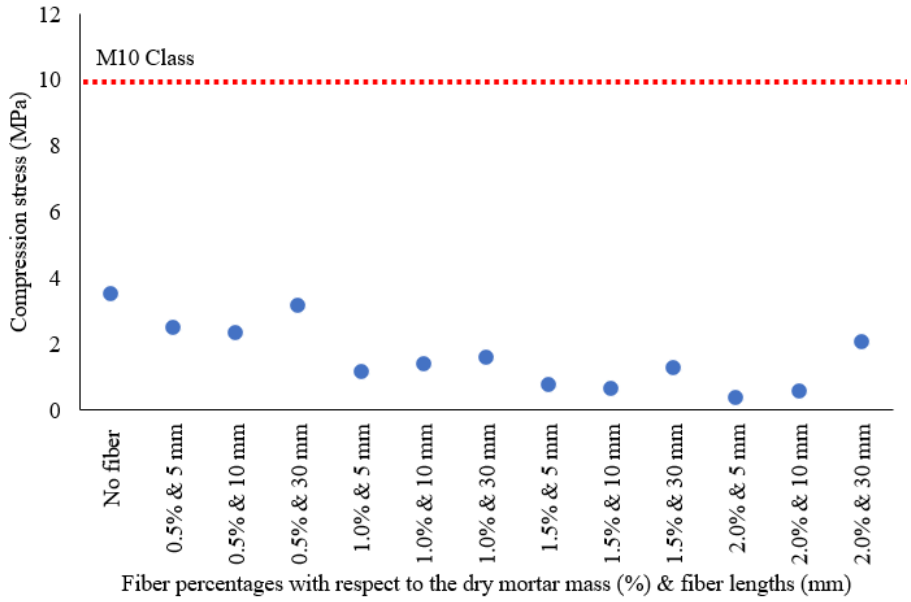

Fig. 5-47. TM and composite TM remained below class M10 (NTC 18 standard).

5.2.3 Thermal properties

The un-strengthened thermal and structural mortars (without fiber), and jute fiber thermal and structural composite mortars insulating performances have been evaluated by comparing their Thermal Conductivity (TC) values.

Fig. 5-48 (Table 5-14) presents the TC values of the structural and thermal mortars evaluated at different temperatures.

After oven drying, the normal thermal mortar has the following TC values: 0.230 W/mK (@10°C), 0.236 W/mK (@20°C) and 0.241 W/mK (@30°C). interestingly the presence of spherical insulating recycled aggregates (Fig. 5-3) provides lower TC values to thermal mortar.

Moreover, the normal SM has the TC values equal to 0.759 W/mK, 0.771 W/mK and 0.793 W/mK respectively (@ 10, 20 and 30°C). Linear trends of the TC have

been observed for all samples, with minimum and maximum values corresponding to 10°C and 30°C, respectively, see Table 5-14 for regression data.

Fig. 5-49 and Fig. 5-50 represent the TC values of the thermal and structural composite mortars, respectively. In these figures only the TC values of the samples after moisture removal through oven drying (for details see Section 5.1.2.3) have been presented. It is evident that in both cases, with the increase in fiber percentages (with respect to the mortar mass) the TC value decreases, therefore it can be demonstrated that the insulating capacity of the composite mortars improve linearly.

Moreover, in the same fiber percentage category (i.e., 0.5%, 1.0%, 1.5% and 2.0% with respect to the mortar mass), it has been observed that the small fibers have better performances than longer ones.

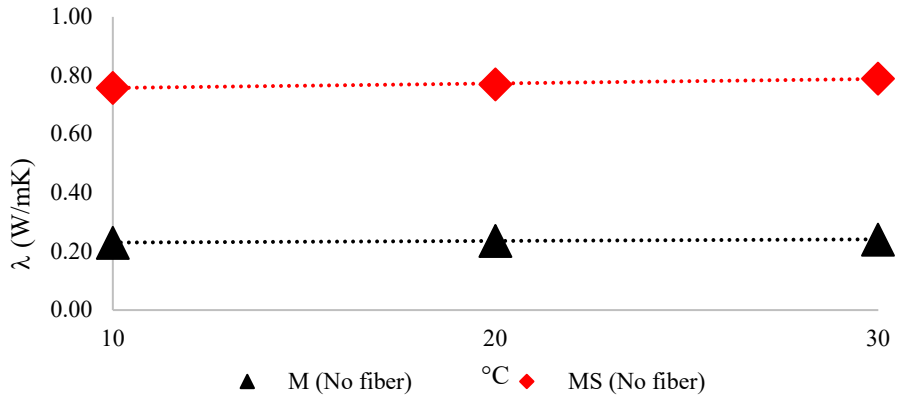

Fig. 5-48.Thermal conductivity comparison: Thermal mortar Vs. Structural mortar, without fiber.

Table 5-14. Linear Regression respect to the thermal conductivity trends

	A	B	R^2
Thermal mortar –> M (No fiber)	0.0016	0.7414	0.9745
Structural mortar – >MS (No fiber)	0.0006	0.2241	0.9958

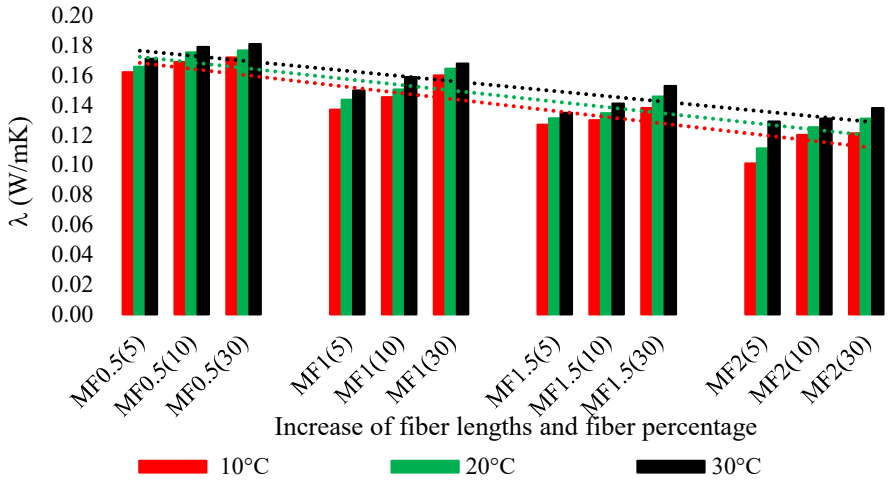

Fig. 5-49. TC after oven drying: Reduction in TC values of the thermal composite mortars with the increase of fiber percentages.

Table 5-15. Linear regression respect to the thermal conductivity tends with fiber percentage increment

	A	B	R^2
Fiber percentage increment @ 10°C	-0.004	0.1724	0.7500
Fiber percentage increment @ 20°C	-0.0038	0.1763	0.7302
Fiber percentage increment @ 30°C	-0.0034	0.1800	0.7461

Comparing the measured TC values (@ 10°C, 20°C and 30°C) of the normal thermal mortar M-(No fiber) with the TC values of the composite samples (i.e., with fibers), we can underline that the TC values always decrease when the fiber percentage and the mean temperature are increased (Fig. 5-49, Table 5-15 and Table 5-17).

The TC decreasing percentage vary in average between 0.1% and 3% with a peak decreasing value equal to 6.5% recorded for the sample MF2(5) from 20°C to 30°C. These decrease in TC, highlight the improvement of the insulating capacity of each composite mix.

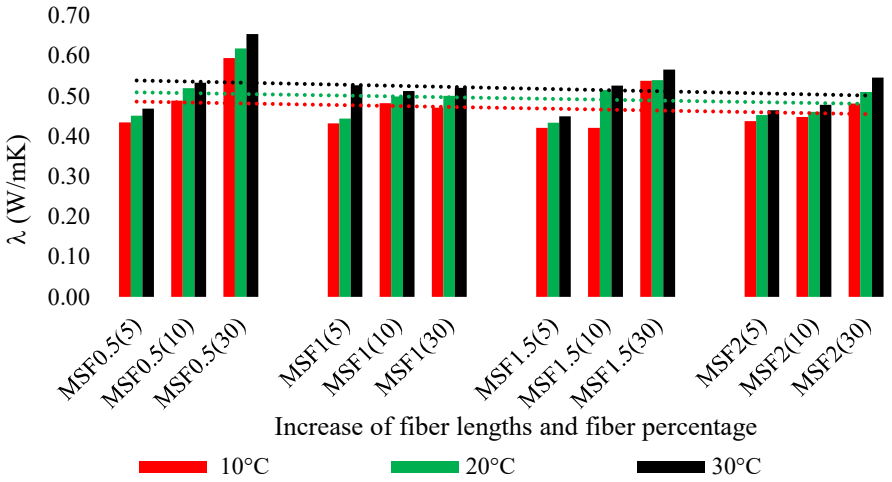

Fig. 5-50. TC after oven drying: Reduction in TC values of the structural composite mortars with the increase of fiber percentages.

Table 5-16.. Linear regression respect to the structural conductivity trends with fiber percentage increment

	A	B	R^2
Fiber percentage increment @ 10°C	-0.0022	0.4885	0.0417
Fiber percentage increment @ 20°C	-0.0021	0.5116	0.0353
Fiber percentage increment @ 30°C	-0.0027	0.5417	0.0533

Moreover, comparing the measured TC values (@ 10°C, 20°C and 30°C) of the normal structural mortar i.e., MS (No fiber) with the TC values of the thermal-composite mortar samples (i.e., with fibers used with respect to mortar mass), here too we have observed that the TC values almost always decrease with increasing mean temperature and fiber percentage (Fig. 5-50, Table 5-16 and Table 5-18).

In this case, the TC decreasing percentage vary in average between 0.1% and 3% with a peak decreasing value equal to 11.4% recorded for the sample MSF1.5(10) from 10°C to 20°C. These decrease in TC, highlight the improvement of the insulating capacity of each individual composite mix.

Table 5-17. The percentage reduction in thermal conductivity value [λ (W/mK)] of the thermal composite mortars, when compared with the sample without fiber i.e. M (No fiber).

	λ [W/mK]		
	@ 10°C	@ 20°C	@ 30°C
M (without fiber)	0.230	0.236	0.241
MF0.5(5)	29.32%	29.66%	28.86%
MF0.5(10)	26.36%	25.58%	25.62%
MF0.5(30)	25.05%	25.08%	24.79%
MF1(5)	40.31%	39.03%	37.67%
MF1(10)	36.69%	36.11%	33.93%
MF1(30)	30.28%	30.25%	30.19%
MF1.5(5)	44.71%	44.29%	43.94%
MF1.5(10)	43.36%	42.89%	41.41%
MF1.5(30)	39.87%	38.10%	36.42%
MF2(5)	55.99%	52.91%	46.40%
MF2(10)	47.71%	46.88%	45.56%
MF2(30)	47.23%	44.38%	42.66%

Table 5-18 The percentage-reduction in thermal conductivity value [λ (W/mK)] of the structural composite mortars, when compared with the sample without fiber i.e. MS (No fiber).

	λ [W/mK]		
	@ 10°C	@ 20°C	@ 30°C
MS (without fiber)	0.759	0.770	0.790
MSF0.5(5)	42.75%	41.46%	40.67%
MSF0.5(10)	35.57%	32.57%	32.51%
MSF0.5(30)	21.67%	19.70%	17.17%
MSF1(5)	43.05%	42.32%	33.29%
MSF1(10)	36.45%	35.17%	35.17%
MSF1(30)	37.90%	35.04%	34.16%
MSF1.5(5)	44.57%	43.69%	43.16%
MSF1.5(10)	44.57%	33.19%	33.46%
MSF1.5(30)	29.06%	29.90%	28.39%
MSF2(5)	42.29%	41.19%	41.21%
MSF2(10)	40.96%	40.14%	39.50%
MSF2(30)	36.59%	33.74%	30.87%

5.2.4 The influence of moisture on Thermal Conductivity (TC)

Table 5-20, Table 5-21 and Table 5-22 present the TC values of all structural mortar and structural composite mortar samples prepared with combinations as stated in Table 5-1.

The TC tests were conducted on each sample on the 10^{th}, 15^{th} , 22^{nd} and 28^{th} day of the natural drying period, while the last TC measurment was done after the oven drying (Fig. 5-22) at a constant temperature of 50°C.

These five mesurements on each samples were done in order to evaluate the influence of moisture on TC values. It was found that the TC value decreased with the reduction of moisture containt in each sample, and it is true for all. Conversely, at complete dry state (after the oven drying), the samples with smallest fiber length and higher fiber percentage (with respect to the dry mortar mass) found to have lowest TC value. The lowest TC value found for the sample MSF0.5(5). Notably the lower TC value means bettter insulation capacity.

Fig. 5-52, Fig. 5-53 and Fig. 5-54 represent the change and decrease in TC with the reduction of moisture in the samples MSF1(30), MS1(10) and MSF1(5) respectively, see Table 5-19 for regression data. This reduction in TC indicates the improvement of samples insulating capacity. From the first TC measurement conducted on the 10^{th} day of natural drying to the forced oven drying TC measurement (when humidity contain quasi-zero): approximately 37.9%, 36.6% and 28.6% reduction in TC and 10.4%, 11.2% and 10.9% reduction in sample masses have been observed for the samples MSF1(30) (Fig. 5-51), MS1(10) (Fig. 5-52) and MSF1(5) (Fig. 5-53), respectively.

It is possible to note that, in average, water presence influences the TC measurement producing 1% TC reduction for 1 g of mass reduction during natural drying. At the end of this period the sample has brought itself to thermodynamic equilibrium with the test environment (the humidity of the laboratory is kept at 60% + - 10%).

Notably the complete drying is achieved (for the samples MSF1(30) on 43th day, MS1(10) on 40th day and MSF1(5) on 44th day) by keeping the sample in the oven at a constant temperature of 50° C for about 10 days, at the end of which the last weight and thermal conductivity measurement was performed.

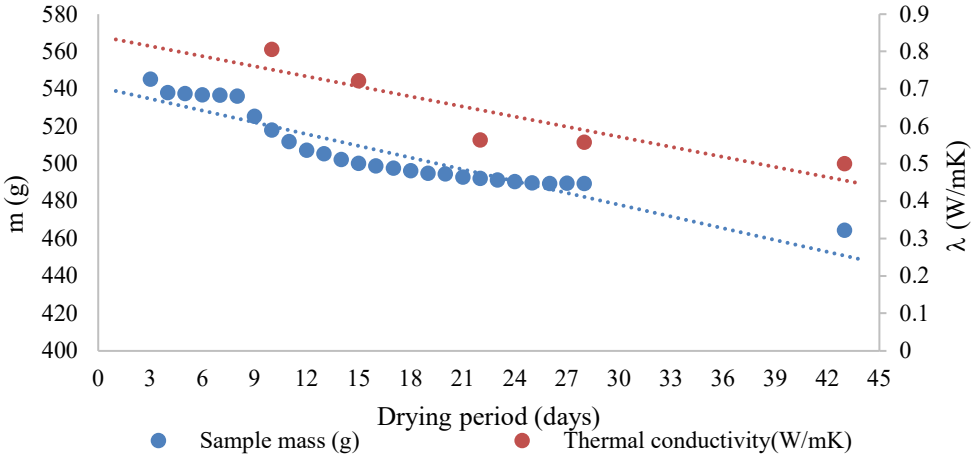

Fig. 5-51. MS1F1(30)T1 - Change in thermal conductivity with respect to the change in sample mass.

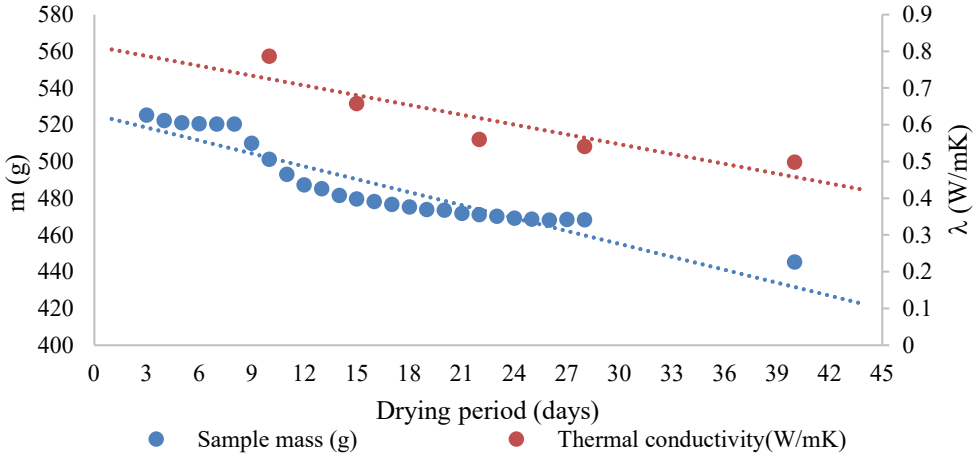

Fig. 5-52. MS1F1(10)T1 - Change in thermal conductivity with respect to the change in sample mass.

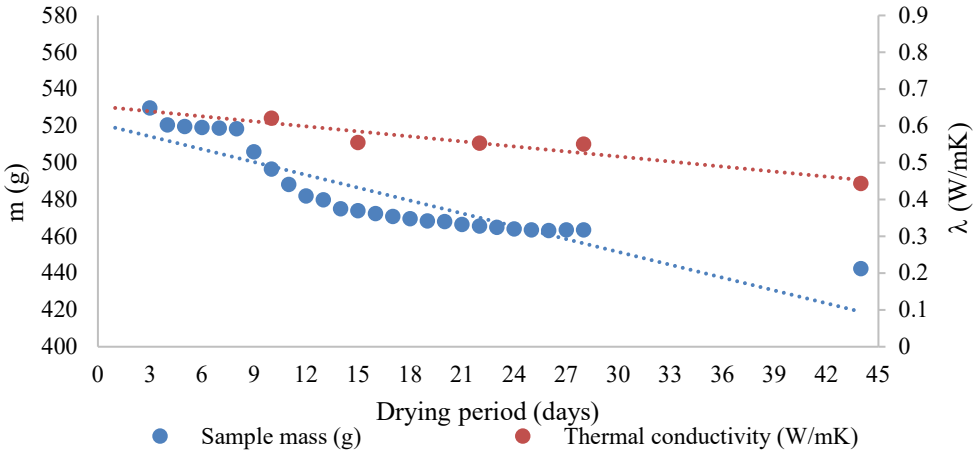

Fig. 5-53. MS1F1(5)T1 - Change in thermal conductivity with respect to the change in sample mass.

Table 5-19. Linear Regression respect to the mass and thermal conductivity trends with respect to the drying period.

		A	B	R2
MS1F1(30)T1 (Fig. 5-51)	Mass (g)	-2.0983	540.96	0.8717
	Thermal conductivity (W/mK)	-0.0090	0.8410	0.8068
MS1F1(10)T1 (Fig. 5-52)	Mass (g)	-2.3496	525.61	0.8680
	Thermal conductivity (W/mK)	-0.0089	0.8140	0.8150
MS1F1(5)T1 (Fig. 5-53)	Mass (g)	-2.3260	521.38	0.8095
	Thermal conductivity (W/mK)	-0.0046	0.6536	0.8888

Table 5-20. Thermal conductivities of the structural mortars and composite mortars

	λ [W/m.K]					
	@10°C	@20°C	@30°C	@10°C	@20°C	@30°C
		MSF0.5(5)			**MSF1(5)**	
10th day of natural drying	0.547	0.566	0.598	0.598	0.621	0.650
15th day of natural drying	0.482	0.511	0.555	0.524	0.555	0.597
22nd day of natural drying	0.449	0.471	0.497	0.537	0.554	0.578
30th day of natural drying	0.451	0.462	0.475	0.533	0.551	0.573
After oven drying	0.434	0.451	0.469	0.432	0.444	0.527
		MSF1.5(5)			**MSF2(5)**	
10th day of natural drying	0.637	0.692	0.757	0.685	0.735	0.741
15th day of natural drying	0.569	0.611	0.647	0.491	0.519	0.564
22nd day of natural drying	0.548	0.569	0.591	0.475	0.491	0.510
30th day of natural drying	0.448	0.466	0.489	0.468	0.482	0.504
After oven drying	0.420	0.433	0.449	0.438	0.453	0.464

Table 5-21. Thermal conductivities of the structural mortars and composite mortars

	λ [W/m.K]					
	@10°C	@20°C	@30°C	@10°C	@20°C	@30°C
	MSF0.5(10)			**MSF1(10)**		
10th day of natural drying	0.707	0.742	0.797	0.744	0.787	0.832
15th day of natural drying	0.522	0.553	0.576	0.608	0.659	0.679
22nd day of natural drying	0.527	0.544	0.566	0.540	0.561	0.577
30th day of natural drying	0.521	0.532	0.549	0.524	0.542	0.573
After oven drying	0.489	0.519	0.533	0.482	0.499	0.512
	MSF1.5(10)			**MSF2(10)**		
10th day of natural drying	0.696	0.749	0.817	0.800	0.866	0.940
15th day of natural drying	0.589	0.624	0.674	0.502	0.547	0.603
22nd day of natural drying	0.520	0.534	0.553	0.460	0.477	0.501
30th day of natural drying	0.503	0.520	0.543	0.437	0.452	0.469
After oven drying	0.420	0.514	0.526	0.448	0.461	0.478

Table 5-22. Thermal conductivities of the structural mortars and composite mortars

	λ [W/m.K]					
	@10°C	@20°C	@30°C	@10°C	@20°C	@30°C
	MSF0.5(30)			**MSF1(30)**		
10th day of natural drying	0.833	0.906	0.974	0.672	0.805	0.851
15th day of natural drying	0.781	0.840	0.898	0.567	0.721	0.736
22nd day of natural drying	0.707	0.729	0.756	0.485	0.563	0.583
30th day of natural drying	0.616	0.635	0.680	0.536	0.557	0.583
After oven drying	0.594	0.618	0.654	0.471	0.500	0.520
	MSF1.5(30)			**MSF2(30)**		
10th day of natural drying	0.746	0.800	0.866	0.658	0.672	0.707
15th day of natural drying	0.569	0.629	0.664	0.558	0.636	0.651
22nd day of natural drying	0.547	0.579	0.599	0.569	0.589	0.617
30th day of natural drying	0.554	0.572	0.592	0.497	0.519	0.574
After oven drying	0.538	0.540	0.566	0.481	0.510	0.546

5.3 Integrated properties and observations

5.3.1 Flexural strength vs strain energy

The force (F) - displacement (δ) curves of some significative thermal mortar samples without fibers (Fig. 5-54) and composite thermal mortar samples with 2% fiber (with respect to the mortar mass) and with 30 mm, 10 mm and 5 mm fiber lengths are shown in Fig. 5-55, Fig. 5-56 and Fig. 5-57, respectively.

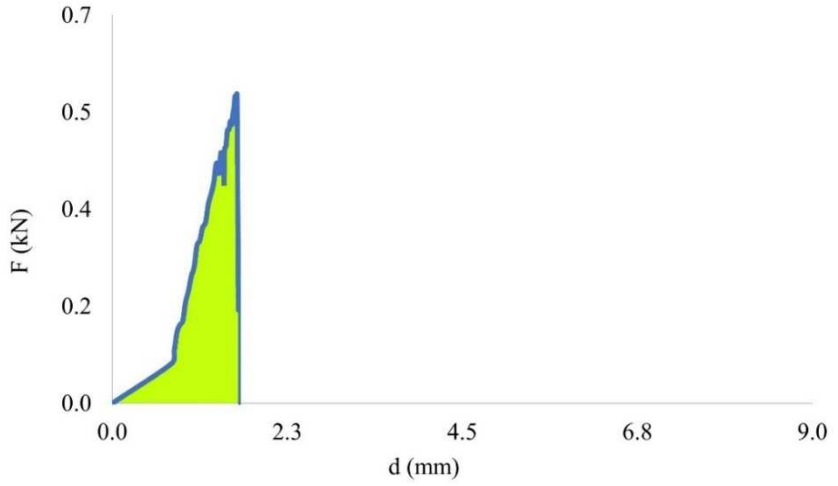

Fig. 5-54. Thermal mortar, strain energy graph of M4M1S3 (without fiber).

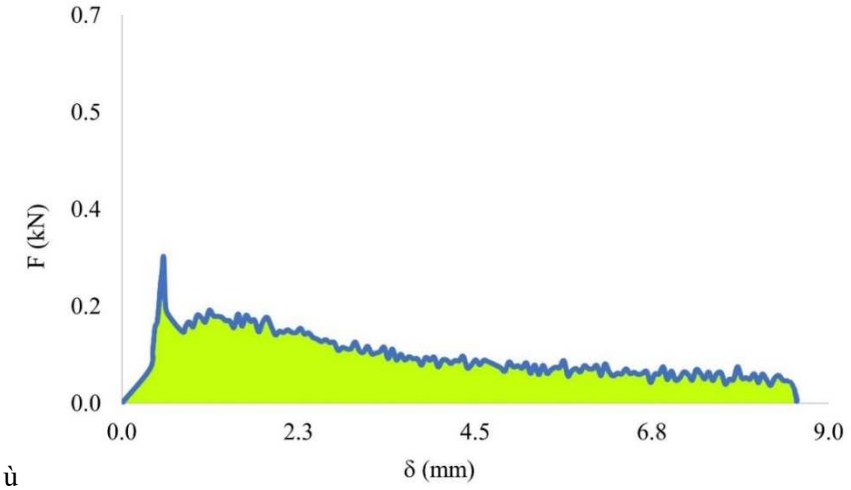

ù

Fig. 5-55. Thermal composite-mortar, strain energy graph of M1F2(30)M1S4.

In the case of the thermal mortar, the strain energy capacity has been increased near about 442% for 30 mm fiber length (Fig. 5-55), 8% for 10 mm fiber length (Fig. 5-56). While decrease in strain energy of -67% for 5 mm fiber length (Fig. 5-57). These comparisons are proposed with reference to the sample M4M1S3 without fiber.

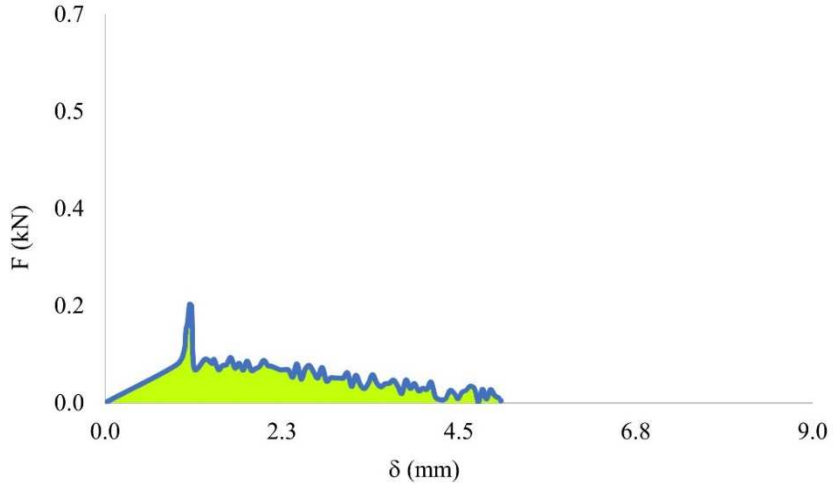

Fig. 5-56. Thermal composite-mortar, strain energy graph of M1F2(10)M1S3.

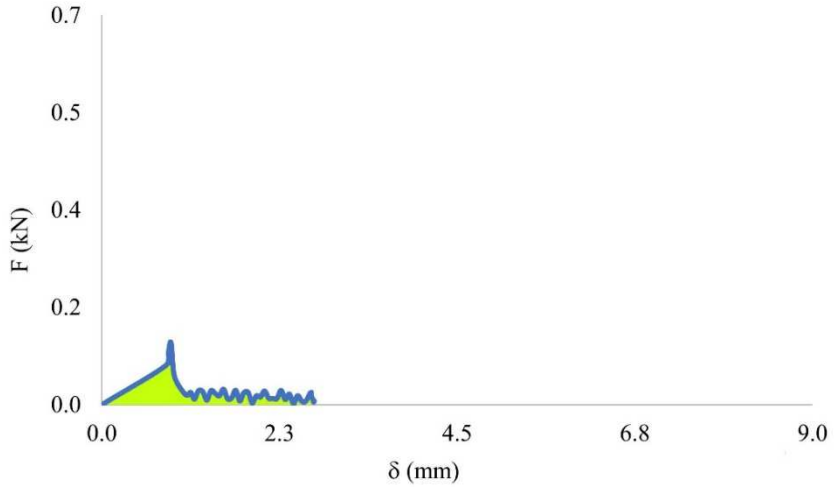

Fig. 5-57. Thermal composite-mortar, strain energy graph of M1F2(5)M2S2.

While the force (F)-displacement (δ) curves of some significative structural mortar samples without fiber (Fig. 5-58) and composite thermal mortar samples with 2% fiber (with respect to the mortar mass) and with 30 mm, 10 mm and 5 mm fiber lengths have shown in Fig. 5-59, Fig. 5-60 and Fig. 5-61, respectively .

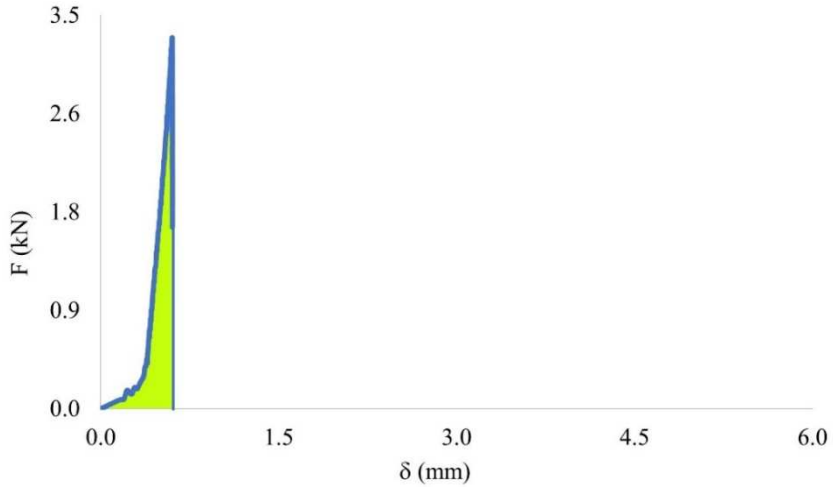

Fig. 5-58. Structural mortar, strain energy graph of MS1M2S2 (without fiber).

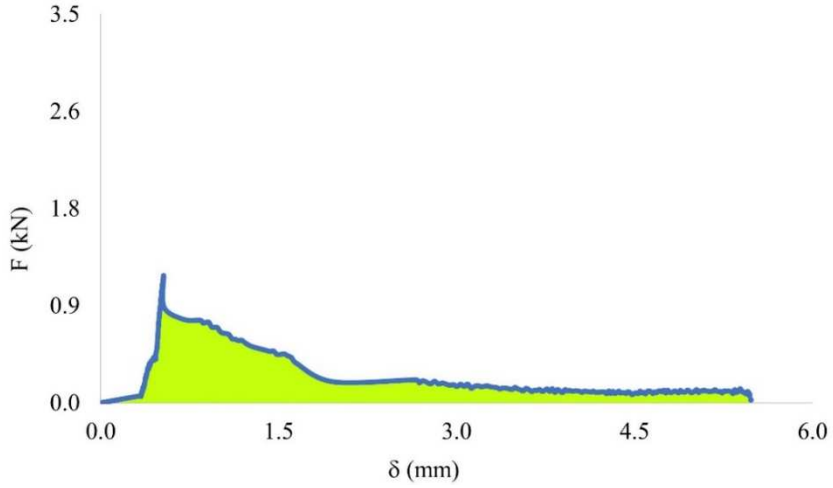

Fig. 5-59. Structural composite-mortar, strain energy graph of MS2F2(30)M2S2.

Instead, in the case of the structural mortar, the strain energy capacity has been increased near about 547% for 30mm fiber length (Fig. 5-59), 217% 10mm fiber length (Fig. 5-60), and 98% for 5mm fiber length (Fig. 5-61). The comparison is done with reference to the sample MS1M2S2 without fiber.

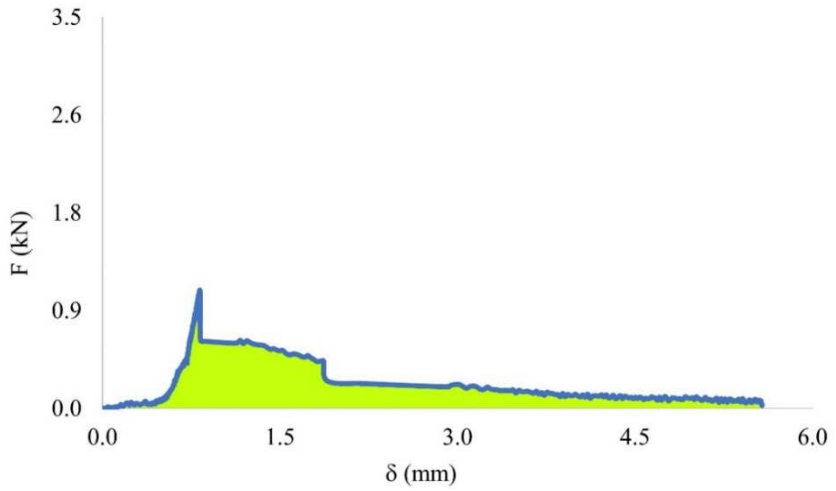

Fig. 5-60. Structural composite-mortar, strain energy graph of MS2F2(10)M2S2.

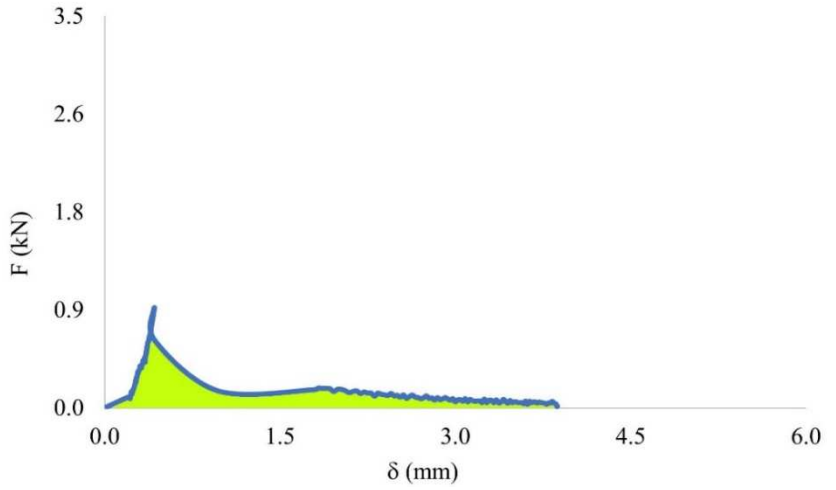

Fig. 5-61. Structural composite-mortar, strain energy graph of MS2F2(5)M1S2.

Fig. 5-62 presents the deformed sample (with 1% 30 mm fibers with respect to the dry mortar mass) at flexural ultimate limit state. It can be clearly seen how the fibers in the cross section lower part still transfer tensile loads even if the mortar matrix is already cracked. Although due to the presence of the embodied fibers, the flexural strength of the composite-samples reduces but the strain energy capacity increases. This improved strain energy capacity is useful when it is necessary to dissipate the effects of extreme loads like earthquakes.

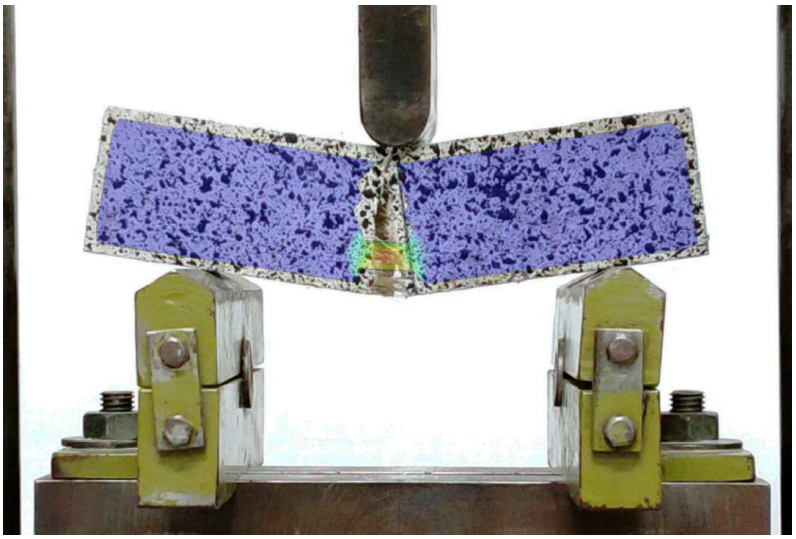

Fig. 5-62. composite SM sample with 1 % fiber (30 mm) with respect to the dry mortar mass

5.3.2 Compressive strength Vs Thermal conductivity

Fig. 5-63 and Fig. 5-64 represent the integrated (thermal and structural) behavior of the thermal and structural composite mortars. It is clearly visible in these graphs that the compression strength reduces gradually with respect to the fiber percentages (from 0.5 to 1%, 1.5% and 2%) and fiber lengths (from 30mm to 10mm and 5mm), as well as the thermal conductivity does the same.

When composite mortars have been compared with non-strengthened mortar sample (without fiber), a drop in compressive strength and improvement in

insulating property (with the reduction of TC value) have been observed. Table 5-23 (composite-TM) and Table 5-24 (composite-SM) represent the average percentage variation in compressive strength and TC, respectively, when compared with mortar sample without fiber.

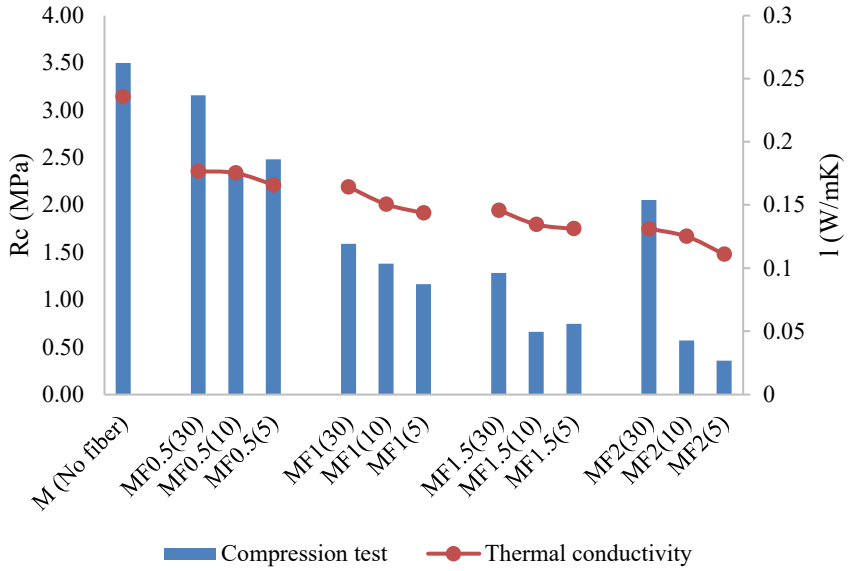

Fig. 5-63. Thermal mortars: compressive strength & thermal conductivity graph

Table 5-23. Integrated comparative behavior of the thermal composite mortars with respect to thermal mortar sample without fiber

Fiber percentage with respect to the mortar mass	Reduction in compressive strength	Improvement in insulating capacity (with reduction in thermal conductivity @ 20°C)
0.5% (avg. of 5 mm, 10 mm and 30 mm)	23.91%	26.77%
1.0% (avg. of 5 mm, 10 mm and 30 mm)	60.62%	35.13%
1.5% (avg. of 5 mm, 10 mm and 30 mm)	74.37%	41.76%
2.0% (avg. of 5 mm, 10 mm and 30 mm)	71.64%	48.06%

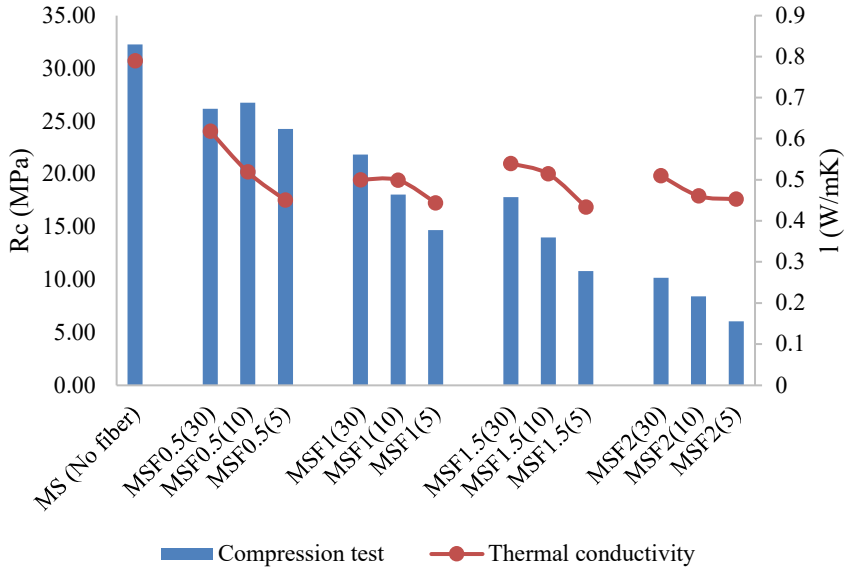

Fig. 5-64. Structural mortars: compressive strength & thermal conductivity graph.

Table 5-24. Integrated comparative behavior of the structural composite mortars with respect to thermal mortar sample without fiber

Fiber percentage with respect to the mortar mass	Fiber percentage with respect to the mortar mass	Improvement in insulating capacity (with reduction in thermal conductivity @ 20°C)
0.5% (avg. of 5 mm, 10 mm and 30 mm)	20.27%	31.24%
1.0% (avg. of 5 mm, 10 mm and 30 mm)	43.63%	37.51%
1.5% (avg. of 5 mm, 10 mm and 30 mm)	56.03%	35.59%
2.0% (avg. of 5 mm, 10 mm and 30 mm)	74.60%	38.36%

Therefore, although the introduction of fiber yields to a lower compressive strength, at the same time it enhances the thermal insulation of composite mortars.

5.4 Conclusions

This chapter has reported the results of experimental tests intended to determine the mechanical and thermal properties of relevance for SM, TM and jute fiber composite mortars (prepared with SM and TM). In this process different jute fiber of lengths 30 mm, 10 mm and 5 mm and different fiber percentages 0.5%, 1.0%, 1.5% and 2.0% (with respect to the mortar masses), of various combinations have been used.

Notably, in our case, all the jute fiber composite mortars have shown ductile behavior and it has been noted that flexural and compressive strengths of the composite specimens have reduced with jute fiber addition, and these reductions linearly increase with the increase in amount/percentage of the fiber and jute fiber lengths also have influenced these values. Similar trend has also been reported by Formisano et al. (2020) for the jute fiber composite mortar, the authors reported to have obtained in average 10% and 25% less the strength and stress, respectively when compared with un-strengthened samples. This could be due to the fact that natural fibers are hydrophobic in nature. As for composite mortar preparation, jute fibers individually absorb and collectively trap water, and after 28 day drying time, when majority of the water get evaporated, it leaves some hollow cavity inside. These cavities are responsible to induce weakness to the composite mortar samples. On the other hand, with the introduction of jute fiber, the uniformity and compactness of the original mortar minimize to have weaker material bonding.

Conversely, the maximum increment in strain energy of more than 500 % and 450 % have been observed for SM and TM composite samples with 2% fiber (30 mm) with respect to the mortar mass. While Formisano et al. (2020) have presented the force-displacement graphs, and authors only talk about the increment in the mean ultimate displacement by 15% due to the addition of fiber, although from graphs it is clearly seeable the improvement of strain energy same as observed by us.

Also, with the induction of fibers TC values have reduced in the case of all composite mortars. But these reduction in TC means the enhancement the insulating capacity of these specimens. The best performer among all SM composite samples

found to be the specimen with 1.5% fiber (5mm) used with respect to the mortar, while in TM composite sample category the specimen with 2.0% fiber (5mm) used with respect to the mortar, with decrease in TC value (improvement in insulation capacity) of more than 40% and 50%, respectively.

Notably, it has been observed that with longer the fiber (30 mm) specimens have optimum strain energy, this is due to the fact that the longer fibers have greater capacity to dissipate energy (load). Contrary, with shorter fiber (5 mm) specimens have better insulation capacity, with reduced TC values. Based on these findings and results, further research activities were also conducted on the masonry wall integrated upgrading.

6. Phase II(a) – Further developments

This chapter is the extension of the works explained in Chapter 5. Additional research work on the mechanical behaviors and thermal performances of composite mortar were mainly conducted, with the aim to improve the results acquired in the Phase II.

Three cases were evaluated in this sub-phase:

1) the first case the thermal and structural composite mortar samples were prepared using the Same Average Water (SAW) for all fiber lengths (30mm, 10mm and 5mm). in this case two different fiber percentages (0.5% and 1%) were used and two different average amounts were calculated for 0.5% fiber (with respect to the dry mortar mass) and 1% fiber (with respect to the dry mortar mass) categories.
2) in the second case the pre-fabricated and pre-present insulation materials (i.e., Recycled Aggregates (RAs)) were separated from the original thermal mortar, and newer thermal composite mortar samples without (No) Recycled Aggregates (nRA) were prepared using all fiber lengths (30 mm, 10mm and 5 mm) and 1% fiber (with respect to the dry mortar mass). In this case too SAW (for all fiber lengths 30mm, 10mm and 5mm) have been used.
3) in the third case the structural composite mortar samples were prepared using Same Water (SW), i.e., same amount which have been used to prepare the normal mortar samples, in the Phase-I. The samples were prepared using all fiber lengths (30 mm, 10 mm and 5 mm) and for 0.5% and 1% fiber (with respect to the mortar mass).

During this sub-phase too, the flexural strength, compression strength and strain energy of each individual composite mortar type was analyzed, and later these values were compared with the mortar samples of same fiber percent (with respect to the dry mortar mass) and fiber lengths from the previous phases. Therefore, the prime objective is to use these refined data and choose the combinations to be used for the thermo-structural masonry upgrading in the next phase.
Notable in this sub-phase none of the composite mortars prepared with SAW or SW were subjected to the thermal conductivity test.

All the above-mentioned tests were conducted in the Material Testing Laboratory of the University of Cagliari, Italy and the Strength Laboratory of the University of Salerno, Italy.

6.1 Materials and methods

In this chapter the themo-mechanical characterization of the newer jute fiber composite Thermal Mortar (TM) and Structural Mortar (SM) are presented. For composite mortar preparation, only two types of jute fibers percentages i.e., 0.5 % respect to the mortar mass and 1 % with respect to the mortar mass have been used.

6.1.1.1 Raw Jute fibers

In this sub-phase, only one or two types of fiber percentages (with respect to the dry mortar mass) have been (Table 6-1) used to prepare the composite mortar (TM and SM) samples.

Table 6-1. Composite TM and SM preparation

		Fiber length categories		
		30mm	10mm	5mm
Composite samples	0.5%	yes	yes	yes
	1.0%	yes	yes	yes

6.1.2 Mortars

Same types of mortars as used in the phase-II. i.e., cement-based Structural Mortars (SM) (Fig. 5-2) and lime based Thermal Mortar (TM) (Fig. 5-3) have been used in this sub-phase too.

6.2 Methods

In addition to the samples as stated in the Phase-II, another three types (mentioned below) of jute fiber composite samples were prepared and later their mechanical behaviors (flexural and compressive) have been studied.

6.2.1 Case 1 – Composite mortars prepared with Same Average Water (SAW) and with Recycled Aggregates (nRA)

In this case the SAW has been used for the preparation of the composite mortars using the 30mm,10mm and 5mm jute fibers and only 0.5% and 1.0 % of jute fibers (with respect to the mortar thermal and structural mortar mass) have been used.

Here the amount of water to be used had been determined by averaging the amount of waters used in the previous experimental phase for TM and for SM composite mortar preparation as in Table 5-3 and Table 5-4, respectively. Therefore, equal amount of water has been used for all three fiber lengths (i.e., 30 mm, 10 mm and 5 mm). This is just contrary to the amount of water used in the Phase-II composite mortar preparation i.e., different amount of water has been used for each fiber lengths.

It is important to highlight that during the TM composite mortar preparation, the pre-fabricated insulation materials have not been separated from the original mortar composition.

The mixing time here was slightly more than that was followed in the phase-I and it was near about 7-10 minutes. Here the mix was prepared by adding fibers not

all together but continuously in smaller amount. Thus, the water also was poured slowly to achieve the mortar mixture with acceptable consistency.

Table 6-2 presents the percentage of mortar, fiber and water, which have been used for the thermal and structural composite mortar preparation.

Table 6-2. Mix design for the composite mortar mixtures.

		Mortar	Fiber	Water
		[%]	[%]	[%]
Thermal composite mortar	0.5% (30 mm, 10 mm, 5 mm) with respect to the dry mortar mass	72.13	0.36	27.51
	1.0% (30 mm, 10 mm, 5 mm) with respect to the dry mortar mass	69.44	0.72	30.86
Structural composite mortar	0.5% (30 mm, 10 mm, 5 mm) with respect to the dry mortar mass	81.44	0.81	36.08
	1.0% (30 mm, 10 mm, 5 mm) with respect to the dry mortar mass	78.36	1.63	42.87

6.2.2 Case 2 – Thermal composite mortars prepared with 1 % fiber (with respect to the dry mortar mass) and without Recycled Aggregates (nRA)

Here only 1.0 % of jute fiber (of lengths of 30mm, 10mm and 5mm) with respect to the thermal mortar dry mass has been mixes with TM without Recycled Aggregates (RA) to prepare the composite mortar.

In this case, the pre-existing insulating RAs (see Fig. 5-3) have been removed from the original mortar using a sieving machine and the SAW has been used for the composite preparation. The composition mixing time and mixing procedure similar to that has been followed in section 6.2.1.

The choice to use the 1% jute fiber (with respect to the dry mortar) for the TM composite mortar preparation was based on the following considerations:

(i) Considering a balance between the integrated properties obtained in the previous measurements .

(ii) Acceptability of these samples as incombustible composites therefore the presence of fiber should be lower and equal to 1%, according to UNI 1350-1.

Table 6-3 presents the percentage of mortar, fiber and water, which have been used for the thermal composite mortar (nRA).

Table 6-3. Mix design for the composite TM (without Recycled Aggregates (RAs)) mixtures.

		Mortar	Fiber	Water
		[%]	[%]	[%]
Thermal composite mortar (without PB)	1.0% (30mm,10mm,5mm) with respect to the dry mortar mass	65.71	0.66	33.63

6.2.3 Case 3 - Thermal mortar without Recycled Aggregates (nRA) and Same water (SW).

In this case, the jute fiber composite-mortars with two different percentages i.e., 0.5% and 1% (with respect to the dry mortar mass) and Same amount of Water (SW).

Here the amount of water has been chosen exactly same as it was used for the normal mortar preparation, in Phase II. The composition mixing time and mixing procedure similar to that has been followed in section 6.2.1.

Table 6-4 reports the details of the mix design which have been used for the TM composite mortar (nRA) preparation.

Notably the combinations of fiber length and fiber percentages (with respect to the mortar mass) of 10mm & 1.0% and 5mm & 1.0% were also prepared using exactly same amount of water (as in Table 6-4), but these two mixture-consistencies have failed the workability tests (shaking table test) and therefore no samples were prepared for these two combination categories.

Table 6-4. Mix design for the structural composite mortar mixtures.

		Mortar	fiber	water
		[%]	[%]	[%]
Thermal composite mortar	0.5% fiber (30 mm, 10mm, 5 mm) with respect to the dry mortar mass	84.32	0.42	15.25
	1.0% fiber (30 mm, 10mm, 5mm) with respect to the dry mortar mass	83.90	0.85	15.25

6.3 Result and discussion

6.3.1 Case 1 - Composite mortars prepared with Same Average Water (SAW) and with Recycled Aggregates (RA)

Composite samples were prepared following the same procedure as mentioned in the section 5.1.2.1. of the Phase-I.

Later, the mechanical properties of the TM and SM composite samples prepared with SAW are evaluated through the flexural and compression tests on 28th day from casting date. The mechanical properties of TM-composite samples are presented in Table 6-5 and Table 6-6 for the flexural tests and Table 6-7 for the compression tests.

While the mechanical properties of SM-composite samples are presented in Table 6-8 and Table 6-9 for the flexural tests and Table 6-10 for the compression tests.

6.3.1.1 TM Composite samples prepared with SAW

For the thermal mortar, it has been observed that the samples cast with SAW (as in Table 6-2) present higher strain energy capacities and flexural strengths, when compared with those same category of samples casted in the Phase-I (i.e., with the same combinations of fiber lengths (30 mm, 10 mm and 5 mm) and fiber percentages with respect to the mortar mass) with different percentage of waters for each combination.

Table 6-5. Thermal composite mortars flexural test properties-1

Sample type	Deflection max. (d)		Strain energy	
	Mean [mm]	Co.V [%]	Mean [kN.mm]	Co.V [%]
M(SAW)F0.5(5)	1.52	3.99	1.08	30.38
M(SAW)F0.5(10)	1.14	46.75	0.65	40.38
M(SAW)F0.5(30)	1.37	22.49	0.86	29.15
M(SAW)F1(5)	1.00	3.47	0.47	10.36
M(SAW)F1(10)	1.07	7.85	0.64	20.86
M(SAW)F1(30)	1.13	2.13	0.90	3.76

Table 6-6. Thermal composite mortars flexural test properties-2

Sample type	Flexural stress (σ)		Flexural strain (ε)		Moment of inertia (I)	
	Mean [MPa]	Co.V [%]	Mean	Co.V [%]	Mean [mm^4]	Co.V [%]
M(SAW)F0.5(5)	2.27	8.42	0.03	3.36	239551.98	2.77
M(SAW)F0.5(10)	2.06	5.55	0.02	46.34	239551.98	2.77
M(SAW)F0.5(30)	2.06	19.19	0.03	21.81	240831.12	2.56
M(SAW)F1(5)	1.49	1.87	0.02	3.97	239551.98	2.77
M(SAW)F1(10)	1.62	7.80	0.02	7.33	239551.98	2.77
M(SAW)F1(30)	1.53	1.85	0.02	2.40	239551.98	2.77

Table 6-5 and Table 6-6 present mechanical properties of TM composite samples prepared with SAW. In Fig. 6-1, the mechanical properties of TM composite samples prepared with various mix were compared (SAW Vs different amount of water for each mix).

When the SAW thermal composite mortar samples were compared with the Phase-I thermal composite mortars of similar category with 0.5% fiber (with respect

to the dry mortar mass), it has been observed that due to the use of SAW, the improvement in *strain energy* of 0.90 kN.mm for of 5 mm fiber length, while increase of 0.45 kN.mm for 10 mm fiber length and increment of 0.28 kN.mm 30 mm fiber length. So as the flexural strengths also improved for same category with 0.5% fiber (with respect to the dry mortar mass) by 1.30 MPa, 1.14 MPa and 0.84 MPa for 5 mm fiber length, 10 mm fiber length and 30 mm fiber length, respectively.

the TM samples prepared with SAW and with 1% fiber (with respect to the dry mortar mass) have demonstrated to have better mechanical (strain energy & *flexural strength*) properties, and these improvements are 0.47 kN.mm & 1.06 MPa for 5 mm fiber length, 0.41 kN.mm & 0.96 MPa for 10 mm fiber lengths and 0.33 kN.mm & 0.90 MPa for 30 mm fiber length, respectively.

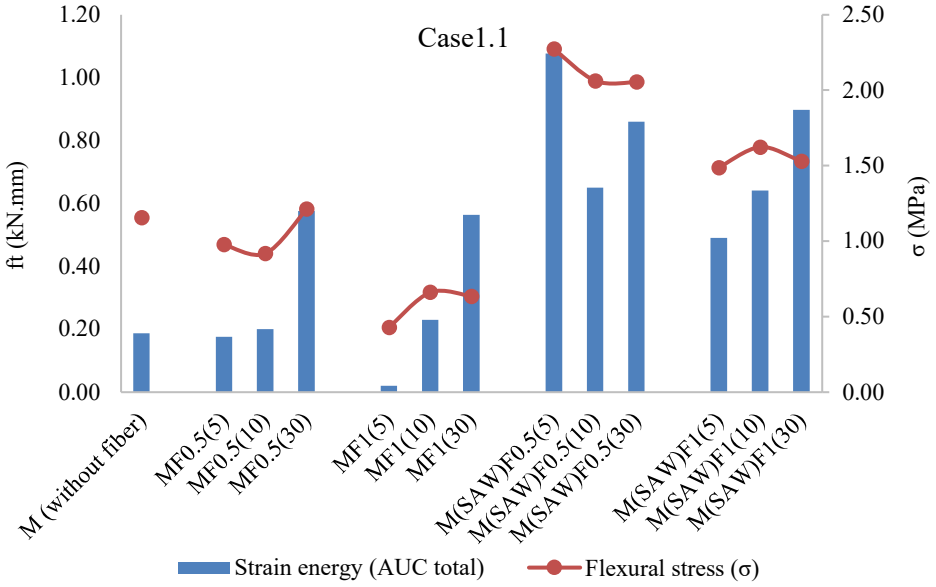

Fig. 6-1. Jute fiber thermal composite mortars flexural test results: SAW Vs. different percentage of water used for different fiber percentage and length combinations.

Table 6-7 presents the compressive strength values of the TM composite samples prepared with SAW. The compressive strengths obtained for the TM

composite samples prepared with SAW (Fig. 6-2) found to be higher, than those of samples casted in Phase -I with different percentage of waters for each same combinations for fiber lengths (mm) and fiber percentages (%) (with respect to the mortar mass).

Table 6-7. Compression tests (@ SAW) – Thermal composite mortars

Sample type	Mean [MPa]	Co.V [%]
M(SAW)F0.5(5)	7.31	6.59
M(SAW)F0.5(10)	6.43	8.56
M(SAW)F0.5(30)	7.84	6.24
M(SAW)F1(5)	4.00	2.75
M(SAW)F1(10)	4.97	3.92
M(SAW)F1(30)	4.90	0.06

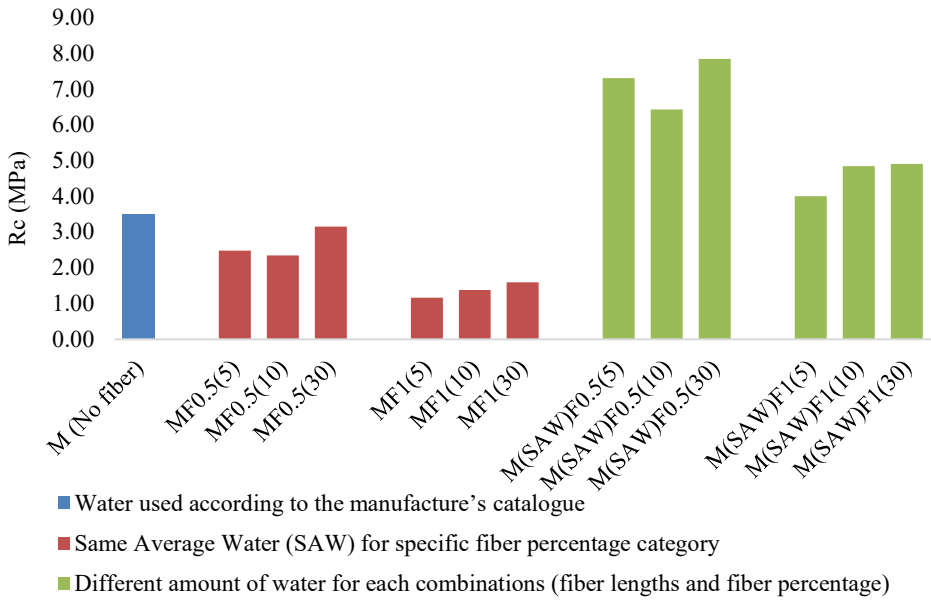

Fig. 6-2. Jute fiber thermal composite mortars compression test results: SAW Vs. different percentage of water used for different fiber percentage and length combinations.

Based on the Fig. 6-2, the improvement in compressive strengths for the combinations of fiber lengths and fiber % (with respect to the dry mortar mass) i.e., 5 mm & 0.5%, 10 mm & 0.5% and 30 mm & 0.5% found to be equal to 4.82 MPa, 4.08 MPa, 4.69 MPa respectively. While for combinations 5 mm & 1.0%, 10 mm & 1.0% and 30 mm & 1.0% obtained compressive strength values are 2.84 MPa, 3.46 MPa and 3.31 MPa, respectively.

6.3.1.2 SM Composite samples prepared with SAW

As for the Structural mortar, it has been observed that the SM composite samples casted with SAW present lower strain energy capacities and flexural strengths (as in Fig. 6-3) than those of same categories of samples casted in the Phase-I (with same combinations for fiber lengths (30 mm, 10 mm and 5 mm) and fiber percentages with respect to the mortar mass) with different percentage of waters for each combination. Table 6-8 and Table 6-9 present mechanical properties of SM composite samples with SAW.

Fig. 6-3 presents the stain energy values, and the flexural strength values of the samples with different category combinations of fiber lengths and fiber percentages (with respect to the dry mortar mass).

Table 6-8. Structural composite mortars flexural test properties-1

Sample type	deflection max. (d)		Strain energy (ft)	
	Mean [mm]	Co.V [%]	Mean [kN.mm]	Co.V [%]
MS(SAW)F0.5(5)	0.51	3.80	0.35	0.89
MS(SAW)F0.5(10)	0.66	26.70	0.46	23.74
MS(SAW)F0.5(30)	0.52	11.16	0.37	24.29
MS(SAW)F1(5)	0.55	4.64	0.41	25.35
MS(SAW)F1(10)	0.76	17.78	0.79	15.28
MS(SAW)F1(30)	0.54	7.93	0.71	24.87

Table 6-9. Structural composite mortars flexural test properties-2

Sample type	Flexural stress (σ)		Flexural strain (ε)		Moment of inertia (I)	
	Mean [MPa]	Co.V [%]	Mean	Co.V [%]	Mean [mm^4]	Co.V [%]
MS(SAW)F0.5(5)	2.08	5.48	0.01	3.18	239578.03	2.41
MS(SAW)F0.5(10)	1.92	6.57	0.01	27.19	239551.98	2.77
MS(SAW)F0.5(30)	1.90	2.82	0.01	11.88	254706.76	1.79
MS(SAW)F1(5)	1.94	5.46	0.01	4.20	241233.71	1.70
MS(SAW)F1(10)	3.27	1.16	0.02	17.74	242608.61	1.64
MS(SAW)F1(30)	3.37	9.10	0.01	7.95	238673.50	0.89

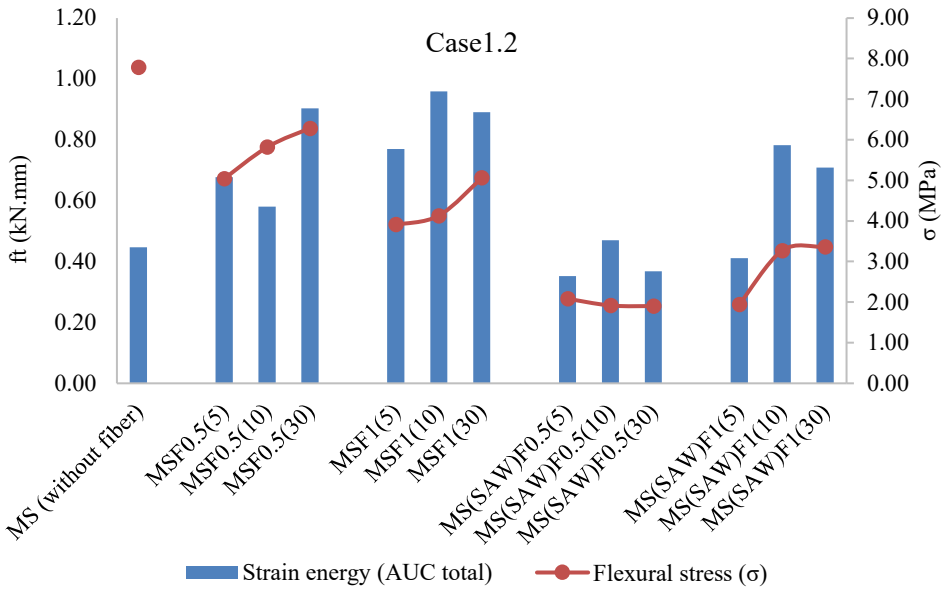

Fig. 6-3. Jute fiber structural composite mortars flexural test results: SAW Vs. different percentage of water used for different fiber percentage and length combinations.

By comparing the SAW structural composite mortars with the Phase-I structural composite mortar samples of 0.5% fiber (with respect to the dry mortar mass), category, it has been observed that, due to the use of SAW, the strain energy decreased (see Fig. 6-3, calculated as MS(SAW)0.5 – MS0.5) near about -0.32 kN.mm for 5 mm fiber length, reductions found to be equal to -0.11 kN.mm for 10 mm fiber length and while, reduction of -0.54 kN.mm have been noticed for 30 mm fiber length.

Although a reduction in strain energy was observed for the mortar samples of 1% fiber (with respect to the dry mortar mass) category, these reductions (see Fig. 6-3, calculated as MS(SAW)1 – MS1) are about -0.36 kN.mm for 5 mm fiber length, -0.18 kN.mm for the 10 mm fiber length and -0.33 for 30 mm fiber length.

Also, decline in flexural strengths of the SM samples prepared with SAW have observed in all combinations of fiber lengths and fiber % (with respect to the dry mortar mass). For 0.5% fiber (with respect to the dry mortar mass) category, these reductions (see Fig. 6-3, calculated as MS(SAW)0.5 – MS0.5) are about -1.97 MPa for 5mm fiber length, -0.86 MPa for 10mm fiber length and -1.70 MPa for fiber length. Similarly, for 1% fiber (with respect to the dry mortar mass) category, these reductions (see Fig. 6-3, calculated as MS(SAW)1 – MS1) are found to be equal to -2.92 MPa for 5mm fiber length, -3.91MPa for 10mm fiber length and -4.38 MPa for 30mm fiber length.

Table 6-10. Compression tests (@ SAW) –structural composite mortars

Sample type	Mean [MPa]	Co.V [%]
MS(SAW)F0.5(5)	7.53	2.24
MS(SAW)F0.5(10)	6.55	6.00
MS(SAW)F0.5(30)	6.52	1.74
MS(SAW)F1(5)	7.53	6.03
MS(SAW)F1(10)	14.78	0.77
MS(SAW)F1(30)	14.31	2.92

Table 6-10 presents the compressive strength values obtained for structural composite mortar samples prepared with SAW. The compressive strengths obtained for the SAW structural composite mortar samples found to be lower in both 0.5% and 1% fiber (with respective to the dry mortar mass) categories.

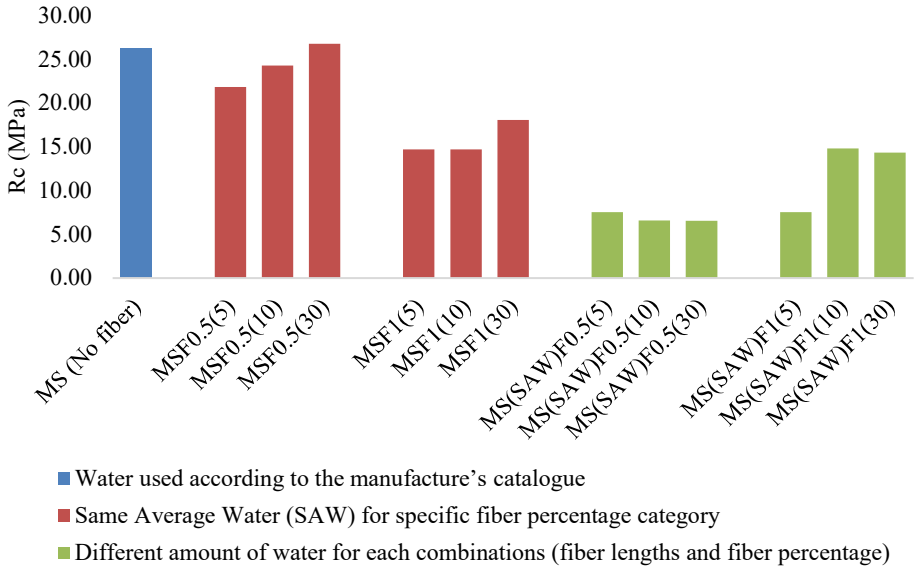

Fig. 6-4. Jute fiber structural composite mortars compression test results: SAW Vs. different percentage of water used for different fiber percentage and length combinations.

Notably, the decrease (see Fig. 6-4, calculated as MS(SAW)0.5 – MS0.5) in compressive strengths for 0.5% fiber (with respect to the dry mortar mass) category observed to be equal to -14.30 MPa for 5mm fiber length, -17.69 MPa for 10mm fiber length and -20.23 MPa for 5mm fiber length.

Similarly, the reduction (see Fig. 6-4, calculated as MS(SAW)1 – MS1) in compressive strengths for 1% fiber (with respect to the dry mortar mass) category found to be -7.16 MPa for 5mm fiber length and -3.72 MPa for 30mm fiber length. Only exception in this category found to be for the 10mm fiber length, in this case improvement 0.10 MPa in compressive strength has been observed.

Actually, exactly opposite behavior has been observed in the case of the structural composite mortars when compared with thermal composite mortar (see, Fig. 6-1 Vs. Fig. 6-3 for flexural strengths and Fig. 6-2 Vs. Fig. 6-4 for compressive strength). This can be explained considering the different properties of the two starting mortars.

Probably the chosen SAW for the structural mortar is far lower than the optimal one while in case of thermal mortar the obtained SAW is prefect to have an optimal mix from the mechanical properties point of view.

6.3.2 Case 2 - TM composite mortars prepared with 1 % fiber (with respect to the dry mortar mass) and without Recycled Aggregates (nRA)

Table 6-11 and Table 6-12 presents the flexural properties of the thermal composite mortars prepared using SAW.

The SAW thermal composite mortar (nRA) samples are compared with the Phase-I thermal composite mortars of similar category compositions of fiber lengths and fiber percentages (with respect to the dry mortar mass) and it has been seen that the thermal composite mortar samples without RA (nRA) prepared with SAW have better mechanical performance and increments in both strain energy capacity and flexural strength have been observed.

Table 6-11. Flexural test properties of the thermal composite mortars (nRA)-1

Sample type	deflection max. (d)		Strain energy (ft)	
	Mean [mm]	Co.V [%]	Mean [kN.mm]	Co.V [%]
M(nRA)(SAW)F1(5)	1.65	22.29	0.55	20.87
M(nRA)(SAW)F1(10)	2.07	3.00	1.18	15.12
M(nRA)(SAW)F1(30)	1.33	17.92	1.73	48.66

Table 6-12. Flexural test properties of the thermal composite mortars (nRA)-2

Sample type	Flexural stress (σ)		Flexural strain (ε)		Moment of inertia (I)	
	Mean [MPa]	Co.V [%]	Mean	Co.V [%]	Mean [mm⁴]	Co. V [%]
M(nRA)(SAW)F1(5)	1.49	2.41	0.03	21.64	239551.9	2.77
M(nRA)(SAW)F1(10)	1.63	2.33	0.04	3.04	239551.9	2.77
M(nRA)(SAW)F1(30)	1.62	0.78	0.03	17.52	239551.9	2.77

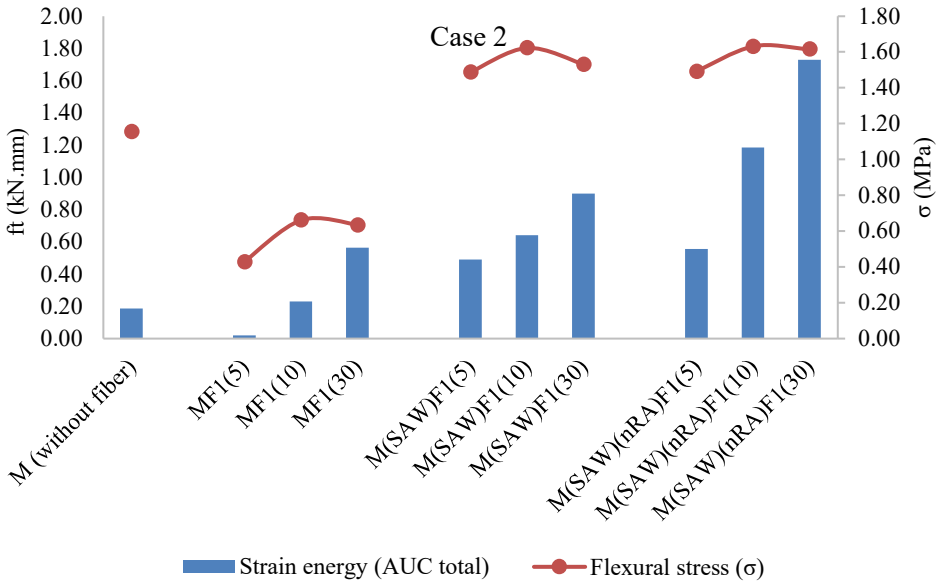

Fig. 6-5. Jute fiber thermal composite mortars flexural test results: nRA Vs. SAW and different percentage of water used for different fiber percentage and length combinations.

The improvement (see Fig. 6-5, calculated as M(SAW)(nRA)F1 – MF1) in strain energy & flexural strength for 1% fiber (with respect to the dry mortar mass) category found to be about 0.54 kN.mm & 1.06 MPa for 5mm fiber length, 0.95

kN.mm & 0.97 MPa for 10mm fiber length and 1.17 kN.mm & 0.98 MPa for 30mm fiber length, respectively.

Similarly, when the SAW thermal composite mortar (nRA) samples are compared with the SAW thermal composite mortar (with inherent insulation materials i.e., PB) samples of 1% fiber (with respect to the dry mortar mass) category, the increment (see Fig. 6-5, calculated as M(SAW)(nRA)F1 – M(SAW)F1) in strain energy & flexural strength obtained equal to 0.06 kN.mm & 0.01 MPa for 5mm fiber length, 0.54 kN.mm & 0.02 MPa for 10mm fiber length and 0.83 kN.mm & 0.09 MPa for 30mm fiber, respectively

Table 6-13 presents the compressive strength values obtained for the thermal composite mortar (nRA) samples prepared with SAW. The compressive strengths obtained for the SAW structural composite mortar samples found to be higher than the Phase-I thermal composite mortar samples and SAW thermal composite mortar (with inherent insulation materials i.e., PB) samples.

Table 6-13. Compressive strength thermal composite without insulating recycled aggregates

Sample type	Mean [MPa]	Co.V [%]
M(nRA)F1(5)	5.27	0.55
M(nRA)F1(10)	5.00	0.96
M(nRA)F1(30)	4.62	1.11

The compression tests have shown very interesting results. Improvement (see Fig. 6-6, calculated as M(SAW)(nRA)F1 – MF1) in compressive strengths for 1% fiber (with respect to the dry mortar mass) category obtained equal to 3.45 MPa for 5mm fiber length, 3.62 MPa for 10mm fiber length and 3.68 MPa for 30mm fiber length. Similarly, increment (see Fig. 6-6, calculated as M(SAW)(nRA)F1 – M(SAW)F1) in compressive strengths for 1% fiber (with respect to the dry mortar

mass) category found to be equal to 0.62 MPa for 5mm fiber length, 0.15 MPa for 10mm fiber length and 3.68 MPa for 30mm fiber length.

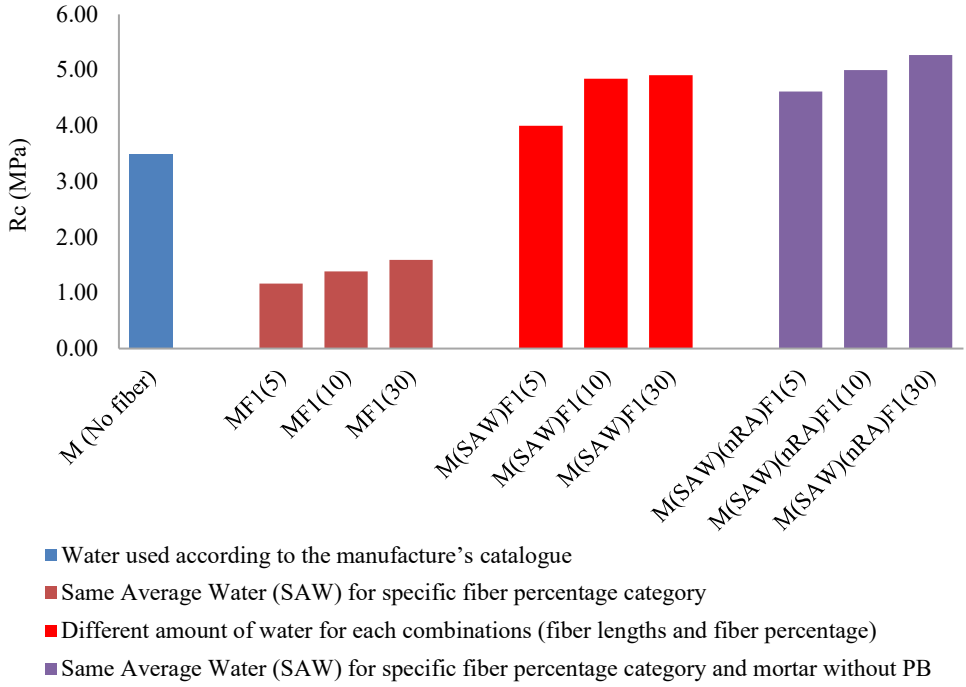

Fig. 6-6. Jute fiber thermal composite mortars compressive strengths: SAW Vs. different percentage of water used for different fiber percentage and length combinations.

6.3.3 Case 3: Thermal mortar without Recycled Aggregates (nRA) and SW.

The flexural properties are reported in Table 6-14 and Table 6-15. In this case it has been observed that the strain energy and flexural strength decrease with the decrease in fiber length and longer fibers demonstrate better mechanical performance in comparison to shorter ones.

The stain energy values and the flexural strength values of the SW structural composite mortars compared with the Phase-I structural composite mortars following the combinations of fiber lengths and fiber percentages (with respect to the dry mortar mass).

When the SW structural composite mortar samples compared with the Phase-I structural composite mortar samples of 0.5% (with respect to the dry mortar mass) category, it has been observed that due to the use of SW, the strain energy increase (see Fig. 6-7, calculated as MS(SW)F0.5 – MSF0.5) by 0.71 for 5mm fiber length, 0.70 kN.mm for 10mm fiber length and 0.92 kN.mm for 30mm fiber length. While the flexural strength reduced (see Fig. 6-7, calculated as MS(SW)F0.5 – MSF0.5) by -1.86 MPa for 5mm fiber length, -2.79 MPa for 10mm fiber length and -2.63 MPa for 30mm fiber length.

Table 6-14. Flexural test properties of the SM with same water-1

	deflection max. (d)		Strain energy (ft)	
	Mean [mm]	Co.V [%]	Mean [kN.mm]	Co.V [%]
MS(SW)F0.5(5)	1.85	2.32	1.39	5.36
MS(SW)F0.5(10)	1.72	10.81	1.28	18.03
MS(SW)F0.5(30)	2.01	8.20	1.82	13.86
MS(SW)F1(30)	2.09	15.41	1.81	15.33

Table 6-15. Flexural test properties of the SM with same water-2

	Flexural stress (σ)		Flexural strain (ε)		Moment of inertia (I)	
	Mean [MPa]	Co.V [%]	Mean	Co.V [%]	Mean [mm^4]	Co.V [%]
MS(SW)F0.5(5)	3.18	0.73	0.04	2.58	236424.26	0.97
MS(SW)F0.5(10)	3.04	9.71	0.04	10.92	234688.15	0.52
MS(SW)F0.5(30)	3.65	7.86	0.04	8.37	220435.97	1.20
MS(SW)F1(30)	3.60	10.46	0.04	15.40	223715.80	0.64

Whereas when the SW structural composite mortar samples compared with the SAW composite mortar samples of 0.5% (with respect to the dry mortar mass) category, the improvement (see Fig. 6-7, calculated as MS(SW)F0.5 – MS(SAW)F0.5) in both strain energy & flexural strength have been obtained by 1.03

kN.mm and 1.10MPa for 5 mm fiber length, 0.81 kN.mm and 1.12 MPa for 10 mm fiber length and 1.45 kN.mm and 1.75 MPa for 30 mm fiber length.

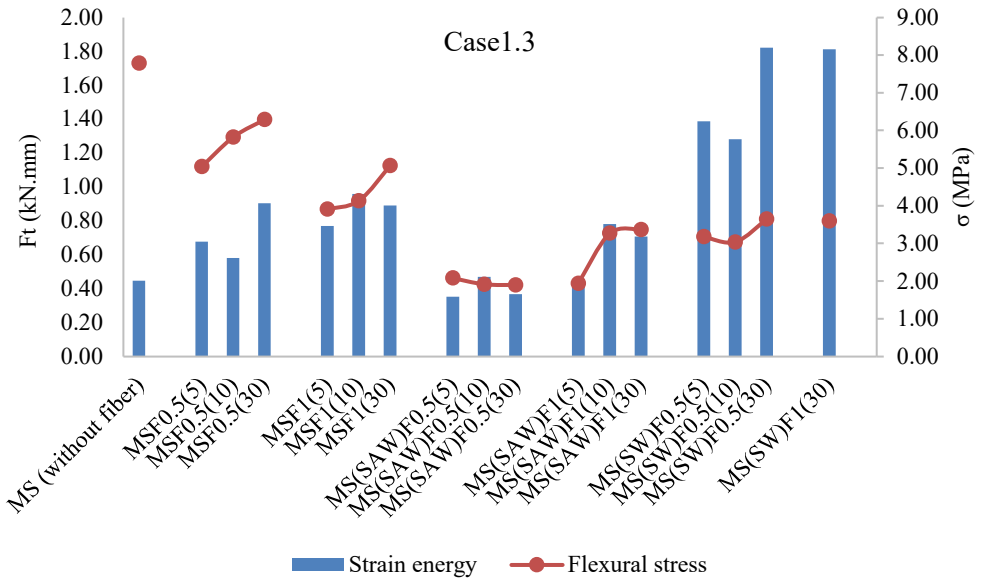

Fig. 6-7. Jute fiber thermal composite mortars flexural test results: SW Vs SAW and nRA and different percentage of water used for different fiber percentage and length combinations.

When the SW structural composite mortar samples compared with the Phase-I structural composite mortar samples of 1% (with respect to the dry mortar mass) category, it has been observed that the SW structural composite mortars have higher strain energy of 0.92 kN.mm and lower flexural strength of -1.47 MPa for 30mm fiber length, (see Fig. 6-7, calculated as MS(SW)F1 – MSF1)

Conversely, when the SW structural composite mortar samples compared with the SAW composite mortar samples of 1% (with respect to the dry mortar mass) category, the SW structural composite mortar samples found to have higher strain energy and flexural strength of 1.10 kN.mm and 0.24 MPa, respectively, (see Fig. 6-7, calculated as MS(SW)F1 – MS(SAW)F1).

Table 6-16 presents the compressive strength values obtained for the structural composite mortar samples prepared with SW.

Table 6-16. Compressive strength for the SM with same water

	Mean [MPa]	Co.V [%]
MS(SW)F0.5(5)	11.66	4.44
MS(SW)F0.5(10)	12.22	4.90
MS(SW)F0.5(30)	12.74	4.62
MS(SW)F1(5)	No samples were prepared due to the mixture-composition failed the workability test	
MS(SW)F1(10)		
MS(SW)F1(30)	12.64	5.30

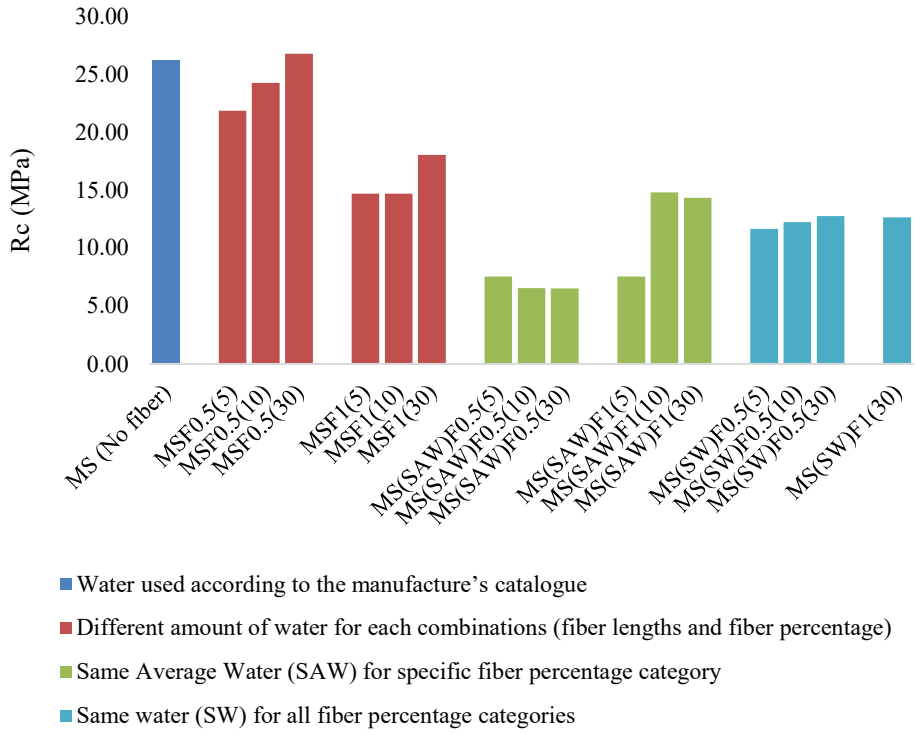

Fig. 6-8. Jute fiber thermal composite mortars compression test results: SW Vs SAW and nRA and different percentage of water used for different fiber percentage and length combinations.

When the SW structural composite mortar samples compared with the Phase-I structural composite mortar samples, of 0.5% (with respect to the dry mortar mass) category, it has been observed that with the application of SW, the compressive strengths of the structural composite mortar samples have reduced (see Fig. 6-8, calculated as MS(SW)F0.5 – MSF0.5) category by -10.17 MPa for 5 mm fiber length, -12.02 MPa for 10 mm fiber length and -14.01 MPa for 30 mm fiber length. Similarly, the compressive strength also has reduced (see Fig. 6-8, calculated as MS(SW)F1 – MSF1) for the 1% fiber (with respect to the dry mortar mass) category by -5.40 MPa for 30mm fiber length.

While just opposite happened for the SW structural composite mortar samples compared with SAW structural composite mortar samples, of 0.5% (with respect to the dry mortar mass), the compressive strength increased (see Fig. 6-8, calculated as MS(SW)F0.5 – MS(SAW)F0.5) by 4.13MPa for 5 mm fiber length, 5.66 MPa for 10 mm fiber length and 6.22 MPa for 30 mm fiber length. While in the 1% fiber (with respect to the dry mortar mass) category, the compressive strength reduced (see Fig. 6-8, calculated as MS(SW)F1 – MS(SAW)F1) by -1.67 MPa for 30mm fiber length.

6.4 Conclusions

In the present chapter it has reported the mechanical properties of the (1) thermal and structural composite mortar samples prepared with 0.5% fiber (30 mm, 10 mm and 5 mm) and 1.0% fiber (30mm, 10mm and 5mm) with respect to the dry mortar mass.

In first case the Same Average Water (SAW) has been used to prepare the mix, for all fiber lengths (30 mm, 10 mm and 5 mm) in a particular fiber % (with respect to the dry mortar mass) category (i.e., 1.05% and 1.0%).

The stain energy, flexural strength and compressive strength improved due to application of SAW, for 0.5% fiber (30 mm, 10 mm and 5 mm) with respect to the

dry mortar mass. While exactly opposite has been observed for 1.0% fiber (30 mm, 10 mm and 5 mm) with respect to the dry mortar mass.

In the second case, the thermal composite mortar samples without nRA (pre-fabricated insulation materials) and with 1.0% fiber (30 mm, 10 mm and 5 mm) with respect to the dry mortar mass, and in this case too, the Same Average Water (SAW) has been used to prepare the mix, for all fiber lengths (30 mm, 10 mm and 5 mm). Here the improvement in the stain energy, flexural strength and compressive strength have been observed.

In the third case, the structural composite mortar samples prepared with 0.5% fiber (30 mm, 10 mm and 5 mm) and 1.0% fiber (30 mm, 10 mm and 5 mm) with respect to the dry mortar mass. In this case to prepare the composite mix, the Same Water (SW) i.e., exactly the same amount of was used which has been used for the normal mortar preparation. Interestingly in this case the mix prepared with 1.0% fiber (with respect to the dry mortar mass) and with fiber lengths 10mm and 5mm, have not passed the workability tests therefore the samples were prepared. Here the samples with SW have demonstrated mix behavior. In this sub-phase none of the composite mortars prepared with SAW or SW were subjected to the thermal conductivity tests.

7. Phase III – In plane cyclic shear test and thermal performance evaluation of masonry walls upgraded with jute-net, jute-diatons and jute-composite mortars.

This chapter aims at analyzing the structural behavior and thermal performance of the hollow-clay brick masonry walls and upgraded hollow-clay brick masonry walls with jute-net, jute-diatons and jute-composite mortar.

Two un-strengthened hollow-clay brick masonry walls have been used as reference, while six hollow-clay brick masonry walls have been upgraded with different combinations of jute fiber products. Whereas a total of five masonry walls has unique reinforcement combinations.

Notably, the jute net and jute diatons have been used for the structural upgrading, while the composite layers have been used particularly for thermal upgrading i.e., to enhance the insulation capacity of the masonry wall.

The jute fiber nets used for the structural upgrading were fabricated with two different dimensions, the 1 x 1 m^2 and 0.9 x 0.7 m^2 and two different inner mesh configurations 2.5 cm x 1.25 cm and 2.5 cm x 2.5 cm.

Whereas jute diation used for masonry upgrading are similar to that of Chapter 4; Section 4.1.3.

While the composite mortars prepared with both structural and thermal mortar (without recycled aggregate) have 1% of jute fiber (length: 30 mm) with respect to the dry mortar mass.

All the masonry walls were upgraded and tests were conducted in the Material Testing Laboratory of the University of Cagliari, Italy and the Strength Laboratory of the University of Salerno, Italy.

7.1 Materials and methods

7.1.1 Raw Jute fibers

Raw jute fibers used are of Bangla Tosha - Corchorus olitorius (golden shine), and for origin, physical characteristics and mechanical behavior, see chapter 4, section 4.1.1, Fig. 4-1. The 30 mm chopped jute fibers were used for the masonry wall upgrading in this phase. For cutting process, see Chapter 4, Fig. 4-4.

7.1.2 Jute fiber diatons

The transversal connectors (Fig.4-9) were prepared in the structural laboratory of the university of Cagliari. These diatons were used for the masonry upgrading purpose. Diaton preparation, physical properties and mechanical behaviors are reported in the Chapter 4, section 4.1.3.

7.1.3 Jute thread and jute net fabrication

Two types of three yarn jute threads have been used for the jute net fabrication. The class 1 mm (see Fig. 4-6) thread was preferred and used for the net fabrication due to its better mechanical performance, for details see the chapter 4, section 4.1.2.

(a): Class 1mm jute thread *(b): Jute net preparation.*

Fig. 7-1. Class 1mm jute threads used for net preparation.

Two different inner mesh configurations 2.5 cm x 1.25 cm (Fig. 7-2.a) and 2.5 cm x 2.5 cm (Fig. 7-3.a) were chosen for the net preparation.

The jute fiber nets were fabricated with two different dimensions, the 1 x 1 m^2 (Fig. 7-2.b and Fig. 7-3.b) for the structural tests and 0.9 x 0.7 m^2 (Fig. 7-3.c) for the thermal conduction tests, respectively.

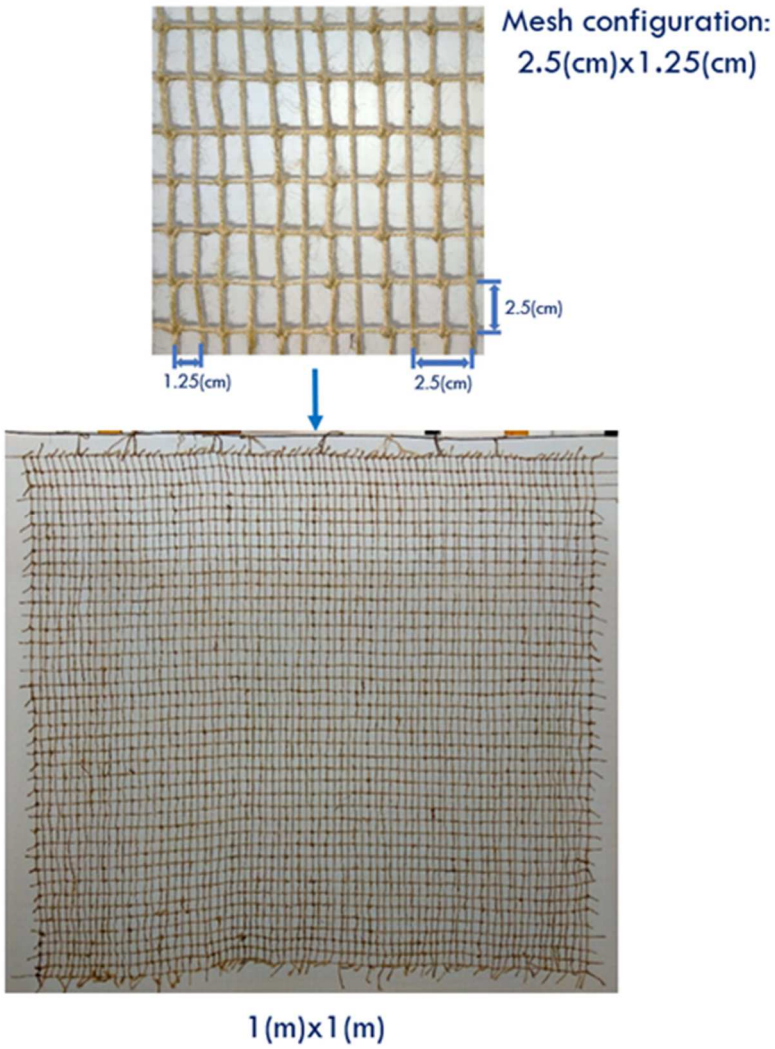

Fig. 7-2. Mesh configuration of 2.5(cm)x1.25(cm) used to prepare the 1(m)x1(m) jute net.

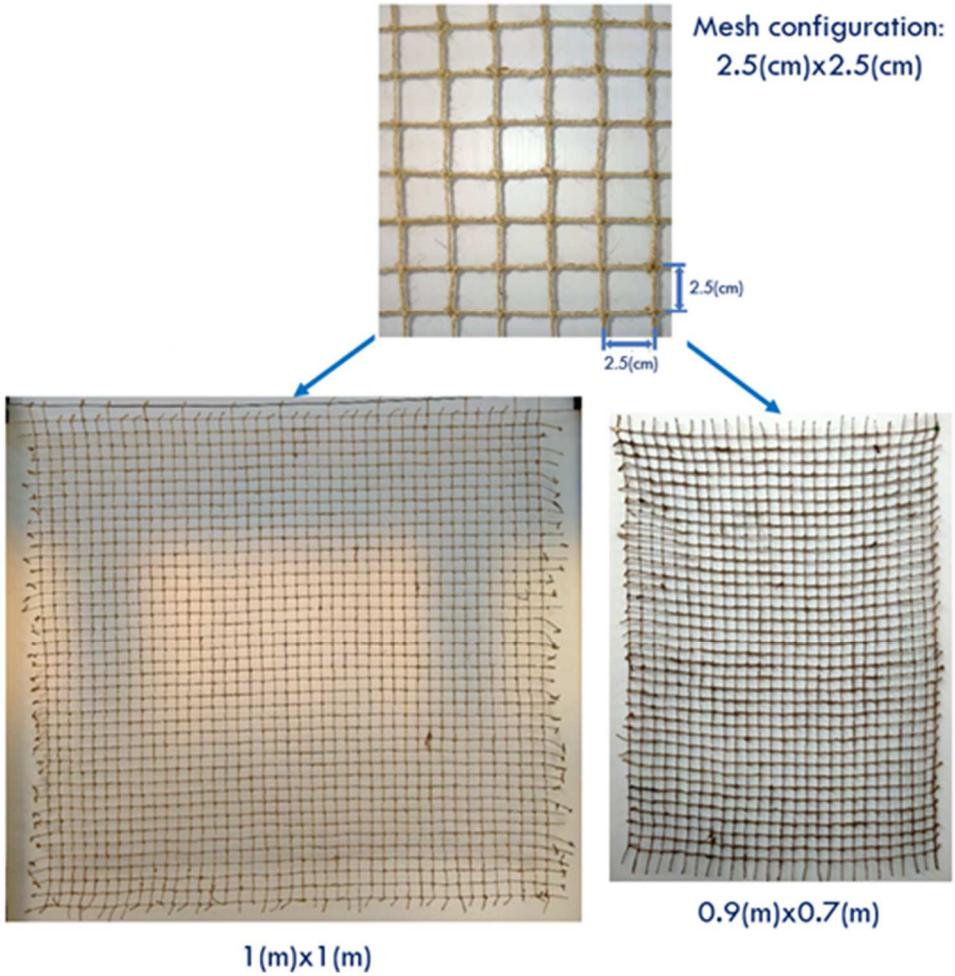

Fig. 7-3. Mesh configuration of 2.5(cm)x2.5(cm) used to prepare 1(m)x1(m) and 0.9(m)x0.7(m) jute nets.

7.1.4 Structural and thermal mortars

Two types of mortars, i.e., Structural Mortar (SM) and Thermal Mortar (TM) (Chapter 5, Section 5.1.1.2, Fig. 5-2, Fig. 5-3). Primarily SM and SM composite mortar have been used for the composite mortar preparations, and these mortars have been also used for masonry wall upgrading purpose.

Here to be noted that the TM (without Recycled Aggregates i.e., RA) and TM (without Recycled Aggregates i.e., RA) composite mortar have been used only

in case for upgrading purpose, and for only one sample which has been used to evaluate the masonry wall's thermal properties and compared with the masonry walls upgraded with SM and SM composite mortars.

7.1.5 Choice of jute fiber length, and the fiber and structural mortar percentages.

Two types of composite mortars have been prepared by mixing 1% of jute fiber (30 mm in length) with SM (Fig 7.4) and TM (without RA) with respect to the dry mortar masses, respectively.

Fig. 7-4. Jute fiber of 30mm, structural mortar (SM), water for masonry wall upgrading.

The choice of fiber length, fiber percentage (with respect to the SM and TM masses) and the amount of water used in the mixture, was based on previous R&D experiments and knowledge gained in Phase I and Phase II, respectively.

Another point which has been considered while selecting 1% of fiber (with respect to the mortar mass) for the composite mixture, is based on EN 13501-1:2019, in which it has been stated that the presence of fiber in an incombustible composite mixture should not be higher than 1%.

Fig. 7-5. Jute fiber – SM mixture

After considering all aspects, findings and results of the earlier phases as mentioned in the aforesaid chapters, the mixture composition of the MSF1(30) has been chosen (ss, Table 5-4) to be used for the composite layer during the masonry walls upgrading.

The best performed, worst performed and the chosen "fiber length and fiber percentage" combination of the mechanical properties for SM summarized in the Table 7-1 and Fig. 7-6, while mechanical properties for TM summarized in the Table 7-2 and Fig. 7-7.

It is important to highlight that the composite mortar used for all the strengthened masonry walls have been prepared used mainly SM, except one, i.e., TM (without Recycled Aggregates (nRA)) has been used.

Table 7-1. Composite SM mixture combinations used for the masonry wall upgrading.

	Best value	Chosen value	Worst value
		Thermal conductivity @ 20°C [W/mK]	
	MSF1(5)	MSF1(30)	MS (No fiber)
Obtained Values	0.444	0.5	0.771
Changes	-13%		5%
		Strain energy [kN.mm]	
	MSF2(30)	MSF1(30)	MS (No fiber)
Obtained Values	2.687	0.89	0.477
Changes	79%		-16%
		Flexural stress [MPa]	
	MS (No fiber)	MSF1(30)	MSF2(5)
Obtained Values	7.789	5.068	3.611
Changes	35%		-40%
		Compressive strength [MPa]	
	MS (No fiber)	MSF1(30)	MSF2(30)
Obtained Values	32.25	21.83	6.03
Changes	32%		-262%

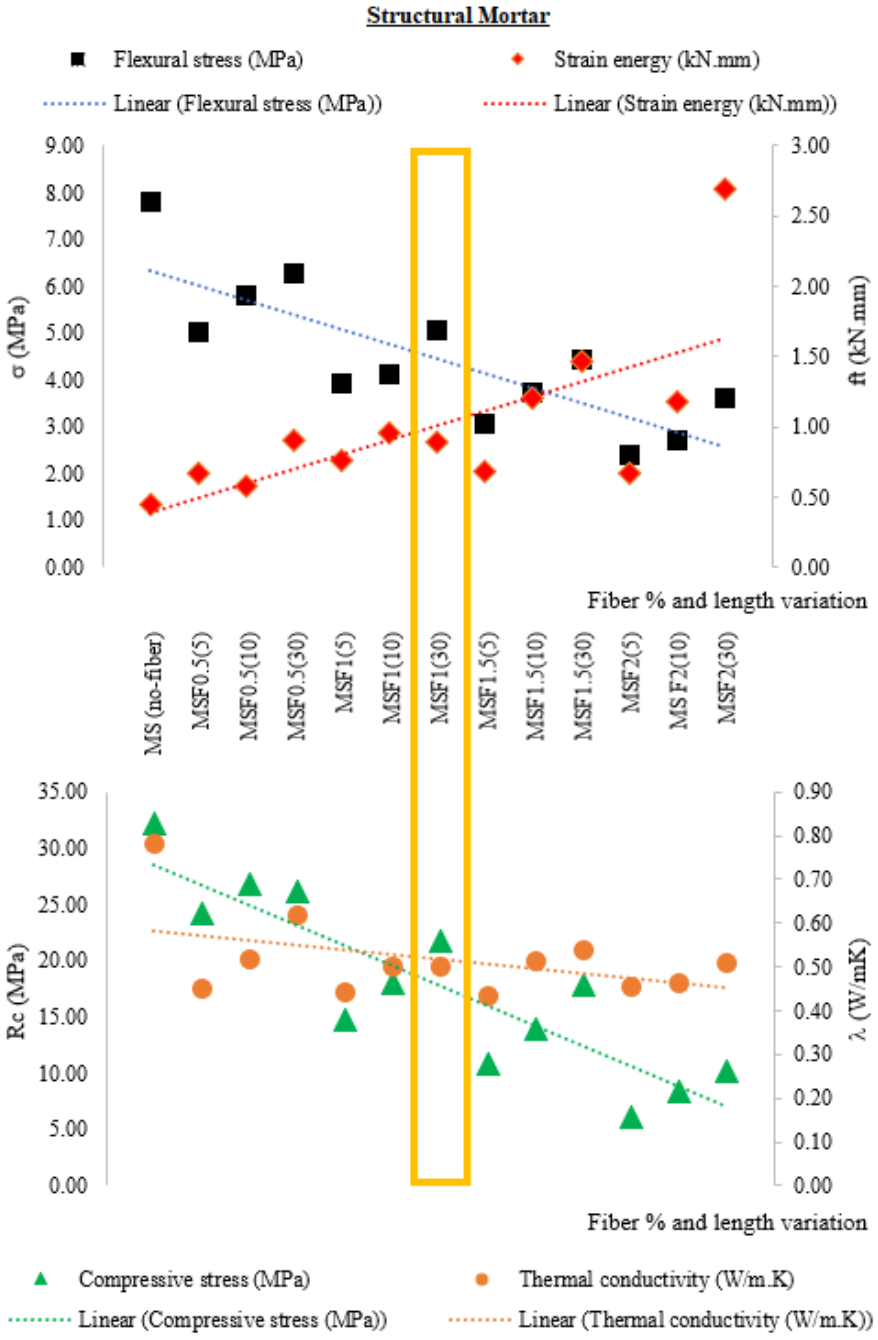

Fig. 7-6. The choice of 30mm fibers and 1% fibers in the mixture with respect to the dry structural mortar (SM) mass

Table 7-2. Composite TM mixture combinations used for the masonry wall upgrading.

	Best value	Chosen value	Worst value
		Thermal conductivity @ 20°C [W/mK]	
	MF2(5)	MF1(30)	no fiber
Obtained Values	0.101	0.168	0.236
Changes	-66%		29%
		Strain energy [kN.mm]	
	MF2(30)	MF1(30)	no fiber
Obtained Values	0.186	0.563	1.095
Changes	-2.027		0.486
		Flexural stress [MPa]	
	no fiber	MF1(30)	MF2(5)
Obtained Values	1.156	0.634	0.283
Changes	0.452	0.000	-1.240
		Compressive strength [MPa]	
	no fiber	MF1(30)	MF2(5)
Obtained Values	3.500	1.590	0.360
Changes	0.546	0.000	-3.417

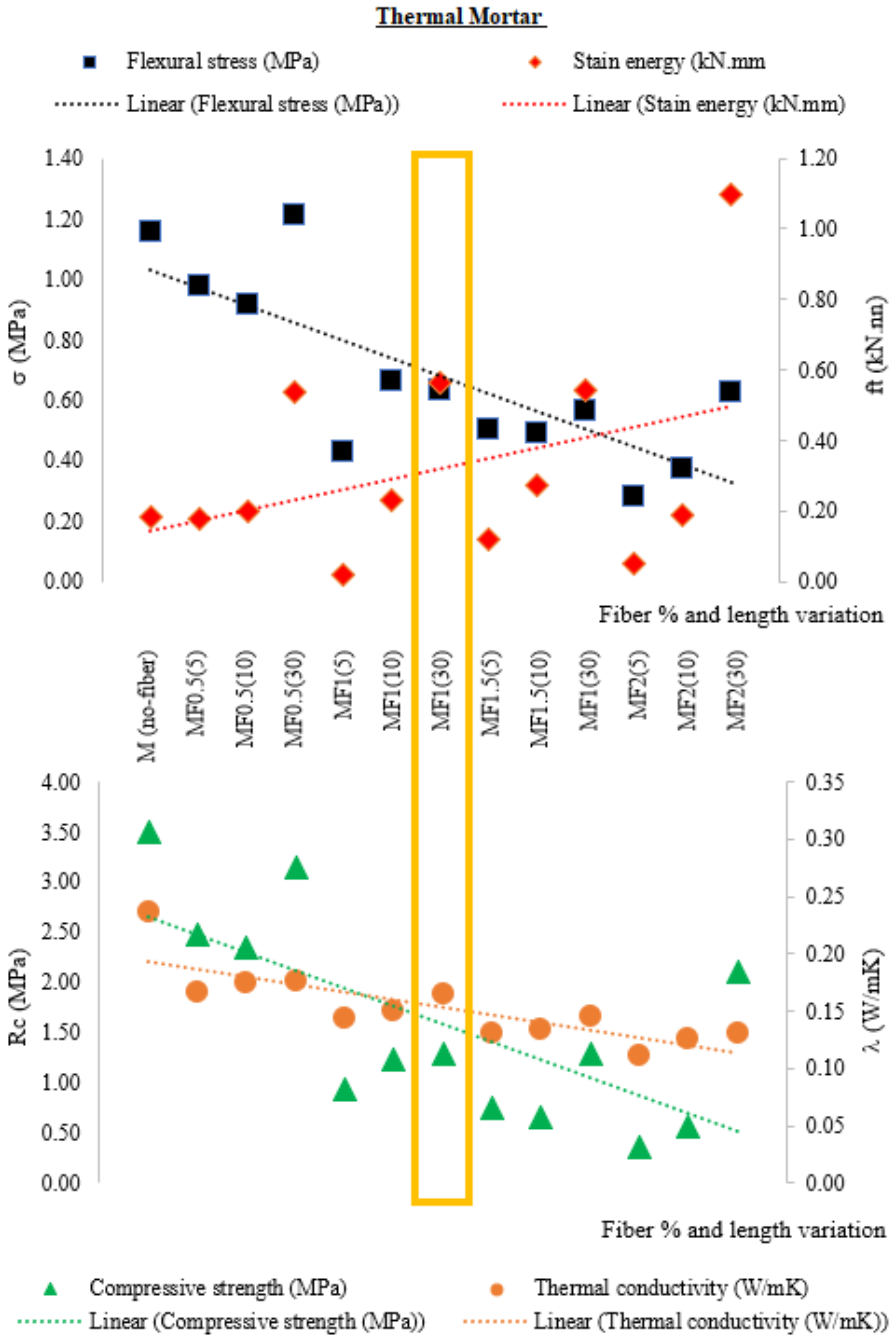

Fig. 7-7. The choice of 30mm fibers and 1% fibers in the mixture with respect to the dry Thermal mortar (TM) mass

7.2 Masonry wall specimens and upgrading schemes

Two un-strengthened and six upgraded masonry walls with various configurations have been prepared in the laboratory of the University of Cagliari. The walls are labelled in sequence using nomenclature Hollow Brick Walls (HBW), i.e., from HBW1 to HBW8. Fig. 7-8 reports various symbols to represent different parts of the upgraded masonry walls.

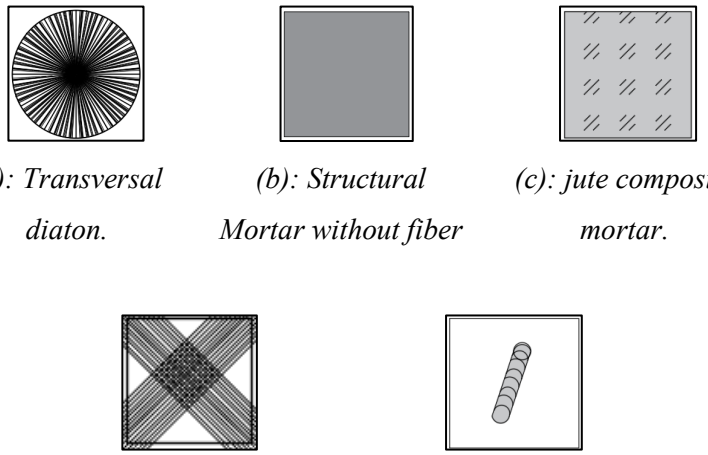

(a): Transversal diaton. *(b): Structural Mortar without fiber* *(c): jute composite mortar.*

(d): Raw intact jute fiber *(e): Tying diaton*

Fig. 7-8. Representation of various items used for masonry upgrading purpose.

- HBW1 (Fig. 7-9 a & c) and HBW2 (Fig. 7-9 b & d) masonry walls were not strengthened. Approximately 40 kN and 80 kN of constant vertical loads were applied to these masonry walls, respectively.
- Both HBW3 (Fig. 7-10.a) and HBW4 (Fig. 7-10.b) walls were strengthened with the jute-net and jute diatons. Jute nets of 1 m^2 (of 2.5 cm x 2.5 cm mesh configuration) were placed on either side of the masonry walls. While four jute diatons (horizontal connectors) were inserted orthogonally through the masonry walls (as in Fig. 7-13.a) to hold the nets and to connect the external surfaces to improve the shear resistance. Thereafter, hollow cavities (of the inserted diatons) were filled

with liquid mortar (Fig. 7-13.b). This was done to reconstruct the structural monolithicity, minimize the weakness and improve the strength of the masonry walls. SM was used for binding the diatons, jute net attachment to the wall and plastering. Vertical loads of approximately 80 kN and 40 kN were applied on HBW3 and HBW5, respectively.

- The masonry walls HBW5 (Fig. 7-11.a) and HBW6 (Fig. 7-11.b) have also four transversal diatons. Here too, the SM was used for initial placement of jute fiber nets on both sides of HBW5 (with 2.5 cm x 1.25 mesh configuration) and HBW6 (with 2.5 cm x 2.5 cm mesh configuration). Thereafter jute-composite mortar prepared with 1% (with respect to the dry mortar weight) jute fiber and 30mm fiber lengths was used for further thermo-structural reinforcement. Approximately 40 kN of constant vertical load was applied on both these masonry walls.
- The HBW7 (Fig. 7-12.a) has been strengthened with only 4 diatons to connect the external surfaces to improve the shear resistance. The diatons were bonded to the masonry wall surfaces using SM and the hollow cavities were filled with liquid mortar, as above.
- In the case of masonry wall HBW8 (Fig. 7-12.b), raw jute fibers were placed diagonally and attached with SM on the wall surfaces, whereas four jute diatons were used to hold these fibers. This reinforcement configuration was chosen to improve the mechanical performance.

The vertical load is about 2% (8 ton) and 1% (4 ton and 3.7 ton) of the maximum vertical load of the masonry wall. For all the above configurations, gradually increasing in-plane cyclic shear loads were applied using three horizontal hydraulic jacks, until the collapse load was reached. Table 7.3 presents list of all masonry walls with their upgrading schemes.

Table 7-3. Masonry wall upgrading scheme.

	Masonry wall nomenclatures	First mortar layer	Net Type	Total net used	Mesh type	Diaton used	Composite mortar used	Second mortar layer
Samples used Structural properties	HBW 1	SM	NO	NO	NO	NO	NO	SM
	HBW 2	SM	NO	NO	NO	NO	NO	SM
	HBW 3	SM	1m x 1m	2	2.5 cm x 2.5 cm	4	NO	SM
	HBW 4	SM	1m x 1m	2	2.5 cm x 2.5 cm	4	NO	SM
	HBW 5	SM	1m x 1m	2	1.25 cm x 2.5 cm	4	SM + 1% (30mm) jute fiber w.r.t. mortar mass	
	HBW 6	SM	1m x 1m	2	2.5 cm x 2.5 cm	4	SM + 1% (30mm) jute fiber w.r.t. mortar mass	
	HBW 7	SM used only to fix diatons	NO	NO	NO	4	SM + 1% (30mm) jute fiber w.r.t. mortar mass	
	HBW 8	SM used only to fix diatons	NO	NO	NO	4	NO	SM
Samples used Thermal Properties	HBW 6 (Same configuration)	SM	0.9m x 0.7m	2	2.5 cm x 2.5 cm	4	SM+1% (30mm) jute fiber w.r.t. mortar mass	
	HBW 6 (Similar configuration)	TM	0.9m x 0.7m	2	2.5 cm x 2.5 cm	4	TM (without RA) + 1% (30mm) jute fiber w.r.t. mortar mass	

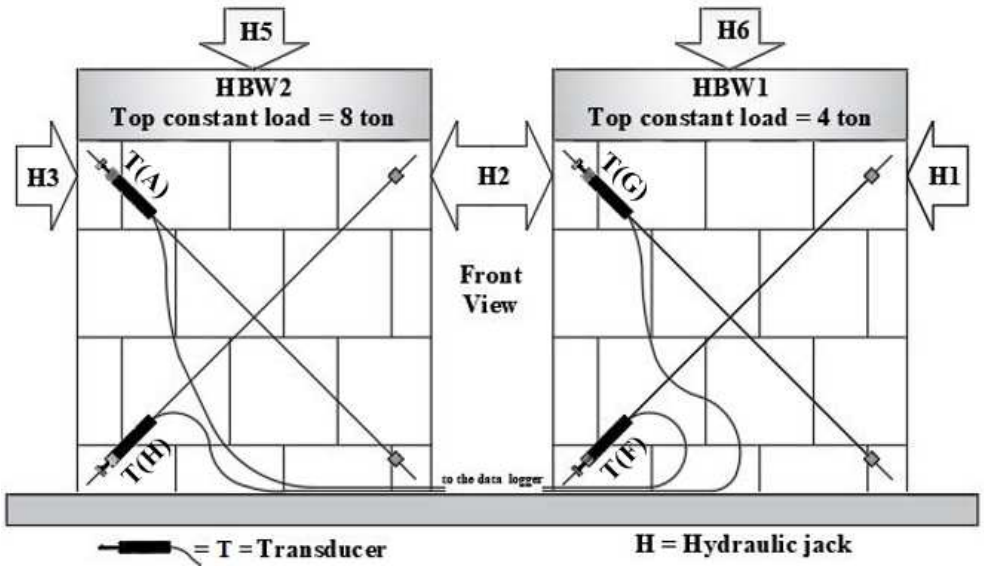

(a): HBW2 front view

(b): HBW1 front view

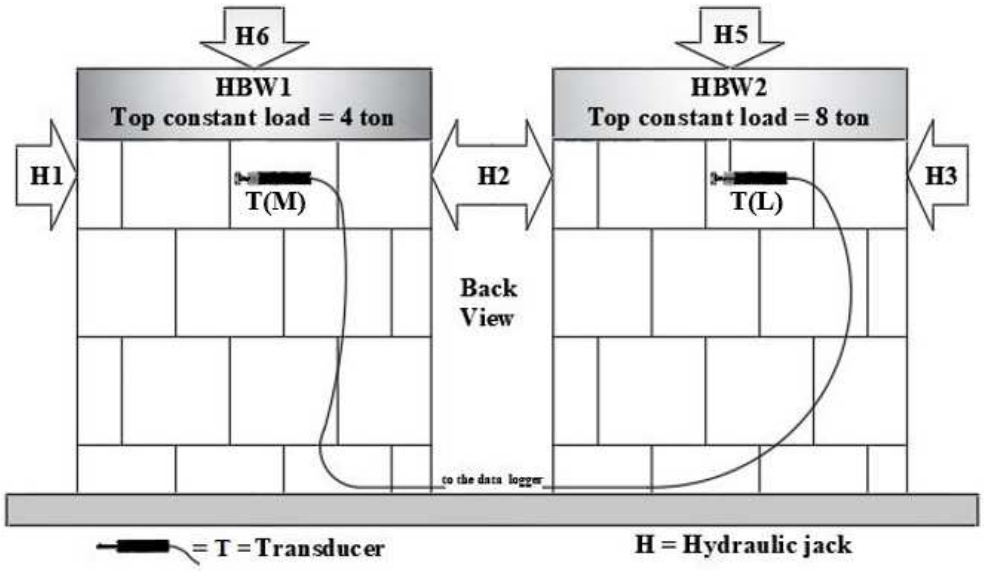

(c): HBW1 back view

(d): HBW2 back view

Fig. 7-9.Masonry walls (HBW1 and HBW2) without reinforcement. Use of hydraulic jacks and displacement measuring schemes.

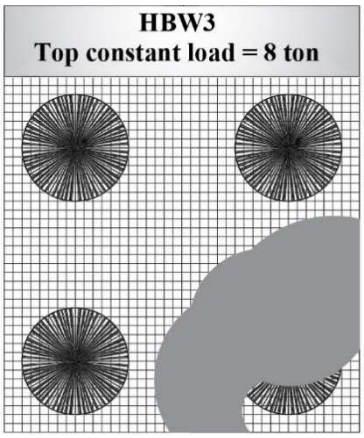

(a): Upgrading configuration: 2.5 cm x 2.5 cm and 4 jute diatons.

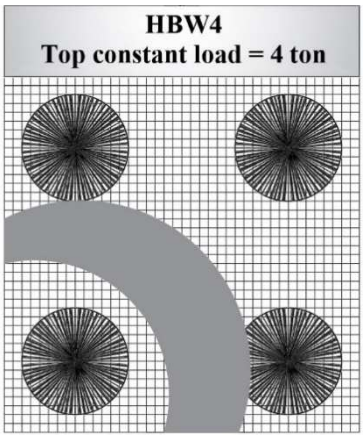

(b): Upgrading configuration 2.5 cm x 2.5 cm and 4 jute diatons.

Fig. 7-10.Masonry walls HBW3 and HBW4 reinforcement schemes.

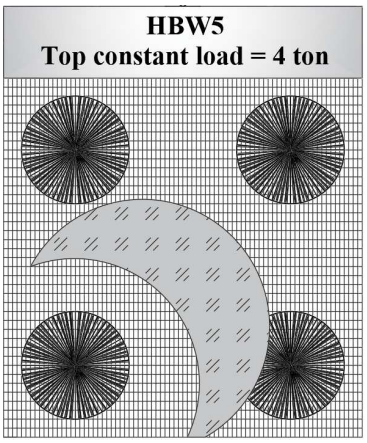

(a): Upgrading configuration: 2.5 cm x 1.25 cm, 4 jute diatons and jute composite mortar (SM).

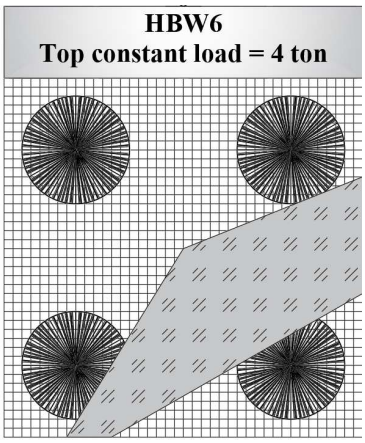

(b): Upgrading configuration: 2.5 cm x 2.5 cm, 4 jute diatons and jute composite mortar (SM).

Fig. 7-11. Masonry walls HBW5 and HBW6 reinforcement schemes.

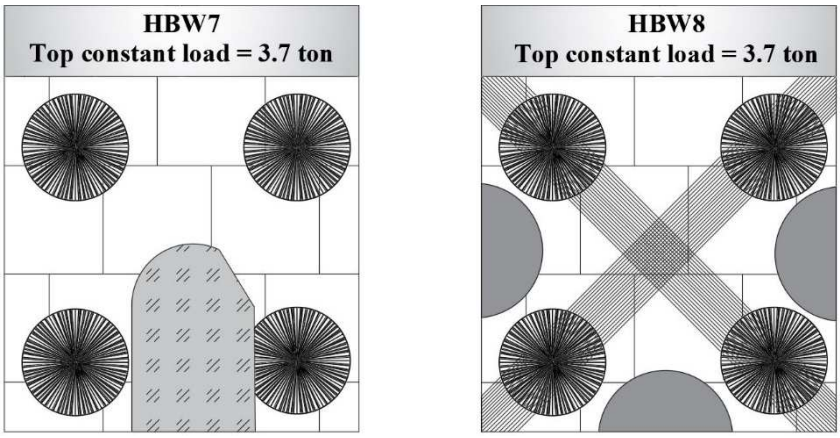

(a): Upgrading configuration: 4 jute diatons and jute composite mortar (SM)l

(b): Upgrading configuration: Long intact raw jute fiber X pattern, 4 jute diatons.

Fig. 7-12. Masonry walls HBW7 and HBW8 reinforcement schemes.

(a): Transversal diaton hole

(b): Transversal jute diaton

(c): Jute diaton holding net.

Fig. 7-13. Jute diaton application scheme.

The transversal diatons (as in Fig.4-9 and Fig. 7-13.b) were placed through the diaton holes (Fig. 7-13.a) and the holes were completely filled and sealed with liquid mortar (Fig. 7-13.b). Thereafter, the diaton edges (front and back) were opened and attached to the net (masonry wall surface) with SM. The HBW6 (Fig. 7-15) wall is upgraded with jute diatons, jute net and structural mortar (same as Fig.

7-11.b). While HBW7 (Fig. 7-16) is retrofitted with jute diatons and jute composite-mortar (SM) HBW7 (same as Fig. 7-12.a).

Fig. 7-14. HBW5 masonry wall upgraded with four jute diatons, 1x1 m^2 jute net (with mesh type 1.25cm x 2.5cm) and jute composite mortar (with 1% fiber (30mm) with respect to dry mortar mass).

Fig. 7-15. HBW6 masonry wall upgraded with four jute diatons, 1x1 m^2 jute net (with mesh type 2.5cm x 2.5cm) and jute composite mortar (with 1% fiber (30mm) with respect to dry mortar mass).

Fig. 7-16. HBW7 masonry wall upgraded with four jute diatons and jute composite mortar (with 1% fiber (30 mm) with respect to dry mortar mass).

7.3 Experimental results: upgraded masonry walls structural characterization

7.3.1 In-plane cyclic shear tests

A total of 8 samples were used for the in-plane cyclic shear test. During these tests, the vertical load was applied at the top of each masonry wall (as in Fig. 7-17), also these walls were subjected to in-plane cyclic reversal loads by means of a set of hydraulic jacks. Horizontal steel beams were placed at the top-surface of the masonry wall structures in order to share the vertical load on the whole top wall surface.

Each wall was subjected to two cycles of growing horizontal loads from the right (hydraulic jack H1 or hydraulic jack H2 depending on the side of the considered wall) and from the left (hydraulic jack H2 or H3 depending on the side of the considered wall). At the end of the horizontal load cycles an ultimate horizontal load was applied until the collapse of the sample.

Each wall was equipped with three displacement Transducers (T) (10 cm long) that convert rectilinear mechanical motion into a variable electric signal that can be digitally recorded. Their nominal displacement is 100 mm, nominal sensitivity 2

mV/V, sensitivity tolerance ± 0.1%, measure resolution 1 μm. Their positions are also represented in Fig. 7-9, Fig. 7-10 Fig. 7-17: two are placed on the front surface to measure diagonal displacements while one is placed on the back surface to record horizontal displacements on every masonry wall, as shown in the Fig. 7-9 and Fig. 7-10, respectively.

(a): Front view: masonry walls equipped with diagonal sensors.

(b): Back view: masonry walls equipped with horizontal sensors.

Fig. 7-17. Wall samples sensors installation scheme..

7.3.2 Masonry wall sample: HBW1

HBW1 denotes a simple not strengthened brick masonry wall. Its vertical load is kept constant and equal to 40 kN, while its load displacement behavior is reported in Fig. 7-18 diagonal displacement transducer G and Fig. 7-19 for diagonal displacement transducer F. While Fig. 7-20 presents the load-displacement relationship based on the horizontal displacement transducers labelled M. In all Figures the green curve represents the first load cycle, while the red one denotes the second load cycle. Deformations and displacements can be negative or positive depending on the direction of the acting forces but excluding Fig 7-18 related to displacement transducer G a good symmetrical behavior has been recorded for HBW1. The asymmetry in Fig 7-18 can be explained with some error in the sensor placement given the results obtained with sensors F and M. The slope of the first load cycle curves in Fig. 7-18 and Fig. 7-19 yields to an average value of the elastic modulus equal to 64 GPa.

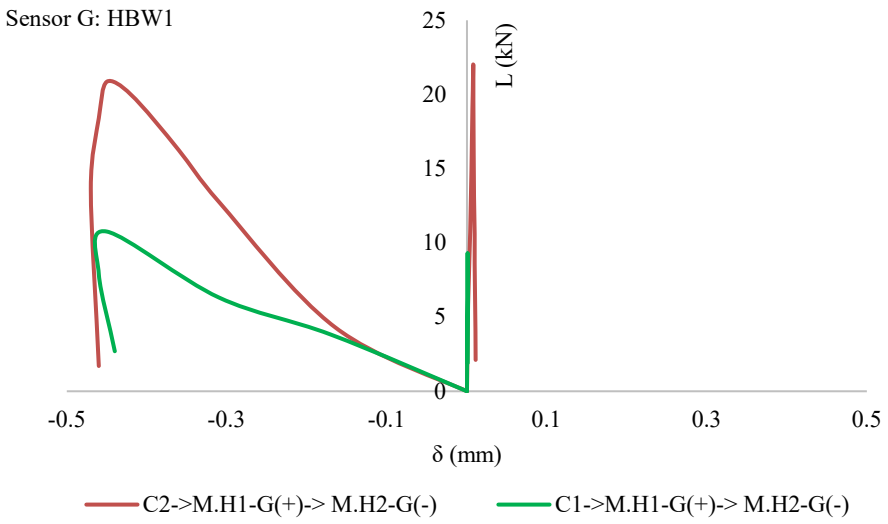

Fig. 7-18. Load-displacement diagrams of the unstrengthened masonry wall HBW1 (when the diagonal sensor G used).

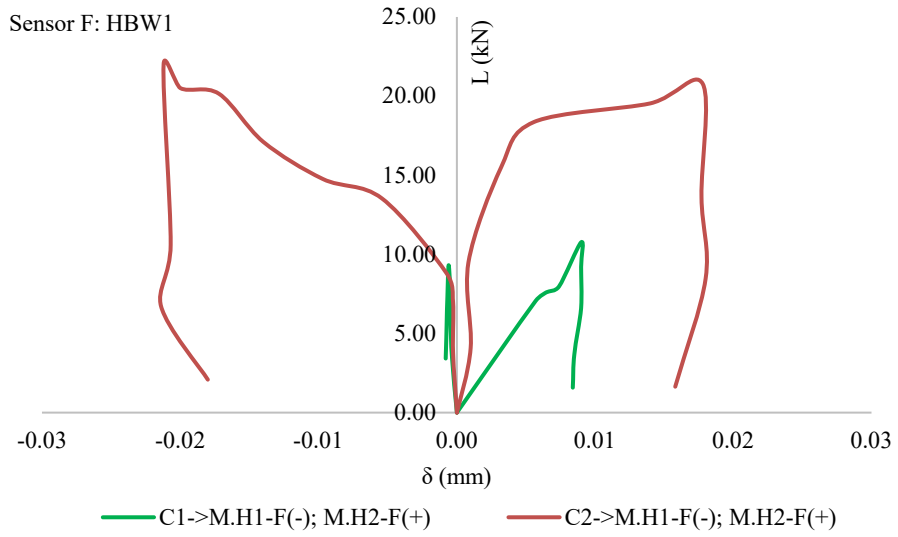

Fig. 7-19. Load-displacement diagrams of the unstrengthened masonry wall HBW1 (when the diagonal sensor F used).

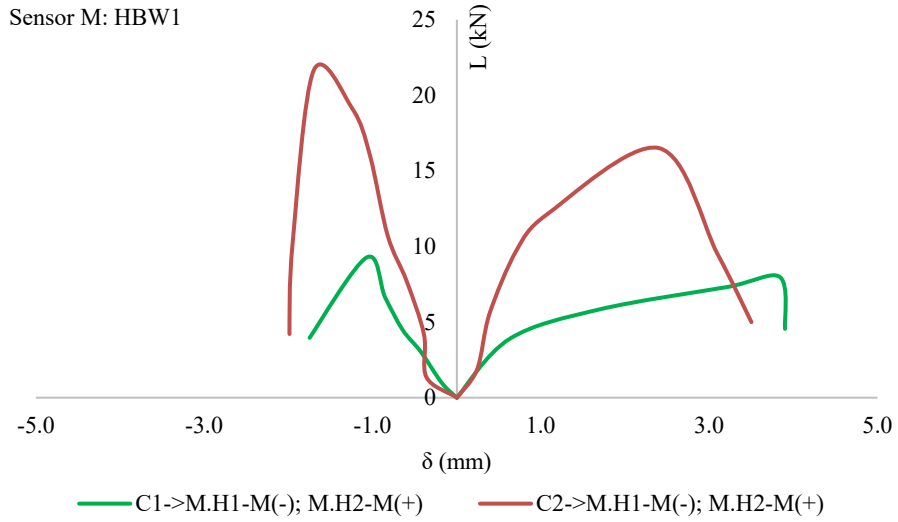

Fig. 7-20. Load-displacement diagram of the unstrengthened masonry wall HBW1 (when the horizontal sensor M used).

7.3.3 Masonry wall sample: HBW2

HBW2 represents another simple not strengthened brick masonry wall. The difference with respect HBW1 is in the vertical load that it is kept constant and equal to 80 kN. Load-displacement behavior is reported in Fig. 7-21 for diagonal displacement transducer A and Fig. 7-22 for diagonal displacement transducer H. Fig. 7-23 presents the load-displacement relationship based on the horizontal displacement transducers labelled L. In all Figures the green curve represents the first load cycle, while the red one denotes the second load cycle. Deformations and displacements can be negative or positive depending on the direction of the acting forces. A symmetrical behavior has been recorded in the latter Fig. 7-23 while the diagonal sensors A and H produced quite different recordings when the horizontal load pushes the wall from left to right or vice versa. Probably also in this case the diagonal sensor placements were not perfect. The slope of the first load cycle curves in Fig. 7-21 and Fig. 7-22 yields to an elastic modulus equal to 300 GPa.

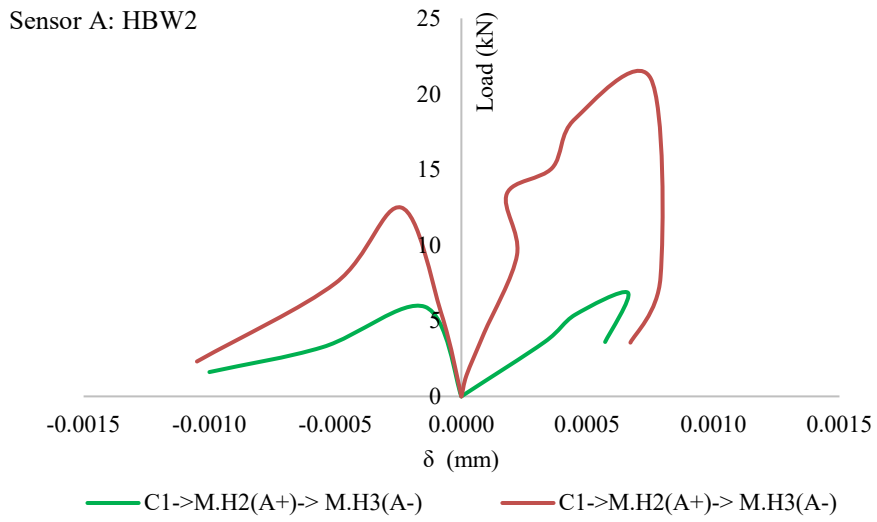

Fig. 7-21. Load-displacement diagrams of the unstrengthened masonry wall HBW2 (when the diagonal sensor A used).

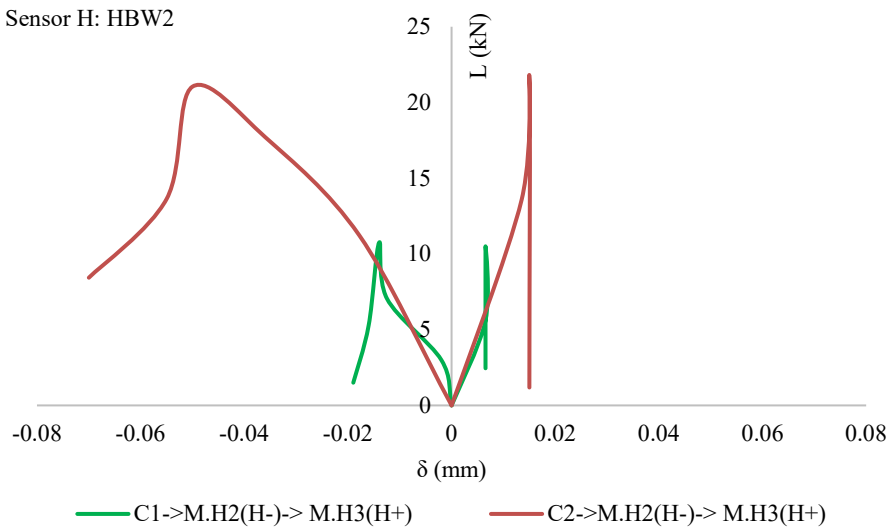

Fig. 7-22. Load-displacement diagrams of the unstrengthened masonry wall HBW2 (when the diagonal sensor H used).

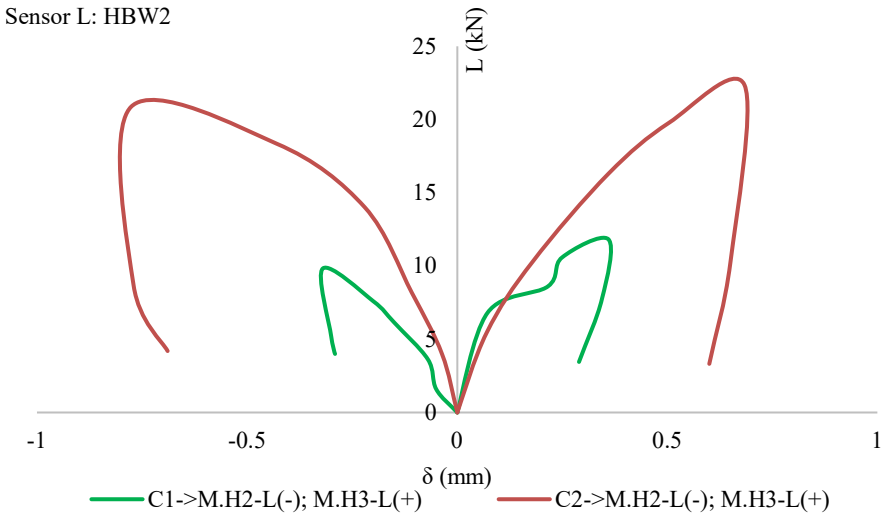

Fig. 7-23. Load-displacement diagram of the unstrengthened masonry wall HBW2 (when the horizontal sensor L used).

7.3.4 Masonry wall sample: HBW3

HBW3 sample was strengthened with the jute-net and jute diatons. Jute nets of 1 m^2 (of 2.5 cm x 2.5 cm mesh configuration) were placed on either side of the wall, while four jute diatons (horizontal connectors) were inserted orthogonally. In this case the vertical load it is kept constant and equal to 80 kN. Load-displacement behavior is reported in Fig. 7-24 for diagonal displacement transducer A and Fig. 7-25 for diagonal displacement transducer H. Fig. 7-26 presents the load-displacement relationship based on the horizontal displacement transducers labelled L. In all Figures the green curve represents the first load cycle, the red one denotes the second load cycle and the black one stands for the third load cycle. Deformations and displacements can be negative or positive depending on the direction of the acting forces. A quite symmetrical behavior has been recorded in all three above mentioned figures apart from the last load cycle in Fig. 7-26 that yields to quite large horizontal displacements. In this specific case probably a small boundary modification at the base of the wall can justify this difference in comparison to other load cycles. If we consider the slope of the first load cycle in Fig. 7-24 and Fig. 7-25 it is possible to estimate that the value of the elastic modulus *E* is equal to 291 GPa.

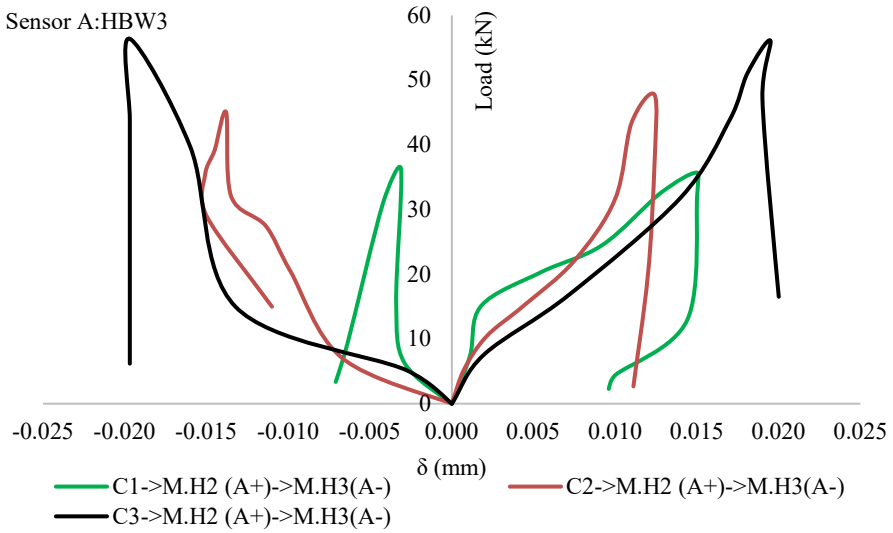

Fig. 7-24. Load-displacement diagrams of the strengthened masonry wall HBW3 (when the diagonal sensor A used).

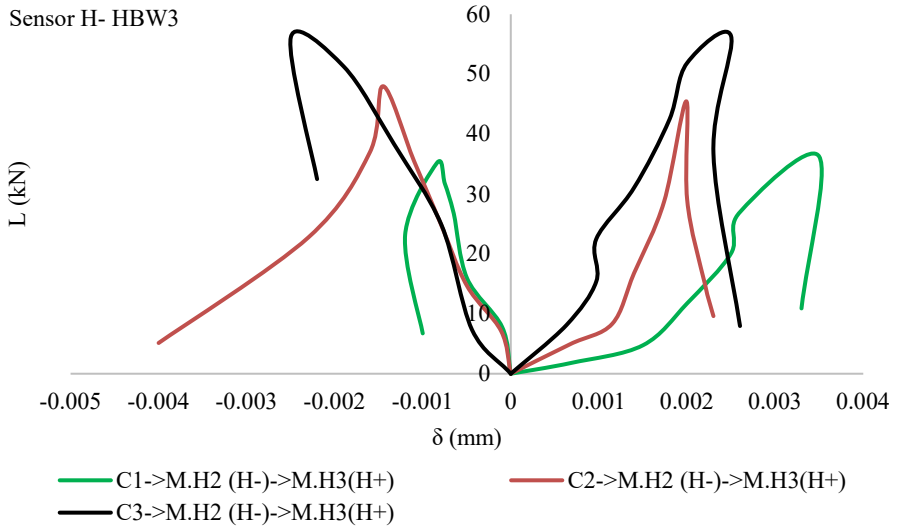

Fig. 7-25. Load-displacement diagrams of the strengthened masonry wall HBW3 (when the diagonal sensor H used).

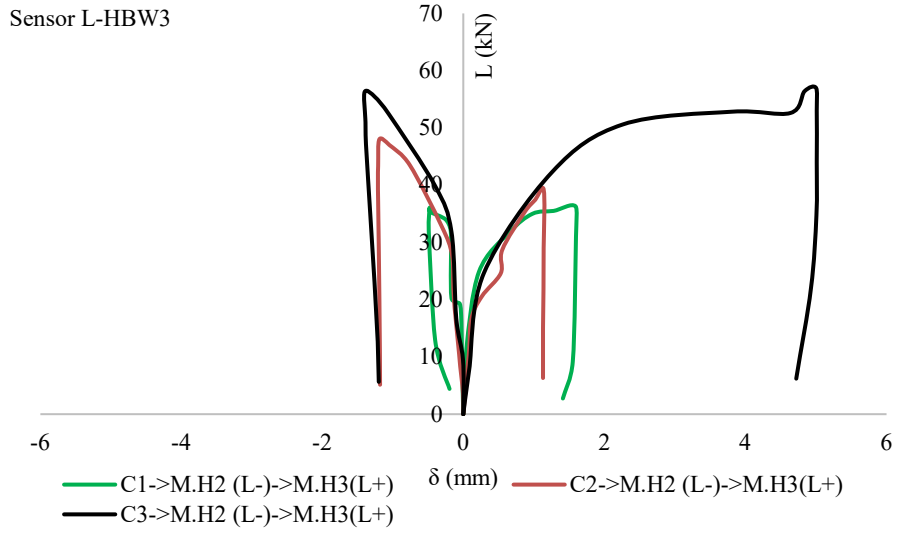

Fig. 7-26. Load-displacement diagram of the strengthened masonry wall HBW3 (when the horizontal sensor L used).

7.3.5 Masonry wall sample: HBW4

HBW4 sample was strengthened with the jute-net and jute diatons. Jute nets of 1 m^2 (of 2.5 cm x 2.5 cm mesh configuration) were placed on either side of the wall, while four jute diatons (horizontal connectors) were inserted orthogonally. In this case the vertical load it is kept constant and equal to 40 kN. Load-displacement behavior is reported in Fig. 7-27 for diagonal displacement transducer G and Fig. 7-28 for diagonal displacement transducer F. Fig. 7-29 presents the load-displacement relationship based on the horizontal displacement transducers labelled M. In all Figures the green curve represents the first load cycle, the red one denotes the second load cycle and the black one stands for the third load cycle. Deformations and displacements can be negative or positive depending on the direction of the acting forces. A quite symmetrical behavior has been recorded in all three above mentioned If we consider the slope of the first load cycle in Fig. 7-27 and Fig. 7-28 it is possible to estimate that the value of the elastic modulus *E* is equal to 14 GPa.

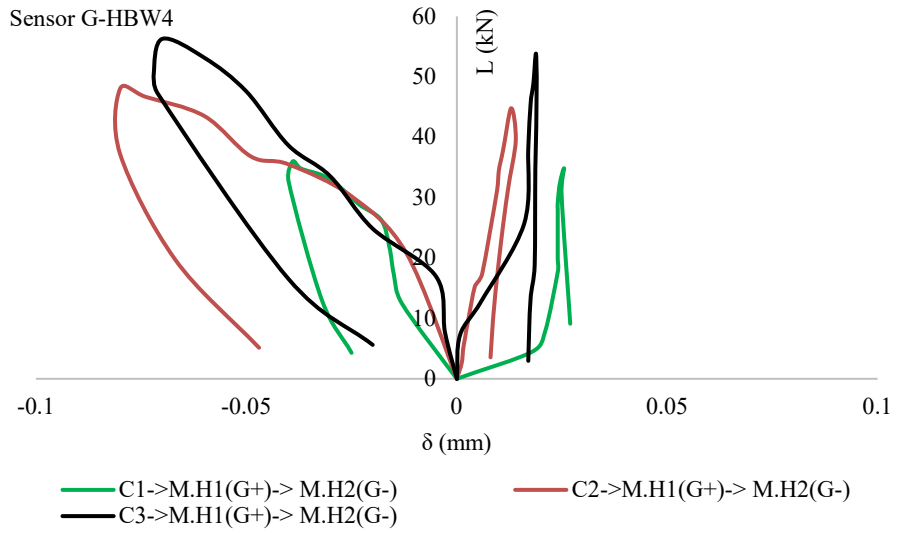

Fig. 7-27. Load-displacement diagrams of the strengthened masonry wall HBW4 (when the diagonal sensor G used).

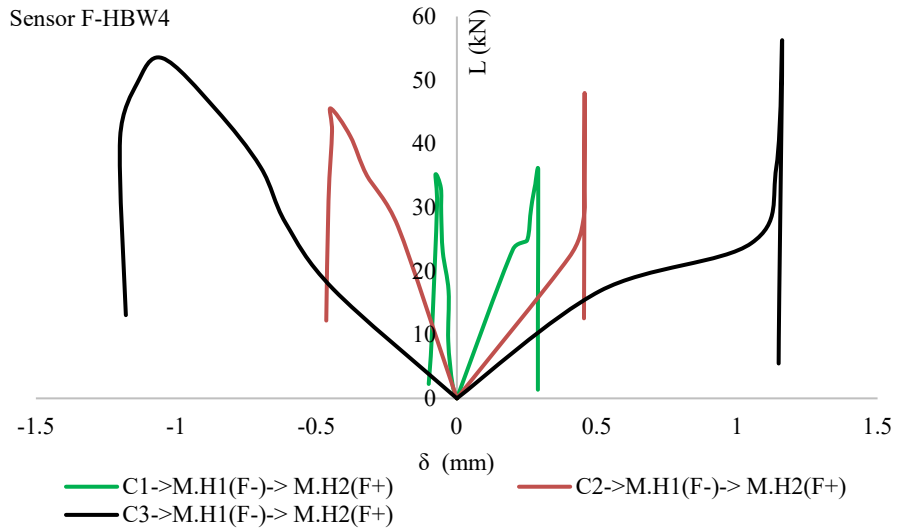

Fig. 7-28. Load-displacement diagrams of the strengthened masonry wall HBW4 (when the diagonal sensor F used).

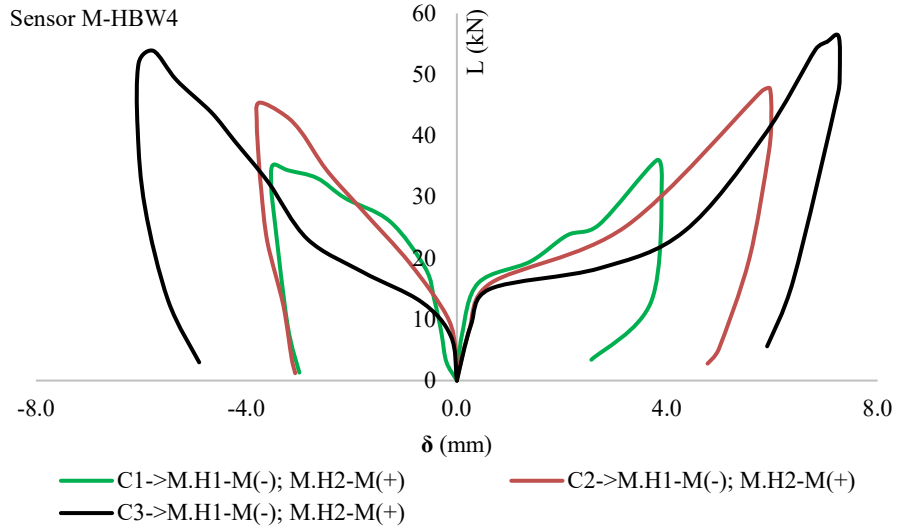

Fig. 7-29. Load-displacement diagram of the strengthened masonry wall HBW4 (when the horizontal sensor M used).

7.3.6 Masonry wall sample: HBW5

Specimen HBW5 was strengthened with four transversal diatons and jute fiber nets on both sides with 2.5 cm x 1.25 mesh configuration. Thereafter jute-composite structural mortar prepared with 1% (with respect to the dry mortar weight) jute fiber and 30mm fiber lengths was used for further thermo-structural reinforcement. 40 kN of constant vertical load was applied on this wall. Load-displacement relationship is reported in Fig. 7-30 for diagonal displacement transducer G and Fig. 7-31 for diagonal displacement transducer F. Fig. 7-32 presents the load-displacement relationship based on the horizontal displacement transducers labelled M. Also in this case, in all Figures the green curve represents the first load cycle, the red one denotes the second load cycle and the black one stands for the third load cycle. Deformations and displacements can be negative or positive depending on the direction of the acting forces. The structural behavior of the wall has not been symmetric in all cases and perhaps some problems in the sensor's placement can explain the differences between the positive and negative strains zones in the above mentioned Figures. If we consider the slope of the first load cycle in Fig. 7-30 and Fig. 7-31 it is possible to estimate that the value of the elastic modulus *E* is equal to 41 GPa.

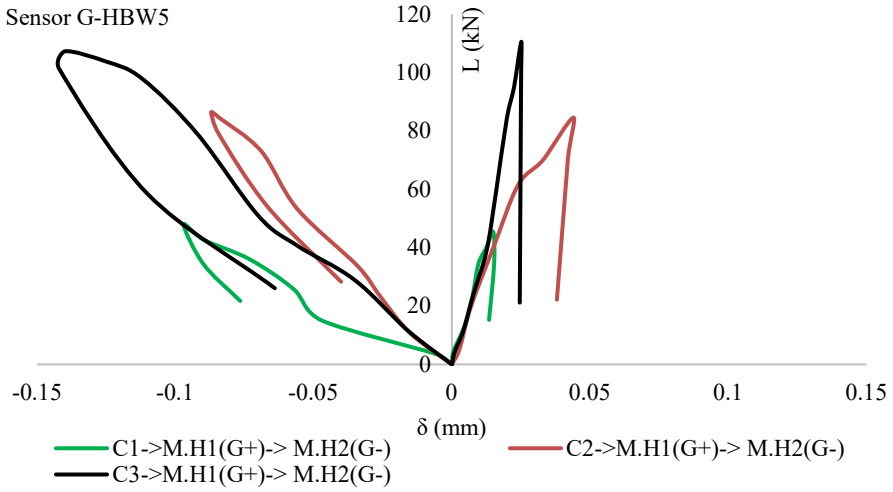

Fig. 7-30. Load-displacement diagrams of the strengthened masonry wall HBW5 (when the diagonal sensor G used).

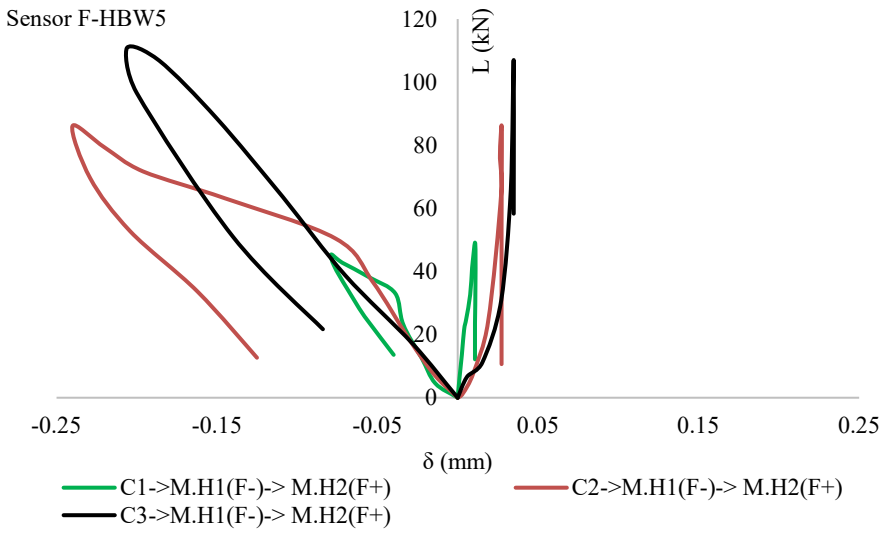

Fig. 7-31. Load-displacement diagrams of the strengthened masonry wall HBW5 (when the diagonal sensor F used).

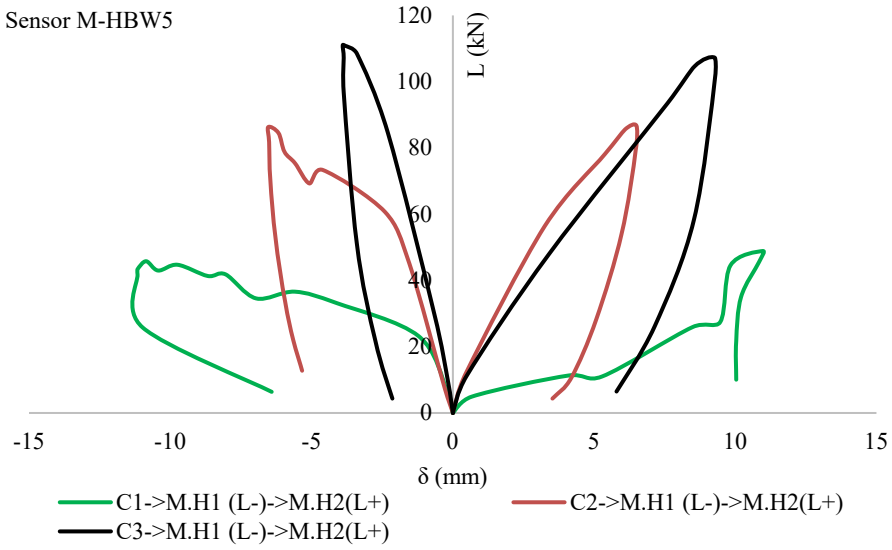

Fig. 7-32. Load-displacement diagram of the strengthened masonry wall HBW5 (when the horizontal sensor M used).

7.3.7 Masonry wall sample: HBW6

Masonry sample HBW6 was strengthened with four transversal diatons and jute fiber nets on both sides with 2.5 cm x 2.5 cm mesh configuration. Thereafter jute-composite structural mortar prepared with 1% (with respect to the dry mortar weight) jute fiber and 30mm fiber lengths was used for further thermo-structural reinforcement. 40 kN of constant vertical load was applied on this wall. Load-displacement relationship is reported in Fig. 7-33 for diagonal displacement transducer A and Fig. 7-34 for diagonal displacement transducer H. Fig. 7-35 presents the load-displacement relationship based on the horizontal displacement transducers labelled L. Also in this case, in all Figures the green curve represents the first load cycle, the red one denotes the second load cycle and the black one stands for the third load cycle. Deformations and displacements can be negative or positive depending on the direction of the acting forces. The structural behavior of the wall has not been symmetric in all cases and a different structural behavior has been recorded when the load is applied from left to right or vice versa. If we consider the slope of the first load cycle in Fig. 7-33 and Fig. 7-34 it is possible to estimate that the value of the elastic modulus E is equal to 22 GPa.

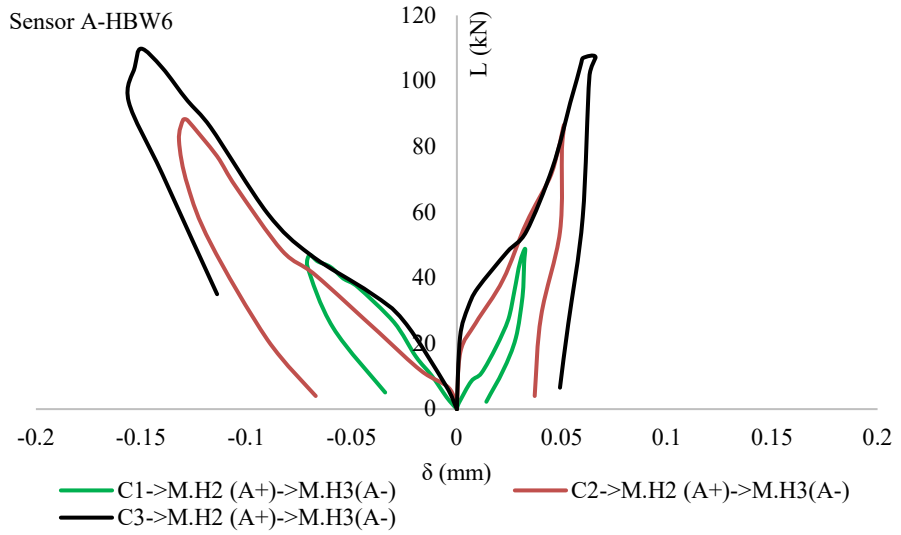

Fig. 7-33. Load-displacement diagrams of the strengthened masonry wall HBW6 (when the diagonal sensor A used).

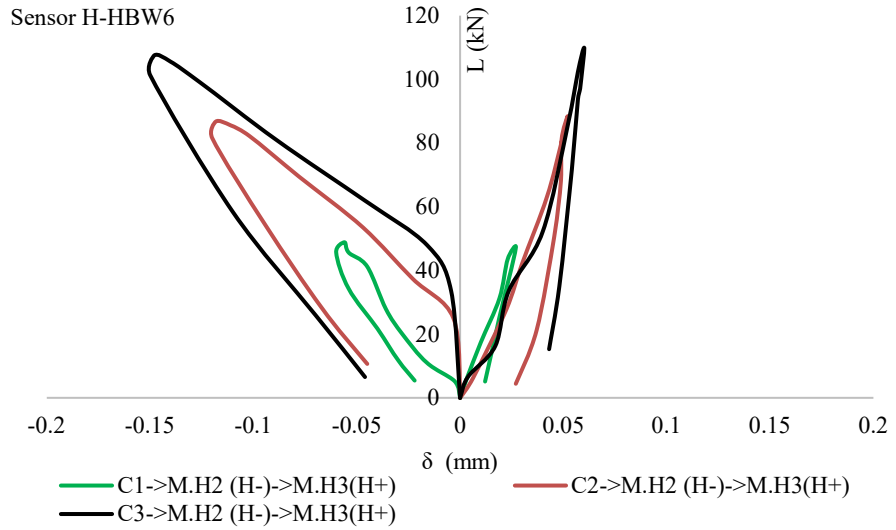

Fig. 7-34. Load-displacement diagrams of the strengthened masonry wall HBW6 (when the diagonal sensor H used).

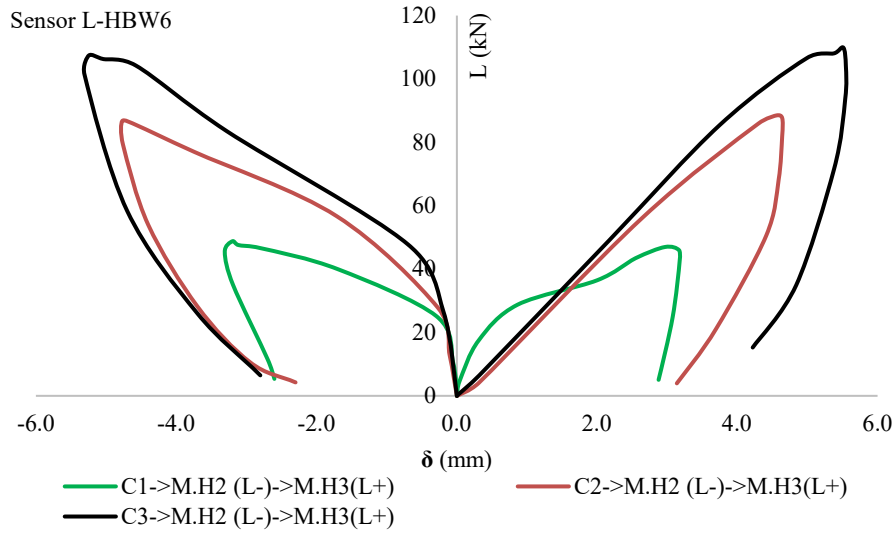

Fig. 7-35. Load-displacement diagram of the strengthened masonry wall HBW6 (when the horizontal sensor L used).

7.3.8 Masonry wall sample: HBW7

Sample HBW has been strengthened with only 4 diatons to connect the external surfaces to improve the shear resistance. The diatons were bonded to the masonry wall surfaces using fiber strengthened SM. 37 kN of constant vertical load was applied and kept constant on this wall. Load-displacement relationship is reported in Fig. 7-36 for diagonal displacement transducer G and Fig. 7-37 for diagonal displacement transducer F. Fig. 7-38 presents the load-displacement relationship based on the horizontal displacement transducers labelled L. Also in this case, in all Figures the green curve represents the first load cycle, the red one denotes the second load cycle and the black one stands for the third load cycle. Deformations and displacements can be negative or positive depending on the direction of the acting forces. The structural behavior of the wall has been almost symmetric in all cases except from Fig. 7-37. If we consider the slope of the first load cycle in Fig. 7-36 and Fig. 7-37 it is possible to estimate that the value of the elastic modulus *E* is equal to 37 GPa.

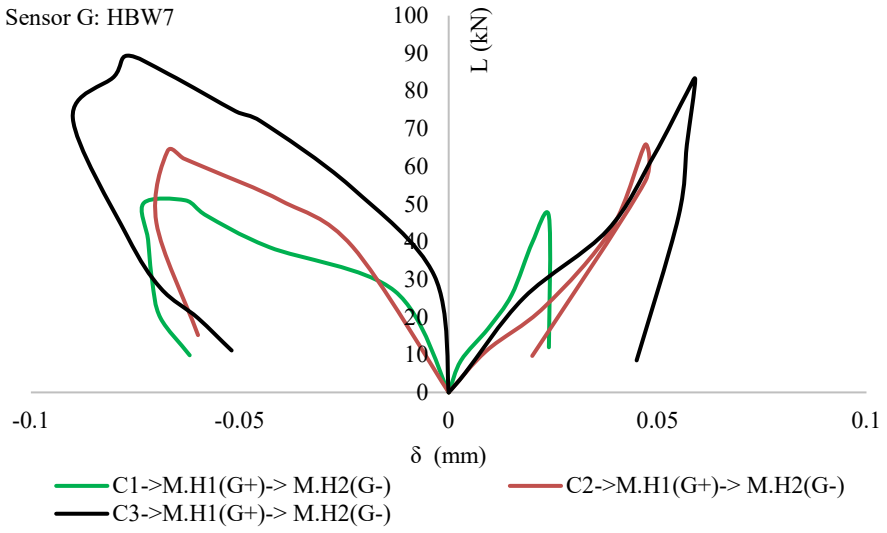

Fig. 7-36. Load-displacement diagrams of the strengthened masonry wall HBW7 (when the diagonal sensor G used).

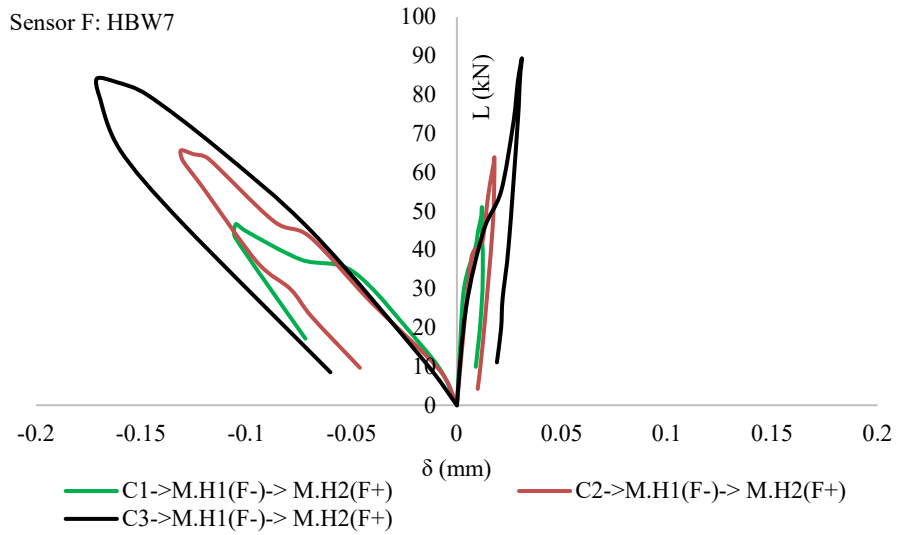

Fig. 7-37. Load-displacement diagrams of the strengthened masonry wall HBW7 (when the diagonal sensor F used).

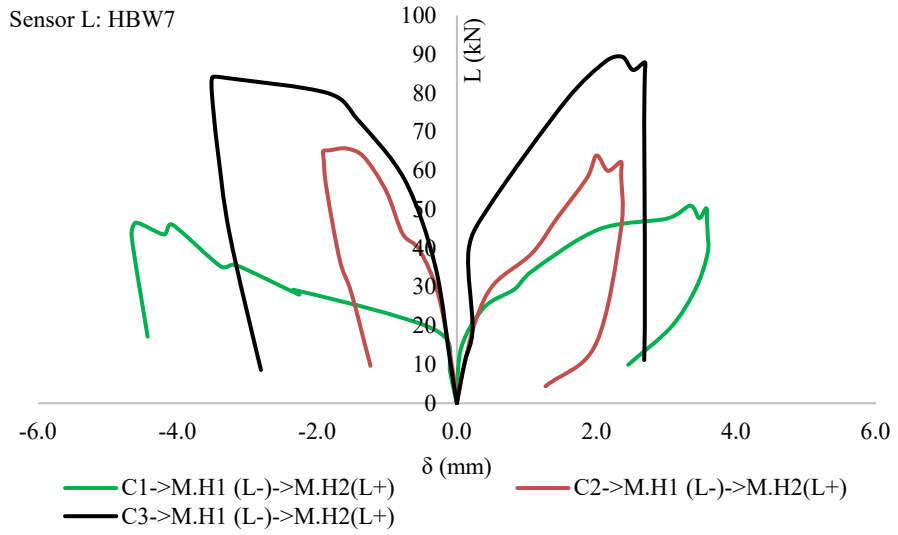

Fig. 7-38. Load-displacement diagram of the strengthened masonry wall HBW1 (when the horizontal sensor L used).

7.3.9 Masonry wall sample: HBW8

Sample HBW8 was strengthened with four transversal diatons and raw jute fibers were placed diagonally and attached with SM on the wall surfaces. 37 kN of constant vertical load was applied and kept constant on this wall. Load-displacement relationship is reported in Fig. 7-39 for diagonal displacement transducer A and Fig. 7-40 for diagonal displacement transducer H. Fig. 7-41 presents the load-displacement relationship based on the horizontal displacement transducers labelled M. Also in this case, in all Figures the green curve represents the first load cycle, the red one denotes the second load cycle and the black one stands for the third load cycle. Deformations and displacements can be negative or positive depending on the direction of the acting forces. After the first load cycle the structural behavior of the wall has not been symmetric, probably there have been some problems in the sensor placement or some modification of boundary conditions. If we consider the slope of the first load cycle in Fig. 7-39 and Fig. 7-40 it is possible to estimate that the value of the elastic modulus *E* is equal to 390 GPa.

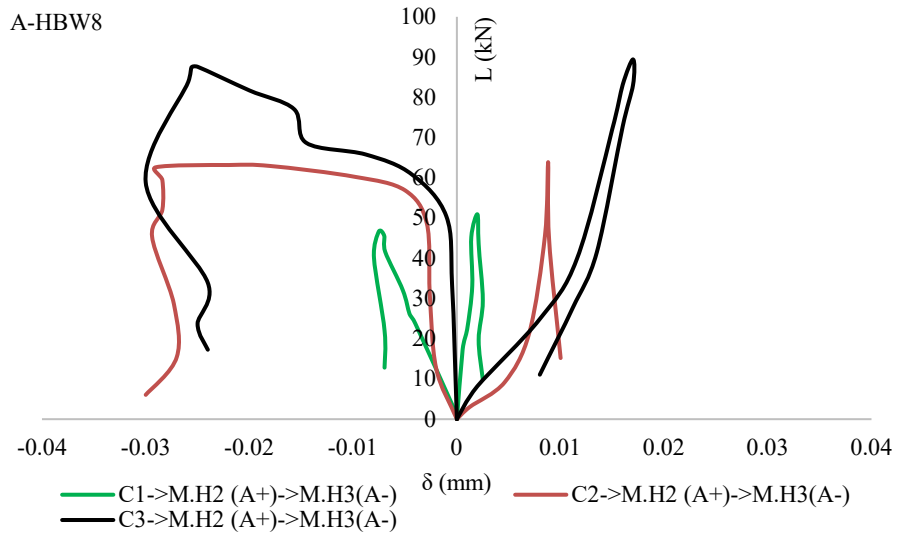

Fig. 7-39. Load-displacement diagrams of the strengthened masonry wall HBW8 (when the diagonal sensor A used).

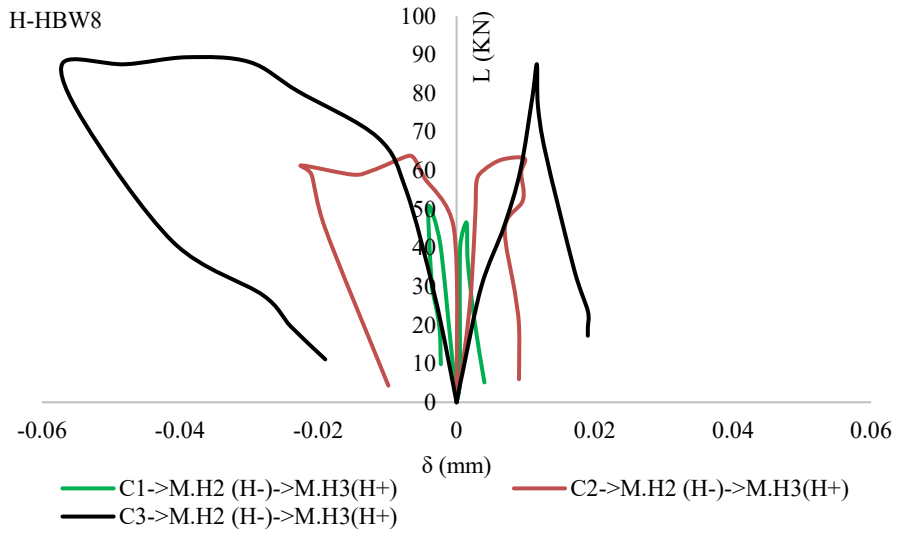

Fig. 7-40. Load-displacement diagrams of the strengthened masonry wall HBW8 (when the diagonal sensor H used).

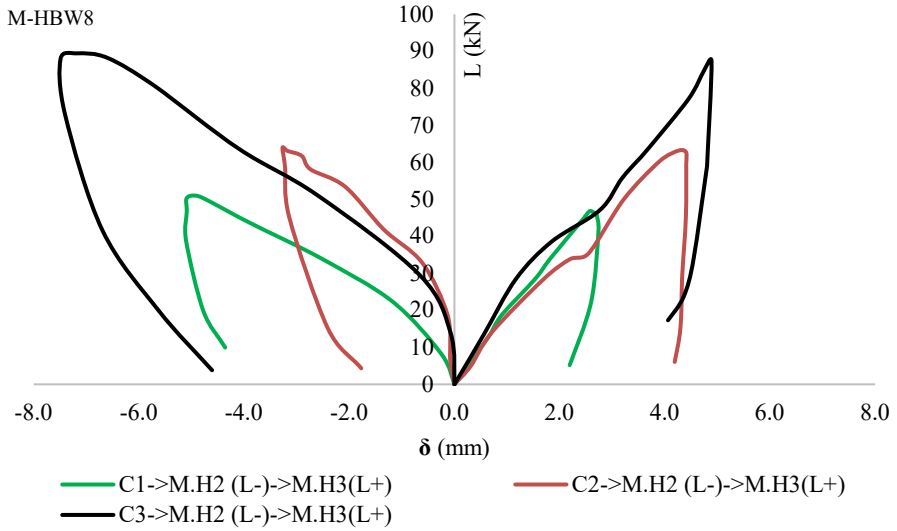

Fig. 7-41. Load-displacement diagram of the strengthened masonry wall HBW1 (when the horizontal sensor M used).

After the above-described load cycles each wall have been subjected to an increasing horizontal load in order to measure the specimen capacity.

Fig. 7-42 presents the load-displacement and which highlights that the natural TRM-system used for masonry upgrading i.e., the strengthened walls have shown better performance than that of hollow brick normal/un-strengthened walls.

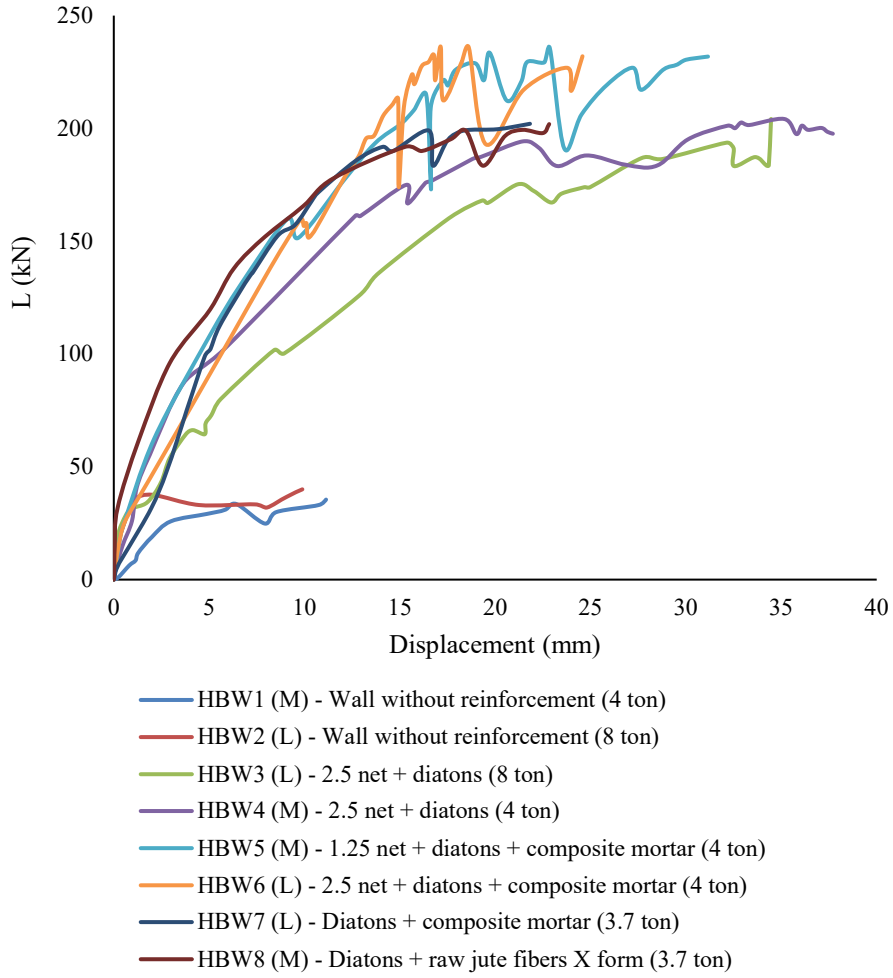

Fig. 7-42. Load-displacement graph, when collapse load was applied (Horizontal sensors).

While in Table 7-4 the maximum loads withstand by each masonry wall and corresponding displacement points have been highlighted. In the maximum displacement obtained by each masonry walls are also presented.

Table 7-4. Applied horizontal load and displacements at collapse.

Masonry wall	Load max	Corresponding displacement	Max displacement
	[kN]	[mm]	[mm]
HBW1 (Sensor-M)	35.41	11.12	11.38
HBW2 (Sensor-L)	40.00	9.88	9.88
HBW3 (Sensor-L)	204.07	34.46	34.46
HBW4 (Sensor-M)	204.17	35.15	37.70
HBW5 (Sensor-M)	235.47	22.87	31.15
HBW6 (Sensor-L)	236.21	17.14	24.57
HBW7 (Sensor-L)	201.97	21.82	21.82
HBW8 (Sensor-M)	201.87	22.82	22.82

7.3.10 Ultimate strengths of the upgraded masonry walls

In this case only four strengthened masonry walls HBW3, HBW4, HBW5 and HBW6 were considered, considering all these walls were upgraded with TRM layer consisting of jute nets and jute fiber diatons. While HBW5 and HBW6 have outer jute fiber composite layer.

According to a well-established approach [CNR-DT 215/2018], the shear capacity of the strengthened wall, $V_{t,R}$ could be determined by calculating the minimum shear capacity of the unstrengthened masonry wall, V_t and the contribution of the TRM, $V_{t,f}$ and summing these two values:

$$V_{t,R} = V_t + V_{t,f} \text{ [kN]} \quad (7.1)$$

where the two term on the right-hand side can be expressed as follows:

(1) The mechanical parameter characterizing the term V_t can be back calculated by considering the results of the experimental tests carried out on the reference (un-strengthened) specimens. While according to the Italian Building Code

(NTC- Circolare n.7 del 21 gennaio 2019 – 8.7.1.16) V_t can be calculated using the below mentioned equation:

$$V_t = H.t.\frac{1.5\,\tau_{0d}}{p}\sqrt{(1+\frac{\sigma_0}{1.5\,\tau_{0d}})}\ [\text{kN}] \quad (7.2)$$

Notably the actual contribution of the un-strengthened masonry wall is equal to the experimental maximum horizontal force applied on the un-strengthened masonry wall during the test (see the Table 7-6).

While the length *(H)*, height *(l)* and thickness *(t)* of the solid clay brick masonry wall are the known values and are equal to 1000 mm, 1000 mm and 200 mm, respectively.

Whereas *P* is the corrective coefficient of the stresses in the cross section, the maximum value i.e., 1.5 has been considered.

The stress due to gravity load, σ_0(MPa) can be calculated using the equation:

$$\sigma_0 = \frac{F_{top}}{H.t}[\frac{N}{mm^2}] \quad (7.3)$$

Therefore, the share stress capacity due to gravity load i.e. τ_{0d} (MPa) could be computed using the equation 7.2 and later the obtained value has been compared with the values provided in the guidelines NTC18.

Table 7-5. Set, measured and calculated in-plane cyclic load test values of the normal (un-upgraded) masonry walls.

	Fixed top load	Experimental maximum horizontal force	stress due to gravity load	share stress capacity due to gravity load
	F_{top} [N]	$V_{t\,exp}$ [N]	σ_0 [MPa]	τ_{0d} [MPa]
HBW1(8ton)	79680	40000	0.3984	0.1073
HBW2(4ton)	39840	35410	0.1992	0.1227

Interestingly, the calculated τ_{0d} (MPa) value (see the Table 7-5) found to fall in-between the range 0.10 – 0.13 [MPa] of the semi-hollow brick wall (i.e., *Muratura in blocchi laterizi semipieni, con giunti verticali a secco (perc. Foratura < 45%)*) as provided in the guidelines NTC18.

Therefore, the overall contribution of the masonry wall, V_t was re-calculated by averaging the two parameters i.e., τ_{od} and σ_0 and using the using the equation 7.1, and the obtained value is equal to 38.01 kN.

(2) The second the mechanical parameter characterizing the term $V_{t,f}$ represents the contribution of the FRCM system and can be calculated according to the Italian Building Code (NTC- Circolare n.7 del 21 gennaio 2019 – 8.7.1.16) using the equation:

$$V_{t,f} = \frac{1}{\gamma_{Rd}} . n_f . t_{vf} . l_f . \alpha_t . \varepsilon_{fd} . E_f \text{ [kN]} \quad (7.4)$$

Notably being a physical parameter, the partial safety factor, γ_{Rd} is considered to be equal to 1.

While n_f represents the total number of the strengthened layers arranged at the sides of the wall (numbers on each side), as both sides of the masonry walls have been retrofitted, therefore n_f is equal to 2.

The equivalent thickness t_{vf} is of a single layer of the TRM system are measured manually (see Table 2).

Whereas l_f is the design dimension of the reinforcement measured orthogonally to the shear force, it can't be longer than length of the masonry wall. Therefore $l_f \leq H$ and is equal to 1000 mm for all the specimens.

α_t is the coefficient to account for reduced tensile strength of fibers when stressed in shear. According to [CNR-DT 215/2018] this value is assumed to equal to 0.80.

E_f is the Young's/elastic modulus of elasticity of dry fabric/textile.

ε_{fd} is the design strain of TRM.

So, the design strength of the TRM system is:

$$\sigma_{fd} = \varepsilon_{fd}.E_f \text{ [MPa]} \quad (7.5)$$

Therefore, the equation 7.3 can be re-written as:

$$V_{t,f} = \frac{1}{\gamma_{Rd}}.n_f.t_{vf}.l_f.\alpha_t.\sigma_{fd} \text{ [kN]} \quad (7.6)$$

Here to be noted that the shear capacity of the strengthened wall, $V_{t,R}$ should be equal to the measured experimental value of the maximum horizontal force (see Table 7-6).

While the contribution of the FRCM system, $V_{t,f}$ should be equal to:

$$V_{t,f} = V_{t,R} - V_t \text{ [kN]} \quad (7.7)$$

The ultimate strength of the TRM system should be equal to,

$$\sigma_{u,f} = \varepsilon_{u,f}.E_f \text{ [MPa]} \quad (7.8)$$

By modifying the equation 4 and using the equation 8, the contribution of the FRCM system at ultimate state could be calculated as,

$$V_{t,f} = \frac{1}{\gamma_{Rd}}.n_f.t_{vf}.l_f.\alpha_t.\sigma_{u,f} \text{ [kN]} \quad (7.9)$$

Therefore, the ultimate strength of the TRM system could be calculated as:

$$\sigma_{u,f} = \frac{V_{t,f}}{\frac{1}{\gamma_{Rd}}.n_f.t_{vf}.l_f.\alpha_t} = \frac{V_{t,R}-V_t}{\frac{1}{\gamma_{Rd}}.n_f.t_{vf}.l_f.\alpha_t} \text{ [MPa]} \quad (7.10)$$

Table 7-6. The ultimate strengths of the TRM system of the tested masonry walls.

	Mesh gap	Equivalent thickness of a single layer of the TRM system	Experimental value of the maximum horizontal force	TRM contribution	Ultimate strength of the TRM
		t_{vf}	$V_{t,R}$	$V_{t,f}$	$\sigma_{u,f}$
	[mm]	[mm]	[N]	[N]	[MPa]
HBW3 (8 ton)	25.0	37.50	204070.00	166056.44	2.768
HBW4 (4 ton)	25.0	37.50	204170.00	166156.44	2.769
HBW5 (4 ton)	12.5	42.50	235470.00	197456.44	2.904
HBW6 (4 ton)	25.0	40.00	236210.00	198196.44	3.097

As in Table 7-6, interestingly the obtained value for the ultimate strength of the TRM system found to be very close to each other, ranging in between 2.768 to 3.097 (MPa).

Notably the HBW5 and HBW6 have been retrofitted with jute nets, jute diatons and jute fiber (30mm and 1% fiber with respect to the mortar mass) composite layers on sides of the masonry wall system. The ultimate strength of the TRM on these two specimens found to be in average 2.77 (MPa).

While HBW3 and HBW4 don't have any composite layers, and the ultimate strength of the TRM on these two specimens found to be in average 3.00 (MPa)

Therefore, it can be said that presence of jute fiber composite layers in the TRM system, has enhanced the ultimate strength of the TRM system by 8.37 %.

7.3.11 Collapses in-plane load tests

The collapse scenario for each wall presents a diagonal crack that represents the edge between a compressive and a tensile stress pattern. Indeed, in the wall specimen subjected to vertical and horizontal load in its plane at ultimate limit state there is the development of a strut and tie system. The strut is almost diagonal connecting the upper side where the hydraulic jack is applying the force with the lower side where there is the boundary condition. The diagonal crack visible see Fig. 7-43.

While the Fig. 7-43 presents the internal skeleton of the masonry wall HBW5, which shows the various layers of the TRM-system. The TRM system starts with a lower mortar layer and on which the net was placed for structural upgrading, thereafter the jute fiber composite upper layer was applied for the masonry wall thermal upgrading.

An interesting collapse has been observed for the masonry wall-HBW3 as in Fig. 7-45. In this case the TRM matrix (textile and mortar) get separated/detached from the substate As possible to see in the Fig. 7-45 jute net used for structural upgrading helps hold the TRM layer.

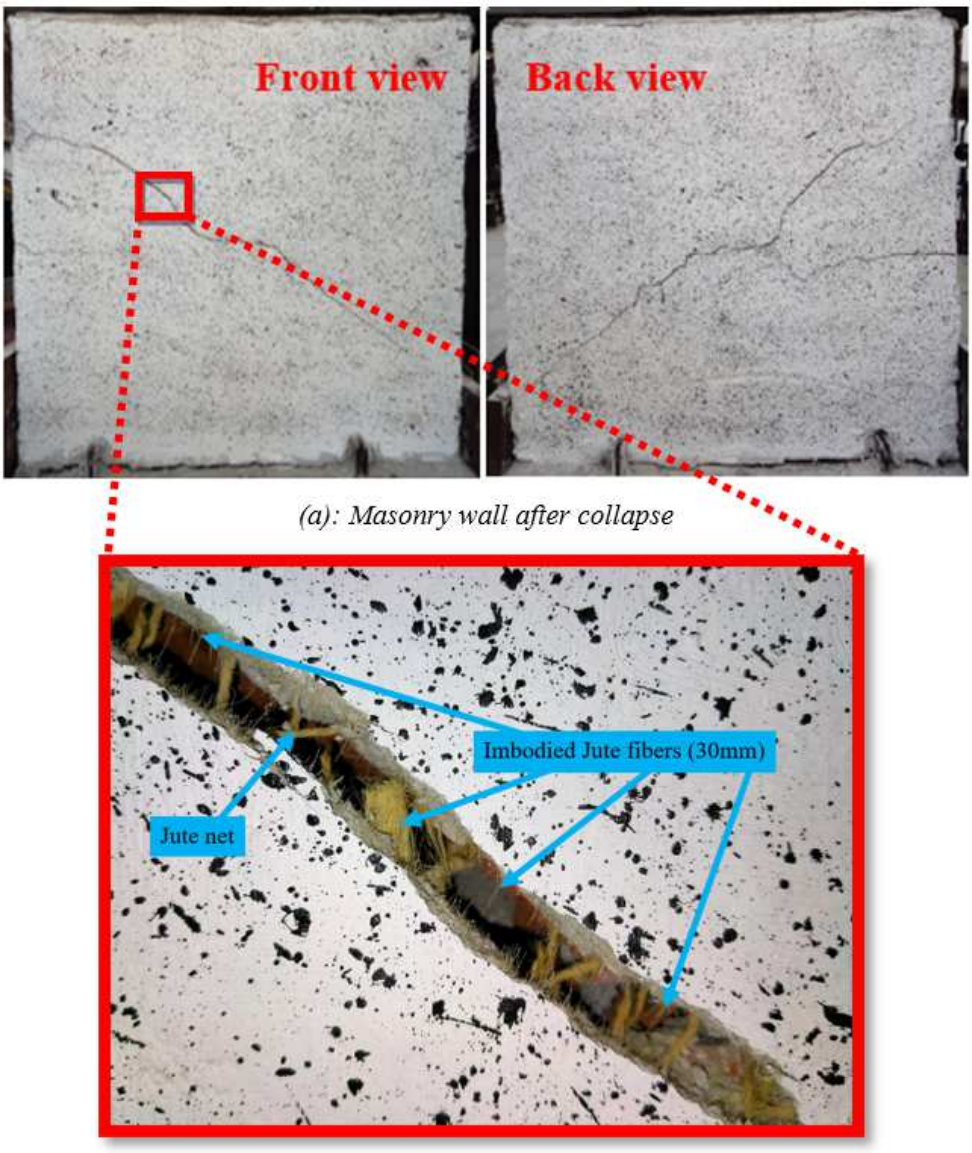

(a): Masonry wall after collapse

(b): Zoomed view of a crack

Fig. 7-43. Masonry wall-HBW5 after collapse

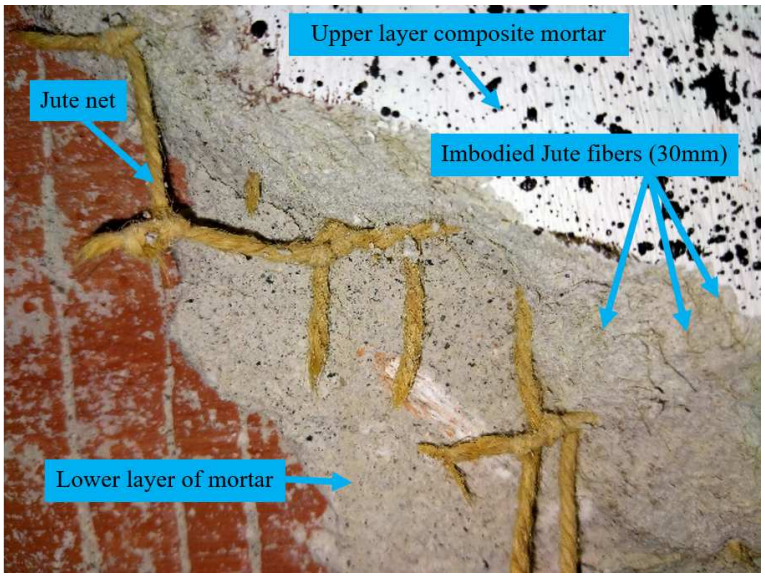

Fig. 7-44. Composite structure (masonry wall-HBW5)

Fig. 7-45. Local collapse of a masonry structure (HBW3)

7.4 Retrofitted masonry walls for thermal characterization

The thermal conductivity measurement of the composite walls was carried out inside the BIEMMETH Climatic Chamber (CC).

Fig. 7-46. Climate Chamber.

Fig. 7-47. Central insulated wall separator of the Climate Chamber.

The CC is installed in the Energy Efficiency Laboratory (LabEE) and it is designed according to the UNI EN 1934:2000. The CC has three parts: there are two chambers and an insulating wall. These two chambers can be set to function as two different desired environments (Fig. 7-47), while the central wall separate the two chambers and in it specimens can be placed to do the tests (Fig. 7-48).

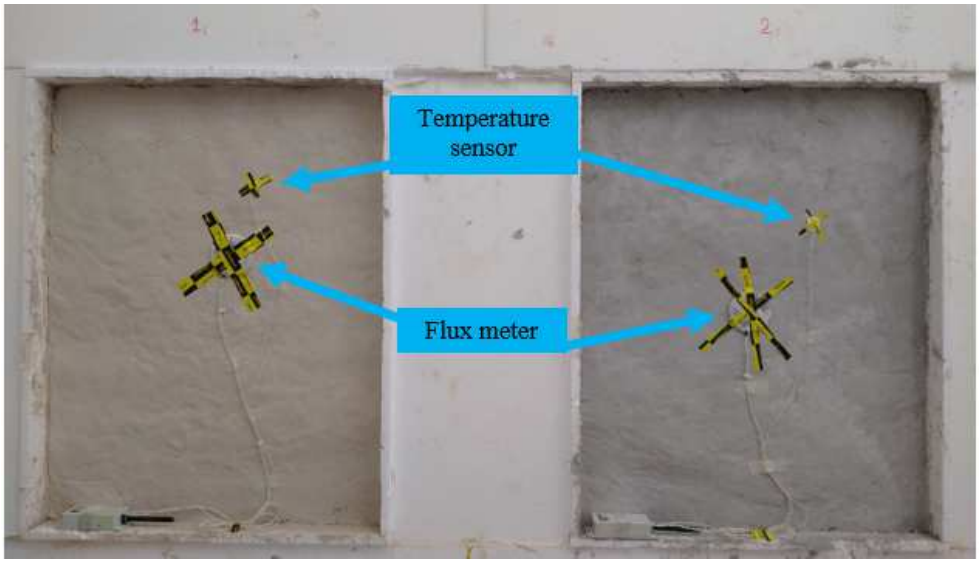

(a): Upgrading configuration: 2.5 cm x 2.5 cm jute fiber nets (both faces), 4 diatons and thermal (without PB)-composite-mortar

(b): Upgrading configuration: 2.5 cm x 2.5 cm jute fiber nets (both faces), 4 diatons and structural composite-mortar

Fig. 7-48. Masonry wall upgrading scheme.

The internal wall which separates the two chambers can accommodate a specimen up to 2.5x2.5x0.7 m.

Generally, a framed ring of insulating material used for smaller specimens and for current experimental purpose a high density (low thermal conductivity < 0.04 W/m^2K) polystyrene has been used. The polystyrene used for this purpose is 30 cm

thick, and it has ensured an unbalancing thermal flow less than 4% of the main thermal flow.

Two strengthened masonry walls with various configurations (as in the below Table 7.7) have been prepared inside the Climate chamber (Fig. 7-47 and Fig. 7-48). Later the thermal conductance measurement of these upgraded masonry walls was conducted.

The first type of upgraded masonry wall (Fig. 7-49) represented as Type 1, (see, Table 7.7) has the same characteristics as of HBW6, see, Fig. 7-11 (b).

While the second type of upgraded masonry wall (Fig. 7-50) represented as Type 2, (see, Table 7.7) is similar to that of HBW6, only in this case the composite mortar mixture has been prepared using the TM (without PB).

The pre-fabricated insulation materials present in the TM, has been removed and replaced with jute fiber.

The final objective is to compare the obtained thermal conductance value of type 1 masonry wall with the type 2 masonry wall.

During the upgrading of the masonry walls, first of all four holes were done on the masonry walls as in Fig. 7-49.(a) and Fig. 7-50.(a), thereafter diatons were placed through these holes and liquid mortar was injected into these holes to fill the gaps, as in Fig. 7-49.(b) and Fig. 7-50.(b).

Then first, very thin layer of mortar was applied to place the jute nets on the surfaces, as in Fig. 7-49.(c) and Fig. 7-50.(c).

After that diaton edges were open, as in Fig. 7-49.(d) and Fig. 7-50.(d) and Fig. 7-49.(e) and Fig. 7-50.(e) represent the upgraded walls with final upper composite layers.

Table 7-7. Masonry wall strengthening scheme.

Masonry wall	Integrated upgrading				
		Structural reinforcement		Thermo-structural reinforcement	
	Mortar type	Jute diatons numbers	Jute net mesh type	Jute fiber configuration in the Composite mortar mixture	
				Fiber length	Fiber percentage
			m^2	mm	%
Type 1: Same as HBW6 Type 2: Similar to HBW6	SM TM (without RA)	4	0.7 x 0.9	30 mm	1 % of fiber with respect to the dry mortar mass
Where, RA is the Recycled Aggregates or prefabricated insulation materials already present in the Thermal Mortar (TM).					

(a): Masonry wall with diaton holes

(b): Diatons placed inside holes + Application of liquid mortar

(c) SM application (lower layer) + Jute net placement

, (d) Application of composite SM (upper layer)

(d): Upgraded masonry wall

Fig. 7-49. Type 1 masonry wall upgradation..

(a): Masonry wall with diaton holes

(b): Diatons placed inside holes + Application of liquid mortar

(c) TM application (lower layer) +Jute net placement

(d) Application of composite TM (upper layer)

(d): Upgraded masonry wall

Fig. 7-50. Type 2 masonry wall upgradation..

The main environmental characteristics of both chambers are summarized in Table 7-8.

Table 7-8. Per-set desired two environment conditions.

Internal room conditions (Hot side)			External ambient conditions (Cold side)		
Temperature (C°)	Humidity (RH%)	Ventilation (m/s)	Temperature (C°)	Humidity (RH%)	Ventilation (m/s)
20	50	1.1	2	50	10.1

The specimens used for the tests have been placed inside the internal wall of the CC, as in Fig. 7-47 and Fig. 7-48. In order to evaluate the thermal conductance of these wall specimens, a total of 2 surface platinum temperature sensors (of class A) and 1 heat flux meter (with accuracy not better than 5% @T=20°C) have been placed on both sides of each specimen, as in Fig. 7-48. One of the temperature sensors is integrated inside the heat flux.

The measurements have been acquired at every 5 min with wireless (the ISM band of 2.4 GHz) and the data have been recorded by a specific data logger with an integrated RAM.

For the tests, steady state conditions (heat fluxes, internal and external temperatures) were considered. This state was achieved generally after ten days of continuous measurements and the values were considered when the cumulative moving average value of the heat flux is maintained within the range of ± 1%, at least for consecutive 24 hours.

Fig. 7-51, Fig. 7-52 and Fig. 7-53 present the continuous measurements of the heat flow, the internal room temperature (of the chamber designated with Room conditions) and external ambient temperature (of the chamber designated with Ambient/outside conditions). In all below graphs it can be seen that the graph trends reach constant values.

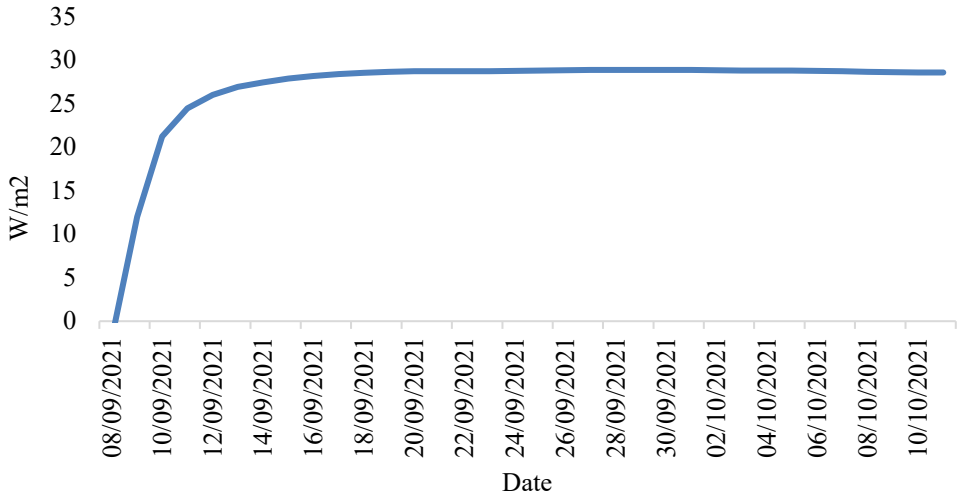

Fig. 7-51.Change in daily heat flow

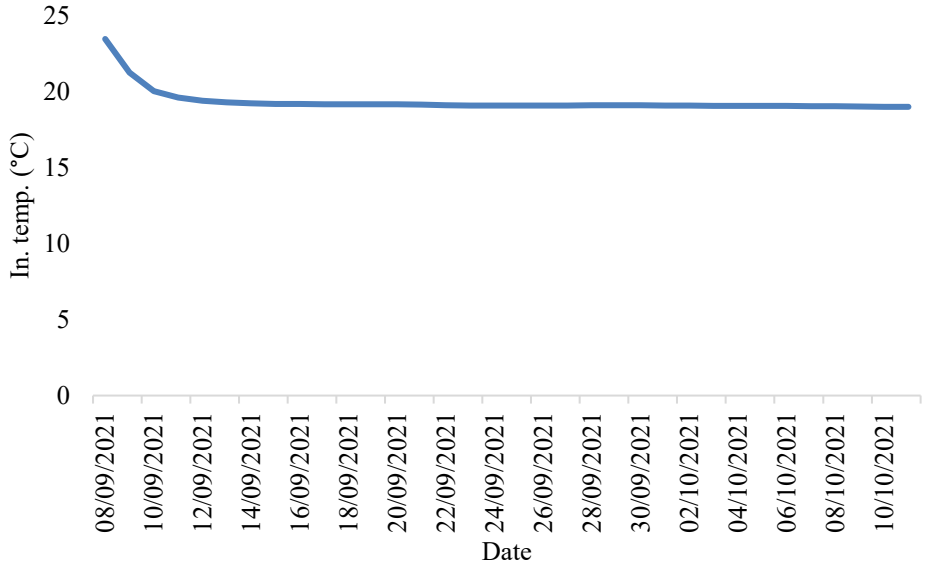

Fig. 7-52.Change in daily internal/room temperature

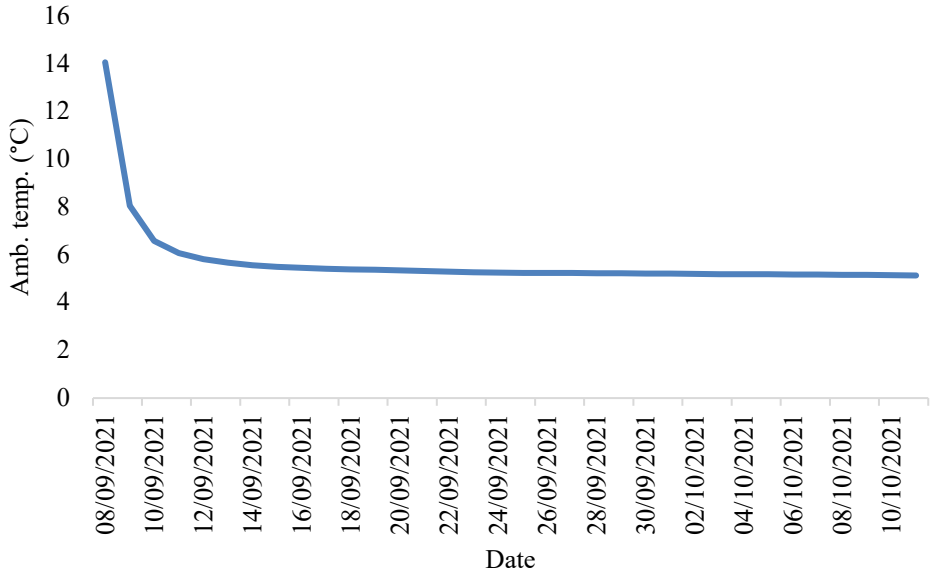

Fig. 7-53. Change in daily ambient temperature

7.4.1 Experimental results: retrofitted masonry walls thermal characterization

7.4.1.1 Thermal conductance measurement

Fig. 7-54 presents a schematic representation of various layers of the hollow brick strengthened composite wall system.

Generally, the heat transfer from indoor condition (with temperature ($T_{in.}$)) to outdoor ambient condition (with temperature ($T_{Amb.}$)) is calculated according to the Equation 7.11:

$$\dot{Q} = U.A.\Delta T\ [\frac{W}{m^2K}] \tag{7.11}$$

where U is the thermal transmittance (W/m^2K); A is the surface area (m^2); $\Delta T = T_{Amb.} - T_{in.}$

$$U = \frac{1}{R_{total}}\ [\frac{W}{m^2K}] \tag{7.12}$$

where R_{Total} is total thermal resistance (m^2K/W).

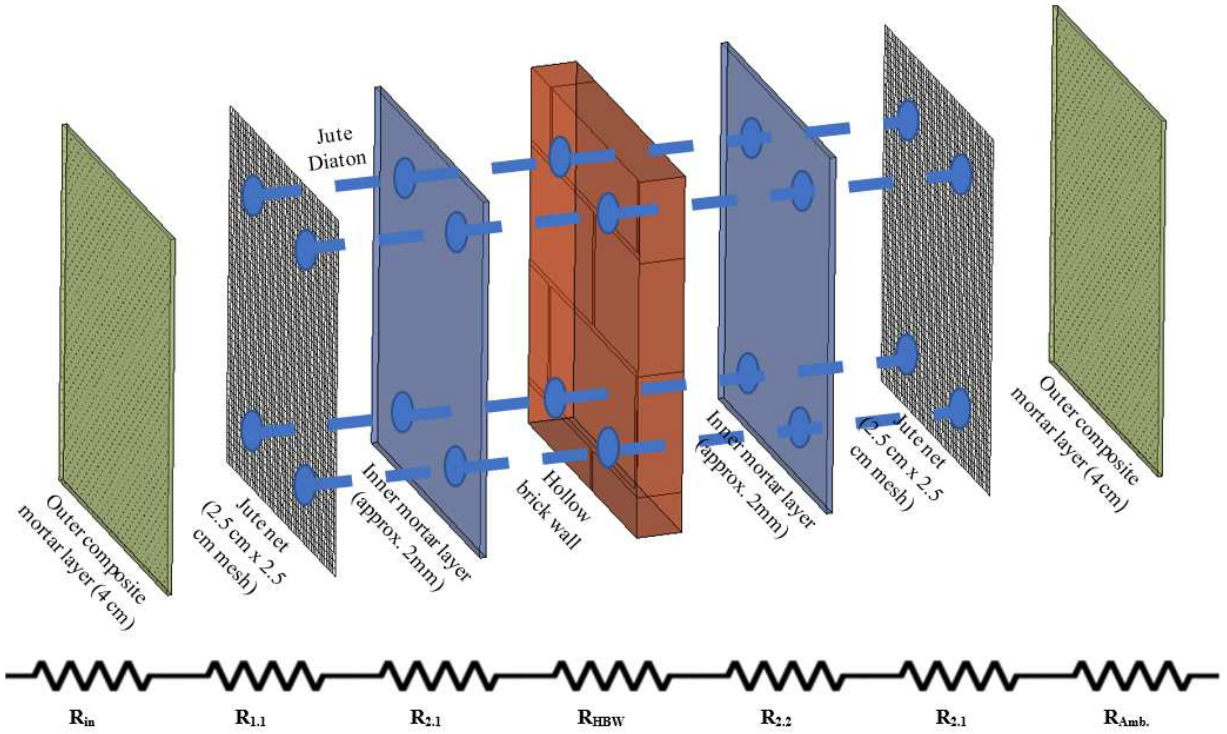

Fig. 7-54. Thermal resistance of the upgraded masonry wall layers.

Table 7-9. Description of each resistance of the masonry wall system.

R_{in}	Indoor resistance
$R_{1.1}$	Composite mortar (towards indoor condition) resistance
$R_{2.1}$	Net + diatons + SM (towards indoor condition) resistance
R_{HBW}	Hollow brick resistance
$R_{2.2}$	Net + diatons + SM (towards indoor condition) resistance
$R_{1.2}$	Composite mortar (towards indoor condition) resistance
R_{Amb}	Ambient/outdoor resistance

During this research work the composite wall systems were built layer by layer. The thermal resistance (m^2K/W) of each layer was calculated (Table 7-10) using the measured heat flow (W/m^2); indoor and out-door temperatures (°C) values. Later the total thermal resistance (m^2K/W) of the composite wall systems were calculated using the equation (Kirchhoff current law):

$$R_{Total.1} = R_{In.} + R_{1.1} + R_{2.1} + R_{HB} + R_{2.2} + R_{1.2} + R_{Amb.} \left[\frac{m^2K}{W}\right] \quad (7.13)$$

Further a normal case, where on the of the masonry wall with SM plaster layers on both sides (Fig. 7-55) was considered.

The thermal resistances $R_{1.1}$ and $R_{2.1}$ (Table 7-12) of only the SM layer calculated using the equation 7.14, when the SM is applied on masonry wall (0.9 m x 0.7 m) with thickness (*S*) about 2 mm. While the thermal conductivity (λ) value of the SM is equal to 0.89 W/mK , obtained in the Phase II was considered.

$$R_{SM} = \frac{S}{A.\lambda} \ [m^2K/W] \quad (7.14)$$

When application of SM was considered on both sides of the masonry wall, the total thermal resistance (m2K/W) using Kirchhoff current law can be written as:

$$R_{Total.2} = R_{In.} + R_{1.SM} + R_{HB} + R_{2.SM} + R_{Amb.} \ [m^2K/W] \quad (7.15)$$

Table 7-10. Thermal resistance of each tested layers of the masonry wall system.

Masonry wall reinforcement mortar type	R_{in}	$R_{1.1}$	$R_{2.1}$	R_{HB}	$R_{2.2}$	$R_{1.2}$	R_{Amb}
Thickness		Approx. 35 mm	Approx. 5 mm		Approx. 5 mm	Approx. 35 mm	
	[m^2K/W]	[m^2K/W]	[m^2K/W]	[m^2K/W]	[m^2K/W]	[m^2K/W]	[m^2K/W]
Type 1: SM	0.040	0.044	0.115	0.394	0.115	0.044	0.13
Type 2: TM(without PB)	0.040	0.050	0.116	0.394	0.116	0.050	0.13

The value of $R_{in\ and}$ R_{Amb} are provided by UNI EN ISO 6946:2018

The measured, calculated and reference thermal resistance values of different layers of the masonry wall only with SM are summarized in the Table 7-12.

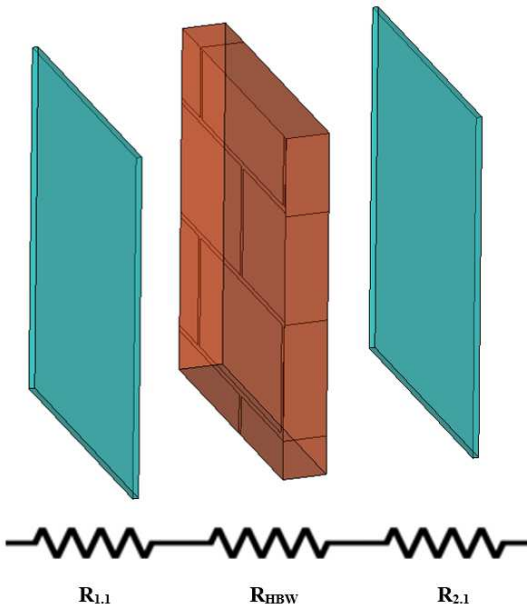

Fig. 7-55. *Thermal resistance of a masonry wall with SM layer.*

Table 7-11. Description of each resistance of the masonry wall system.

R_{in}	Indoor resistance
$R_{1.1}$ and $R_{2.1}$	SM pater layer

Thereafter the thermal transmittance value of normal masonry wall (U_{HBW}), masonry wall with mortar plaster (U_{HBW+SM}) and composite masonry wall ($U_{HBW+NTRM}$) were calculated by using the Equation 7.12. and summarized in Table 7-13.

The thermal transmittance (U_{HBW+SM}) of the masonry wall with only SM plaster layers (Fig. 7-55) was calculated and compared with the composite wall system (Table 7-13).

Table 7-12. Thermal resistance of each layer of the masonry wall with SM applied on surfaces.

Masonry wall reinforcement mortar type	R_{in} (Indoor)	$R_{1.SM}$ (Structural mortar layer)	R_{HB} (Hollow brick wall)	$R_{2.SM}$ (Structural mortar layer)	R_{Amb} (Ambient)
Thickness		2 mm		2 mm	
	m^2K/W	m^2K/W	m^2K/W	m^2K/W	m^2K/W
SM	0.040	0.0039	0.3935	0.0039	0.130
The value of $R_{in\ and}$ R_{Amb} are provided by UNI EN ISO 6946:2018					

Table 7-13. Thermal transmittance: Hollow brick masonry wall Vs Hollow brick strengthened composite wall system.

Masonry wall reinforcement mortar type	U_{HBW} (Hollow Brick wall)	U_{HBW+SM} (Masonry wall + SM)	$U_{HBW+NTRM}$ (Composite wall system)
	[W/m^{2}K]	W/m^{2}K	[W/m^{2}K]
Type 1: SM	1.77 (Same as HBW1 & HBW2)	1.750	1.135 (Same as HBW6)
Type 2: TM (without PB)		x	1.115 (Similar to HBW6)

Table 7-13 presents the comparison between a hollow brick wall and upgraded composite walls. It has been found that, due to the application of raw jute fibers in various forms (jute fiber nets, jute fiber diatons and jute fiber composite mortar) for thermo-structural upgrading, in both cases i.e., for Type 1 and Type 2 masonry walls the thermal transmittance value reduced, which is desired to improve the energy efficiency of a building.

7.5 Integrated behavior

To evaluate the integrated behavior and the performance of the TRM system used for upgrading the masonry wall, the HBW6 has been considered.

The HBW6 has been upgraded with jute nets (with mesh 2.5 cm x 2.5 cm), jute fiber diatons and jute fiber composite mortar. The jute net and jute diatons have been used for the structural strengthening, while the composite layers have been used particularly for thermal upgrading i.e., to enhance the insulation capacity of the masonry wall.

Due to the application of NFTRM system used for HBW6, the overall improvement of the withstanding the overall load capacity increased by 465.84%, when compared with masonry wall without strengthening and upgrading.

The presence of jute fiber composite layers in HBW6's TRM system (jute net + jute diatons + jute fiber composite layer), also help in enhancing the ultimate strength of the TRM system by 11.87 % when compared with the TRM system composed of only jute nets and jute diatons.

Interestingly the composite layer also responsible for enhancing the insulating capacity of the masonry wall, represented in terms of thermal transmittance by 36.05% when compared without strengthening and upgrading.

7.6 Conclusions

This chapter highlights the duel upgrading strategy of the masonry walls, for this purpose hollow brick masonry walls were structurally strengthened and thermally upgraded with jute fiber derived products. Subsequently their structural behavior (through in-plane cyclic shear tests) and thermal properties (the thermal conductivity measurement using a Climatic Chamber) were evaluated and compared with the not-strengthened masonry wall.

The Natural Fiber (NF) TRM system is composed of jute nets (with mesh 2.5 cm x 2.5 cm and 2.5 cm x 1.25 cm), jute fiber diatons. Due to the application of NFTRM system, improvement in ultimate strengths of the upgraded masonry walls (HBW3, HBW4, HBW5 and HBW6), ranging in between 2.768 to 3.097 (MPa). In the case of HBW5 and HBW6, due to application of jute fiber composite layers on the outer-face of the TRM system, enhancement in the ultimate strength of the TRM system by 8.37 % in average has been observed. Interestingly in some cases, for TRM matrix (textile and mortar) debonding at matrix-to-substrate interface has been observed.

On the other hand, the outer composite-layers (NFTRM system) has improved the thermal transmittance of the upgraded masonry walls. When composite upgraded wall is compared with non-upgraded wall, the reduction in thermal transmittance found to be around 0.65 (W/m^2K).

Although these experiments (in-plane cyclic shear tests and the thermal conductivity measurement) have demonstrated improvement in strength and enhancement in insulating capacity of the upgraded masonry walls, but further research would be necessary to conduct to determined right thickness of the TRM system, number of fiber net layers should be used in the TRM system, durability of the TRM system etc.

8. Phase IV - Mechanical behavior and thermal performance of left-over jute-net fiber composite mortar

This part of the project was developed subsequently after the phase III, due to the availability of the jute net fibers leftovers or scraps during the jute net fabrication.

As it has been mentioned previously the mortar nominated with “TM” already has the pre-fabricated insulation materials, which are mainly expanded perlite/polystyrene granules or Recycled Aggregates (RA). These recycled aggregates take up to 1/3 of the total product or the mortar mass.

Notably the jute fiber is known to be bio-degradable, recyclable and also available abundantly, being the second largest produced vegetal fiber.

In this phase the jute fibers scraps were recycled to replace the prefabricated recycled aggregates. This was done to reduce the carbon footprint and mainly to improve the sustainability of the overall project.

In this chapter the mechanical behavior and thermal performance of the recycled jute net fiber composite mortar (without RA) were evaluated by comparing it with normal Thermal Mortar (TM) samples (with RA). These recycled jute fiber scraps were added with the aim to improve both structural and thermal properties.

8.1 Materials and methods

This particular activity has been conducted, while keeping in mind the global or overall sustainability of the project. Therefore, the residual jute fibers were collected during the net fabrication (class 1 mm threads used) and sustainable Recycled Jute

Fiber Composite Mortar (RJFCM) were prepared, by mixing the recycled fiber with the Thermal Mortar (TM) (without pre-fabricated insulation materials i.e., nRA).

8.1.1 Materials

8.1.1.1 Recycled jute net fiber

Recycled jute fibers were collected during the net fabrication processes. Interestingly, these recycled jute net fibers (Fig. 8.2) were used to replace the pre-fabricated insulation materials (Fig. 8-1) present in the original TM.

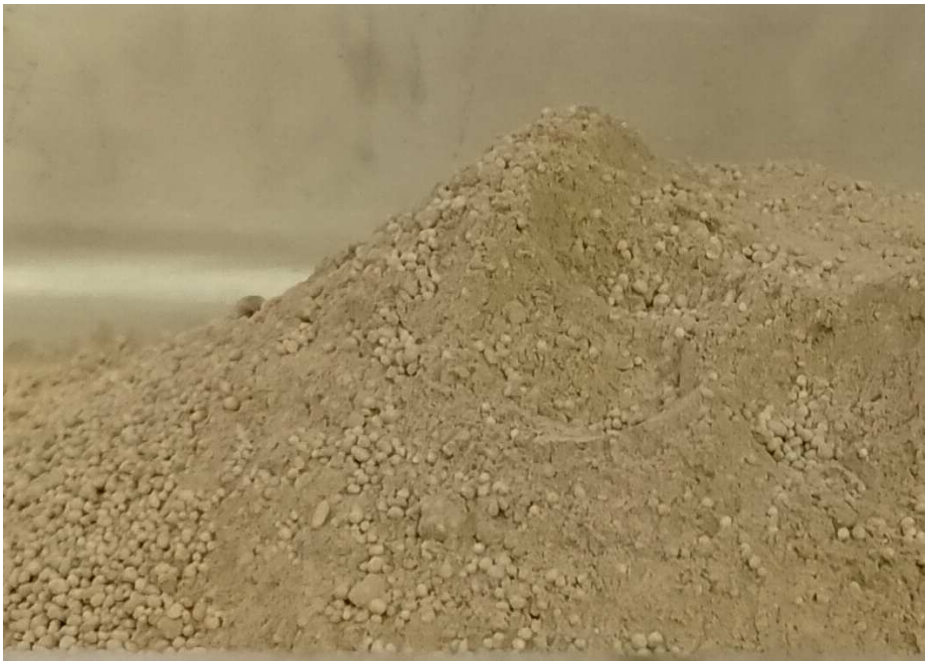

Fig. 8-1. Original thermal mortar (TM) with recycled aggregates (RA).

The recycled jute net fibers have the same characteristics as of the class 1 mm jute threads (see Chapter 4 for details) used for the net preparation. The sizes of these recycled scrap fibers found to be ranging from 5 mm to 50 mm (Fig. 8-4.b), while some of these fibers also have knot(s) (Fig. 8-4.c).

Fig. 8-2. Amount of water, thermal mortar (without PB) and recycled jute net fibers

8.1.1.2 Mortar

The TM is classification and the composition of the TM are explained in Chapter 5. The original TM has the inherent insulation materials (i.e., PBs) which take nearly up to 33% mortar mass (Table 8-1).

8.1.2 Test procedure

8.1.2.1 jute fiber composite mortars preparation.

The standard UNI EN 1015-2: 2007 was followed for the recycled jute-net fiber composite mortars without recycled aggregates (Fig. 5-3 and Fig. 8-1) preparation and these were grouped under M(nRA)F6.5(NF). Whereas nRA and NF used to express samples without/No Recycled Aggregates and Net Fiber, respectively.

The recycled jute-net fiber composite mortars later were compared with the normal TM samples with RA are nominated and grouped under M (without fiber).

Approximately 444.27 kg/m^3 of recycled aggregates can be present in a normal mortar sample, and these recycled aggregates have been replaced with 77.5 kg/m^3 recycled jute thread fibers.

A power sifting machine (Fig need to put) was used to separate the pre-present insulation materials (Fig. 8-3.c) and powder mortar (without PB) (Fig. 8-3.d) from the original mortar (Fig. 8-3.a).

Therefore, only the separated powder mortar (lime based) (Fig. 8-3.d) has been used for the composite mortar preparation.

The jute net fiber scraps (Fig. 8-3.e) were collected from the net fabrication (Fig. 8-3.b) were used to replace the pre-fabricated insulation materials (i.e., PBs).

Table 8-1 presents the amount of jute fiber and water have been used for the mortar mixtures.

After adding the adequate amount of water (as in Table 8-1), the mixture was stirred (Fig. 8-3.f) approximately for 2+3+3 minutes, in three stages.

Table 8-1. Composition TM samples without PB and with recycled jute-net fiber.

Sample type	Insulation materials	Percentage of insulation materials (jute net fiber) with respect to mortar mass	Water used for the mixture
		[%]	[%]
M(nRA)F6.5(NF)	Jute net fiber (Added externally replacing PB)	6.33	58

The mixture (mortar + fiber) consistency and workability were determined by using the shaking table tests as explained in the chapter 5, section 5.1.2.1.

Thereafter two types of samples were prepared: for mechanical tests (Fig. 8-3.g) and for thermal conductivity tests (Fig. 8-3.h)

The sample curing procedure and period were exactly the same way as explained in the Chapter 5, Section 5.1.2.1.

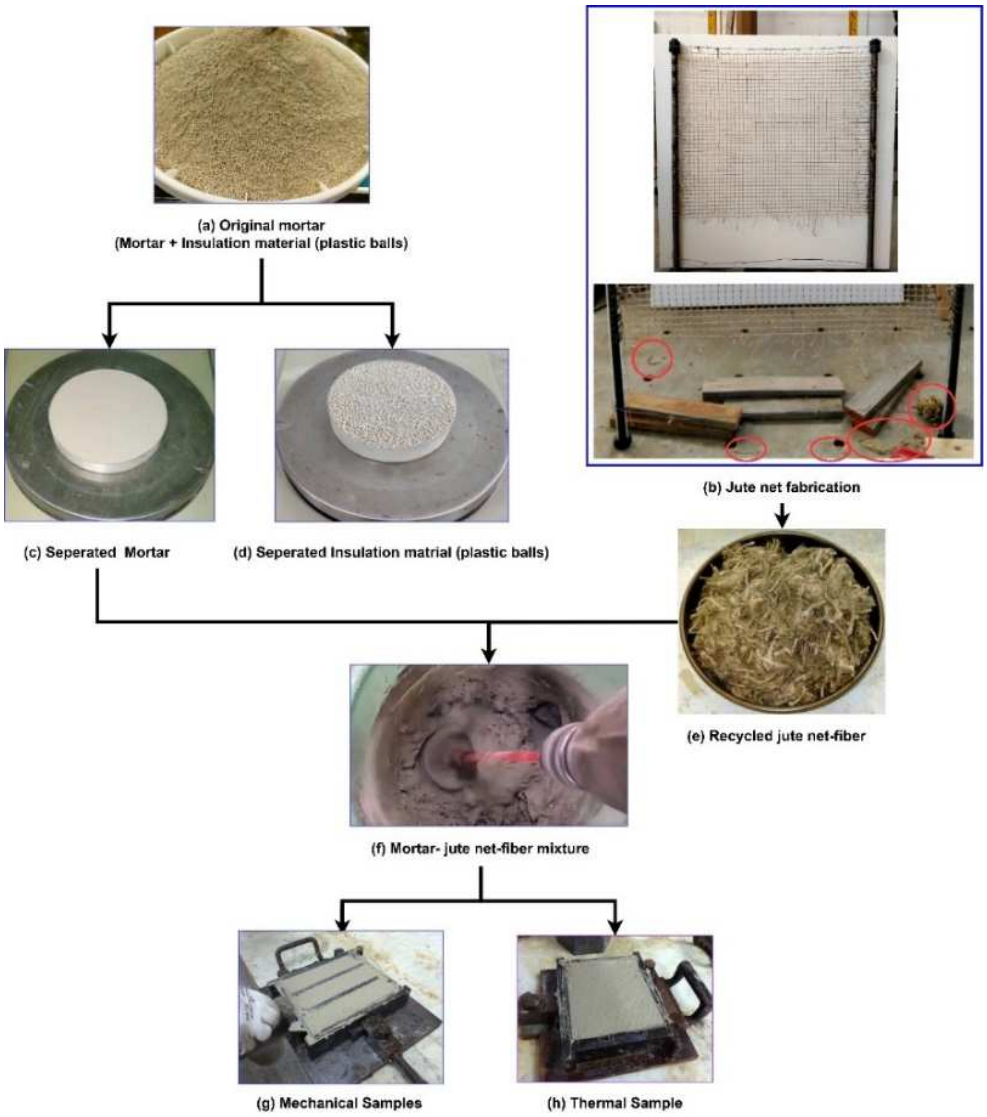

Fig. 8-3. The recycled jute net fiber composite mortar preparation scheme

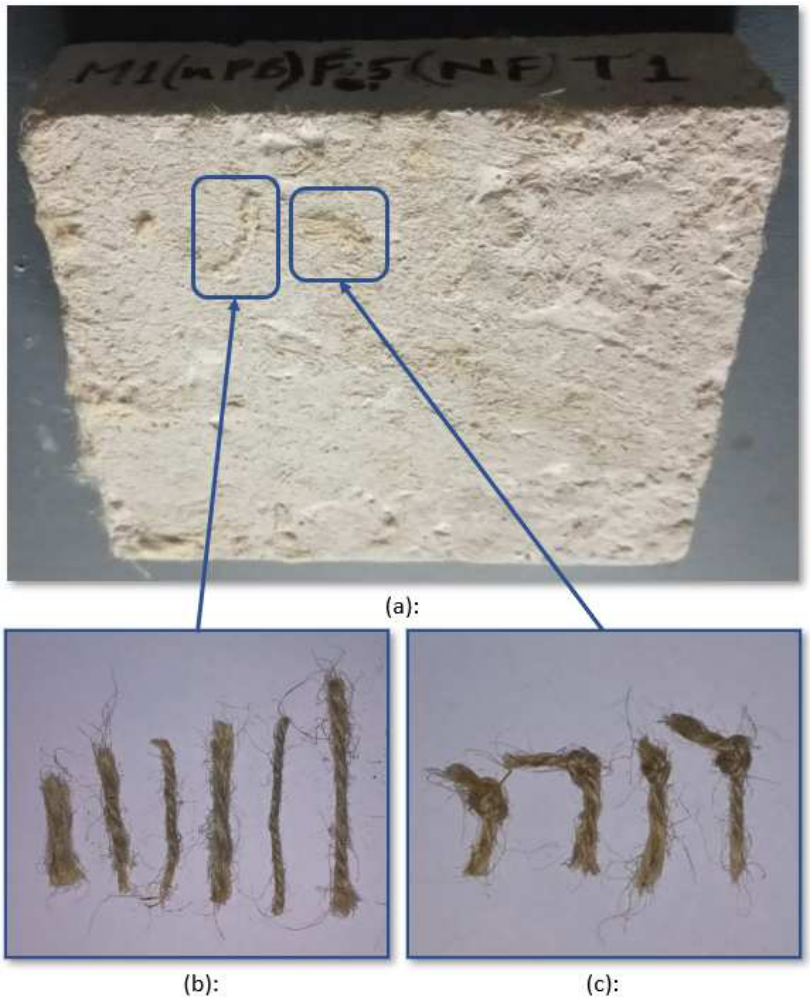

Fig. 8-4. (a) Thermal sample (160 x 140 x 40 mm^3) with imbodied recycled jute net fiber, (b) Thread fiber pieces of various sizes; (b) Presence of knots in some of the recycled jute net fibers

8.1.2.2 Mechanical Property Tests

Table 8-2 and Table 8-3 present the flexural properties (based on the tests as in Fig. *8-5*) of the RJFCM sample. To know more about the standard used, procedure followed for the test and the machine, please see, Chapter 5.

Fig. 8-5. Flexural strength test: sample M(nRA)F6.5(NF)M1S1.

Table 8-2. Thermal composite mortars with Flexural properties-1

Sample type	deflection max. (d)		Stain energy	
	Mean [mm]	Co.V [%]	Mean [kN.mm]	Co.V [%]
M(nRA)F6.5(NF)	0.531	11.540	1.362	25.756

Table 8-3. Thermal composite mortars with Flexural properties-2

Sample type	Flexural stress (σ)		Flexural strain (ε)		Moment of inertia (I)	
	Mean [MPa]	Co.V [%]	Mean	Co.V [%]	Mean [mm^4]	Co.V [%]
M(nRA)F6.5(NF)	0.578	19.152	0.011	9.623	244668.562	8.548

Table 8-4 reports the compressive strength (based on the tests as in Fig. 8-6) value of the RJFCM sample. To know more about the standard used, test procedures and the machine, see Chapter 5.

Fig. 8-6. Compression test: sample M(nRA)F6.5(NF)M1S1

Table 8-4. Thermal composite mortars compressive strength

Sample type	Mean [MPa]	Co.V [%]
M(nRA)F6.5(NF)	19.51	26.54

8.1.2.3 Thermal Property Tests

Thermal conductivity tests were run on the RJFCM samples (160 x 140 x 40 mm^3) without recycled aggregates (nRA) and with recycled jute net fiber (M(nRA)F6.5(NF)) (Fig. 8-7) to evaluate the thermal characteristics and

performances. The TC measuring procedure, the heat flow meter instrument (TAURUS TCA 300). Table 8-5 presents the thermal conductivity values of the RJFCM sample, the measurements conducted at 10°C, 20°C and 30°C.To know more about the standard used, test procedures and the machine, please see, chapter 5, section 5.1.2.2.

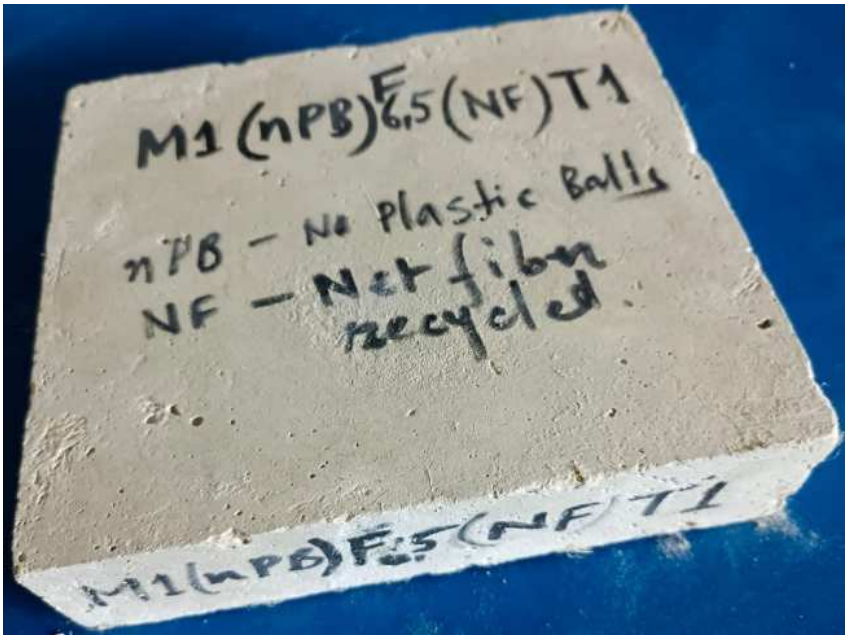

Fig. 8-7. RJFCM sample: M1(nRA)F6.5(NF)T1.

Table 8-5. Thermal conductivity tests: insulation capacity of the RJFCM

Sample type	λ (after oven drying @ 50°C) [W/mK]		
	@ 10°C	@ 20°C	@ 30°C
M(nRA)F6.5(NF)	0.213	0.218	0.225

Fig. 8-8. Thermal conductivity test: sample M(nRA)F6.5(NF)T2.

8.2 Result and discussion

8.2.1 Experimental results: Mechanical behavior of the recycled jute-net fiber composite mortars

The mechanical behaviors of each prismatic sample (160 x 40 x 40 mm^3) were evaluated through flexural (Fig. 8 5) and compressive (Fig. 8 6) strengths.

The tests were conducted on the 28th day of casting, and the strain energy (U), the flexural strength (f_t) and flexural strain of each sample were determined. In this case, when the mechanical results of the normal thermal mortar sample M (No fiber & with RA) was compared with the recycled jute fibers i.e., M(nRA)F6.5(NF), and it was observed that the flexural strength (as in Fig. 8-2) clearly reduced, while the stain energy (Fig. 8-2) and compressive strength (Table 8-4) have been increased.

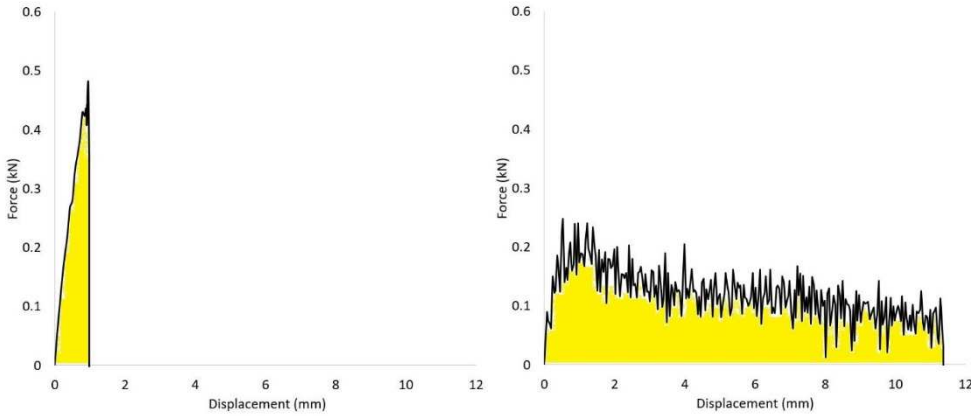

(a): Normal thermal mortar (without fiber and with insulation materials (Recycled aggregates)

(b): Thermal mortar M(nRA)F6.5(NF) with recycled jute net-fiber and without materials (Recycled aggregates)

Fig. 8-9. Strain energy graphs: sample without fiber Vs sample with 6.5% (with respect to the mortar mass) fiber.

Therefore, with the addition of jute fibers (recycled residual from net fabrication), in the place of pre-fabricated insulation materials (i.e., PB was present in the original mortar), it has been observed that the stain energy more than 600% (Fig. 8-9.b) when these values were compared with the samples without fiber and with PB (Fig. 8-9.a). Interestingly the compressive strengths also found to be improved about 400%.

The presence of unequal and longer fibers (without knots, see Fig. 8-4.b and with knots, see Fig. 8-4.c) have helped in binding and gripping mortar materials better than that of PBs. Therefore, the presence of imbodied fibers in composite samples have helped in absorbing and dissipating the applied load.

Notably, during the flexural tests, the samples with fibers (and without PB) have shown ductile behavior, while the same samples have shown rigid behavior during the compression test.

The increment of strain energy was due to the fact that these recycled jute fibers are the smaller pieces come from jute thread, therefore their individual tensile

strength capacity collectively augment the tensile behavior resulting in higher strain energy. While the samples prepared with TM with RAs have higher flexural strength (found to be 50% more when recycled jute fibers were added in the place of PBs) due to the fact that the PBs are spherical therefore provide better uniformity in a composite sample.

While fibers imbodied in samples are responsible for discontinuity. When natural (jute) fibers are used for a composite mixture, these fibers absorb water by itself and as well as trap water collectively. Therefore, when the composite sample dry and this process is responsible to create void in the fiber matrix (three yarn jute fiber thread pieces).

8.2.2 Experimental results: thermal properties of the recycled jute-net fiber composite mortars

It can be concluded that by replacing the pre-fabricated RA from the original mortar and by adding around 6.5% (with respect to dry mortar mass) the recycled jute thread fibers, it is possible to improve also the insulating capacity of the composite mortars.

Table 8-6 shows the reduction of thermal conductivity at every temperature range, therefore these reductions highlight the improvement in the insulation capabilities of the RJFCM. The reduction in TC of 0.017 W/mK at 10°C, of 0.018 W/mK at 20°C and of 0.016 W/mK at 30°C, respectively have been observed when PBs were replaced with the recycled jute-net fibers.

Table 8-6. Change in thermal properties with addition of jute fiber and removal of insulation materials: the sample M(nRA)F6.5(NF) Vs. M(without fiber).

Thermal conductivity (λ) [W/mK]		
@ 10°C	@ 20°C	@ 30°C
- 7.98 %	- 8.26 %	-7.11 %

nRA = No Recycled aggregates; NF = Net Fiber

8.3 Conclusions

The recyclability of the residual jute fiber from net fabrication process and its applicability in the production of new recycled natural fiber composite material have been evaluated in this paper. Moreover, the thermo-structural behaviors of the composite material and its potential use as duel-upgrading (i.e., structural and thermal) purposes have been studied.

In this process, the insulation materials (expanded perlite/polystyrene granules or recycled aggregates) already present in the commercial dry-mixed mortar have been replaced with the above-mentioned recycled jute-net fibers.

Interestingly, promising results have been obtained with the improvement in strain energy and thermal conductivity. Only three jute net-fiber composite mortar samples mechanical and thermal properties have been evaluated and compared with the normal TM (with RA and without fiber) mortar, during this phase of the research work. Therefore, further studies need to be conducted to assess the feasibility of using these fibers in construction and building sector.

9. Digital Image Correlation (DIC)

This chapter highlights the use of Digital Image Correlation (DIC) method to analyze and determine, the cracks opening (mm) in the deformed specimens, before reaching the ultimate displacement point. For the DIC analysis, very popular GOM correlate software has been used.

Notably, as stated by Janeliukstis et al. (2021), the DIC was already in use in 1980s, while nowadays DIC used to determine the geometry, displacement, and string. Interestingly DIC is getting popular among scientists and researchers being a non-contact fill-filed measuring procedure. It is an optical method to measure 2D or 3D coordinates for evaluation of required parameters (displacement and strain) Deák et al. (2018).

As stated in Górszczyk et al. (2019), Janeliukstis et al. (2021), the measurements and analysis of the displacement or deformation of the targeted specimen using DIC system subjected to following steps:

1. Surface preparation: before starting the tests, under-observation specimen(s) to be tinted with white paint and after drying, the black dots/sprinkles have to be stochastically sprayed on the surface painted with white background (as can be seen in Fig 9.3 and Fig 9.4)
2. Calibration of a device according to the required procedure (using the DIC system calibration): Through DIC analysis software it is possible define the quality of the analyzing pictures. Therefore, to have the optimum DIC results the camera spatial resolution and the working distance between the camera(s) and the target object should be correctly calibrated. Prior to the tests, by putting pictures in DIC software the various camera parameters could/should be adjusted, like focal point, acquisition rate, resolution as required, etc.

3. Illumination: Light adjustment is an important factor for taking good pictures, therefore high-intensity illumination is necessary to have high-quality images.
4. Taking and recording images of the targeted object or material surface during the test(s): It is important to note that picture taking interval should be synchronized with the load-displacement measuring instrument, to have correct correlation between the taken pictures and measured data during analysis. As in Fig. 9-1(a), 2D-DIC are applied for planer objects, where single camera is used to measure the in-plane deformations Górszczyk et al. (2019). While Fig. 9-1(b) represents 3D-DIC scheme which mainly used for non-planer objects, in this case two cameras are needed to take pictures from different directions Górszczyk et al. (2019).

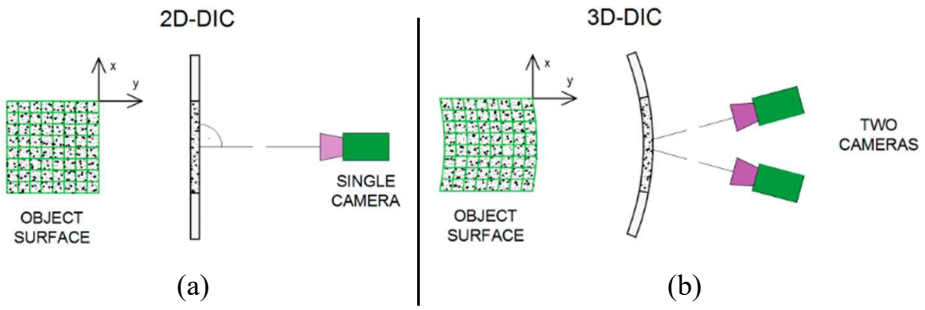

Fig. 9-1. DIC image recording scheme Górszczyk et al. (2019).

5. DIC analysis (evaluation) using a specialized computer program (software): various software are available in the market for DIC analysis. While GOM correlate is free software and very easily can be used for pictures elaboration and analysis.
6. Visualization of the results.

9.1 Materials and methods

The Digital Image Correlation (DIC) method has been used to analysis the cracks of the deformed samples. The investigation has been made with the help of the GOM correlate software.

9.1.1 Materials

Some composite prismatic samples (used for mechanical tests) and upgraded masonry wall specimens were used for the DIC analysis. Both prismatic samples and masonry wall specimens were painted with white color (Fig. 9-2) and later black color was sprayed over white surfaces (as in Fig. 9-3 for prismatic sample and Fig. 9-4 for upgraded masonry wall specimen).

Fig. 9-2.Painting of masonry wall with white color.

Fig. 9-3. Black spots/pattern surface of the sample MS1(SW)F0.5(5)M1S3.

Fig. 9-4. Black spots/pattern surface of the wall specimen HBW5.

9.1.2 Methods

The camera is mounted exactly in front, and perfectly parallel to the targeted center of the surface. Fig. 9-5 represents the camera configuration as used during the test for the masonry wall specimen. The camera resolution and acquisition time interval were selected to be 1920 x1080 pixel and 0.5 sec., respectively. Whereas the focal distance was around 237 cm. While two artificial lights were also used to have uniform light on the surface, therefore, to have better quality pictures for DIC analysis.

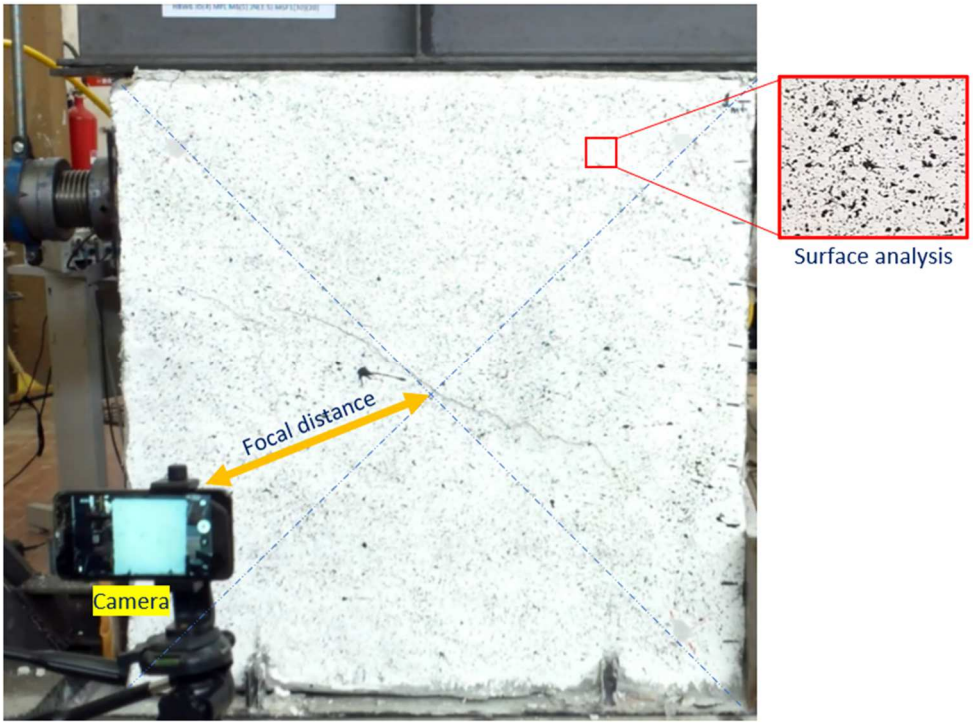

Fig. 9-5. Camera setup.

A total of 15 pictures were selected for the DIC analysis (Fig. 9-6), for the composite prismatic sample's cases. This selection of these pictures has been considered and selected from various phases. Pictures from 1 to 6 represents, zero load to peak load (at this point the sample collapse and drop in the graph can be

seen), pictures from 7 to 15 represents post-peak phases, where load gradually decrease and crack in samples increase until ultimate state represents with picture 15.

The main objective of this analysis is to determine the crack opening distance between two broken or separated parts.

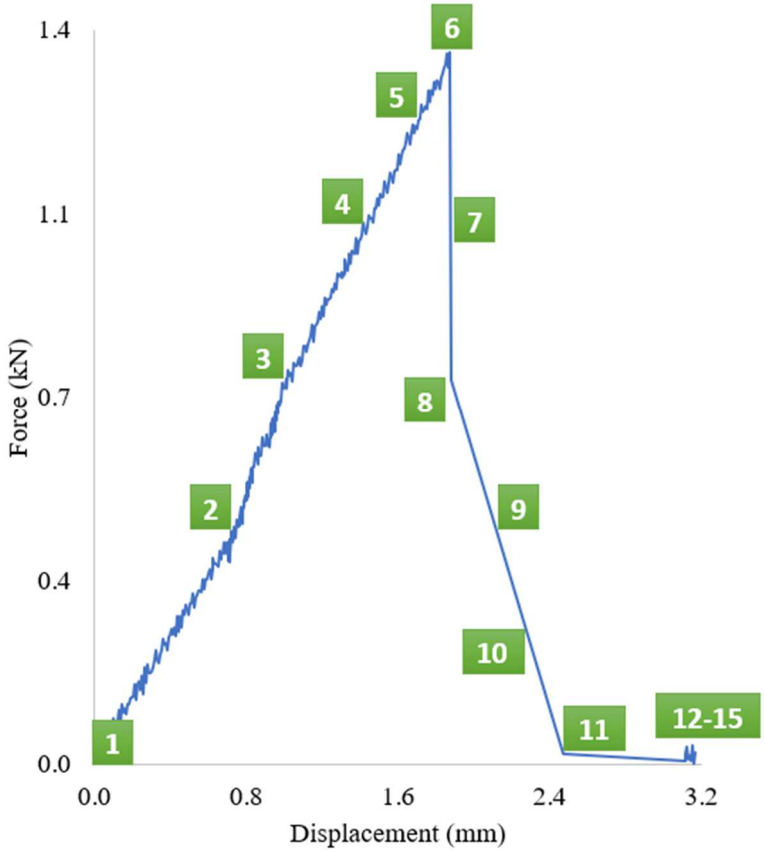

Fig. 9-6. Selected pictures underlined with number in green boxes, on a force-displacement curve of the sample MS(SW)F0.5(10)M1S1.

9.2 Analysis

DIC analysis has been done using the GOM correlate software. Fig. 9-7, Fig. 9-8, Fig. 9-9 and Fig. 9-10 represents DIC analysis of the crack openings at ultimate

displacement state (Table. 9.1) of the applied load, for the samples MS(SW)F1(30)M1S1, MS(SW)F0.5(30)M1S1, MS(SW)F0.5(10)M1S1 and MS(SW)F0.5(5)M1S3, respectively. Fig. 9-11 represents the progressive crack dimension with respect to each picture from 1 to 15.

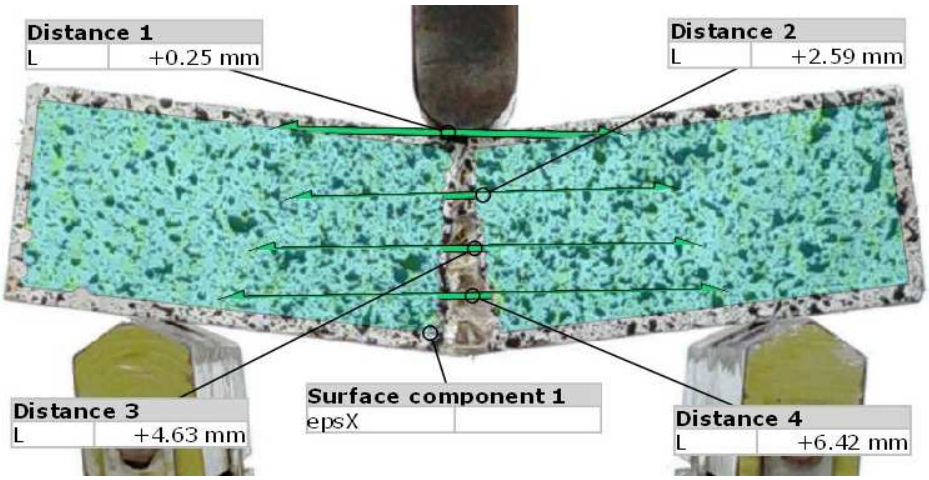

Fig. 9-7. DIC analysis of the sample MS(SW)F1(30)M1S1.

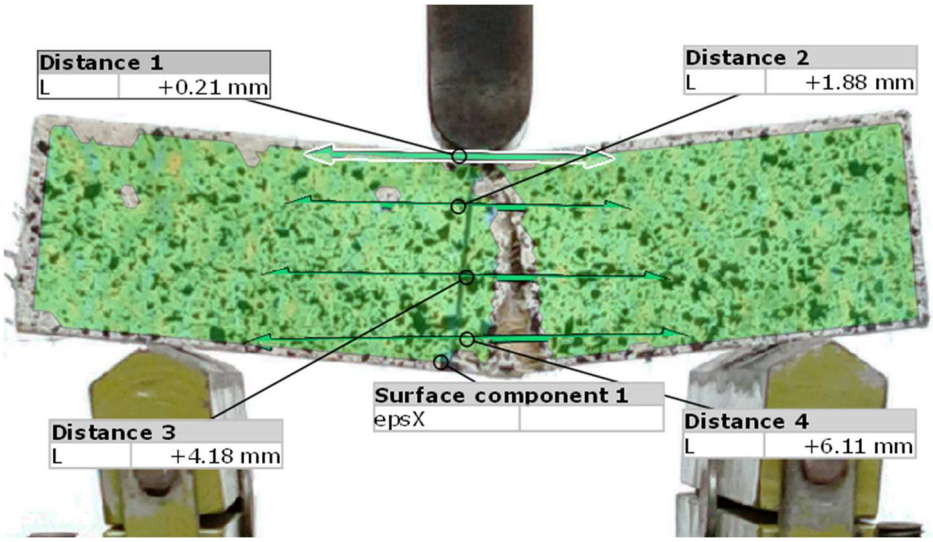

Fig. 9-8. DIC analysis of the sample MS(SW)F0.5(30)M1S1.

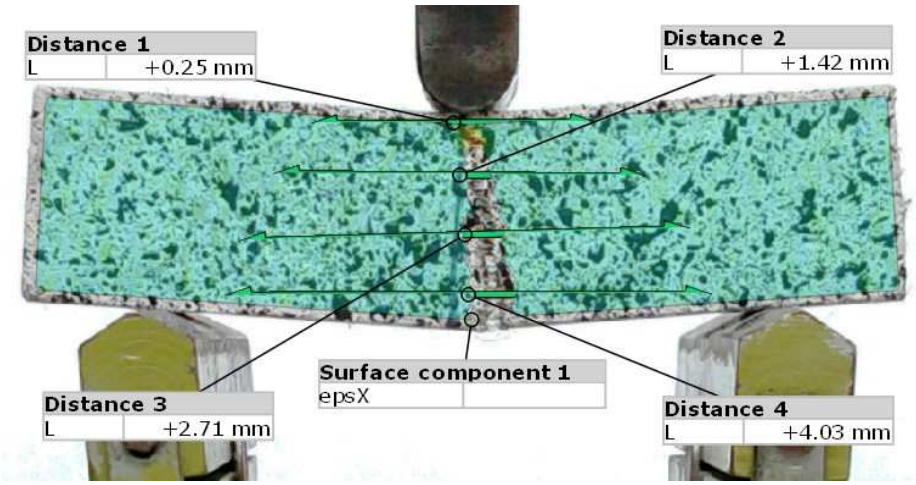

Fig. 9-9. DIC analysis of the sample MS(SW)F0.5(10)M1S1.

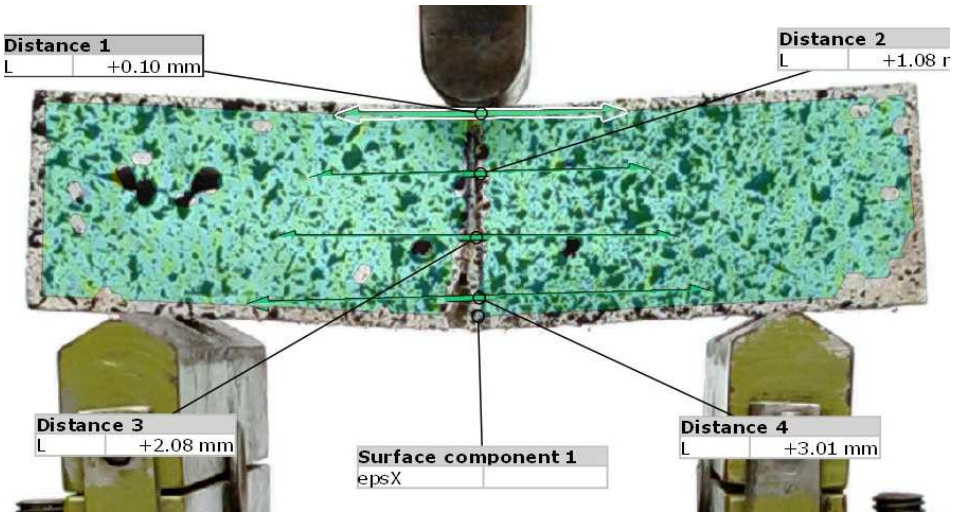

Fig. 9-10. DIC analysis of the sample MS(SW)F0.5(5)M1S3.

It is evident that the longer fibers help in binding/holding the broken parts together avoiding complete collapse of the samples. This could be demonstrated for the composite samples with 0.5% fiber (with respect to the mortar mass) and imbodied with 30mm long fibers, the crack/openings are 34% and 50% higher than that of samples imbodied with 10mm and 5mm long fiber, respectively (Table 9.1).

Wider cracks, i.e., about 5% larger opening has been noted that the higher percentage of fiber presence (for 30 mm long fibers) (Table 9.1).

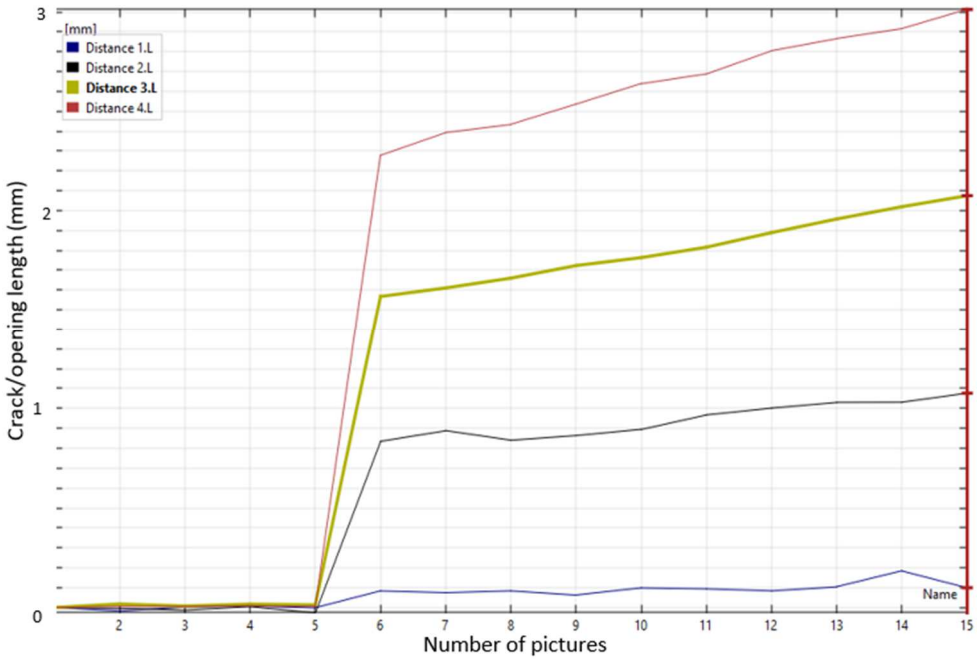

Fig. 9-11. Increase in crack/opening (mm) with progress from Picture 1 to picture 15; of the sample MS(SW)F0.5(10)M1S1.

Table 9-1. Prism samples crack measurements through DIC analysis.

Fiber percentage and fiber length combinations	Ultimate crack/opening dimension (length)	Ultimate displacement point corresponding to applied Load
	[mm]	[mm]
MS(SW)F1(30)M1S1	6.42	5.98
MS(SW)F0.5(30)M1S1	6.11	4.64
MS(SW)F0.5(10)M1S1	4.03	3.22
MS(SW)F0.5(5)M1S3	3.01	3.17

All masonry walls were prepared for the DIC analysis, but only two cases are presented here:

(1) HBW3 masonry wall reinforce with TRM configuration consist of 1 m x 1 m jute net with mesh pattern of 2.5 cm x 2.5 cm, four jute fiber diatons, structural mortar. The wall was subjected to a top load of 8 tons.

(2) HBW5 masonry wall reinforce with TRM configuration consist of 1m x 1m jute net with mesh pattern of 1.25cm x 2.5 cm, four jute fiber diatons, jute fiber (30mm fiber length and 1% of fiber with respect to the dry mortar mass) composite structural mortar. This wall was subjected to a fixed top load of 4 ton.

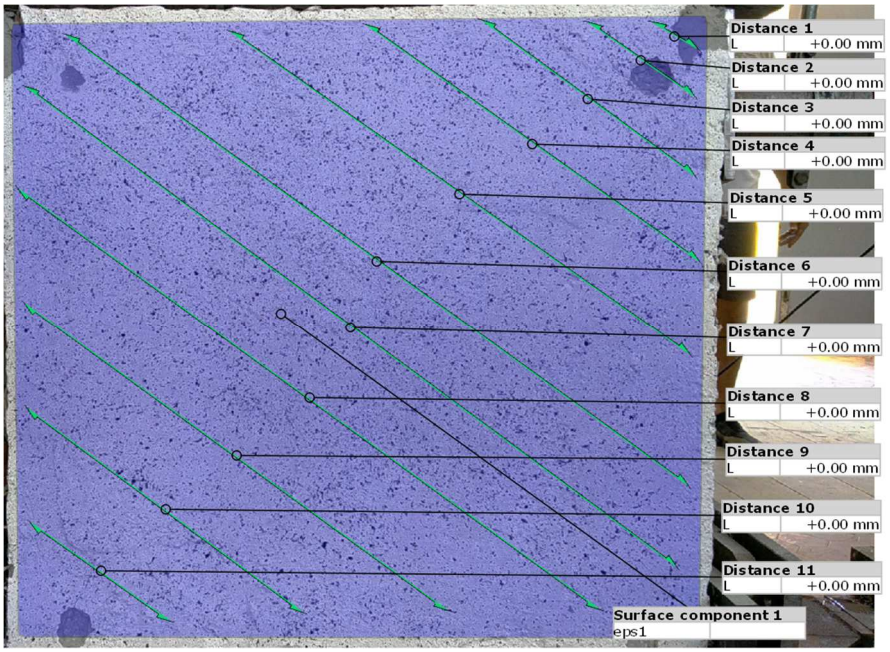

Fig. 9-12. DIC analysis of the retrofitted masonry wall HBW3, before applying the horizontal load.

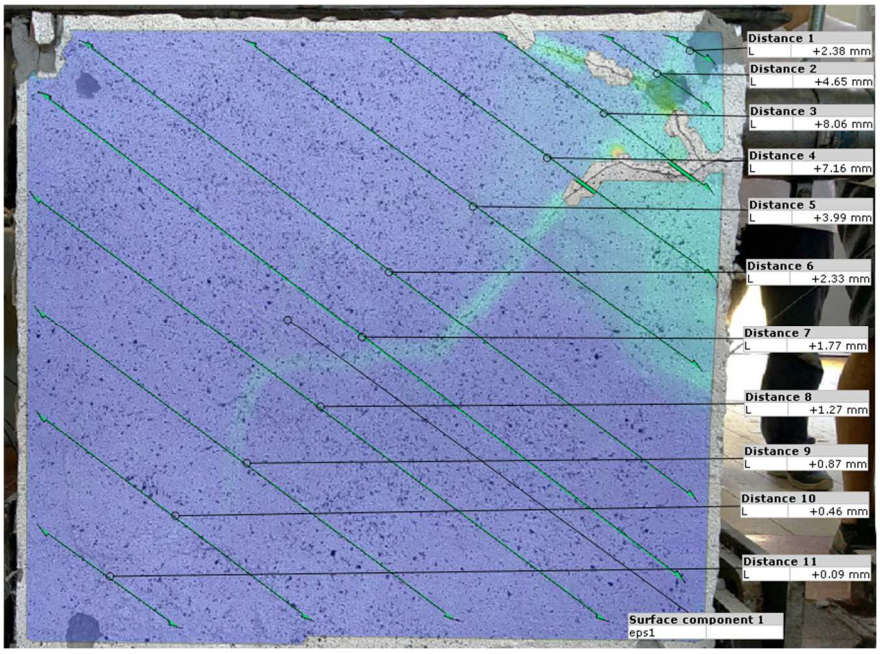

Fig. 9-13. DIC analysis of the retrofitted masonry wall HBW3, when maximum crack or opening observed.

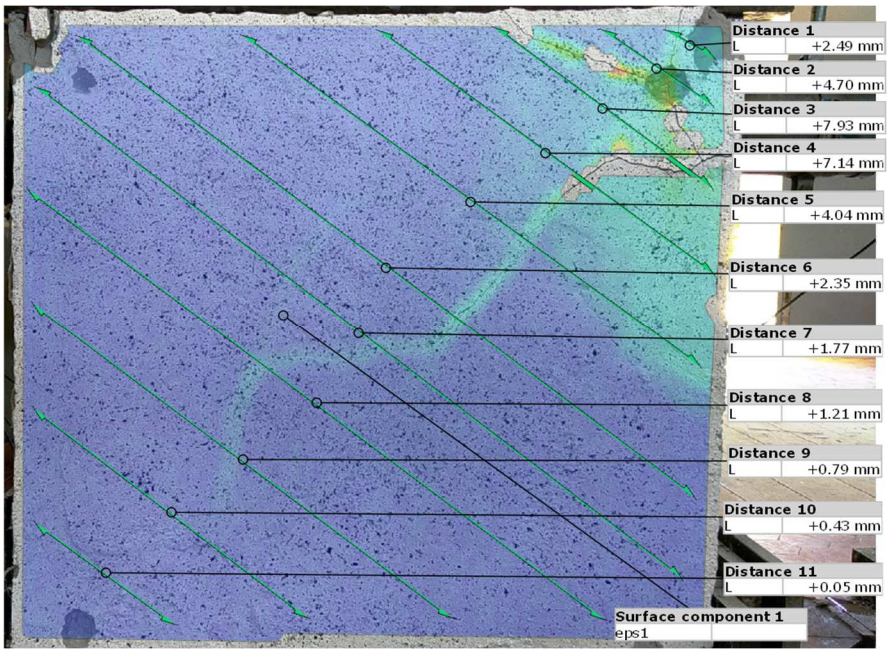

Fig. 9-14. DIC analysis of the retrofitted masonry wall HBW3, at ultimate state after completing the test.

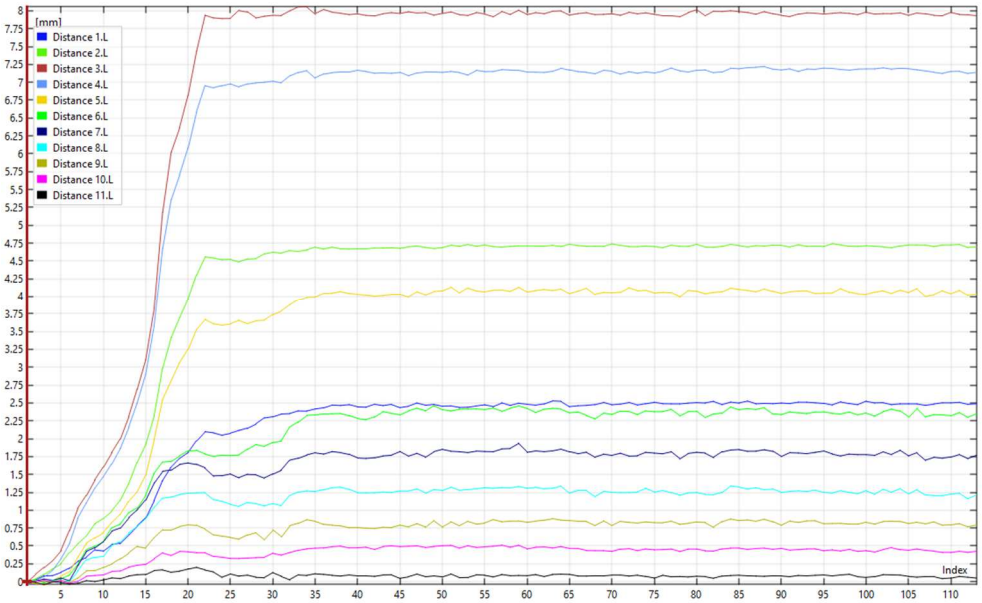

Fig. 9-15. The crack or opening trends of the masonry wall HBW3.

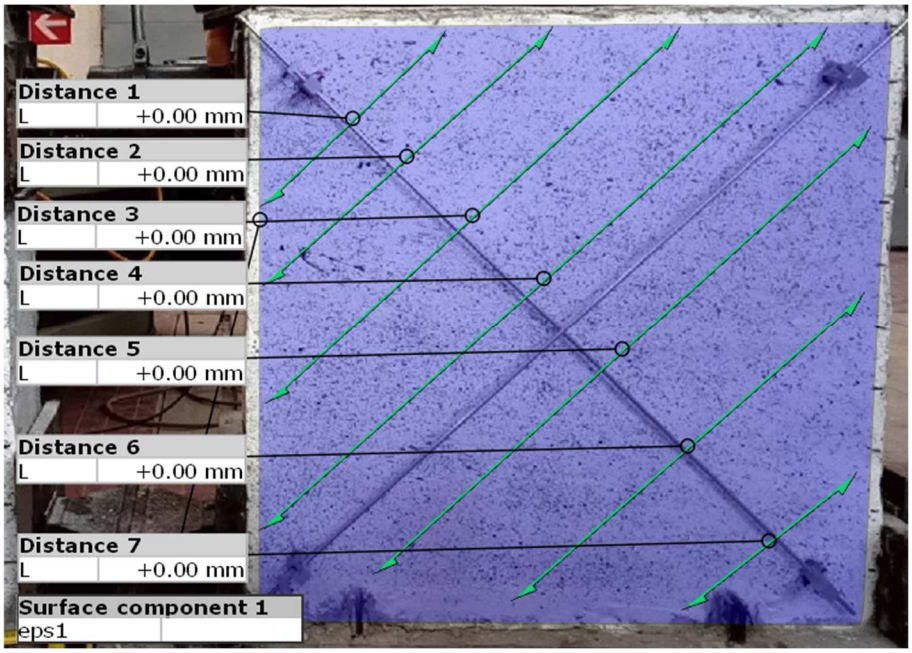

Fig. 9-16. DIC analysis of the retrofitted masonry wall HBW5, before applying the horizontal load.

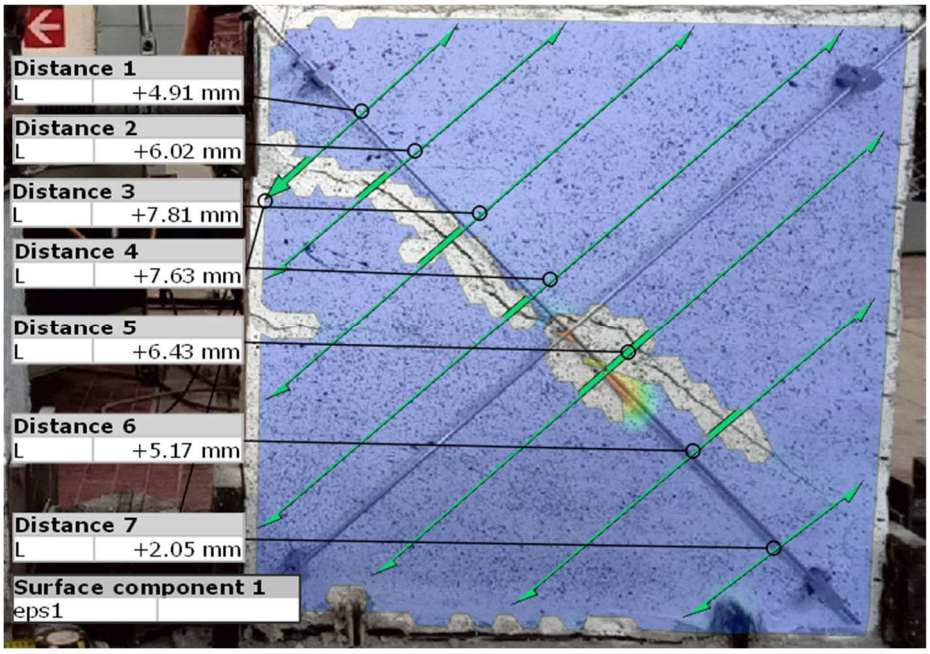

Fig. 9-17. DIC analysis of the retrofitted masonry wall HBW5, when maximum crack or opening observed.

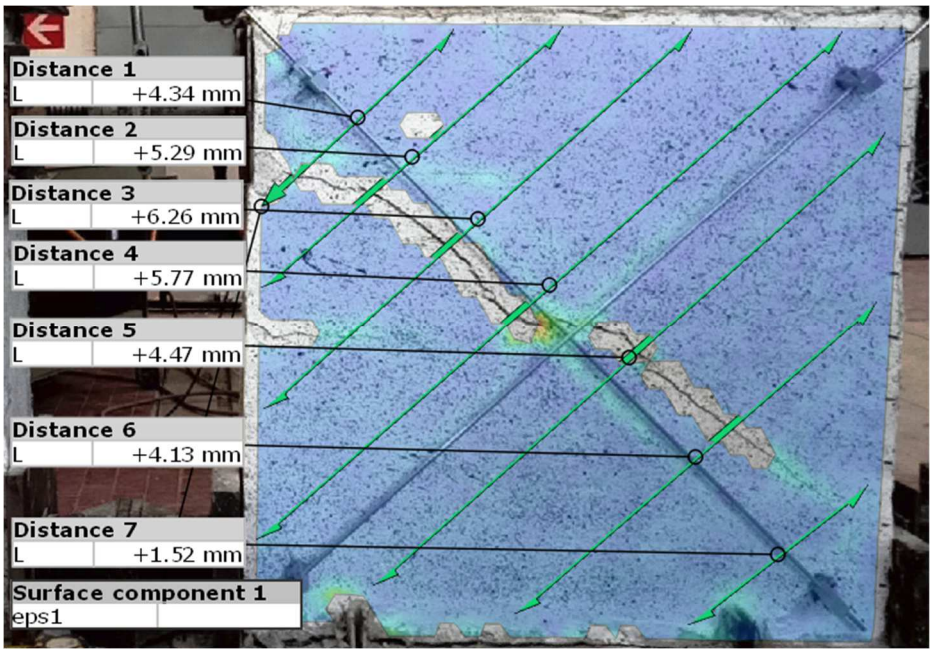

Fig. 9-18. DIC analysis of the retrofitted masonry wall HBW3, at ultimate state after completing the test.

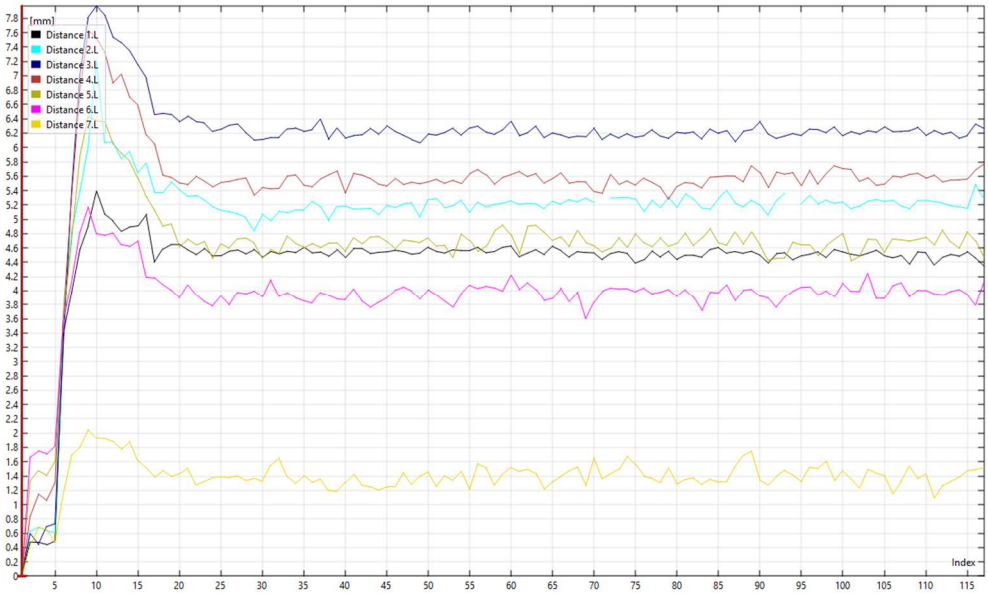

Fig. 9-19. The crack or opening trends of the masonry wall HBW3.

Table 9-2. Masonry wall specimens crack measurements through DIC analysis.

Fiber percentage and fiber length combinations.	The largest crack observed in the retrofitted masonry wall.
	[mm]
HBW3	8.06
HBW5	7.81

Fig. 9-12, Fig. 9-13 and Fig. 9-14 represent various phases of the DIC analysis of the HBW3 masonry walls. While Fig. 9-16, Fig. 9-17 and Fig. 9-18 and represent various phases of the DIC analysis of the HBW5 masonry wall.

Whereas in Fig. 9-15 and Fig. 9-19 shows the development and fluctuation of cracks with the development time and applied horizontal loads on masonry walls HBW3 and HBW5, respectively. For both cases around 115 plus pictures were used for the DIC analysis of the crack's behavior and patterns.

Table 9.2 represents the largest crack observed on the retrofitted masonry walls HBW3 and HBW5. Here to be noted that the “Distance” expressed in the above pictures from Fig. 9-7 to Fig. 9-19 is the crack or opening observed in samples and specimens.

9.3 Conclusion

The main objective of the DIC analysis was to study the crack behavior or pattern occurred in the masonry wall specimens, during the in-plane cyclic load tests. Interesting phenomenon have been observed.

Generally, the main crack occurs with the application of maximum load and at this point the crack length between two broken parts found to be maximum. Thereafter the gap remains quasi constant.

Further studies could be made to synchronize the crack pattern with respect to the applied loads.

10. Carbon-footprint of the masonry wall upgrading process, with jute fiber products

The Construction and Building (C&B) sector is directly responsible for global warming, as this sector is liable to pollute the environment by adding 39% and 36% of the total CO_2 emission to the atmosphere globally and in the EU, respectively, this is due to the fact that C&B sector needs about 36% and 40% of the total energy consumption in the world and in EU, respectively.

As already it has been stated previously that particularly the carbon, glass, aramid, steel fibers and PBO (Polyparaphenylene benzobisoxazole) are used for structural reinforcement or upgrading purposes. Notably use of these fibers hugely impacts the cost and on the environment. These fibers need (from cradle to gate) huge amount of energy during their production process, consequently the carbon foot-print is very high.

When compared with the man-made fibers, the natural plant fibers have much lower strength and also lack in applicable knowledge, standards and guidelines.

While recently the use of nature fibers is getting momentum, especially among the scientific and research community due these fibers availability, recyclability, bio-degradability and lower cost of production and final product.

Two interesting research works can be found on TRM upgrading with hemp fiber by Menna et al. (2015) and flex fiber by Ferrara et al. (2020).

During this PhD research activity, jute fiber products: raw fiber, net and diatons have been used for the upgrading of masonry walls (see chapter 7).

Therefore, in this chapter the impact of the jute fiber application in terms of energy consumption and carbon-foot print have been evaluated.

10.1 Carbon-footprint and energy consumption evaluation

Before calculating the overall energy consumption and carbon-foot print, a data collection flow chart was drawn (Fig 10.1) to easily identify the steps/points at which the data need to be collected.

Various sources have been used to collect the overall data, like on field survey has been conducted and rest of the information have been collected from the literature review.

During the on field survey, a questionnaire has been prepared for the jute fiber cultivators (Fig. 10-1). The below mentioned questions have been asked during the interview:

1) How much jute fiber you get from 1 bigha land?
2) Cost of cultivation?
3) Selling price?
4) How much water necessary for jute plant cultivation?
5) How much electricity necessary for jute plant cultivation?
6) Motor/pumping capacity (kW or hp)?
7) How many hours the motor is on?

Fig. 10-1. Jute plant cultivator.

Here it is to be noted that the bigha is a traditional unit of measurement of area of a land, and commonly used among farmers in the state of West Bengal, India. Where, 1 [bigha] is equivalent to 0.251 [Hectare]. In average 450 [kg] jute fiber can be produced from 1 [hectare] of cultivated land. Whereas the cost of jute plant cultivation and selling price of the fiber found to be equal to $ 437.56 and $ 1312.67 respectively in average per hectare. While the farmers could not directly answer to the question number 4 and 5. Therefore, they have been further asked two questions (question number 6 and 7) and it has been derived that in average 74 [kWh] electricity need per hectare for pumping water for 5 [hours], in average.

Fig. 10-2. The jute mill company visited during survey.

Further, a questioner also has been prepared for the mill: "Ganges Jute Pvt. Ltd., West Bengal, India" (Fig. 10-2), to collect data on jute processing and thread production. The below mentioned questions have been asked to the General Manager of the aforesaid company:

1) How much raw jute fiber (kg or other value) is necessary to produce 1 (kg or other value) threads (for both cases 1mm and 2mm thread)?
2) Procedure or steps followed from raw jute fiber to threads.

3) How much electricity is necessary at each process/step (or total electricity need for the production)?
4) Electricity price - Rs/kWh?
5) How much water is necessary at each process/step (or total electricity need for the production)?
6) Water cost?
7) What are capacities of the machines (Watt) used during the production? (1mm and 2mm)
8) What is done with the waste jute?
9) Jute buying cost?
10) Threads (1mm and 2mm) selling price?
11) Other important information would like to share?

Nearabout 100 [kg] of raw jute is necessary to produce 1 [kg] of thread (true for both thread dimensions: 1mm and 2mm). Whereas, about 8 [%] of the total fibers come out as waste product and these are used for energy production for self-consumption.

Based on the provided information by the jute mill, about 0.475 [kWh] electricity and 0.2 [liter] of water are necessary for every kg of thread production. Electricity and water cost of the jute-mill are about $ 0.10 per kWh, while water cost is $ 0.03 per 1000 liter of water. No information on the capacity of the machines is provided by the mill for privacy. Raw jute fiber buying and thread selling prices are $ 0.78 per kg and $ 1.12 per kg respectively.

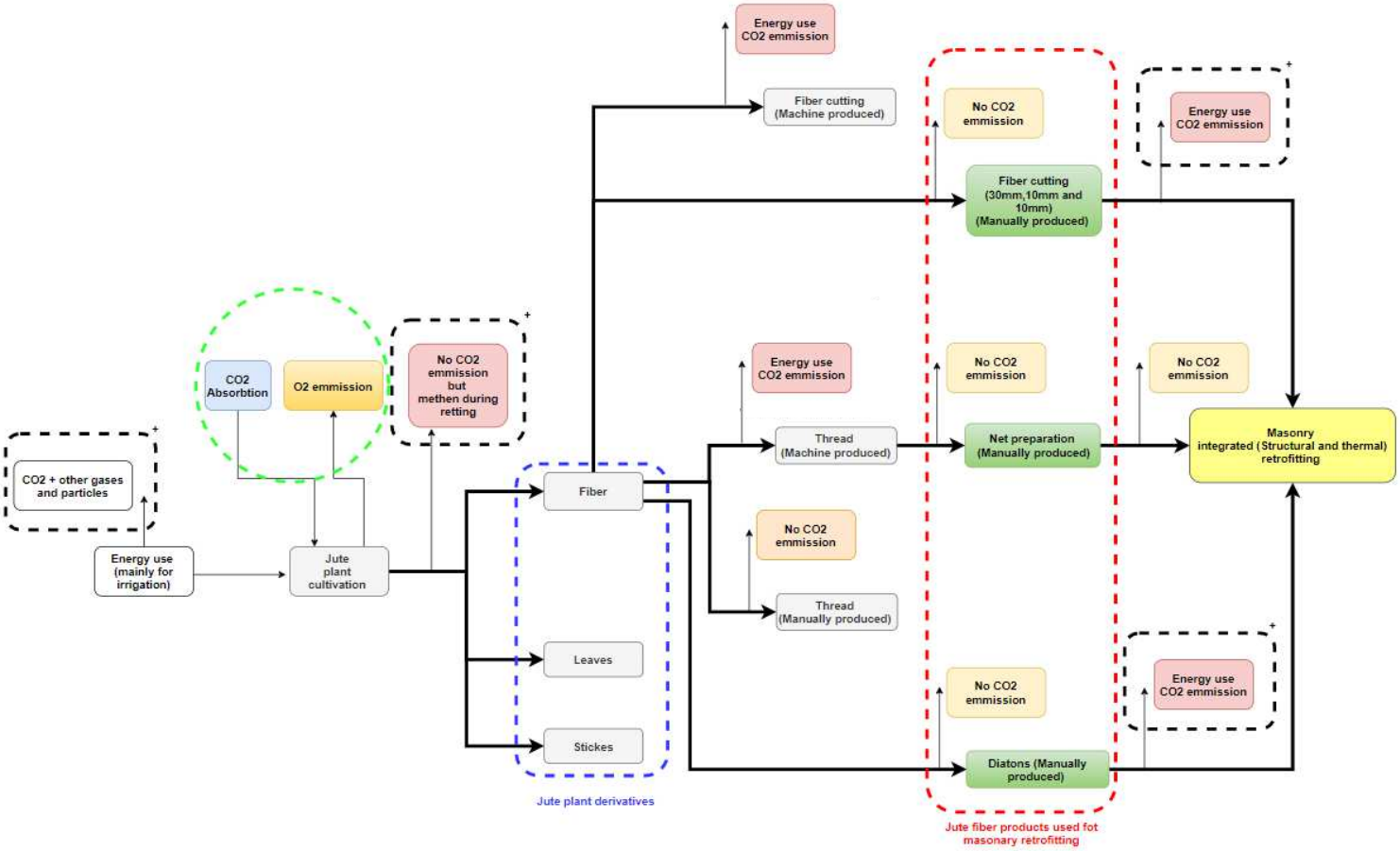

Fig. 10-3. Self-prepared Flow chart to determine the CO_2 emission and energy requirement at each step.

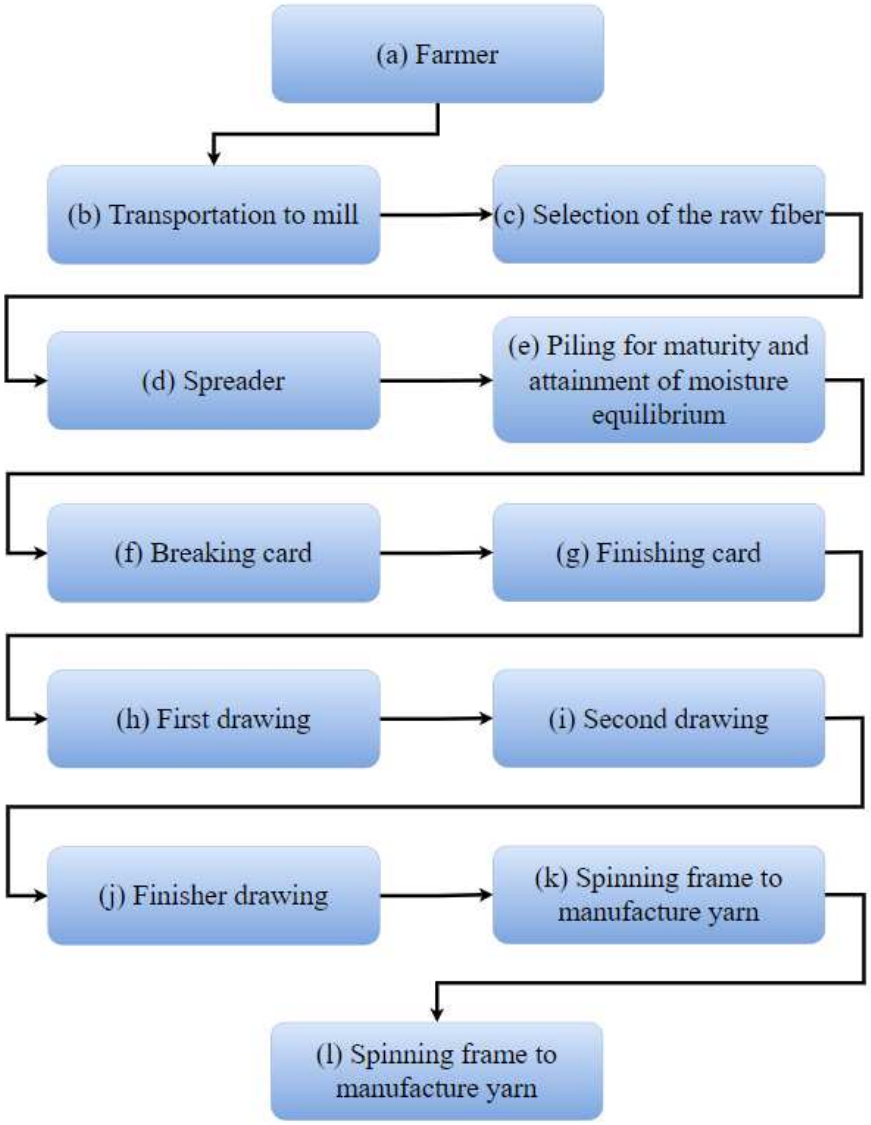

Fig. 10-4. Flow chart for jute processing.

Fig. 10-4 presents the jute thread production processing flow chart. The step starts from jute plant cultivation.

After jute fibers arrive at the mill, they were selected grade wise based on their quality and uniform morahs. The selected jute fibers processed through the spreader machine (Fig. 10-5 and Fig. 10-3.d). During this phase the water-rice bran oil

mixture is sprayed on fibers, and this is done to soften the fibers. The fibers were rolled and piled together and left for few days to achieve the require maturity.

After reaching the maturity, the lower part of the jute fibers is chopped off with a cutting knife, due to fact that this portion is not suitable for thread processing.

Rest of the uniform jute fiber portions are fed into the breaker card (Fig. 10-5 and Fig. 10-3.f) and these fibers are processed to obtain small units and further these were passed through the finisher card (Fig. 10-7 and Fig. 10-3.g) to obtain further tinner and regular in the rolled sliver form. Thereafter the rolled slivers are processed through three consecutive stages of the drawing frames (Fig. 10-8 and Fig. 10-3.h, Fig. 10-3.i and Fig. 10-3.j) to further attenuates and regularizes the slivers. The crimped slivers obtained at the end of the finisher drawing frame are further processed through the spinning frame (Fig. 10-9 and Fig. 10-3.k) where the application of suitable draft converts it into twisted yarns. Thereafter these yarns are also used to prepare fabrics as required (Fig. 10-10 and Fig. 10-3.l).

Fig. 10-5. Spreader machine.

Fig. 10-6. Breaker carding.

Fig. 10-7. Finisher carding.

Fig. 10-8. Drawing machine.

Fig. 10-9. Spinning machine.

Fig. 10-10. Victor loom for fabric manufacturing.

One of the major advantages of jute plant cultivation is that the process purifies the air by absorbing CO_2 and emitting O_2 (Islam et al. 2012). According to Niloy A.C (2021), about 11000 (kgO_2/hectare) of oxygen produce and around 15000 ($kgCO_2$/hectare) of carbon dioxide get absorbed during each cultivation period.

10.2 Major findings and Carbon-footprint analysis of the project

A total of 7 upgraded masonry walls were considered for the calculation. For masonry upgrading purpose, about 2.5 [kg] (equivalent to 249.8 [kg] of raw jute fiber) of jute thread, 1.4 [kg] of chopped fiber (30 mm long) used for composite mortar preparation and 1.12 [kg] of long raw fiber have been used for diaton preparation.

Therefore, calculation has been done considering the total raw jute fiber needed for the upgrading

Therefore back-calculation has been done to evaluate the amount of oxygen emitted and CO_2 absorbed during the plantation period.

Thereafter amount of energy and electricity needed at each step are determined and respective CO_2 has been evaluated.

Here to be noted that many other factors like transportation, fiber processing, pesticides, fertilizer induced N_2O emissions, fertilizer, seeds, field operations etc. are also responsible for the greenhouse gas emissions, therefore here by considering all possible sources, the total CO_2 equivalent emission has been considered, based on the data available in de Beus et al. (2019).

Table 10-1. Carbon-dioxide emission and energy needed at each step.

	O_2 emission	CO_2 Absorption	CO_2 emission	Electricity necessary during
	[g O_2]	[g CO_2]	[g CO_2]	[kWh]
Jute Plant cultivation + Jute fiber production	1547045.21	2109607.11	6968.36	0.10
Jute thread production	X	X	791.35	118.66
Masonry upgrading	X	X	5591.20	23.20
Greenhouse gas emissions in CO2 equivalent (considering transportation, fiber processing, pesticides, fertilizer induced N_2O emissions, fertilizer, seeds, field operations etc)	X	X	138768.80	X
Total	1547045.21	2109607.10	152119.71	141.96

The CO_2 absorption by jute plants during the plantation period is considered and compared with overall CO_2 emission, the net CO_2 balance is calculated around 1957487.40 [g CO_2] using the values of absorbed CO_2 and emitted CO_2 from Table 10-1, when the calculation has been done based on the equivalent jute fibers necessary for masonry upgrading.

Therefore, it could be demonstrable that use of natural fiber, like jute in our case can reduce the carbon-footprint by absorbing CO_2 and emitting O2 , from and to the atmosphere. Therefore, enhance the overall sustainability of the project.

10.3 Conclusions

The prime objective of the carbon footprint analysis for the masonry walls upgrading with the jute fiber driven products (raw jute fibers (30 mm long), net and diation), is to determine the sustainability and environmental feasibility of the process and the project.

Results obtained are highly enthusiastic and demonstrated that the optimum use of natural fiber can reduce the carbon-footprint and also could contribute to the overall sustainability of the overall project.

11. Conclusions

This thesis has analyzed many relevant aspects about the possible use of Jute fibers composite, intended as a technical solution for integrated structural/thermal upgrading of existing masonry walls.

The overall research activity mainly was developed in three phases, which started by characterizing the geometry and mechanics of fibers, proceeded by analyzing the thermo-mechanical properties of the mortars including just as both short fibers and reinforcing net and end up with the investigation of thermo-structural performances of TRM strengthened masonry walls.

Some of the interesting findings of this research work and related activities are summarized and highlighted below:

Phase I (fiber-scale)

At the fiber level, the jute fiber and its products (threads and diatons) have demonstrated promising mechanical properties. The average mechanical properties of the raw fibers are the following: Strain Energy of 0.77 Nmm, Tensile Strength 215.11 of MPa, Maximum Axial Strain 0f 0.0131 and Elastic Modulus of 127 16.97 GPa. Whereas the stain energy and tensile strength of the class 1 mm thread found to be 103 kN.mm and 112.45 MPa, respectively, while for class 2 mm thread theses values are 2.05 kN.mm and 56.95 MPa, respectively.

Therefore, being a vegetal fiber, the strength of jute and its products are significantly lower than those mostly used commercially like steel, glass, basalt fibers etc.

Also, jute threads from both classes were treated in different aging conditions and later theses threads were subjected to tensile strength tests, to determine their durability. It has been observed that thinner thread, i.e., class 1 mm thread without

and with aging treatment is better performer, therefore it has been chosen to prepare the nets for TRM masonry strengthening. For both types of jute threads, it has been observed that they do not significantly lose their strength when treated in salty and alkaline solutions, while threads treated in distilled water loose nearabout 50% of their original strengths.

The raw jute fiber and threads have demonstrated to have high water absorption capacity, similar to that of all other natural fibers.

Therefore, to reduce the water absorbability, and to improve the durability and strength of the raw jute fiber, it is highly advisable that the jute fiber need to be treated before their use.

Phase II (TRM scale)

At the composite system level, two types of composite mortars have been prepared using Thermal Mortar (TM) and Structural Mortar (SM) with three different fiber lengths (i.e., 30 mm, 10 mm and 5 mm) and four different fiber percentages (0.5%, 1.0%, 1.5% and 2.0%) with respect to the dry mortar mass.

Due to the application of fiber drop in flexural strength has been observed in all composite samples when compared with sample without fiber. The flexural strength decreased with the increase in fiber percentage.

Maximum drop in flexural strength of nearabout 1 MPa and more than 5.5 MPa has been observed with 2% fiber (5 mm) with respect to the mortar mass for composite TM and SM, respectively.

A maximum improvement in strain energy of near about 1 kN.mm and more than 2 kN.mm have been obtained for SM and TM composite samples with 2% fiber (30 mm) with respect to the mortar mass.

While drop of 81% and 89% in compressive strengths for SM and TM composite samples, respectively has been observed for specimens with 2% fiber (5 mm) used respect to the mortar mass.

Furthermore, the presence of fibers has influenced in lowering the TC values, consequently enhancing the insulating capacity of these specimens. The best

performer in this category found to be SM with 1.5% fiber (5 mm) used with respect to the mortar and TM with 2.0% fiber (5 mm) used with respect to the mortar, the measured reduction in TC value in average found to be more than 45 % and 52 %, respectively.

The application of jute fibers has both positive and negative effects. Although, on the one hand, the flexural and compressive strengths reduced with fiber addition, on the other hand, the strain energy capacity and insulation capacity of the composite materials have improved significantly. All composite mortars have shown ductile behavior. This improved strain energy capacity is useful when it is necessary to dissipate the effects of extreme loads like earthquakes.

This compensating nature of the jute fiber composite mortar (derived building materials) could be used for the integrated upgrading purpose.

One of the main problems, which has been observed during the mortar-fiber mixture, is related to the hydrophobic nature of the jute fiber, in particular when the chopped fibers (5 mm, 10 mm and 30 mm) come in contact with water, they tend to form small spherical balls and behave like sponge to absorb extra water in its cavity. Therefore, further research should be conducted to have uniform distribution of fiber in the composite mixture, including some pre-treatment of the chopped jute fibers. More combinations (fiber percentage and fiber length) need to be studied to obtain the best mixture for integrated (structural and thermal) upgrading.

Phase III (structural scales)

At masonry wall integrated (structural and thermal) upgrading level, the hollow brick walls were upgraded with various jute fiber products like:

1) Jute fiber nets (with mash configuration of “2.5 cm x 2.5 cm” and “2.5 cm x 1.25 cm” (to know more about the fabrication process and specification see Chapter 7).
2) Jute diatons (to know more about the fabrication process and specification see Chapter 4). Main purpose of diatons is to hold the nets (both sides of

the wall) and to connect the external surfaces to improve the shear resistance.

3) Jute fiber composite mortars, prepared with structural and thermal (without recycled aggregates) and copped 30 mm long jute fibers. In the mixture 1% jute fibers were used with respect to the dry mortar mass (to know more about the reason behind this choice see Chapter 5 and Chapter 6).

The jute net and jute diatons have been used for the structural strengthening, while the composite layers have been used particularly for thermal upgrading i.e., to enhance the insulation capacity of the masonry walls.

In this level two un-strengthened masonry walls and other six strengthen masonry walls were subjected to in-plane cyclic shear tests.in the strength laboratory of the University

While another two masonry walls were subjected to step-by-step thermal conductivity measurement. Staring from wall without reinforcement and then with various layers of the TRM system one after another. At the end the thermal transmittance of the upgraded walls was calculated.

The tests have demonstrated improvement in shear strength capacity of the upgraded masonry walls. The minimum and maximum load capacity improvement of the upgraded masonry wall found to 164.17 kN for HBW8 (upgraded with long intact raw jute fiber X pattern, 4 jute diatons.) and 198.51 kN for HBW6 (upgraded with jute nets, jute diatons and jute fiber composite mortars), when compared with non-upgraded masonry wall.

Thermal performance of the upgraded masonry wall same as HBW6 configuration has been evaluated and the reduction in thermal transmittance of 0.639 m^2K/W has been obtained, when compared with non-upgraded masonry wall.

Form aforesaid experiments it can be concluded that there are many aspects which need to be looked into before upgrading a masonry wall with Natural Fiber (NF) TRM system. As there are no specific standard or guidelines are available

particularly on NFTRM system and upgrading process, therefore it would be necessary and recommended to focus more on the preliminary tests to evaluate strength and configuration of the NFTRM systems following guidelines and recommendation like RILEM TC 250-CSM, ACI 549 and CNR DT (2018) available for general TRM system.

At the end the overall carbon foot-print of the project or more precisely the sustainability of the use of jute fiber and its products for masonry upgrading has been evaluated. Interestingly it has been found that use of jute fiber and it derived products have positive carbon foot-print effects on our environment and this is due to the positive CO_2 balance. Which can be expresses as i.e., more CO_2 have been absorbed from the environment than it has been produced or emitted, during the whole process, from jute plant cultivation to jute fiber and it derived products application for masonry upgrading.

Reference

AC 434–1011-R1 (2018) Acceptance criteria for masonry and concrete strengthening using fiber-strengthened cementitious matrix (FRCM) composite systems. ICC Evaluation Service, LLC: Birmingham, AL, USA

ACI 549.4R-13 (2013) Guide to design and construction of externally bonded fabric strengthened cementitious matrix (FRCM) systems for repair and strengthening concrete and masonry structures; ACI Committee 549: Farmington Hills, MI, USA

Ahmed, A., Qayoum, A. and Mir, F.Q., 2019. Investigation of the thermal behavior of the natural insulation materials for low temperature regions. *Journal of Building Engineering*, *26*, p.100849.

Aizi, D.E. and Kaid-Harche, M., 2020, December. Mechanical Behavior of Gypsum Composites Strengthened with Retama monosperma Fibers. In *Proceedings* (Vol. 63, No. 1, p. 40). MDPI.

Akhoundi, F., Vasconcelos, G. and Lourenço, P., 2018. In-plane behavior of infills using glass fiber shear connectors in textile strengthened mortar (TRM) technique. *International Journal of Structural Glass and Advanced Materials Research*, *2*(1), pp.1-14.

Akhoundi, F., Vasconcelos, G., Lourenço, P., Silva, L.M., Cunha, F. and Fangueiro, R., 2018. In-plane behavior of cavity masonry infills and strengthening with textile strengthened mortar. *Engineering Structures*, *156*, pp.145-160.

Alecci, V., Barducci, S., D'Ambrisi, A., De Stefano, M., Focacci, F., Luciano, R. and Penna, R., 2019. Shear capacity of masonry panels repaired with composite materials: Experimental and analytical investigations. *Composites Part B: Engineering*, *171*, pp.61-69.

Alfano, F.R. and Santoli, L.D., 2017. Energy efficiency and HVAC systems in existing and historical buildings. In *Historical Buildings and Energy* (pp. 45-53). Springer, Cham.

Ali Shah, S.M., Shahzada, K., Gencturk, B. and Memon, S.A., 2017. Retrofitting of full-scale confined masonry building using ferro-cement overlay. *Journal of Performance of Constructed Facilities*, *31*(5), p.04017079. DOI.org/10.1061/(ASCE)CF.1943-5509.0001060

Almeida, C., Guedes, J.P., Arêde, A., Costa, C.Q. and Costa, A., 2012. Physical characterization and compression tests of one leaf stone masonry walls. *Construction and Building Materials*, *30*, pp.188-197.

AL-Zubaidi, A.B., 2018, May. Effect of natural fibers on mechanical properties of green cement mortar. In *AIP Conference Proceedings* (Vol. 1968, No. 1, p. 020003). AIP Publishing LLC.

Amaral, M.C.D., Zonatti, W.F., Silva, K.L.D., Karam Junior, D., Amato Neto, J. and Baruque-Ramos, J., 2018. Industrial textile recycling and reuse in Brazil: case study and considerations concerning the circular economy. *Gestão & Produção*, *25*, pp.431-443.

Antov, P., Savov, V. and Neykov, N., 2017. Utilization of agricultural waste and wood industry residues in the production of natural fiber-strengthened composite materials. *International Journal–Wood, Design, and Technology*, *6*, pp.64-71.

Arifuzzaman, S. and Saatcioglu, M., 2012. Seismic Retrofit of Load Bearing Masonry Walls by FRP sheets and Anchors Sheets and Anchors. In *Proceedings of the 15th World Conference on Earthquake Engineering*.

Army US. 1993. Standard Practice for Shotcrete. US Army corps of Engineers, Washington, USA. Engineer Manual No. 1110-2-2005, *20020626*, p.123.

Arunavathi, S., Eithiraj, R.D. and Veluraja, K., 2017, May. Physical and mechanical properties of jute fiber and jute fiber strengthened paper bag with tamarind seed gum as a binder-An eco-friendly material. In *AIP Conference Proceedings* (Vol. 1832, No. 1, p. 040026). AIP Publishing LLC.

Ascione, F., Lamberti, M., Napoli, A. and Realfonzo, R., 2020. Experimental bond behavior of Steel Strengthened Grout systems for strengthening concrete elements. *Construction and Building Materials*, *232*, p.117105.

Asdrubali, F., D'Alessandro, F. and Schiavoni, S., 2015. A review of unconventional sustainable building insulation materials. *Sustainable Materials and Technologies*, *4*, pp.1-17.

Ashraf, M., Khan, A.N., Naseer, A., Ali, Q. and Alam, B., 2012. Seismic behavior of unstrengthened and confined brick masonry walls before and after ferrocement overlay retrofitting. *International Journal of Architectural Heritage*, *6*(6), pp.665-688.

Ashraf, M.A., Zwawi, M., Taqi Mehran, M., Kanthasamy, R. and Bahadar, A., 2019. Jute based bio and hybrid composites and their applications. *Fibers*, *7*(9), p.77.

Babaeidarabad, S., De Caso, F. and Nanni, A., 2014. URM walls strengthened with fabric-strengthened cementitious matrix composite subjected to diagonal compression. *Journal of Composites for Construction*, *18*(2), p.04013045.

Bakis, C.E., Bank, L.C., Brown, V., Cosenza, E., Davalos, J.F., Lesko, J.J., Machida, A., Rizkalla, S.H. and Triantafillou, T.C., 2002. Fiber-strengthened polymer composites for construction-state-of-the-art review. *Journal of composites for construction*, *6*(2), pp.73-87.

Bambach, M.R., 2020. Direct comparison of the structural compression characteristics of natural and synthetic fiber-epoxy composites: flax, jute, hemp, glass and carbon fibers. *Fibers*, *8*(10), p.62.

Banthia, N., 2019. Advances in sprayed concrete (shotcrete). In *Developments in the Formulation and Reinforcement of Concrete* (pp. 289-306). Woodhead Publishing.ISBN: 978-0-08-102616-8.

Barbosa, M.C., Rosa, S.E.S.D., Correa, A.R., Dvorsak, P. and Gomes, G., 2004. Setor de fibras sintéticas e suprimento de intermediários petroquímicos.

Barducci, S., Alecci, V., De Stefano, M., Misseri, G., Rovero, L. and Stipo, G., 2020. Experimental and analytical investigations on bond behavior of basalt-FRCM systems. *Journal of Composites for Construction*, *24*(1), p.04019055.

Basaran, H., Demir, A. and Bagci, M., 2013. The behavior of masonry walls with strengthened plaster mortar. *Advances in Materials Science and Engineering*, *2013*.

Benmansour, N., Agoudjil, B., Gherabli, A., Kareche, A. and Boudenne, A., 2014. Thermal and mechanical performance of natural mortar strengthened with date palm fibers for use as insulating materials in building. *Energy and Buildings*, *81*, pp.98-104.

Benzar, B.E., Park, M., Lee, H.S., Yoon, I. and Cho, J., 2020. Determining retrofit technologies for building energy performance. *Journal of Asian Architecture and Building Engineering*, *19*(4), pp.367-383.

Bera, T., Mohanta, N., Prakash, V., Pradhan, S. and Acharya, S.K., 2019. Moisture absorption and thickness swelling behaviour of luffa fibre/epoxy composite. *Journal of Strengthened Plastics and Composites*, *38*(19-20), pp.923-937.

Bernat, E., Gil, L., Roca, P. and Escrig, C., 2013. Experimental and analytical study of TRM strengthened brickwork walls under eccentric compressive loading. *Construction and Building Materials*, *44*, pp.35-47.

Bhatt, P. and Goe, A., 2017. Carbon fibres: production, properties and potential use. *Mater. Sci. Res. India*, *14*(1), pp.52-57.

Bisby, L.A., Williams, B.K., Green, M.F. and Kodur, V.K., 2002, May. Studies on the fire behaviour of FRP strengthened and/or strengthened concrete members. In 2nd International Conference on the Durability of Fibre Strengthened Polymer Composites for Construction.

Bischof, P. and Suter, R., 2014. Retrofitting masonry walls with carbon mesh. *Polymers*, *6*(2), pp.280-299.

Borri, A., Corradi, M., Sisti, R., Buratti, C., Belloni, E. and Moretti, E., 2016. Masonry wall panels retrofitted with thermal-insulating GFRP-strengthened jacketing. *Materials and Structures*, *49*(10), pp.3957-3968.

Buchan, P.A. and Chen, J.F., 2007. Blast resistance of FRP composites and polymer strengthened concrete and masonry structures–A state-of-the-art review. *Composites Part B: Engineering*, *38*(5-6), pp.509-522.

Can, Ö., 2018. Investigation of seismic performance of in-plane aligned masonry panels strengthened with Carbon Fiber Strengthened Polymer. *Construction and Building Materials*, *186*, pp.854-862.

Cascardi, A., Leone, M. and Aiello, M.A., 2020. Transversal joining of multi-leaf masonry through different types of connector: Experimental and theoretical investigation. *Construction and Building Materials*, *265*, p.120733.

Chand, N. and Fahim, M., 2020. *Tribology of natural fiber polymer composites*. Woodhead publishing.

Christou, P. and Elliotis, M., 2016. Construction and retrofit methods of stone masonry structures in cyprus. *The Open Construction & Building Technology Journal*, *10*(1).

Chuang, S.W. and Zhuge, Y., 2005. Seismic retrofitting of unstrengthened masonry buildings–a literature review. *Australian Journal of Structural Engineering*, *6*(1), pp.25-36.

CNR DT 215/2018, Guide for the Design and Construction of Externally Bonded Fibre Strengthened Inorganic Matrix Systems for Strengthening Existing Structures, 2020

CNR-DT, National Research Council, 2018. Guide for the design and construction of externally bonded fibre strengthened inorganic matrix systems for strengthening existing structures. CNR-DT, 215, p.2018.

CNR, D., 2004. 200/2004. Guide for the Design and Construction of Externally Bonded FRP Systems for Strengthening Existing Structures.

Codispoti, R., Oliveira, D.V., Olivito, R.S., Lourenço, P.B. and Fangueiro, R., 2015. Mechanical performance of natural fiber-strengthened composites for the strengthening of masonry. *Composites Part B: Engineering*, *77*, pp.74-83.

Dalalbashi, A., Ghiassi, B., Oliveira, D.V. and Freitas, A., 2018. Fiber-to-mortar bond behavior in TRM composites: effect of embedded length and fiber configuration. *Composites Part B: Engineering*, *152*, pp.43-57.

de Beus, N., Carus, M. and Barth, 2019, PRESS RELEASE (DE/EN): Natural fibres show outstandingly low CO2 footprint compared to glass and mineral fibres 2019– nova-Institute updates its reference study for the automotive and insulation industry. (https://renewable-carbon.eu/news/natural-fibres-show-outstandingly-low-co2-footprint-compared-to-glass-and-mineral-fibres/ (Accessed on 27 July 2022).

De Santis, S., Carozzi, F.G., de Felice, G. and Poggi, C., 2017. Test methods for textile strengthened mortar systems. Composites Part B: Engineering, 127, pp.121-132.

De Santis, S., De Canio, G., de Felice, G., Meriggi, P. and Roselli, I., 2019. Out-of-plane seismic retrofitting of masonry walls with Textile Strengthened Mortar composites. *Bulletin of Earthquake Engineering*, *17*(11), pp.6265-6300.

De Santoli, L. and DÁmbrosio Alfano, F.R., 2014. Energy efficiency and HVAC systems in existing and historical buildings. *The Rehva European HVAC Journal*, *51*(6), pp.44-48.

De Vuyst, P., Dumortier, P., Swaen, G.M., Pairon, J.C. and Brochard, P., 1995. Respiratory health effects of man-made vitreous (mineral) fibres. *European Respiratory Journal*, *8*(12), pp.2149-2173.

Deák, P. and Kowalik, M., 2018. Composite aircraft joint experimental testing with digital image correlation (Doctoral dissertation, Instytut Techniki Lotniczej i Mechaniki Stosowanej).

Dell'Isola, M., D'Ambrosio Alfano, F.R., Giovinco, G. and Ianniello, E., 2012. Experimental analysis of thermal conductivity for building materials depending on moisture content. *International Journal of Thermophysics*, *33*(8), pp.1674-1685.

Deopura, B.L. and Padaki, N.V., 2015. Synthetic textile fibres: polyamide, polyester and aramid fibres. In *Textiles and Fashion* (pp. 97-114). Woodhead Publishing.

Dong, K., Sui, Z.A., Jiang, J. and Zhou, X., 2019. Experimental study on seismic behavior of masonry walls strengthened by strengthened mortar cross strips. *Sustainability*, *11*(18), p.4866.

EC (European Commission), 2019. New rules for greener and smarter buildings will increase quality of life for all Europeans. Brussels. https://ec.europa.eu/info/news/new-rules-greener-and-smarter-buildings-will-increase-quality-life-all-europeans-2019-apr-15_en#:~:text=Buildings%20are%20responsible%20for%20approximately,CO2%20emissions%20in%20the%20EU.&text=Therefore%2C%20more%20renovation%20of%20existing,CO2%20emissions%20by%20about%205%25 (Accessed on November 02,2019)

EC nZEB 2020 European Commission, Nearly zero-energy buildings, available online at https://ec.europa.eu/energy/topics/energy-efficiency/energy-efficient-buildings/nearly-zero-energy-buildings_en (Accessed on 27 July 2022).

EC, 2030 C&E framework , European Commission, 2030 climate & energy framework, https://ec.europa.eu/clima/eu-action/climate-strategies-targets/2030-climate-energy-framework_en (Accessed on 27 July 2022).

EC. (2019b). Brussels. (European Commission), EPBD (Energy performance of buildings directive).

Echarri, V., Espinosa, A. and Rizo, C., 2017. Thermal transmission through existing building enclosures: Destructive monitoring in intermediate layers versus non-destructive monitoring with sensors on surfaces. Sensors, 17(12), p.2848.

El Azhary, K., Chihab, Y., Mansour, M., Laaroussi, N. and Garoum, M., 2017. Energy efficiency and thermal properties of the composite material clay-straw. *Energy Procedia*, *141*, pp.160-164.

Elanchezhian, C., Vijaya Ramnath, B., Ramakrishnan, G., Rajendrakumar, M., Naveenkumar, V. and Saravanakumar M.K., 2018. Review on mechanical properties of natural fiber composites., Materials Today: Proceedings, Volume 5, Issue 1, Part 1, Pages 1785-1790, ISSN 2214-7853.

Elfordy, S., Lucas, F., Tancret, F., Scudeller, Y. and Goudet, L., 2008. Mechanical and thermal properties of lime and hemp concrete ("hempcrete") manufactured by a projection process. *Construction and Building Materials*, *22*(10), pp.2116-2123.

ElGawady MA, Lestuzzi P, Badoux M. Retrofitting of masonry walls using shotcrete. In2006 NZSEE Conference, Paper 2006 Mar (Vol. 45).

EN 1015-11:2019; Italian National Unification. Methods of test for mortar for masonry - Part 11: Determination of flexural and compressive strength of hardened mortar, UNI: Milan, Italy, 2019

EN 1015-2:2007, Methods of Test for Mortar for Masonry—Part 2: Bulk Sampling of Mortars and Preparation of Test Mortars, 2007.

EN 1015-3:2007 - Methods of Test for Mortar for Masonry—Part 3: Determination of Consistence of Fresh Mortar (by Flow Table); 2007.

EN 12667: 2002; Thermal Performance of Building Materials and Products-Determination of Thermal Resistance by Means of Guarded Hot Plate and Heat Flow Meter Methods-Products of High and Medium Thermal Resistance; 2002.

EN 12939:2002; Italian National Unification. Thermal Performance of Building Materials and Products—Determination of Thermal Resistance by Means

of the Hot Plate with Guard Ring and the Heat Flow Meter Method—Thick Products with High and Medium Thermal Resistance; UNI: Milan, Italy, 2002

EN 1946-3; CEN, European Committee for Standardization. Thermal Performance of Building Products and Components—Specific Criteria for the Assessment of Laboratories Measuring Heat Transfer Properties—Part 3: Measurements by the Guarded Heat Flow Meter Method; Brussels, Belgium, 1999.

EN 1998 Eurocode 8: Design of structures for earthquake resistance, 2004. https://eurocodes.jrc.ec.europa.eu/showpage.php?id=138.

EN 998-1, Specification for Mortar for Masonry – Part 1: Rendering and Plastering Mortar, Comité Européen de Normalisation, Brussels, 2010.

EN ISO 1350-1:2019;Fire classification of products in building elements - Part1: classification based on fire reaction test results., 2019

EP, C.E.U. (European Parliament, Council of the European Union). 2018. Energy Performance of Buildings 2018/844/EU. https://ec.europa.eu/energy/topics/energy-efficiency/energy-efficient-buildings/energy-performance-buildings-directive_en. (Accessed on 15 November 2020)

Facconi, L., Lucchini, S.S., Minelli, F., Grassi, B., Pilotelli, M. and Plizzari, G.A., 2021. Innovative method for seismic and energy retrofitting of masonry buildings. Sustainability, 13(11), p.6350.

Faella, C., Martinelli, E., Nigro, E. and Paciello, S., 2010. Shear capacity of masonry walls externally strengthened by a cement-based composite material: An experimental campaign. *Construction and Building Materials*, *24*(1), pp.84-93.

Ferrandez-García, M.T., Ferrandez-Garcia, C.E., Garcia-Ortuño, T., Ferrandez-Garcia, A. and Ferrandez-Villena, M., 2020. Study of waste jute fibre

panels (corchorus capsularis L.) agglomerated with Portland cement and starch. *Polymers*, *12*(3), p.599.

Ferrara, G., 2021. *Flax-TRM Composite Systems for Strengthening of Masonry: From Material Identification to Structural Behavior*. Springer Nature.

Ferrara, G., Caggegi, C., Gabor, A. and Martinelli, E., 2019. Experimental study on the adhesion of basalt textile strengthened mortars (TRM) to clay brick masonry: the influence of textile density. *Fibers*, *7*(12), p.103.

Ferrara, G., Caggegi, C., Martinelli, E. and Gabor, A., 2020. Shear capacity of masonry walls externally strengthened using Flax-TRM composite systems: Experimental tests and comparative assessment. *Construction and Building Materials*, *261*, p.120490.

Ferreira, J.M., Capela, C., Manaia, J. and Costa, J.D., 2016. Mechanical properties of woven mat jute/epoxy composites. *Materials Research*, *19*, pp.702-710.

Ferretti, E., 2019. Wire Ropes and CFRP Strips to Provide Masonry Walls with Out-Of-Plane Strengthening. *Materials*, *12*(17), p.2712.

Formisano, A., Chiumiento, G. and Dessì, E.J., 2020. Laboratory Tests on Hydraulic Lime Mortar Strengthened With Jute Fibres. *The Open Civil Engineering Journal*, *14*(1).

Formisano, A., Chiumiento, G. and Fabbrocino, F., 2019, September. Experimentation on lime mortars strengthened with jute fibres: Mixture workability and mechanical strengths. In *Conference of the Italian Association of Theoretical and Applied Mechanics* (pp. 1869-1880). Springer, Cham.

Formisano, A., Dessì Jr, E. and Landolfo, R., 2017, November. Mechanical-physical experimental tests on lime mortars and bricks strengthened with hemp. In *AIP conference proceedings* (Vol. 1906, No. 1, p. 090006). AIP Publishing LLC.

Fossetti, M. and Minafò, G., 2016. Strengthening of masonry columns with BFRCM or with steel wires: An experimental study. *Fibers*, *4*(2), p.15.

Francesconi, L., Pani, L. and Stochino, F., 2016. Punching shear strength of strengthened recycled concrete slabs. *Construction and Building Materials*, *127*, pp.248-263.

Furtado, A., Rodrigues, H., Arêde, A. and Varum, H., 2020. Impact of the Textile Mesh on the Efficiency of TRM Strengthening Solutions to Improve the Infill Walls Out-of-Plane Behaviour. *Applied Sciences*, *10*(23), p.8745.

Gattesco, N. and Boem, I., 2015. Experimental and analytical study to evaluate the effectiveness of an in-plane reinforcement for masonry walls using GFRP meshes. *Construction and Building Materials*, *88*, pp.94-104.

Giresini, L., Paone, S. and Sassu, M., 2020. Integrated cost-analysis approach for seismic and thermal improvement of masonry building façades. *Buildings*, *10*(8), p.143.

Giresini, L., Puppio, M.L. and Taddei, F., 2020. Experimental pull-out tests and design indications for strength anchors installed in masonry walls. *Materials and Structures*, *53*(4), pp.1-16.

Gkournelos, P.D., Triantafillou, T.C. and Bournas, D.A., 2020. Integrated structural and energy retrofitting of masonry walls: Effect of in-plane damage on the out-of-plane response. Journal of Composites for Construction, 24(5), p.04020049.

Gopinath, A., Kumar, M.S. and Elayaperumal, A., 2014. Experimental investigations on mechanical properties of jute fiber strengthened composites with polyester and epoxy resin matrices. *Procedia Engineering*, *97*, pp.2052-2063.

Górszczyk, J., Malicki, K. and Zych, T., 2019. Application of digital image correlation (DIC) method for road material testing. Materials, 12(15), p.2349.

Günaslan, S.E., Karaşin, A. and Öncü, M.E., 2014. Properties of FRP materials for strengthening. *International Journal of Innovative Science, Engineering & Technology*, *1*(9), pp.656-660.

Gupta, M.K., Srivastava, R.K. and Bisaria, H., 2015. Potential of jute fibre strengthened polymer composites: a review. Int. J. Fiber Text. Res, 5(3), pp.30-38.

GVR (Grand view research). 2017. Fiber Strengthened Polymer (FRP) Composites Market Analysis By Fiber Type (Glass, Carbon, Basalt, Aramid), By Application (Automotive, Construction, Electronic, Defense), By Region, And Segment Forecasts, 2018 – 2025. Report ID: GVR-2-68038-006-4. https://www.grandviewresearch.com/industry-analysis/fiber-strengthened-polymer-frp-composites-market (Accessed on November 15, 2020)

Hari, R. and Mini, K.M., 2019. Mechanical and durability properties of sisal-Nylon 6 hybrid fibre strengthened high strength SCC. *Construction and Building Materials*, *204*, pp.479-491.

Hemeda, S., 2018, November. Carbon Fiber Strengthened Polymers (CFRP) for Strengthening and Seismic Retrofitting of Historic Circular Masonry Stone Columns. In *International Congress and Exhibition" Sustainable Civil Infrastructures: Innovative Infrastructure Geotechnology"* (pp. 114-137). Springer, Cham.

IMED (2015); Italian Ministry of Economic Development, Inter-Ministerial Decree 26 June 2015 - Application of the methods of calculation of the energy performance and definition of requirements and minimum requirements for buildings, June 2015.

Isfeld, A.C., Moradabadi, E., Laefer, D.F. and Shrive, N.G., 2016. Uncertainty analysis of the effect of grout injection on the deformation of multi-wythe stone masonry walls. *Construction and Building Materials*, *126*, pp.661-672.

Islam, M.S. and Ahmed, S.J., 2018. Influence of jute fiber on concrete properties. *Construction and Building Materials*, *189*, pp.768-776.

Islam, M.S. and Ahmed, S.K., 2012. The impacts of jute on environment: An analytical review of Bangladesh. *J. Environ. Earth Sci*, *5*, pp.24-31.

Islam, M.S., Saito, J.A., Emdad, E.M., Ahmed, B., Islam, M.M., Halim, A., Hossen, Q.M.M., Hossain, M.Z., Ahmed, R., Hossain, M.S. and Kabir, S.M.T., 2017. Comparative genomics of two jute species and insight into fibre biogenesis. *Nature plants*, *3*(2), pp.1-7.

ISO 10077-1:2017; Thermal performance of windows, doors and shutters — Calculation of thermal transmittance — Part 1: General; 2017.

ISO 2062:2009, Textiles – yarns from packages – determination of single-end breaking force and elongation at break using constant rate of extension (CRE) tester, 2009

ISO 8301:1991, International Organization for Standardization. Thermal Insulation—Determination of Steady-State Thermal Resistance and Related Properties—Heat Flow Meter Apparatus; Geneva, Switzerland, 1991.

Janeliukstis, R. and Chen, X., 2021. Review of digital image correlation application to large-scale composite structure testing. Composite Structures, 271, p.114143.

Jirawattanasomkul, T., Ueda, T., Likitlersuang, S., Zhang, D., Hanwiboonwat, N., Wuttiwannasak, N. and Horsangchai, K., 2019. Effect of natural fibre strengthened polymers on confined compressive strength of concrete. *Construction and Building Materials*, *223*, pp.156-164.

Kalali, A. and Kabir, M.Z., 2012. Cyclic behavior of perforated masonry walls strengthened with glass fiber strengthened polymers. *Scientia Iranica*, *19*(2), pp.151-165.

Karlos, K., Tsantilis, A. and Triantafillou, T., 2020. Integrated seismic and energy retrofitting system for masonry walls using textile-reinforced mortars combined with thermal insulation: experimental, analytical, and numerical study. Journal of Composites Science, 4(4), p.189.

Kim, Y.K. and Chalivendra, V., 2020. Natural fibre composites (NFCs) for construction and automotive industries. In *Handbook of natural fibres* (pp. 469-498). Woodhead Publishing.

Koutas, L.N. and Bournas, D.A., 2020. Confinement of masonry columns with textile-strengthened mortar jackets. *Construction and Building Materials*, *258*, p.120343.

Kutz, M., 2006. Heat-transfer calculations. McGraw-Hill Education.

Kuzik, Marc D., Alaa E. Elwi, and JJ Roger Cheng. "Cyclic flexure tests of masonry walls strengthened with glass fiber strengthened polymer sheets." *Journal of Composites for Construction* 7, no. 1 (2003): 20-30.

Lei, Z., Qu, J.T. and Wang, Y., 2014. Strengthening of RC-brick masonry walls with opening using basalt fiber strengthened polymer. In *Advanced Materials Research* (Vol. 1021, pp. 63-67). Trans Tech Publications Ltd.

Liuzzi, S., Rubino, C., Stefanizzi, P., Petrella, A., Boghetich, A., Casavola, C. and Pappalettera, G., 2018. Hygrothermal properties of clayey plasters with olive fibers. *Construction and Building materials*, *158*, pp.24-32.

Lizundia, B., Lizundia, B., Longstreth, M., Kren, A. and Abrams, D.P., 1997. *Development of procedures to enhance the performance of rehabilitated URM buildings*. US Department of Commerce, National Institute of Standards and Technology.

Longo, F., Cascardi, A., Lassandro, P. and Aiello, M.A., 2021. Energy and seismic drawbacks of masonry: A unified retrofitting solution. Journal of Building Pathology and Rehabilitation, 6, pp.1-24.

Mahltig, B. and Kyosev, Y., 2018. Inorganic and composite fibers: production, properties, and applications.

Mahmood, H. and Ingham, J.M., 2011. Diagonal compression testing of FRP-retrofitted unstrengthened clay brick masonry wallettes. *Journal of Composites for Construction*, *15*(5), pp.810-820.

Majumder, A., Canale, L., Mastino, C.C., Pacitto, A., Frattolillo, A. and Dell'Isola, M., 2021. Thermal characterization of recycled materials for building insulation. *Energies*, *14*(12), p.3564.

Marcari, G., Manfredi, G., Prota, A. and Pecce, M., 2007. In-plane shear performance of masonry panels strengthened with FRP. *Composites Part B: Engineering*, *38*(7-8), pp.887-901.

Martínez-Barrera, G., del Coz-Díaz, J.J., Álvarez-Rabanal, F.P., Gayarre, F.L., Martínez-López, M. and Cruz-Olivares, J., 2020. Waste tire rubber particles modified by gamma radiation and their use as modifiers of concrete. *Case Studies in Construction Materials*, *12*, p.e00321.

Masuelli, M. 2013. Introduction of fibre-strengthened polymers− polymers and composites: concepts, properties and processes. In: Fiber Strengthened Polymers, The Technology Applied for Concrete Repair.

Masuelli, M. ed., 2013. *Fiber strengthened polymers: the technology applied for concrete repair*. BoD–Books on Demand.

Menna, C., Asprone, D., Durante, M., Zinno, A., Balsamo, A. and Prota, A., 2015. Structural behaviour of masonry panels strengthened with an innovative hemp fibre composite grid. *Construction and Building materials*, *100*, pp.111-121.

Mistretta, F., Stochino, F. and Sassu, M., 2019. Structural and thermal retrofitting of masonry walls: An integrated cost-analysis approach for the Italian context. *Building and Environment*, *155*, pp.127-136.

Mohanty, A.K. and Misra, M., 1995. Studies on jute composites—a literature review. *Polymer-Plastics Technology and Engineering*, *34*(5), pp.729-792.

Momoh, E.O. and Dahunsi, B.I.O., 2017. Suitability of oil-palm-broom-fibres as reinforcement for laterite-based roof tiles. International Journal of Software & Hardware Research in Engineering, 5(4), pp.27-35.

Mouritz, A.P. 2012. Manufacturing of fibre–polymer composite materials. Introduction to Aerospace Materials; Woodhead Publishing: Sawston, UK; Cambridge, UK. 10:303-37.

Mustafaraj, E., Yardim, Y., Corradi, M. and Borri, A., 2020. Polypropylene as a retrofitting material for shear walls. *Materials*, *13*(11), p.2503.

Nedwell, P.J. and SWAMY, R., 1994. Ferrocement, proceedings of the Fifth international Symposium on Ferrecement. *UMIST, Manchester, 6–9 September 1994. London: E & FN Spon, 1994. 28-30. Print*.

Niloy, A.C., 2021. Jute: Solution to Global Challenges and Opportunities of Bangladesh. SEISENSE Business Review, 1(2), pp.59-75.

Nouri, K., Alam, M.A., Mohammadhassani, M., Jumaat, M.Z.B. and Abna, A.H., 2015. Development of jute rope hybrid composite plate using carbon fibre. Structural Engineering and Mechanics, 56(6), pp.1095-1113.

NTC18 Italian building code 'Norme Tecniche per le Costruzioni ' Ministero delle infrastrutture e dei Trasporti. https://www.gazzettaufficiale.it/eli/gu/2018/02/20/42/so/8/sg/pdf. (Accessed on 10 February 2020)

Ortega, J., Vasconcelos, G., Rodrigues, H., Correia, M. and Lourenço, P.B., 2017. Traditional earthquake resistant techniques for vernacular architecture and local seismic cultures: A literature review. *Journal of Cultural Heritage*, *27*, pp.181-196.

Oskouei, A.V., Jafari, A., Bazli, M. and Ghahri, R., 2018. Effect of different retrofitting techniques on in-plane behavior of masonry wallettes. *Construction and Building Materials*, *169*, pp.578-590.

Osugi, R., Takagi, H., Liu, K. and Gennai, Y., 2009, November. Thermal conductivity behavior of natural fiber-strengthened composites. In *Proceedings of the Asian pacific conference for materials and mechanics, Yokohama, Japan* (pp. 13-16).

Padalu, P.K.V.R., Singh, Y. and Das, S., 2019. Out-of-plane flexural strengthening of URM wallettes using basalt fibre strengthened polymer composite. *Construction and Building Materials*, *216*, pp.272-295.

Padalu, P.K.V.R., Singh, Y. and Das, S., 2020. Cyclic two-way out-of-plane testing of unstrengthened masonry walls retrofitted using composite materials. *Construction and Building Materials*, *238*, p.117784.

Pani, L., Francesconi, L., Rombi, J., Mistretta, F., Sassu, M. and Stochino, F., 2020. Effect of parent concrete on the performance of recycled aggregate concrete. *Sustainability*, *12*(22), p.9399.

Papanicolaou, C., Triantafillou, T. and Lekka, M., 2011. Externally bonded grids as strengthening and seismic retrofitting materials of masonry panels. *Construction and Building Materials*, *25*(2), pp.504-514.

Pittau, F., Malighetti, L.E., Iannaccone, G. and Masera, G., 2017. Prefabrication as large-scale efficient strategy for the energy retrofit of the housing stock: An Italian case study. *Procedia Engineering*, *180*, pp.1160-1169.

Pohoryles, D.A., Maduta, C., Bournas, D.A. and Kouris, L.A., 2020. Energy performance of existing residential buildings in Europe: A novel approach combining energy with seismic retrofitting. *Energy and buildings*, *223*, p.110024.

Prota, A., Marcari, G., Fabbrocino, G., Manfredi, G. and Aldea, C., 2006. Experimental in-plane behavior of tuff masonry strengthened with cementitious matrix–grid composites. *Journal of Composites for Construction*, *10*(3), pp.223-233.

Punurai, W., Kroehong, W., Saptamongkol, A. and Chindaprasirt, P., 2018. Mechanical properties, microstructure and drying shrinkage of hybrid fly ash-basalt fiber geopolymer paste. *Construction and Building Materials*, *186*, pp.62-70.

Rahman, A. and Ueda, T., 2016. In-plane shear performance of masonry walls after strengthening by two different FRPs. *Journal of composites for construction*, *20*(5), p.04016019.

Rajak, D.K., Pagar, D.D., Menezes, P.L. and Linul, E., 2019. Fiber-strengthened polymer composites: Manufacturing, properties, and applications. *Polymers*, *11*(10), p.1667.

Raoof, S. M., & Bournas, D. A. (2017). TRM versus FRP in flexural strengthening of RC beams: Behaviour at high temperatures. *Construction and building materials*, 154: 424-437.

Rashid, K., Haq, E.U., Kamran, M.S., Munir, N., Shahid, A. and Hanif, I., 2019. Experimental and finite element analysis on thermal conductivity of burnt clay bricks strengthened with fibers. *Construction and Building Materials*, *221*, pp.190-199.

Raut, A.N. and Gomez, C.P., 2016. Thermal and mechanical performance of oil palm fiber strengthened mortar utilizing palm oil fly ash as a complementary binder. *Construction and Building Materials*, *126*, pp.476-483.

Ray, D., Sarkar, B.K., Rana, A.K. and Bose, N.R., 2001. Effect of alkali treated jute fibres on composite properties. *Bulletin of materials science*, *24*(2), pp.129-135.

Razmi, A. and Mirsayar, M.M., 2017. On the mixed mode I/II fracture properties of jute fiber-strengthened concrete. *Construction and Building Materials*, *148*, pp.512-520.

Righetti, L., Edmondson, V., Corradi, M. and Borri, A., 2016. Fiberglass grids as sustainable reinforcement of historic masonry. *Materials*, *9*(7), p.603.

RILEM TC 250-CSM, Technical Committee RILEM, 232-TDT (Wolfgang Brameshuber) (2016) Recommendation of RILEM TC 232-TDT: test methods and design of textile strengthened concrete. Mater Struct 49(12):4923–4927

Saba, N., Md Tahir, P. and Jawaid, M., 2014. A review on potentiality of nano filler/natural fiber filled polymer hybrid composites. *Polymers*, *6*(8), pp.2247-2273.

Sakthivel, P.B. and Jagannathan, A., 2011. Ferrocement construction technology and its applications–A Review.

Saleem, A., Medina, L., Skrifvars, M. and Berglin, L., 2020. Hybrid polymer composites of bio-based bast fibers with glass, carbon and basalt fibers for automotive applications—A review. *Molecules*, *25*(21), p.4933.

Saleem, M.A., Abbas, S. and Haider, M., 2016. Jute fiber strengthened compressed earth bricks (FR-CEB)–a sustainable solution. *Pakistan Journal of Engineering and Applied Sciences*.

Sassu, M., Giresini, L., Bonannini, E. and Puppio, M.L., 2016. On the use of vibro-compressed units with bio-natural aggregate. *Buildings*, *6*(3), p.40.

Shabdin, M., Attari, N.K. and Zargaran, M., 2018. Experimental study on seismic behavior of Un-Strengthened Masonry (URM) brick walls strengthened with shotcrete. *Bulletin of Earthquake Engineering*, *16*(9), pp.3931-3956.

Shahriar Kabir, M., Hossain, M., Mia, M., Islam, M., Rahman, M., Hoque, M.B. and Chowdhury, A.M., 2018. Mechanical properties of gamma-irradiated natural fiber strengthened composites. In *Nano Hybrids and Composites* (Vol. 23, pp. 24-38). Trans Tech Publications Ltd.

Shamsuddoha, M., Islam, M.M., Aravinthan, T., Manalo, A. and Lau, K.T., 2013. Effectiveness of using fibre-strengthened polymer composites for underwater steel pipeline repairs. *Composite Structures*, *100*, pp.40-54.

Siddiqui, M.Z., Everett, J.W. and Vieux, B.E., 1996. Landfill siting using geographic information systems: a demonstration. *Journal of environmental engineering*, *122*(6), pp.515-523.

Silva, P.F., Yu, P. and Nanni, A., 2008. Monte Carlo simulation of shear capacity of URM walls retrofitted by polyurea strengthened GFRP grids. *Journal of Composites for Construction*, *12*(4), pp.405-415.

Sivaraja, S.S., Thandavamoorthy, T.S., Vijayakumar, S., Mosesaranganathan, S., Rathnasheela, P.T. and Dasarathy, A.K., 2013. GFRP Strengthening and Applications of Unstrengthened Masonry wall (UMW). *Procedia Engineering*, *54*, pp.428-439.

Smits, J. 2016. Fiber-strengthened polymer bridge design in the Netherlands: Architectural challenges toward innovative, sustainable, and durable bridges. Engineering. 2(4):518-27.

Sonnenschein, R., Gajdosova, K. and Holly, I., 2016. FRP Composites and their Using in the Construction of Bridges. *Procedia engineering*, *161*, pp.477-482.

Srinivasababu, N., Rao, K.M.M. and Kumar, J.S., 2009. Experimental determination of tensile properties of okra, sisal and banana fiber strengthened polyester composites. *Indian Journal of Science and Technology*, *2*(7), pp.35-38.

Stratford, T., Pascale, G., Manfroni, O. and Bonfiglioli, B., 2004. Shear strengthening masonry panels with sheet glass-fiber strengthened polymer. *Journal of Composites for Construction*, *8*(5), pp.434-443.

Tempesta, G., 2018. Seismic retrofit of historical masonry walls by means of natural basalt fiber strips system (BFRP). Pre-modern concepts and innovative materials. In *MATEC Web of Conferences* (Vol. 242, p. 01014). EDP Sciences.

Townsend T, 2019. Natural Fibres and the World Economy July 2019. https://dnfi.org/coir/natural-fibres-and-the-world-economy-july-2019_18043/ (Accessed on 27 July 2022).

Townsend, T., 2020. World natural fibre production and employment. In *Handbook of natural fibres* (pp. 15-36). Woodhead Publishing.

Triantafillou, T.C., Karlos, K., Kapsalis, P. and Georgiou, L., 2018. Innovative structural and energy retrofitting system for masonry walls using textile reinforced mortars combined with thermal insulation: In-plane mechanical behavior. Journal of Composites for Construction, 22(5), p.04018029.

Triantafillou, T.C., Karlos, K., Kefalou, K. and Argyropoulou, E., 2017. An innovative structural and energy retrofitting system for URM walls using textile reinforced mortars combined with thermal insulation: Mechanical and fire behavior. Construction and Building Materials, 133, pp.1-13.

UN SDG (2020). The-Sustainable Development-Goals. https://sdgs.un.org/goals

UNDP (2022), Housing and living conditions https://www.teamstoendpoverty.org/wq_pages/en/visages/logement.php (Accessed on 27 July 2022).

UNFCCC (2015). Adoption of the Paris Agreement. Report No. FCCC/CP/2015/L.9/Rev.1, http://unfccc.int/resource/docs/2015/cop21/eng/l09r01.pdf. (Accessed on 21 September 2022)

UNI / TR 11552: 2014; Abacus of the structures constituting the opaque envelope of the buildings - Thermophysical parameters; 2014.

UNI 10351:1994; Building materials. Thermal conductivities and vapour permeabilities; 1994.

UNI EN 1015-2:2007, Methods of test for mortar for masonry - Part 2: Bulk sampling of mortars and preparation of test mortars

UNI EN 13501-1:2019-Fire classification of construction products and building elements - Part 1: Classification using data from reaction to fire tests

UNI EN 1934:2000; Thermal performance of buildings - Determination of thermal resistance by means of the hot runner method with thermo-fluxmeter – Masonry, 2000.

UNI EN ISO 10456:2008; Building materials and products - Hygrothermal properties - Tabulated design values and procedures for determining declared and design thermal values; 2008.

UNI EN ISO 6946:2018; Building components and building elements - Thermal resistance and thermal transmittance - Calculation methods; 2018.

Valenza, A., Fiore, V., Nicolosi, A., Rizzo, G., Scaccianoce, G. and Di Bella, G., 2015. Effect of sheep wool fibres on thermal-insulation and mechanical properties of cement matrix. *Academic Journal of Civil Engineering*, *33*(2), pp.40-45. DOI.org/10.26168/icbbm2015.5

Van Den Einde L, Zhao L, Seible F (2003), Use of FRP composites in civil structural applications. Construction and building materials, 2003, 17.6-7: 389-403.

Van Hoolst, T. and Rivoldini, A., 2014. Interior structure and evolution of Mars. In Encyclopedia of the solar system (pp. 379-396). Elsevier.

Vintzileou, E. and Tassios, T.P., 1995. Three-leaf stone masonry strengthened by injecting cement grouts. Journal of Structural Engineering, 121(5), pp.848-856.

Vintzileou, E., Mouzakis, C., Adami, C.E. and Karapitta, L., 2015. Seismic behavior of three-leaf stone masonry buildings before and after interventions: Shaking table tests on a two-storey masonry model. Bulletin of Earthquake Engineering, 13(10), pp.3107-3133.

Vosper, F.C. and Wiersma, B.J., 1988. Residential heat loss.

Wallin, J., 2014. Investigating Different Opportunities to Increase Energy Efficiency in Buildings by Retrofitting Heat Pump Coupled Heat Recovery Systems (Doctoral dissertation, KTH Royal Institute of Technology).

Wang, C., Sarhosis, V. and Nikitas, N., 2018. Strengthening/retrofitting techniques on unstrengthened masonry structure/element subjected to seismic loads: A literature review. *Open Construction and Building Technology Journal*, *12*(1), pp.251-268.

Warnar, J., 1996. Shotcrete in Seismic Repair and Retrofit. *Special Publication*, *160*, pp.299-314.

World Bank. (2021). The Global Economy.com, Rural population, percent - Country rankings. https://www.theglobaleconomy.com/rankings/rural_population_percent/ (Accessed on 27 July 2022).

Wu, Z., Wu, Y. and Fahmy, M.F., 2020. Structures strengthened with bonded composites. Woodhead Publishing. In book: Structures Strengthened with Bonded Composites (pp.1-85). Doi.org/10.1016/B978-0-12-821088-8.00001-1

Yan, L., Kasal, B. and Huang, L., 2016. A review of recent research on the use of cellulosic fibres, their fibre fabric strengthened cementitious, geo-polymer and polymer composites in civil engineering. *Composites Part B: Engineering*, *92*, pp.94-132.

Yun, K.K., Y.S. Baek, S.Y. Han and Y.G. Kim. 2019. Plastic Shrinkage Properties of Natural Fiber Strengthened Shotcrete. in "Shotcrete for Underground Support XIV", Matthias Beisler, ILF Consulting Engineers Asia, Ltd., Thailand Preedee Ngamsantikul, Thailand Underground and Tunneling Group (TUTG), Thailand Herbert Klapperich, TU Freiberg, Germany Eds, ECI Symposium Series, Nov 17-22. https://dc.engconfintl.org/shotcrete_xiv/8

Zakaria, M., Ahmed, M., Hoque, M.M. and Islam, S., 2017. Scope of using jute fiber for the reinforcement of concrete material. *Textiles and clothing sustainability*, *2*(1), pp.1-10.

Zaman, A., Gutub, S.A. and Wafa, M.A., 2013. A review on FRP composites applications and durability concerns in the construction sector. *Journal of Strengthened Plastics and Composites*, *32*(24), pp.1966-1988.

Zhao, J., Cai, G., Cui, L., Si Larbi, A. and Daniel Tsavdaridis, K., 2017. Deterioration of basic properties of the materials in FRP-strengthening RC structures under ultraviolet exposure. *Polymers*, *9*(9), p.402.

Zhou, D., Lei, Z. and Wang, J., 2013. In-plane behavior of seismically damaged masonry walls repaired with external BFRP. *Composite Structures*, *102*, pp.9-19.

Zukowski, B., dos Santos, E.R.F., dos Santos Mendonça, Y.G., de Andrade Silva, F. and Toledo Filho, R.D., 2018. The durability of SHCC with alkali treated curaua fiber exposed to natural weathering. Cement and Concrete Composites, 94, pp.116-125.